Photopolymer Systems for Holography and Additive Manufacturing

by

MARVIN D. ALIM

B.S., Carnegie Mellon University, 2013

M.S., Carnegie Mellon University, 2014

A thesis submitted to the

Faculty of the Graduate School of the

University of Colorado in partial fulfillment

of the requirement for the degree of

Doctor of Philosophy

Materials Science and Engineering

2019

ProQuest LLC
789 East Eisenhower Parkway
P.O. Box 1346
Ann Arbor, MI 48106 - 1346

This thesis entitled:

Photopolymer Systems for Holography and Additive Manufacturing

written by Marvin Dion Alim

has been approved for the Materials Science and Engineering

_____

Christopher N. Bowman, Committee Chair

_____

Robert R. McLeod, Committee Member

Date _____

The final copy of this thesis has been examined by the signatories, and we find that both the content and the form meet acceptable presentation standards of scholarly work in the above mentioned discipline.

Alim, Marvin Dion (PhD, Materials Science and Engineering)

Photopolymer Systems For Holography and Additive Manufacturing

Thesis directed by Professor Christopher N. Bowman and Professor Robert R. McLeod

This thesis is focused on the advancement of enabling photopolymer materials for holography and additive manufacturing. The first part of this thesis covers the design, synthesis and implementation of novel chemistries in two-stage holographic photopolymers. First, photopolymerizable high refractive index monomers (n_D/20ºC: 1.60 – 1.67) with enhanced solubilities were developed and employed in two-stage photopolymers, achieving high refractive index modulations (peak-to-mean Δn) of up to 0.03 in transmission holograms (pitch spacing ~ 1 μm); competitive with state-of-the-art commercial materials. These materials were also investigated towards alternative recording methods such as the facile optical fabrication of millimeter-scale flexible gradient refractive index (GRIN) lenses. In general, using efficient thiol-X chemistries, a diverse set of liquid acrylate writing monomers with a balanced set of properties (viscosity, color, dispersion, solubility etc.) were obtained. Correspondingly, a general and scalable synthetic strategy was devised that significantly expanded the thiol-X monomer toolbox for realizing high refractive index step-growth (photo)polymers. This highly modular approach enabled precise control over the monomer structure. Using only commercially available starting materials, synthesized thiol and diallyl ether monomers (n_D/20ºC > 1.64) formed low viscosity thiol-ene resins (< 200 cP) that exhibited rapid and high conversions, achieving high refractive index values (n_D/20ºC) up to 1.665. Separately, aspects of configuring the network in two-stage systems with

dynamic covalent chemistries were developed to enable stress relaxation during and after holographic exposure.

The second part of this thesis comprises the foundational study of photopolymerizable thermoplastics, a unique class of high molecular weight polymers (> 10^4 g/mol) rapidly fabricated with light in seconds. This includes the investigation of photopolymerized linear thiol-ene polymers that subsequently crystallize within minutes at ambient to form mechanically strong and tough semicrystalline materials. Fundamental structure-property studies revealed a unique sub-class of polymers characterized by elastomeric-like elongations (~800%) with thermoplastic-like tensile strength and toughness values of 25 MPa and 100 MJ/m^3 respectively. The potential of these materials for vat photopolymerization additive manufacturing was conclusively demonstrated using commercial 3D printers achieving good patterning resolutions at standard print times. The salient feature of being able to dissolve or melt otherwise mechanically robust 3D printed objects opens the door to a new class of intrinsically recyclable and reprocessable 3D printable photopolymers.

To my parents and siblings

ACKNOWLEDGEMENTS

I would like to thank both my advisors Prof. Christopher Bowman and Prof. Robert McLeod for giving me the opportunity to be a graduate student in their respective groups. Bob and Chris have both continuously assembled a diversely talented group of wonderful people to learn from and enjoy laughs with. Being a member of these two (+1) labs has been an incredible privilege. I would like to thank Prof. Jeffrey Stansbury, Prof. Timothy White and Prof. Yifu Ding for serving on my thesis committee and giving their time, ideas, and resources.

I would like to thank all the Bowman, McLeod and Stansbury group members that I have had the pleasure of interacting with. I would like to thank Adam Dobson, Dr. Adam Urness, Alex Anderson, Alexander Flores, Alina Martinez, Archish Muralidharan, Dr. Austin Baranek, Dr. Alan Aguirre Soto, Dr. Benjamin Fairbanks, Dr. Benjamin Kowalski, Dr. Brady Worrell, Dr. Callie Fiedler-Higgins, Camila Uzcategui, Charlie Rackson, Dr. Chen Wang, Dr. Danielle Konetski, Dr. Darren Forman, Dr. David Glugla, David Miller, Dawei Zhang, Dr. Devatha Nair, Dillon Love, Eftalda Becka, Dr. Gayla Lyon, Dr. Hanbyul Song, Dr. Heidi Culver, Izabelle Berman, Dr. Jacob Friedlein, Dr. Jasmine Sinha, John Hegert, Juan Hernandez, Justine Wagner, Kangmin Kim, Katelyn Long, Dr. Lewis Cox, Dr. Maciej Podgórski, Dr. Martha Bodine, Dr. Matthew McBride, Dr. Mauro Claudino, Megan Renny, Dr. Mingli Ni, Nancy Sowan, Neil Baugh, Nicholas Bongiardana, Dr. Parag Shah, Philip Nystrom, Sijia Huang, Dr. Sudheendran Mavila, Dr. Tao Gong, Dr. Tao Liu, Taylor Goodrich, Xiance Wang, Dr. Xinpeng Zhang, Dr. Xun Han, Dr. Zhenzhen Liu, and Dr. Zhibin Wen for their invaluable guidance and insights throughout the years. Aside from these groups, I have been fortunate to work with

several talented graduate students and post-docs in various groups including the Ding group, the Srubar group, and the White RPM group, I would also like to acknowledge the help and supported provided by Amelia Davenport, Neil Cramer and Trevor Goldman at Colorado Photopolymer Solutions.

I am especially grateful to the following people for sharing their time, knowledge and skills with me. Darren Forman, for taking me under his wing and guiding me at the start. Matthew McBride, for mentoring me throughout my graduate schooling. Chen Wang, for being a role model in getting things done. Brady Worrell, for his wisdom and constant willingness to help. Amy Sullivan, for helping me immensely with writing, presenting and my research overall through her insanely delicious cookies. David Glugla, for being an excellent research compadre on multiple successful projects (Chapter 3). David Miller, for providing continuous optics support whenever needed and his time and efforts on the GRIN project (Chapter 4). Maciej Podgórski, for helpful discussions and his help with the thiol-X and dynamic networks projects (Chapters 5 – 6). Sudheendran Mavila, for patiently teaching me how to synthesize chemicals and working with me on all the high refractive index monomers and dynamic networks work (Chapters 3 – 6). Kimberly Childress, for being a tireless and indispensable partner on the thermoplastics project (Chapters 7 – 8).

I would like to also acknowledge Facebook, Konica Minolta, the National Institute of Health, and the National Science Foundation for providing funding for this research.

Most of all, I would like to thank my family for their love and support. My parents have sacrificed enormously for me to get to this point and I owe them everything.

Table of Contents

List of Tables

List of Figures

List of Schemes

Introduction

1.1 Overview

Photopolymers are arguably one of the most facile and rapid methods of producing materials on demand. Using readily available wavelengths (300-500 nm) at mild intensities (1-100 mW/cm^2), photopolymerization rapidly converts a liquid into a solid in a matter of seconds; usually accompanied by orders of magnitude increase in modulus. Critically, the power of light crucially enables both spatial and temporal control over the material fabrication and development of physical properties. Unsurprisingly, photopolymers are used across multiple fields including coatings, dental restoratives, adhesives, holographic recording materials and additive manufacturing (3D printing). In particular with the latter two applications, non-uniform light exposure (i.e. patterned illumination) enables the formation of high quality, functional objects and optical devices not possible with current methods. However, despite the unparalleled convenience and utility of photopolymers, an overwhelming majority of photopolymers rely on chain-growth (meth)acrylate systems. While an enormous range of material properties can be accessed through the vast catalog of commercially available (meth)acrylate monomers, realizing the full potential of either holography or 3D printing requires a critical leap beyond this useful but limited materials platform. This thesis describes the development of critically enabling polymeric materials primarily based on novel high refractive index thiol-X ‘click’ chemistries for holography and 3D printing.

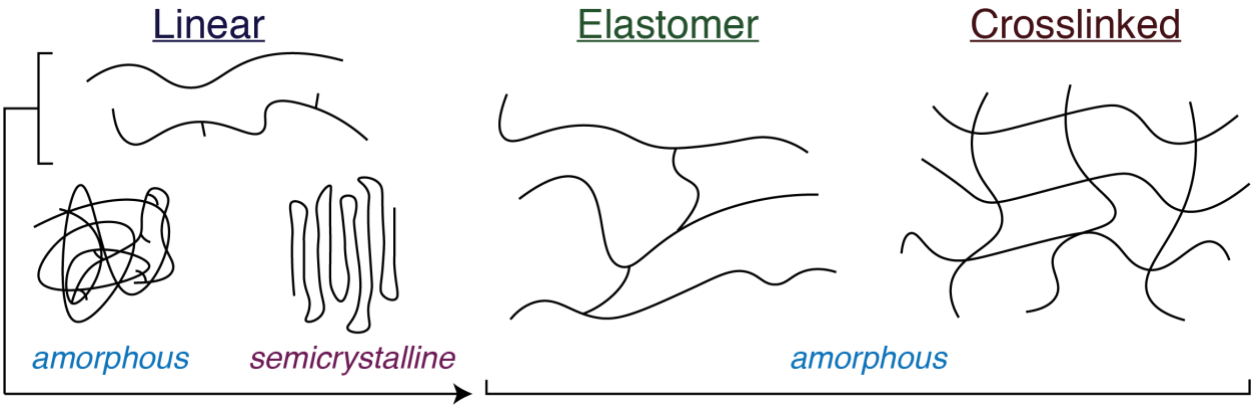

Scheme 0-1. Traditional classifications of polymeric materials according to their structural morphology. Linear, or branched, polymers can range from completely amorphous forming random coils or semicrystalline. Elastomers are loosely crosslinked and thus capable of large, reversible extensibility. Crosslinked polymers are three-dimensional networks that are irreversible.

1.2 Polymers

1.2.1 Linear vs. crosslinked polymers

Polymers can be characterized by their structural morphology ranging from linear to crosslinked as illustrated in Scheme 0-1.[1-3] Within this thesis, polymers on both ends of the spectrum are pertinent for their distinct properties and characteristics.

Linear polymers, traditionally termed thermoplastics, consist of long, linear or branched (but not crosslinked) chains. While chains can form physical entanglements with each other, upon heating they can soften and undergo macroscopic flow, making them amenable to reshaping or reprocessing.[1, 2] This distinct rheological behavior has set the standard for modern polymer manufacturing processing techniques such as injection molding and extrusion to make the workhorse materials of modern society such as poly(ethylene) (PE) or poly(ethylene terephthalate) (PET). As the chains in linear polymers are primarily associated via intermolecular forces, depending on the structural moieties present and thermal history, a limited subset of linear polymers can organize to

form partially crystalline domains.[4] Some examples include PE, polypropylene,[5] polylactides,[6] polyamides and polyesters.

In contrast to linear polymers, crosslinked network polymers, i.e. thermosets, possess a permanent three-dimensional network comprising irreversible chemical bonds that provide mechanical strength, thermal stability and chemical resistance but also prevents macroscopic flow upon heating.[7] Consequently, thermosets are typically amorphous and cannot be reshaped, reprocessed or melted at elevated temperatures. Elastomers (or rubbers) represent an intermediate third class of polymeric materials whereby crosslinks are present at much lower concentrations than thermosets resulting in a weakly crosslinked material that can exhibit large elastic (i.e. reversible) elongations. Together, these classes of polymers encompass an extraordinary array of unique and useful material properties impacting a wide scope of applications and industries today.

Amongst the available methods of forming crosslinked polymers, photopolymerizations are a powerful tool for on-demand and spatially defined formation. Photopolymers, the focus of this thesis, refer to the light induced formation of polymeric materials from low molecular weight monomers usually in the liquid state.[8] Classical photopolymerizations involve using ultra-violet (λ = 220 – 380 nm) or visible irradiation (λ = 400 – 700 nm) to cure a light-sensitive liquid resin composed of photoinitiator(s)[8-12] and a mixture of monomers, oligomers and additives without solvent at ambient conditions. Photopolymerizations offer distinct advantages over other conventional polymerization techniques including rapid reaction kinetics, convenience, low volatile organic compounds (VOCs) emission, and spatio-temporal control.[13] As a result,

photopolymers are used extensively as coatings, adhesives, dental restorative materials,[14-16] and in 3D printing.[17-21] However, due to requirements on reactivity rates and final mechanical properties, an overwhelming majority of photopolymerizations are limited to chain-growth (meth)acrylates as the monomers/oligomers to generate crosslinked networks.

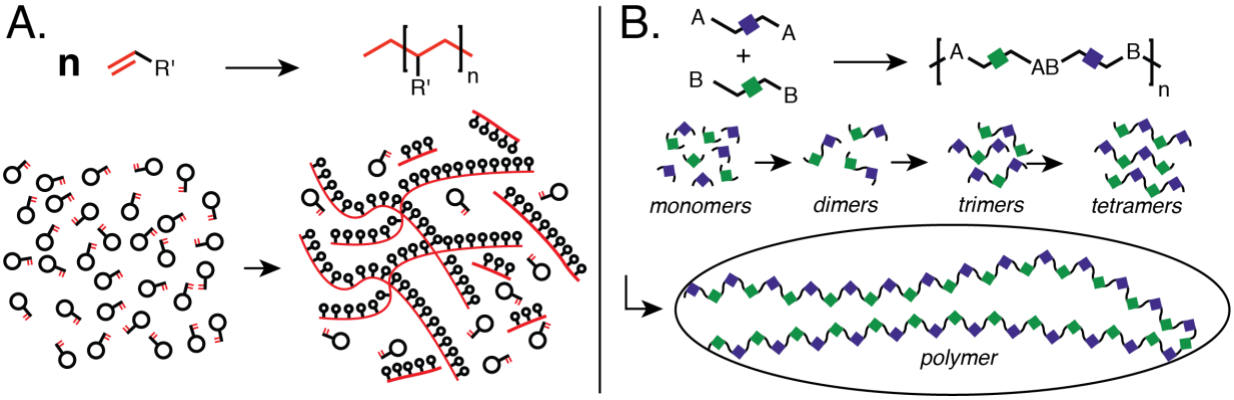

Scheme 0-2. Comparison of chain-growth and step-growth polymers. A) Schematic of a monofunctional vinyl monomer such as a (meth)acrylate) polymerizing to give a relatively large dispersity in molecular weights. B) Schematic for a AA and BB step-growth polymerization whereby low to high molecular weight species are gradually formed.

1.2.2 Chain-growth vs. step-growth polymers

The mechanism of polymerization is a key determinant on the final properties of polymers as described in Scheme 0-2. In chain-growth polymers, such as (meth)acrylates, molecular weight increases dramatically with a propagating radical adding to many carbon-carbon double bonds to low overall functional group conversions.[1, 2] A consequence of this early haphazard buildup of molecular weight is a highly heterogeneous formation of polymers. In linear systems this is characterized by high polydispersity values while in crosslinked systems gelation occur at very low monomer conversions. This has deleterious effects on shrinkage stresses and overall

uniformity of the material because of large variations in conversion. In contrast, step-growth polymerizations proceed in a gradual, stepwise manner forming low to high molecular weight species (i.e. dimers then trimers then tetramers and so on) sequentially.[1, 2] This leads to a steady increase in molecular weight with the formation of high molecular weight species and gelation occurring at higher conversions for step-growth networks than in chain-growth networks. This critical gel point conversion, ρ_c, for step-growth networks can be estimated by the Flory-Stockmayer equation[3, 22]:

$$\rho_C = \sqrt{\frac{1}{r(f_A-1)(f_B-1)}} \quad (1)$$

where r is the molar ratio ($0 < r \leq 1$) between the reactants (i.e. stoichiometric ratio), f_A is the average functionality of reactant A, and f_B is the average functionality of reactant B. Thus, significant control is afforded by the modulation of the stoichiometry as well as the functionalities of monomers present in a given formulation system. In general, step-growth polymer networks are more homogeneous (as characterized by sharp glass transitions) and exhibit lower shrinkage stresses due to dissipation through viscous flow. Furthermore, from a monomer structure design standpoint, step growth polymers incorporate the moieties linked to the reactive functionalities within the backbone of the polymer whilst in chain growth polymers the moieties reside exclusively as side chains as shown in Scheme 0-2. This restriction of only carbon-carbon main chains with (meth)acrylate polymers means there are intrinsic limitations on the scope of accessible material properties. On the other hand, step-growth polymers offer greater degrees of freedom in design than their chain-growth counterparts as desirable moieties can be built directly in to the backbone of the polymer.[23] Overall, designing novel step-growth

monomers represents a tangible route to achieving a tunable range of material properties in photopolymers beyond what is achievable with classical (meth)acrylate systems.

1.2.3 Thiol-X family of 'click' reactions

'Click' chemistry, as proposed by Kolb, Finn and Sharpless in 2001,[24] describes a class of reactions that are generally rapid, modular and highly efficient. Ideally, these reactions produce a single stereoselective product under mild, ambient conditions. The thiol-X family of 'click' reactions[25, 26] describes the collection of efficient and quantitative reactions in which a thiol readily undergoes either a radical or anionic-mediated reaction.[25, 26] In this section, specific thiol-X reactions directly relevant to this thesis will be discussed, including the radical-mediated thiol-ene reaction,[27-29] the thiol-Michael addition reaction,[30] the thiol-epoxide nucleophilic ring-opening reaction[31, 32] and the thiol-halide nucleophilic substitution reaction[33] as outlined in Scheme 0-3.

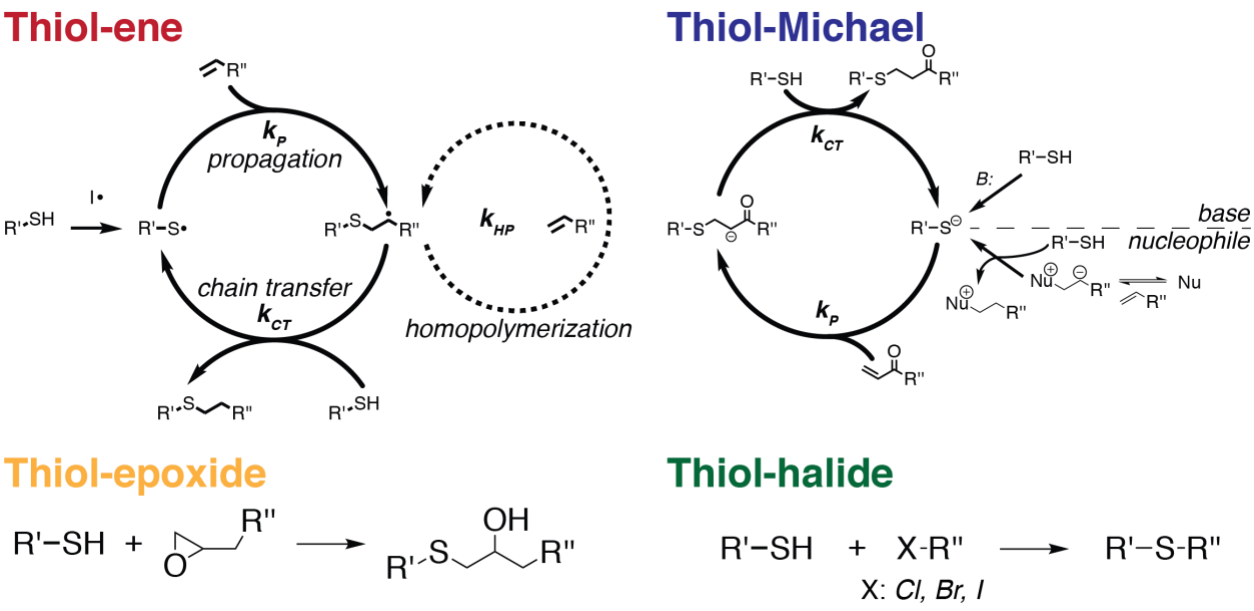

Scheme 0-3. Overview of several thiol-X reactions for small molecule and polymer synthesis. The thiol-ene reaction is a radical-mediated process that undergoes an

alternating sequence of propagation and chain transfer. The thiol-Michael reaction is the anion-mediated analog entailing the reaction of thiols with electron-deficient vinyls to form a thioether linkage. The thiol-epoxide reaction involves the nucleophilic ring-opening of epoxides by thiolate anions to produce a thioether with a free secondary hydroxyl group. The thiol-halide reaction is the efficient nucleophilic substitution of thiols into halide compounds.

1.2.3.1 Thiol-ene reaction

The thiol-ene 'click' reaction is the most prominent and comprehensively investigated of all thiol-X reactions.[25-27, 34, 35] The thiol-ene reaction, studied since 1905, involves the radical-based addition of a thiol and a vinyl (carbon-carbon double bond) to form a thioether linkage.[25, 26] As illustrated in Scheme 0-3, thiol-ene reactions uniquely undergo a radical-mediated step-growth reaction involving an alternating sequence of propagation of a thiyl radical to a vinyl (ene) group and chain transfer of the hydrogen from a thiol to regenerate a thiyl radical. Conveniently, thiol-ene polymerizations rely upon the same toolbox of radical photo, thermal or redox initiators as used for conventional free radical polymerizations. However, thiol-ene polymerizations possess the distinct advantage of reduced oxygen sensitivity[12, 36-39] over their chain-growth counterparts as unreactive peroxy radicals chain transfer to thiols to form reactive thiyl radicals. It is worth mentioning that while the thiol-ene reaction is widely reported to occur with virtually any type of vinyl under the appropriate conditions, instances with significant double bond homopolymerization are generally not considered to be a thiol-ene reaction.[25, 26]

1.2.3.2 Thiol-Michael reaction

The thiol-Michael addition reaction is the anionic analog to the thiol-ene, producing the same reaction product via an anionic intermediate instead of a radical intermediate[30]. The thiol-Michael reaction primarily involves the reaction of thiols with

electron-deficient vinyls including (meth)acrylates, vinyl sulfones and maleimides.[40] Typical approaches involve using either a base[30, 41, 42] or nucleophile catalyst[41, 43] with either method proceeding via an anionic mechanism. For the base-catalyzed thiol-Michael reaction, the thiolate anion is generated first from the deprotonation of the thiol by a base. Next, nucleophilic attack of the thiolate anion on electrophilic β-carbon on the vinyl (typically the rate limiting step) generates a highly basic carbon-centered anion intermediate that sequentially deprotonates another thiol to form the thioether product and regenerate the thiolate anion to complete the reaction cycle. In the case of the nucleophile-catalyzed pathway, the nucleophiles do not function as a base and act as a nucleophile to attack a vinyl to generate the highly basic carbon-centered anion intermediate responsible for starting the reaction cycle.

1.2.3.3 Thiol-Epoxide and Thiol-Halide reactions

Other thiol-X reactions that are especially useful for monomer synthesis are the thiol-epoxide nucleophilic ring opening reaction[31] and the thiol-halide nucleophilic substitution.[33] The base-catalyzed thiol-epoxy reaction is an efficient method to produce intermediate compounds containing flexible, sulfur-containing thioether linkages with free, labile hydroxyl groups. These hydroxyl groups are readily converted into a variety of (photo)polymerizable moieties including (meth)acrylates, allyl ethers, alkynes and norbornenes. Similarly, the base-catalyzed thiol-halide reaction is a robust and versatile route to monomer intermediates containing thioether linkages from a broad range of commercially available or easily synthesized halide-functionalized starting materials.

In this thesis, the thiol-epoxy and thiol-halide reactions are exploited to achieve the efficient and scalable synthesis of photopolymerizable high refractive index monomers. These monomers are typically used in chain-growth (meth)acrylate photopolymerizations or a step-growth thiol-ene. The Thiol-Michael reaction is used towards facile uniform network formation with excess thiol groups pendent.

1.2.4 High refractive index polymers

Polymers are important alternative optical materials to inorganic glass due to advantages in ease of processing, weight, impact resistance, and versatility in controlling other material properties of interest.[44] Optical materials over the visible spectrum are usually first considered in terms of their transmittance (T), refractive index (n) and the dispersion, typically expressed by the Abbe number (V). Refractive index is an intrinsic material property defined as,

$$n = \frac{c}{v} \tag{2}$$

where c is the speed of light in vacuum and v is the phase velocity of light in the medium.[45] For a given lens curvature, higher refractive index materials afford higher focusing power thus enabling thinner, lighter optical elements. Similarly in gradient refractive index materials, higher refractive indices provide greater dynamic range and latitude in optical design. However, within the scope of polymers, refractive index values typically range from 1.3 to 1.7 with a majority of organic compounds falling in the 1.4 to 1.55 range.[46] Therefore, polymers with refractive index values exceeding 1.6 are generally considered as being high refractive index polymers. Refractive index values for a given material change with respect to wavelength and this dependence is called dispersion. Within the visible spectrum, dispersion is quantified by the Abbe number,

$$V = \frac{n_D - 1}{n_F - n_C} \quad (3)$$

where n_D, n_F and n_C refer to the refractive index values at the sodium *D* (589.3 nm), hydrogen *F* (486.1 nm) and hydrogen *C* (656.3 nm) lines, respectively. One can predict the approximate refractive index of a given polymer using group contribution theory[46] and the Lorentz-Lorenz equation[47, 48] defined as,

$$n = \sqrt{\frac{1 + 2[R]/V_0}{1 - 2[R]/V_0}} \quad (4)$$

where [R] is the molar refraction and V_0 is the molar volume. It is well reported that atoms and groups with high molar refractions ([R]) and low molar volumes (V_0) such as sulfur, chalcogenides, heavy halogens (Cl, Br and I) and aromatic groups are effective contributors to increasing refractive index. Based on this, work to develop high refractive index polymers have led to remarkably high values achieved using multiple synthetic approaches.[47, 48] In particular increasing sulfur content has been shown to be an effective route that when taken to its extreme, i.e. polysulfides, can lead to refractive index values in excess of 2.[49, 50] However, a number of these strategies forfeit other important considerations such as color,[50, 51] dispersion, processability (viscosity and solubility), synthetic accessibility (involving multiple steps or inefficient yields), scalability or combinations thereof. Crucially, the majority of reports on high refractive index polymers are produced thermally[47, 48] (typically via polycondensation reactions) with only a small subset involving monomers that are subsequently photopolymerizable.

1.2.5 Covalent adaptable networks (CANs)

In this thesis, the utilization of covalent adaptable networks to augment the optical properties is investigated. The CANs paradigm[52-56] is a relatively new exploration

characterized by the incorporation of dynamic covalent chemistry[57] (DCC), i.e. triggerable, reversible covalent bonds, in crosslinked networks to enable dynamic bond exchange upon an applied stimulus (such as light, heat or select chemical triggers). The motivation for developing CANs materials is to bridge the divide in properties and behavior between thermosets and thermoplastics to obtain a material exploiting the best of both worlds. In general, CANs can be categorized as being either reversible addition (and condensation) or reversible exchange reaction type.[54] A key distinction between these two being the reaction sequence of the bond rearrangement. With reversible addition (and condensation) reactions, such as the Diels-Alder reaction,[58-62] a bond-breaking, bond-forming sequence occurs. However, reversible exchange reactions, such as transesterification,[63-66] follow a bond-forming, bond-breaking sequence. A key takeaway being that in reversible addition reactions, crosslink density is adjustable whereas in reversible exchange reactions, crosslink density is conserved. Numerous types of DCC have been implemented into CANs materials with the dynamic exchange process being either triggered *on-demand* using an applied stimulus or continuous[52, 54, 67, 68].

Since a majority of the use cases for polymer optics require ambient temperature operation, thermally-activated CANs requiring elevated temperatures for bond exchange are generally less applicable. In this respect, light-activated CANs are advantageous in having the capability to spatially pattern the required static-to-dynamic transition within a material. Aside from the constraint for room temperature dynamic exchange, additional requirements pertaining to optical polymers exist including the need for transparent and colorless materials. Taking this into account, suitable DCC that will be explored in this

thesis include: allyl sulfide,[69] and thioesters[70] as summarized in Scheme 0-4. Allyl sulfides undergo addition-fragmentation chain transfer (AFT) in which a generated radical species reacts with an AFT functional group to form a carbon-centered radical intermediate that can fragment in multiple ways to (re)generate the AFT unit and a radical species. Allyl sulfides have been successfully incorporated to photoinduce plasticity in crosslinked networks,[69] and thus, photoinduce stress relaxation allowing for programmed actuation,[71] reduced shrinkage stress,[15, 72, 73] mechanophotopatterning,[74] reconfigured surface patterns via nanoimprint lithography[75], and controlled liquid crystal alignment in liquid crystalline networks.[76] Fundamentally, allyl sulfides are radical-mediated and radical lifetimes are short, bond exchange effectively only occurs when there is appropriate irradiation of the finite amount of photoinitiator present to generate the required radical species. This may be considered a detriment or limitation to long, continuous or repeatable exchange and so a solution to this is the thiol-thioester exchange reaction, or transthioesterification, that undergoes an anion-mediated process and can be designed to be continuously dynamic or only dynamic on-demand (i.e. static).[70, 77-79] Recently implemented and studied in bulk crosslinked polymers,[70, 77, 78] the thioester exchange occurs rapidly upon generation of a thiolate anion from a base or nucleophile, which attacks a thioester to generate new thiol and thioester products.

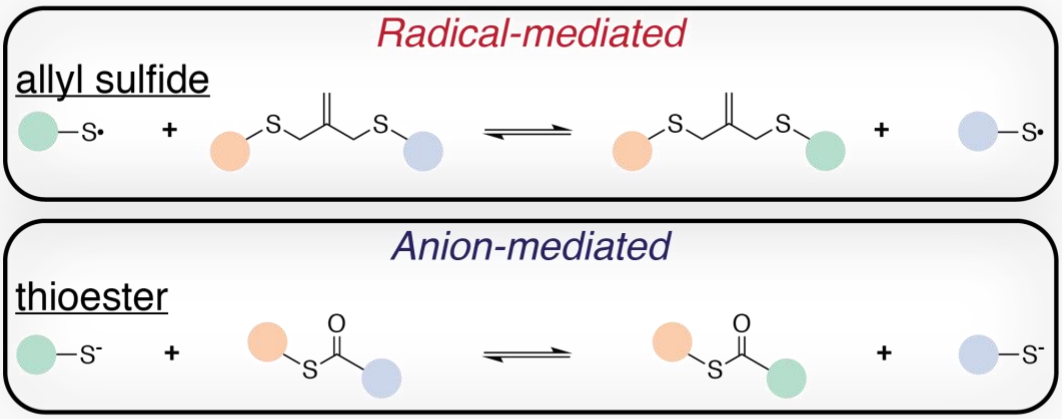

Scheme 0-4. Overview of select dynamic covalent chemistries useful for optical polymers. The allyl sulfide being radical mediated relies on the use of an initiator and thus will have a finite timeframe for dynamic exchange. In contrast, the transthioesterification exchange reaction is anion-mediated and thus long-lived dynamic exchange is possible provided that thiolate anion is present in the system.

1.2.6 Two-stage photopolymers

As introduced earlier, photopolymer materials responsive to spatially modulated light can enable advanced functions and capabilities via the localized programming of material properties. This is conveniently achieved with the two-stage photopolymer paradigm, generally defined as polymer systems that utilize different (ideally orthogonal) polymerization chemistries and stimuli (one of which being light) to access a wide and distinct range in material properties such as modulus, glass transition temperature, refractive index, etc.[80-83] This materials design approach coupled with the power of light offers unique advantages over conventional polymerization systems to tune properties with highly defined spatial and temporal control in a convenient manner. Applied to the

field of optics, two-stage photopolymers represent candidate recording materials for holography and other functional refractive index (phase) structures.[84] Typical systems consist of a stage 1 network (or matrix) and a photosensitive stage 2 writing chemistry. The general scheme involves an initial thermal cure of a solid rubbery matrix (stage 1), typically of lower refractive index ($n < 1.5$). This matrix acts as a framework through which dissolved species (writing monomer and photoinitiator) freely diffuse and undergo photopolymerization during a subsequent patterned irradiation step. This patterned light exposure spatially controls the polymerization (stage 2) according to the light intensity profile, consuming the reactive monomer species in the exposed regions and inducing mass transport of the additional monomer from the unexposed regions into the exposed regions to enhance the developing refractive index structure. The net outcome is a phase structure that ideally corresponds directly to the exposure pattern recorded in a thin, transparent polymeric film. As such, there is significant interest to use two-stage materials to record functional optical elements such as diffraction gratings, waveguides, mirrors, filters, lenses, etc. capable of high efficiencies and performance. When recorded using holography, these refractive index structures are collectively known as holographic optical elements (HOEs). These HOEs serve as key components in devices and systems where lightweight, compact sizes and configurable shape are essential. Regardless of the exposure patterning technique, a key enabling performance metric amongst two-stage photopolymers is the achievable refractive index modulation (Δn). In general, the Δn dictates the maximum diffraction efficiency for a given thickness as well as how many multiplexed holograms can be recorded in a given volume. To achieve practically relevant diffraction efficiencies, peak-to-mean Δn on the order of 10^{-2} are

critical with a majority of HOE applications requiring Δn approaching 0.05. In addition to Δn, other demands such as transparency, sensitivity, color, scatter (haze) are equally important for practical applications, thus requiring thoughtful design of high refractive index writing monomers as well as their judicious incorporation in a two-stage photopolymer system.

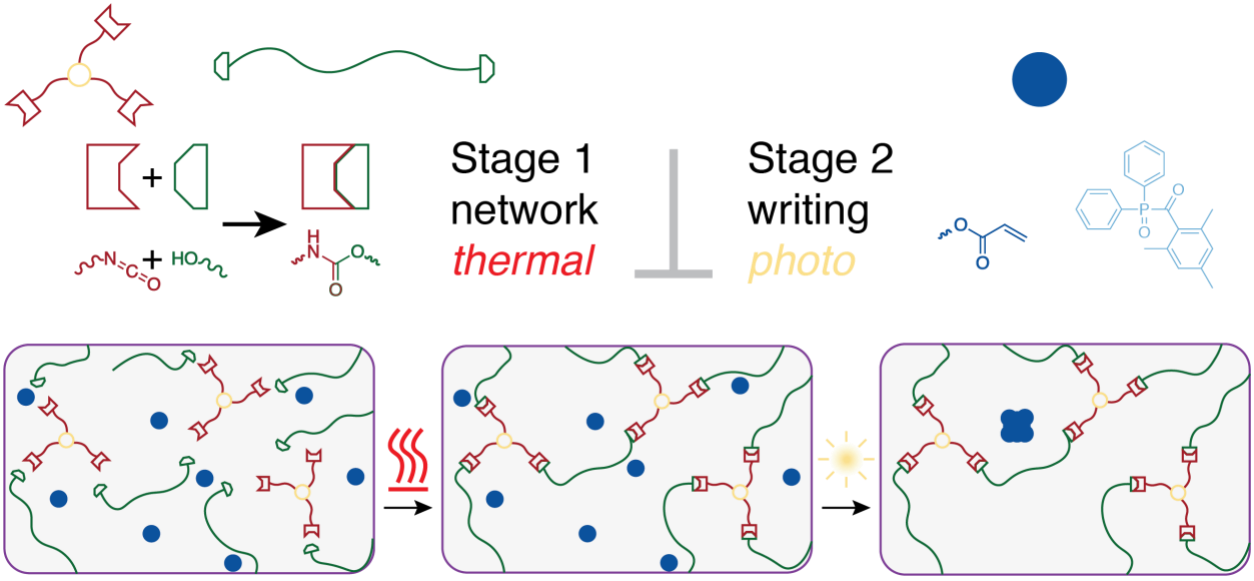

Scheme 0-5. Schematic illustration of a candidate two-stage system for holographic photopolymers. A stage 1 network is formed by thermally curing multifunctional alcohol and isocyanate monomers to form a loosely crosslinked, sub-ambient glass transition temperature network with good optical transparency and no color. Dissolved within this matrix framework, is the writing chemistry comprising the high refractive index acrylate writing monomer and a Type I photoinitiator such as TPO. A photosensitive film irradiated with a spatially modulated pattern results in a corresponding recording of the refractive index structure.

As shown in Scheme 0-5, a prototypical two-stage system for holographic photopolymers entails a thermally cured polyurethane matrix for the stage 1 network, (formed by the reaction of multifunctional alcohols and isocyanates) and high refractive

index acrylates as the writing monomer(s) with photoinitiator comprising the stage 2 writing chemistry. These set of reactions provide excellent orthogonality and modularity with the best overall combination of recording performance and stability[84]. In terms of two-stage formulation design, there is a broad range of commercially available multifunctional alcohol and isocyanate monomers to form low refractive index ($n < 1.5$), loosely crosslinked, low T_g networks. Similarly, the same set of photoinitiators used in other photopolymer applications are generally applicable (with some consideration of spectral absorption, photobleaching and overall efficiency). However, in the case of high refractive index acrylate monomers, which is the primary driver for refractive index contrast, there are limited available options. Furthermore, judicious selection of each component is required to ensure mutual compatibility to avoid noticeable phase separation.

1.3 Holography

Holography, invented in 1948 by Denis Gabor,[85] is the sub-field of optics based on using interference of coherent beams to record the entire information of the wavefront (i.e. phase and amplitude).[86] Unique to holography, upon appropriate conditions, the amplitude and phase of the recorded wavefront can be reconstructed completely using a single beam making it distinct to any other form of optical recording such as photography. Holography has been used in a variety of fields including data storage, displays, art, security, sensors and HOEs. Specifically, HOEs are central to this thesis as they combine holography and photopolymers to fabricate high quality, complex and custom optics not otherwise possible through conventional means.

Hologram performance is typically characterized by its diffraction efficiency, η, defined as the ratio of the powers of the reconstructed (diffracted) beam to that of the incident reference (readout) beam.

$$\eta = \frac{P_{diffracted}}{P_{incident}} \quad (5)$$

There are several types and classifications of holograms and depending on the type of hologram, they can exhibit different properties or limits in theoretical diffraction efficiencies (up to 100%).

1.3.1 Classifications of holograms

Three distinctions are used to classify holograms. The first classification is whether the modulation is in amplitude or phase. The second classification is based on the finite thickness of the hologram in comparison to the spacing of the recorded interference pattern. Lastly, holograms are classified based on the recording geometry used, with implications on their specific diffractive properties.

1.3.1.1 Amplitude vs phase modulation holograms

Amplitude modulation holograms entail a variation in absorption and typically do not produce bright images (because of light lost due to absorption). In contrast, a phase modulation hologram involves a change in the refractive index or thickness of the material proportional to the holographic interference intensity pattern.

1.3.1.2 Thin and thick holograms

A hologram can be either thin or thick and is commonly considered in terms of the relative length scales of the holographic material thickness and the pitch spacing of the interference fringes.[87] With thin holograms (also known as a surface hologram) the

thickness of the recording medium is close or less than the fringe spacing and thus operates in the Raman-Nath regime whereby multiple diffracted waves are produced. However, with thick holograms the recorded structure occupies the entire volume and characteristically exhibits Bragg selectivity. This means the hologram produces a single fundamental diffracted order only within a specific range of angles and wavelengths. The difference in whether a given hologram is thin or thick has been typically determined by the Klein-Cook *Q* parameter[88] although the more appropriate parameter would be to use the ρ parameter,[89] defined as

$$\rho = \frac{\lambda_0^2}{\Lambda^2 n_0 \Delta n} \quad (6)$$

where λ_0 is the vacuum wavelength of light, Λ is the grating spacing, n_0 is the mean refractive index, and Δn is the modulation of the refractive index. A hologram with a $\rho \leq 1$ operates in the Raman-Nath regime and hence holograms with $\rho \gg 1$ operate in the Bragg regime.[89] A key takeaway point from Equation 6 is that a thin material can still be considered a volume hologram (i.e. thick hologram).

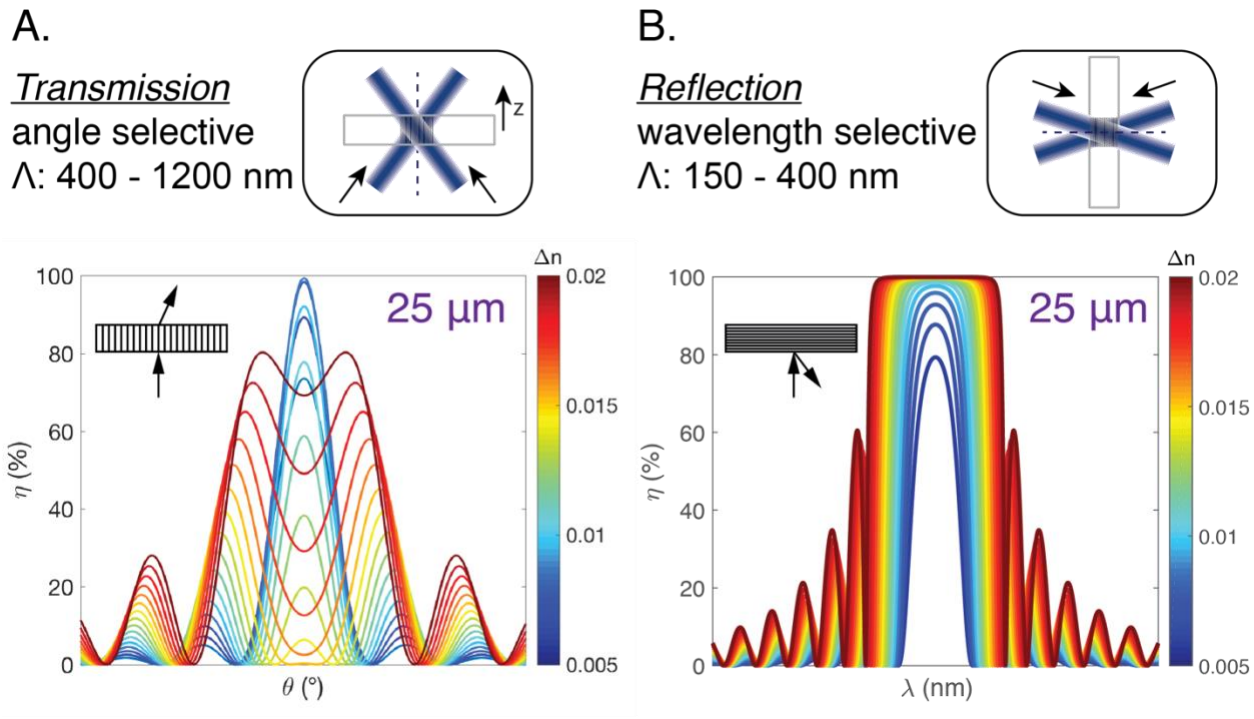

Scheme 0-6. Overview of volume holograms. A) Transmission holograms are recorded using recording beams incident on the same side to the material and thus the diffracted beam is transmitted. Transmission holograms are generally selective in angle and can overmodulate (go 'beyond' 100% diffraction efficiency) as either thickness or Δn increases. B) Reflection holograms are recorded when incident exposure beams interfere from opposing sides of the material. Reflection holograms are relatively selective in wavelength and produce a diffracted beam in reflection upon readout.

1.3.1.3 Transmission vs reflection holography

The simplest hologram is one recorded by the interference of two plane waves which generate a standing sinusoidal intensity pattern. The recording pitch, Λ, of this hologram is given by the equation,

$$\Lambda = \frac{\lambda}{2sin\theta} \tag{7}$$

where λ is the recording wavelength in the medium of refractive index n and θ is the half-angle between the two recording beams in the material. Depending on how the recording beams interfere with respect to the media, we can classify holograms as being either transmission or reflection. As shown in Scheme 0-6, transmission

holograms are recorded by beams interfering from the same side of the media while reflection holograms are generated with the recording beams incident on opposite sides of the material. This key difference leads to different properties and characteristics summarized in Scheme 0-6 such as the overmodulation of transmission holograms (diffraction efficiency going to a 100% and then below with a deviation from the classical $sinc^2$ profile) as thickness or Δn increases beyond a critical point.

In this thesis, we exclusively focus on phase modulated, volume holograms of both reflection and transmission type that can theoretically achieve up to a 100% in diffraction efficiency. These recorded holograms have some acceptance range in angle and wavelength (i.e. angular and spectral selectivity) that scales inversely with thickness of the material. Therefore, by increasing the thickness of a material to say 500 μm, it is possible to record multiple weak overlapping holograms (known as multiplexing) with minimal crosstalk upon readout.

Coupled wave theory is used to analyze volume holograms.[90, 91] Experimentally, the diffraction efficiencies of recorded volume holograms are typically measured as a function of angle or wavelength to produce characteristic $sinc^2$-like angular or spectral selectivity profiles respectively. These diffraction efficiency profiles are fit to Kogelnik coupled wave theory[90] to obtain numerical evaluations of the refractive index modulation (Δn) and the thickness of the recorded grating.

1.3.2 Requirements for holography

The first governing requirement for the successful recording of a hologram is the stability of the interference pattern generated from multiple beams. Thus, monochromatic light sources with high spatial and temporal coherence are essential

precluding most light sources such as white light, mercury lamps and LEDs.[86, 92] Only a small subset of lasers (i.e. narrow linewidth) are practically suitable for holography as the coherence length of the laser needs to be larger than the path length difference between each beam. This roughly translates to requiring a coherence length greater than 1 m (ideally) which corresponds to a linewidth of < 100 MHz. In addition to selecting an appropriate laser one must also maximize the mechanical and thermal stability of the entire optical system to produce consistent, low-noise holograms. Despite taking these precautions, imperfections on the materials also lead to undesirable nonlinearity effects like reduced fringe contrast, spurious noise gratings, scatter, shrinkage and laser speckle.[86] Therefore, it is important to note that experimentally, imperfect diffraction efficiency angular or spectral scans are rather common and can be due to the optics and/or the material.

1.3.3 Photopolymers as holographic recording materials

In this section the brief history and evolution of high refractive index modulation ($\Delta n \geq 0.01$) photopolymers as holographic recording materials will be examined with more comprehensive reviews available elsewhere.[93, 94] Holographic photopolymers, first reported in 1969 by Close *et al.*,[95] are arguably the candidate recording materials for realizing the technological promise of holography for its collective benefit of high refractive index modulation, photosensitivity, self-processing nature, tunability and cost. Despite a multitude of photopolymer-based materials having been reported, they generally comprise two components that differ in refractive index: 1) writing chemistry, and 2) binder/matrix.[96] A key process occurring in the majority of these materials is the photoinduced mass transport of the mobile writing chemistry species within the

relatively immobile binder/matrix upon selective irradiation/photopolymerization. Early high Δn materials developed and commercialized by DuPont were distinct in their use of thermoplastic polymers such as polyvinyl alcohol (PVA) or cellulose acetate butyrate (CAB) as the inert 'binder' with acrylates as the writing monomers. However, these non-crosslinked-based materials generally suffered from stability issues as well as high sensitivities to humidity and temperature. The next major conceptual development in materials design came from Bell Labs with the replacement of the thermoplastic binder with a crosslinked matrix.[97] In particular, the matrix chemistry, initially an epoxy-amine system, was designed to be orthogonal in its reaction to the free radical polymerization-based writing chemistry. This allowed for the efficient materials design of photosensitive dimensionally stable films cast between optically flat substrates displaying a good balance in the multiple properties of interest. From an academic standpoint, the design scheme enabled the discretization of the multiple components with a majority of the research focus based on the writing chemistry side including the incorporation of thiol chain transfer agents,[98] high refractive index organic[99] and inorganic[100-102] nanoparticles, the development of low shrinkage novel cyclic allyl sulfide ring opening monomers[103] and the use of thiol-X monomers.[81, 82, 101, 104] Following this orthogonal two-stage platform, recent material developments have been mostly dominated by the industrial space. Covestro AG launched a product line called Bayfol HX, based on roll-to-roll processing, of panchromatic sensitive recording materials up to 20 μm thick capable of Δn between 0.02 and 0.05 depending on the recording geometry and pitch. Similarly, Akonia Holographics hold patents on the introduction of dynamic range enhancing dopants (DREDs), essentially compounds with functional groups that

immobilize to the matrix in addition to functional groups that act as free radical traps for growing polymer chains. In these commercial materials, formulations of additive(s), photoinitiator(s), writing monomer(s) and matrix chemistries are highly optimized for recording performance.

1.4 Additive manufacturing

Additive manufacturing, commonly referred to as 3D printing, is a technology involving the computer-controlled production of three-dimensional objects from computer-aided design (CAD) models, typically using a point-by-point or layer-by-layer approach.[105, 106] On the industrial level 3D printing enables the capability for rapid prototyping on designs, especially ones that involve complex assembly steps, avoiding material waste and incurring substantial costs for low-volume production.[19] For consumers, 3D printing provides the opportunity for high degrees of customization and personalization in many product areas that can translate to better overall fit and performance. In general, 3D printing also opens up new unforeseen possibilities for object production not possible through conventional means. Light-based 3D printing, or vat photopolymerization,[18, 19, 21, 107] is arguably the most rapidly developing and disruptive of the 3D printing technologies for its collective advantages of speed, resolution, convenience and versatility.[21] The majority of vat photopolymerizations are based on stereolithography (SLA)[108] which can be further sub-divided based on the optics employed. In digital light processing (DLP),[109] an incoherent light source (typically an LED) is paired with a digital micromirror device (DMD) to project an entire patterned layer at once to print layer-by-layer. In laser-based SLA a scanning laser exposes the two-dimensional pattern of a given layer on a point-by-point basis.[18, 19, 21]

While significant technological breakthroughs and advancements have developed over the printing technology aspect itself,[17, 20, 110, 111] the available choices in photopolymer materials are relatively restricted.[19, 21] This is essentially because 3D printing resins require photopolymerizable resins capable of fast reaction rates and the ability to pattern at reasonably high resolutions (several microns). The photopolymer also needs to be mechanically robust during and after the printing for the printed object to be functional. For these reasons, photopolymers for 3D printing are almost exclusively (meth)acrylate-based systems. Amongst this class of monomers, there are also inherent resin viscosity constraints as SLA printers commonly involve a build head that gets continuously lifted vertically away from the vat after each layer exposure to allow for resin reflow. This effectively limits the range of obtainable material properties attainable with (meth)acrylates. Currently, the most viable materials approach to go beyond the restricted material properties space of (meth)acrylates has been to employ a two-stage system[107] involving the design of (meth)acrylate oligomers containing hindered urea bonds that are capable of reverting at elevated temperatures. However, fundamental constraints persist in being restricted to only (meth)acrylate-based polymers. In light of this, the later chapters of this thesis explores a unique sub-class of thiol-ene monomers that enable a novel suite of properties in 3D printing photopolymers.

1.5 Research overview

This thesis is split into two parts. The first part, Chapters 3-7, cover materials development toward designing high performance two-stage holographic photopolymers. The second part encompasses materials development for vat photopolymerization

additive manufacturing. Chapter 3 details the design and synthesis of efficient high refractive index acrylate writing monomers with enhanced solubilities in two-stage photopolymers. Chapter 4 describes using developed high Δn holographic materials for the design and fabrication of soft, flexible gradient refractive index (GRIN) lenses. Chapter 5 expands on using the thiol-ene reaction as high refractive index writing chemistry detailing a scalable and modular synthetic strategy towards suitable monomers. Chapter 6 investigates how stage 1 networks can be modified to be an active participant in the recording process. The second part of this thesis (Chapters 7 & 8) encompasses novel, enabling photopolymerizable thermoplastics for 3D printing. Chapter 7 investigates the concept of photopolymerizable thermoplastics and their detailed characterization. Finally, Chapter 8 examines the viability of applying photopolymerizable thermoplastics towards additive manufacturing.

References

1. Odian, G. G., Principles of polymerization. **2004**.

2. Young, R. J.; Lovell, P. A., Introduction to polymers. **2011**.

3. Flory, P. J., Molecular Size Distribution in Three Dimensional Polymers. I. Gelation1. *J. Am. Chem. Soc.* **1941,** *63* (11), 3083-3090.

4. Mandelkern, L., *Crystallization of polymers*. Cambridge Univ Press: [Place of publication not identified], 2010.

5. Nogales, A.; Hsiao, B. S.; Somani, R. H.; Srinivas, S.; Tsou, A. H.; Balta-Calleja, F. J.; Ezquerra, T. A., Shear-induced crystallization of isotactic polypropylene with different molecular weight distributions: in situ small-and wide-angle X-ray scattering studies. *Polymer* **2001,** *42* (12), 5247-5256.

6. Sarasua, J.-R.; Rodríguez, N. L.; Arraiza, A. L.; Meaurio, E., Stereoselective Crystallization and Specific Interactions in Polylactides. *Macromolecules* **2005,** *38* (20), 8362-8371.

7. Flory, P. J., Constitution of Three-dimensional Polymers and the Theory of Gelation. *The Journal of Physical Chemistry* **1942,** *46* (1), 132-140.

8. Decker, C., Light-induced crosslinking polymerization. *Polymer International* **2002,** *51* (11), 1141-1150.

9. Allen, N. S., Photoinitiators for UV and visible curing of coatings: Mechanisms and properties. *Journal of Photochemistry and Photobiology A: Chemistry* **1996,** *100* (1-3), 101-107.

10. Fouassier, J. P.; LalevÈe, J., Photoinitiators for Polymer Synthesis : Scope, Reactivity, and Efficiency. **2013**.

11. Eibel, A.; Fast, D. E.; Gescheidt, G., Choosing the ideal photoinitiator for free radical photopolymerizations: predictions based on simulations using established data. *Polymer Chemistry* **2018,** *9* (41), 5107-5115.

12. Decker, C.; Jenkins, A. D., Kinetic approach of oxygen inhibition in ultraviolet- and laser-induced polymerizations. *Macromolecules* **1985,** *18* (6), 1241-1244.

13. Chatani, S.; Kloxin, C. J.; Bowman, C. N., The power of light in polymer science: photochemical processes to manipulate polymer formation, structure, and properties. *Polymer Chemistry* **2014,** *5* (7), 2187-2201.

14. Park, H. Y.; Kloxin, C. J.; Scott, T. F.; Bowman, C. N., Covalent adaptable networks as dental restorative resins: Stress relaxation by addition–fragmentation chain transfer in allyl sulfide-containing resins. *Dent. Mater.* **2010,** *26* (10), 1010-1016.

15. Park, H. Y.; Kloxin, C. J.; Abuelyaman, A. S.; Oxman, J. D.; Bowman, C. N., Novel dental restorative materials having low polymerization shrinkage stress via stress relaxation by addition-fragmentation chain transfer. *Dent. Mater.* **2012,** *28* (11), 3-9.

16. Podgorski, M.; Becka, E.; Claudino, M.; Flores, A.; Shah, P. K.; Stansbury, J. W.; Bowman, C. N., Ester-free thiol-ene dental restoratives-Part A: Resin development. *Dent. Mater.* **2015,** *31* (11), 1255-1262.

17. Tumbleston, J. R.; Shirvanyants, D.; Ermoshkin, N.; Janusziewicz, R.; Johnson, A. R.; Kelly, D.; Chen, K.; Pinschmidt, R.; Rolland, J. P.; Ermoshkin, A.; Samulski, E. T.; DeSimone, J. M., Continuous liquid interface production of 3D objects. **2015,** *347* (6228), 1349-1352.

18. Stansbury, J. W.; Idacavage, M. J., 3D printing with polymers: Challenges among expanding options and opportunities. *Dent. Mater.* **2016,** *32* (1), 54-64.

19. Ligon, S. C.; Liska, R.; Stampfl, J.; Gurr, M.; Mulhaupt, R., Polymers for 3D Printing and Customized Additive Manufacturing. *Chem. Rev.* **2017,** *117* (15), 10212-10290.

20. Shusteff, M.; Browar, A. E. M.; Kelly, B. E.; Henriksson, J.; Weisgraber, T. H.; Panas, R. M.; Fang, N. X.; Spadaccini, C. M., One-step volumetric additive manufacturing of complex polymer structures. *Sci. Adv.* **2017,** *3* (12), eaao5496.

21. Layani, M.; Wang, X. F.; Magdassi, S., Novel Materials for 3D Printing by Photopolymerization. *Adv. Mater.* **2018,** *30* (41), 7.

22. Stockmayer, W. H., Theory of Molecular Size Distribution and Gel Formation in Branched Polymers II. General Cross Linking. **1944,** *12* (4), 125-131.

23. Hawker, C. J.; Wooley, K. L., The Convergence of Synthetic Organic and Polymer Chemistries. *Science* **2005,** *309* (5738), 1200-1205.

24. Kolb, H. C.; Finn, M. G.; Sharpless, K. B., Click Chemistry: Diverse Chemical Function from a Few Good Reactions. *Angew. Chem.-Int. Edit.* **2001,** *40* (11), 2004-2021.

25. Hoyle, C. E.; Bowman, C. N., Thiol–Ene Click Chemistry. *Angew. Chem.-Int. Edit.* **2010,** *49* (9), 1540-1573.

26. Lowe, A. B.; Bowman, C. N., *Thiol-X chemistries in polymer and materials science*. RSC Publishing: Cambridge, 2013; p xvii, 317 pages.

27. Kade, M. J.; Burke, D. J.; Hawker, C. J., The power of thiol-ene chemistry. *J. Polym. Sci. A Polym. Chem.* **2010,** *48* (4), 743-750.

28. Lowe, A. B., Thiol-ene “click” reactions and recent applications in polymer and materials synthesis. *Polymer Chemistry* **2010,** *1* (1), 17-36.

29. Hoyle, C. E.; Lowe, A. B.; Bowman, C. N., Thiol-click chemistry: a multifaceted toolbox for small molecule and polymer synthesis. *Chem. Soc. Rev.* **2010,** *39* (4), 1355-1387.

30. Nair, D. P.; Podgorski, M.; Chatani, S.; Gong, T.; Xi, W. X.; Fenoli, C. R.; Bowman, C. N., The Thiol-Michael Addition Click Reaction: A Powerful and Widely Used Tool in Materials Chemistry. *Chem. Mat.* **2014,** *26* (1), 724-744.

31. Brändle, A.; Khan, A., Thiol–epoxy ‘click’ polymerization: efficient construction of reactive and functional polymers. *Polymer Chemistry* **2012,** *3* (12), 3224-3227.

32. Stuparu, M. C.; Khan, A., Thiol-epoxy “click” chemistry: Application in preparation and postpolymerization modification of polymers. *J. Polym. Sci. Part A: Polym. Chem.* **2016,** *54* (19), 3057-3070.

33. Fernández-Rodríguez, M. A.; Shen, Q.; Hartwig, J. F., A General and Long-Lived Catalyst for the Palladium-Catalyzed Coupling of Aryl Halides with Thiols. *J. Am. Chem. Soc.* **2006,** *128* (7), 2180-2181.

34. Lowe, A. B., Thiol–ene “click” reactions and recent applications in polymer and materials synthesis: a first update. *Polymer Chemistry* **2014,** *5* (17), 4820-4870.

35. Xi, W. X.; Scott, T. F.; Kloxin, C. J.; Bowman, C. N., Click Chemistry in Materials Science. *Adv. Funct. Mater.* **2014,** *24* (18), 2572-2590.

36. Ligon, S. C.; Husár, B.; Wutzel, H.; Holman, R.; Liska, R., Strategies to Reduce Oxygen Inhibition in Photoinduced Polymerization. *Chem. Rev.* **2014,** *114* (1), 557-589.

37. O'Brien, A. K.; Bowman, C. N., Impact of Oxygen on Photopolymerization Kinetics and Polymer Structure. *Macromolecules* **2006,** *39* (7), 2501-2506.

38. Goodner, M. D.; Bowman, C. N., Development of a comprehensive free radical photopolymerization model incorporating heat and mass transfer effects in thick films. *Chemical Engineering Science* **2002,** *57* (5), 887-900.

39. O'Brien, A. K.; Cramer, N. B.; Bowman, C. N., Oxygen inhibition in thiol–acrylate photopolymerizations. **2006,** *44* (6), 2007-2014.

40. Chatani, S.; Nair, D. P.; Bowman, C. N., Relative reactivity and selectivity of vinyl sulfones and acrylates towards the thiol-Michael addition reaction and polymerization. *Polymer Chemistry* **2013,** *4* (4), 1048-1055.

41. Chatani, S.; Sheridan, R. J.; Podgorski, M.; Nair, D. P.; Bowman, C. N., Temporal Control of Thiol-Click Chemistry. *Chem. Mat.* **2013,** *25* (19), 3897-3901.

42. Xi, W. X.; Krieger, M.; Kloxin, C. J.; Bowman, C. N., A new photoclick reaction strategy: photo-induced catalysis of the thiol-Michael addition via a caged primary amine. *Chem. Commun.* **2013,** *49* (40), 4504-4506.

43. Chan, J. W.; Hoyle, C. E.; Lowe, A. B.; Bowman, M., Nucleophile-Initiated Thiol-Michael Reactions: Effect of Organocatalyst, Thiol, and Ene. *Macromolecules* **2010,** *43* (15), 6381-6388.

44. Dislich, H., Plastics as Optical Materials. *Angew. Chem.-Int. Edit.* **1979,** *18* (1), 49-59.

45. Born, M.; Wolf, E.; Bhatia, A. B., *Principles of optics electromagnetic theory of propagation, interference and diffraction of light*. Cambridge Univ. Press: Cambridge, 2016.

46. Gharagheizi, F.; Ilani-Kashkouli, P.; Kamari, A.; Mohammadi, A. H.; Ramjugernath, D., Group Contribution Model for the Prediction of Refractive Indices of Organic Compounds. *Journal of Chemical & Engineering Data* **2014,** *59* (6), 1930-1943.

47. Liu, J.-g.; Ueda, M., High refractive index polymers: fundamental research and practical applications. *Journal of Materials Chemistry* **2009,** *19* (47), 8907-8919.

48. Higashihara, T.; Ueda, M., Recent Progress in High Refractive Index Polymers. *Macromolecules* **2015,** *48* (7), 1915-1929.

49. Chung, W. J.; Griebel, J. J.; Kim, E. T.; Yoon, H.; Simmonds, A. G.; Ji, H. J.; Dirlam, P. T.; Glass, R. S.; Wie, J. J.; Nguyen, N. A.; Guralnick, B. W.; Park, J.; Somogyi, Á.; Theato, P.; Mackay, M. E.; Sung, Y.-E.; Char, K.; Pyun, J., The use of elemental sulfur as an alternative feedstock for polymeric materials. *Nature Chemistry* **2013,** *5*, 518.

50. Griebel, J. J.; Namnabat, S.; Kim, E. T.; Himmelhuber, R.; Moronta, D. H.; Chung, W. J.; Simmonds, A. G.; Kim, K.-J.; van der Laan, J.; Nguyen, N. A.; Dereniak, E. L.; Mackay, M. E.; Char, K.; Glass, R. S.; Norwood, R. A.; Pyun, J., New Infrared Transmitting Material via Inverse Vulcanization of Elemental Sulfur to Prepare High Refractive Index Polymers. *Adv. Mater.* **2014,** *26* (19), 3014-3018.

51. Lim, J.; Pyun, J.; Char, K., Recent Approaches for the Direct Use of Elemental Sulfur in the Synthesis and Processing of Advanced Materials. *Angew. Chem.-Int. Edit.* **2015,** *54* (11), 3249-3258.

52. Kloxin, C. J.; Scott, T. F.; Adzima, B. J.; Bowman, C. N., Covalent Adaptable Networks (CANs): A Unique Paradigm in Cross-Linked Polymers. *Macromolecules* **2010,** *43* (6), 2643-2653.

53. Bowman, C. N.; Kloxin, C. J., Covalent Adaptable Networks: Reversible Bond Structures Incorporated in Polymer Networks. *Angew. Chem.-Int. Edit.* **2012,** *51* (18), 4272-4274.

54. Kloxin, C. J.; Bowman, C. N., Covalent adaptable networks: smart, reconfigurable and responsive network systems. *Chem. Soc. Rev.* **2013,** *42* (17), 7161-7173.

55. Chen, X.; Dam, M. A.; Ono, K.; Mal, A.; Shen, H.; Nutt, S. R.; Sheran, K.; Wudl, F., A Thermally Re-mendable Cross-Linked Polymeric Material. **2002,** *295* (5560), 1698-1702.

56. Cromwell, O. R.; Chung, J.; Guan, Z., Malleable and Self-Healing Covalent Polymer Networks through Tunable Dynamic Boronic Ester Bonds. *J. Am. Chem. Soc.* **2015,** *137* (20), 6492-6495.

57. Rowan, S. J.; Cantrill, S. J.; Cousins, G. R. L.; Sanders, J. K. M.; Stoddart, J. F., Dynamic Covalent Chemistry. **2002,** *41* (6), 898-952.

58. Sheridan, R. J.; Bowman, C. N., A Simple Relationship Relating Linear Viscoelastic Properties and Chemical Structure in a Model Diels-Alder Polymer Network. *Macromolecules* **2012,** *45* (18), 7634-7641.

59. Sheridan, R. J.; Bowman, C. N., Understanding the process of healing of thermoreversible covalent adaptable networks. *Polymer Chemistry* **2013,** *4* (18), 4974-4979.

60. Berg, G. J.; Gong, T.; Fenoli, C. R.; Bowman, C. N., A Dual-Cure, Solid-State Photoresist Combining a Thermoreversible Diels-Alder Network and a Chain Growth Acrylate Network. *Macromolecules* **2014,** *47* (10), 3473-3482.

61. Lyon, G. B.; Baranek, A.; Bowman, C. N., Scaffolded Thermally Remendable Hybrid Polymer Networks. *Adv. Funct. Mater.* **2016,** *26* (9), 1477-1485.

62. Tasdelen, M. A., Diels–Alder “click” reactions: recent applications in polymer and material science. *Polymer Chemistry* **2011,** *2* (10), 2133-2145.

63. Montarnal, D.; Capelot, M.; Tournilhac, F.; Leibler, L., Silica-Like Malleable Materials from Permanent Organic Networks. *Science* **2011,** *334* (6058), 965-968.

64. Denissen, W.; Winne, J. M.; Du Prez, F. E., Vitrimers: permanent organic networks with glass-like fluidity. *Chem. Sci.* **2016,** *7* (1), 30-38.

65. Demongeot, A.; Groote, R.; Goossens, H.; Hoeks, T.; Tournilhac, F.; Leibler, L., Cross-Linking of Poly(butylene terephthalate) by Reactive Extrusion Using Zn(II) Epoxy-Vitrimer Chemistry. *Macromolecules* **2017,** *50* (16), 6117-6127.

66. Rottger, M.; Domenech, T.; van der Weegen, R.; Nicolay, A. B. R.; Leibler, L., High-performance vitrimers from commodity thermoplastics through dioxaborolane metathesis. *Science* **2017,** *356* (6333), 62-65.

67. Zou, W. K.; Dong, J. T.; Luo, Y. W.; Zhao, Q.; Xie, T., Dynamic Covalent Polymer Networks: from Old Chemistry to Modern Day Innovations. *Adv. Mater.* **2017,** *29* (14), 18.

68. Bowman, C. N.; Kloxin, C. J. J. A. C. I. E., Covalent adaptable networks: reversible bond structures incorporated in polymer networks. **2012,** *51* (18), 4272-4274.

69. Scott, T. F.; Schneider, A. D.; Cook, W. D.; Bowman, C. N., Photoinduced plasticity in cross-linked polymers. *Science* **2005,** *308* (5728), 1615-1617.

70. Worrell, B. T.; McBride, M. K.; Lyon, G. B.; Cox, L. M.; Wang, C.; Mavila, S.; Lim, C. H.; Coley, H. M.; Musgrave, C. B.; Ding, Y. F.; Bowman, C. N., Bistable and photoswitchable states of matter. *Nat. Commun.* **2018,** *9*, 7.

71. Scott, T. F.; Draughon, R. B.; Bowman, C. N., Actuation in Crosslinked Polymers via Photoinduced Stress Relaxation. **2006,** *18* (16), 2128-2132.

72. Park, H. Y.; Kloxin, C. J.; Abuelyaman, A. S.; Oxman, J. D.; Bowman, C. N., Stress Relaxation via Addition-Fragmentation Chain Transfer in High T-g, High Conversion Methacrylate-Based Systems. *Macromolecules* **2012,** *45* (14), 5640-5646.

73. Park, H. Y.; Kloxin, C. J.; Fordney, M. F.; Bowman, C. N., Stress Reduction and T-g Enhancement in Ternary Thiol-Yne-Methacrylate Systems via Addition-Fragmentation Chain Transfer. *Macromolecules* **2012,** *45* (14), 5647-5652.

74. Kloxin, C. J.; Scott, T. F.; Park, H. Y.; Bowman, C. N., Mechanophotopatterning on a Photoresponsive Elastomer. *Adv. Mater.* **2011,** *23* (17), 1977-1981.

75. Cox, L. M.; Li, Z.; Sowan, N.; Nair, D.; Xiao, J.; Bowman, C. N.; Ding, Y., Reconfigurable surface patterns on covalent adaptive network polymers using nanoimprint lithography. *Polymer* **2014,** *55* (23), 5933-5937.

76. McBride, M. K.; Hendrikx, M.; Liu, D. Q.; Worrell, B. T.; Broer, D. J.; Bowman, C. N., Photoinduced Plasticity in Cross-Linked Liquid Crystalline Networks. *Adv. Mater.* **2017,** *29* (17), 6.

77. Wang, C.; Mavila, S.; Worrell, B. T.; Xi, W. X.; Goldman, T. M.; Bowman, C. N., Productive Exchange of Thiols and Thioesters to Form Dynamic Polythioester-Based Polymers. *ACS Macro Lett.* **2018,** *7* (11), 1312-1316.

78. Wang, C.; Goldman, T. M.; Worrell, B. T.; McBride, M. K.; Alim, M. D.; Bowman, C. N., Recyclable and repolymerizable thiol-X photopolymers. *Mater. Horizons* **2018,** *5* (6), 1042-1046.

79. Worrell, B. T.; Mavila, S.; Wang, C.; Kontour, T. M.; Lim, C. H.; McBride, M. K.; Musgrave, C. B.; Shoemaker, R.; Bowman, C. N., A user's guide to the thiol-thioester exchange in organic media: scope, limitations, and applications in material science. *Polymer Chemistry* **2018,** *9* (36), 4523-4534.

80. Nair, D. P.; Cramer, N. B.; Gaipa, J. C.; McBride, M. K.; Matherly, E. M.; McLeod, R. R.; Shandas, R.; Bowman, C. N., Two-Stage Reactive Polymer Network Forming Systems. *Adv. Funct. Mater.* **2012,** *22* (7), 1502-1510.

81. Peng, H. Y.; Wang, C.; Xi, W. X.; Kowalski, B. A.; Gong, T.; Xie, X. L.; Wang, W. T.; Nair, D. P.; McLeod, R. R.; Bowman, C. N., Facile Image Patterning via Sequential Thiol-Michael/Thiol-Yne Click Reactions. *Chem. Mat.* **2014,** *26* (23), 6819-6826.

82. Peng, H. Y.; Nair, D. P.; Kowalski, B. A.; Xi, W. X.; Gong, T.; Wang, C.; Cole, M.; Cramer, N. B.; Xie, X. L.; McLeod, R. R.; Bowman, C. N., High Performance Graded Rainbow Holograms via Two-Stage Sequential Orthogonal Thiol-Click Chemistry. *Macromolecules* **2014,** *47* (7), 2306-2315.

83. Iha, R. K.; Wooley, K. L.; Nyström, A. M.; Burke, D. J.; Kade, M. J.; Hawker, C. J., Applications of Orthogonal “Click” Chemistries in the Synthesis of Functional Soft Materials. *Chem. Rev.* **2009,** *109* (11), 5620-5686.

84. Bruder, F.-K.; Hagen, R.; Rölle, T.; Weiser, M.-S.; Fäcke, T., From the Surface to Volume: Concepts for the Next Generation of Optical–Holographic Data-Storage Materials. *Angew. Chem.-Int. Edit.* **2011,** *50* (20), 4552-4573.

85. Gabor, D., A New Microscopic Principle. *Nature* **1948,** *161*, 777.

86. Toal, V., Introduction to holography. **2012**.

87. Gaylord, T. K.; Moharam, M. G., Thin and thick gratings: terminology clarification. *Appl. Opt.* **1981,** *20* (19), 3271-3273.

88. Klein, W. R.; Cook, B. D., Unified Approach to Ultrasonic Light Diffraction. *IEEE Transactions on Sonics and Ultrasonics* **1967,** *14* (3), 123-134.

89. Moharam, M. G.; Young, L., Criterion for Bragg and Raman-Nath diffraction regimes. *Appl. Opt.* **1978,** *17* (11), 1757-1759.

90. Kogelnik, H., Coupled wave theory for thick hologram gratings. *The Bell System Technical Journal* **1969,** *48* (9), 2909-2947.

91. Moharam, M. G.; Gaylord, T. K., Rigorous coupled-wave analysis of planar-grating diffraction. *J. Opt. Soc. Am.* **1981,** *71* (7), 811-818.

92. Hariharan, P., *Basics of holography*. Cambridge University Press: Cambridge, 2002.

93. Kowalski, B. A.; McLeod, R. R., Design concepts for diffusive holographic photopolymers. *J. Polym. Sci. Part B: Polym. Phys.* **2016,** *54* (11), 1021-1035.

94. Guo, J.; Gleeson, M. R.; Sheridan, J. T., A Review of the Optimisation of Photopolymer Materials for Holographic Data Storage. *Physics Research International* **2012,** *2012*, 16.

95. Close, D. H.; Jacobson, A. D.; Margerum, J. D.; Brault, R. G.; McClung, F. J., HOLOGRAM RECORDING ON PHOTOPOLYMER MATERIALS. **1969,** *14* (5), 159-160.

96. Colburn, W. S.; Haines, K. A., Volume Hologram Formation in Photopolymer Materials. *Appl. Opt.* **1971,** *10* (7), 1636-1641.

97. Dhar, L.; Hale, A.; Katz, H. E.; Schilling, M. L.; Schnoes, M. G.; Schilling, F. C., Recording Media That Exhibit High Dynamic Range for Digital Holographic Data Storage. *Opt. Lett.* **1999,** *24*, 487.

98. Guo, J.; Fujii, R.; Ono, T.; Klepp, J.; Pruner, C.; Fally, M.; Tomita, Y., Effects of chain-transferring thiol functionalities on the performance of nanoparticle-polymer composite volume gratings. *Opt. Lett.* **2014,** *39* (23), 6743-6746.

99. Tomita, Y.; Urano, H.; Fukamizu, T.-a.; Kametani, Y.; Nishimura, N.; Odoi, K., Nanoparticle-polymer composite volume holographic gratings dispersed with ultrahigh-refractive-index hyperbranched polymer as organic nanoparticles. *Opt. Lett.* **2016,** *41* (6), 1281-1284.

100. Hata, E.; Tomita, Y., Order-of-magnitude polymerization-shrinkage suppression of volume gratings recorded in nanoparticle-polymer composites. *Opt. Lett.* **2010,** *35* (3), 396-398.

101. Mitsube, K.; Nishimura, Y.; Nagaya, K.; Takayama, S.; Tomita, Y., Holographic nanoparticle-polymer composites based on radical-mediated thiol-yne photopolymerizations: characterization and shift-multiplexed holographic digital data page storage. *Opt. Mater. Express* **2014,** *4* (5), 982-996.

102. Suzuki, N.; Tomita, Y.; Kojima, T., Holographic recording in TiO2 nanoparticle-dispersed methacrylate photopolymer films. **2002,** *81* (22), 4121-4123.

103. Choi, K.; Chon, J. W. M.; Gu, M.; Malic, N.; Evans, R. A., Low-Distortion Holographic Data Storage Media Using Free-Radical Ring-Opening Polymerization. *Adv. Funct. Mater.* **2009,** *19* (22), 3560-3566.

104. Hata, E.; Mitsube, K.; Momose, K.; Tomita, Y., Holographic nanoparticle-polymer composites based on step-growth thiol-ene photopolymerization. *Opt. Mater. Express* **2011,** *1* (2), 207-222.

105. Gibson, I.; Rosen, D. W.; Stucker, B., *Additive Manufacturing Technologies: Rapid Prototyping to Direct Digital Manufacturing*. Springer-Verlag Berlin: Berlin, 2010; p 1-459.

106. Huang, S. H.; Liu, P.; Mokasdar, A.; Hou, L., Additive manufacturing and its societal impact: a literature review. *Int. J. Adv. Manuf. Technol.* **2013,** *67* (5-8), 1191-1203.

107. Poelma, J.; Rolland, J., Rethinking digital manufacturing with polymers. *Science* **2017,** *358* (6369), 1384-1385.

108. Melchels, F. P. W.; Feijen, J.; Grijpma, D. W., A review on stereolithography and its applications in biomedical engineering. *Biomaterials* **2010,** *31* (24), 6121-6130.

109. Lee, M. P.; Cooper, G. J. T.; Hinkley, T.; Gibson, G. M.; Padgett, M. J.; Cronin, L., Development of a 3D printer using scanning projection stereolithography. *Scientific Reports* **2015,** *5*, 9875.

110. de Beer, M. P.; van der Laan, H. L.; Cole, M. A.; Whelan, R. J.; Burns, M. A.; Scott, T. F., Rapid, continuous additive manufacturing by volumetric polymerization inhibition patterning. *Sci. Adv.* **2019,** *5* (1), eaau8723.

111. Kelly, B. E.; Bhattacharya, I.; Heidari, H.; Shusteff, M.; Spadaccini, C. M.; Taylor, H. K., Volumetric additive manufacturing via tomographic reconstruction. *Science* **2019**, eaau7114.

Objectives

This thesis encompasses the rational design of novel photopolymerizable chemistries and their implementations to achieve benchmark standards for both two-stage holographic photopolymers and photopolymerizable thermoplastics. The central hypothesis is that thiol-X ‘click’ reactions can realize enabling material properties and performance in photopolymer systems for holography and additive manufacturing. To test this hypothesis, the following aims were devised:

Specific Aim 1: Design and synthesize photopolymerizable monomer(s) suitable as writing monomers in two-stage systems targeting both refractive index and solubility in the first stage network.

Specific Aim 2: Implementation of improved writing monomer(s) in two-stage systems and characterization of achievable Δn via bulk refractive index measurements and transmission holography.

Specific Aim 3: Implement network adaptability to enable relaxation of stresses induced by photopolymerization recording. Internal stresses built up due to polymerization result in birefringence and deleterious optical performance. The ability to relax stresses generated from photopolymerization would enhance performance of recorded optical elements.

Specific Aim 4: Enable the photopolymerization of mechanically robust linear polymers for 3D printing.

In specific aim 1, a general synthetic route to photopolymerizable monomers was developed using thiol-X chemistries to obtain a broad range of liquids with high refractive index values exhibiting typically fast reaction kinetics and quantitative conversions. Importantly, synthesized writing monomers demonstrate good solubility in stage 1 polyurethane networks. Effective solubility limits can restrict the available writing

chemistry available for generating a refractive index contrast. Improving writing monomer solubility in a given matrix also serves to minimize the possibilities of encountering optical deficiencies such as reduced transparency or increased scatter (haze) due to phase separation.

In specific aim 2, the outcomes of specific aim 1 was utilized by implementing developed writing monomers into a candidate polyurethane matrix. At elevated writing monomer loadings high quality holographic two-stage photopolymers capable of peak-to-mean Δn up to 0.03 in 1 μm transmission gratings were achieved. High performance formulations were also used for the recording of various diffractive optical elements.

In specific aim 3, network modifications are considered to enable stress relaxation and/or promote participation of the network during stage 2 recording. This was primarily achieved by incorporating specific dynamic covalent chemistries (i.e. allyl sulfide) to enable dynamic bond exchange with the primary goal of inducing plasticity to an otherwise static network.

In specific aim 4, a system of bifunctional thiol-ene monomers were studied for the rapid photopolymerization of linear polymers with robust mechanical properties not seen in typical linear photopolymers. Specific systems also exhibited varying degrees of crystallinity with interesting rheological and mechanical properties. A candidate system was employed for the vat photopolymerization 3D printing of thermoplastic objects that can subsequently be melted and reprocessed.

Summary of Work

This work advanced the field of photopolymerizations for both optical/holography and 3D printing applications in multiple ways. First, the approaches developed for new photopolymerizable high refractive index monomers significantly expanded upon the limited set of writing monomers capable of achieving high refractive index (n_D/20°C >

1.6) bulk materials as well as achieving high Δn values (> 0.02) in two-stage photopolymers. Next, the investigation of using dynamic covalent chemistries in the stage 1 network represents an entirely new approach for overcoming key intrinsic constraints faced in two-stage holographic photopolymers. Finally, the ability to rapidly photopolymerize mechanically robust linear polymers shatters a major preconception over the formation of linear polymers using light. Overall, the material properties and performance presented in the subsequent chapters are at the high end if not the state of the art.

High Dynamic Range (Δn) Two-Stage Photopolymers via Enhanced Solubility of a High Refractive Index Acrylate Writing Monomer

Manuscript published under the same title in ACS Applied Materials & Interfaces, 2018, 10, 1, 1217-1224

Holographic photopolymers capable of high refractive index modulation (Δn) on the order of 10^{-2} are integral for the fabrication of functional holographic optical elements that are useful in a myriad of optical applications. In particular, to address the deficiency of suitable high refractive index writing monomers for use in two-stage holographic formulations, here we report a novel high refractive index writing monomer, 1,3-bis(phenylthio)-2-propyl acrylate (BPTPA), simultaneously possessing enhanced solubility in a low refractive index (n = 1.47) urethane matrix. Examined in comparison to a widely used high refractive index monomer, 2,4,6-tribromophenyl acrylate (TBPA), BPTPA exhibited superior solubility in a stage 1 urethane matrix of approximately 50% with a 20% higher refractive index increase per unit amount of writing monomer for stage 2 polymerizations. Formulations with 60 wt% loading of BPTPA exhibit a peak-to-mean holographic Δn ~ 0.029 without obvious deficiencies in transparency, color or scatter. To the best of our knowledge, this value is the highest reported in the peer-reviewed literature for a transmission hologram. The capabilities and versatility of BPTPA-based formulations are demonstrated at varying length scales via demonstrative refractive index gradient structure examples including direct laser write (DLW), projection mask lithography of a 1”-diameter Fresnel lens and ~100% diffraction

efficiency volume transmission holograms with a 1-μm fringe spacing in 11 μm thick samples.

1.6 Introduction

Two-stage photopolymers are an ideal framework for designing materials capable of accessing a wide range of material properties (mechanical, thermal, optical, electrical etc.) on demand using light.[1-3] A valuable implementation of the two stage paradigm is in designing recording materials (often referred to as holographic photopolymers)[4-13] for appropriate refractive index (phase) structures using various optical exposure techniques (such as photolithography,[14] direct laser write (DLW),[15] two-photon lithography[16] and holography)[4-13] to generate a refractive index contrast (Δn) between the bulk material and the recorded feature(s). In particular, the advent of augmented reality (AR) devices has spurred a rising interest to use photopolymers to fabricate holographic optical elements (HOEs) capable of complex, yet high quality, optical functions with thin, light and flexible form factors.[17]

The general scheme involves an initial thermal cure of a solid rubbery matrix (stage 1), typically of lower refractive index ($n < 1.5$). This matrix acts as a framework through which dissolved species (writing monomer and photoinitiator) freely diffuse and undergo photopolymerization during a subsequent patterned irradiation step. This patterned light exposure spatially controls the polymerization (stage 2) according to the light intensity profile, consuming the reactive monomer species in the exposed regions and inducing mass transport of additional monomer from the unexposed regions into the exposed regions to enhance the developing refractive index structure. The net outcome is a phase structure that ideally corresponds directly to the exposure pattern recorded in

a thin, transparent polymeric film. The primary development goal for practical application is to maximize the material's available dynamic range, i.e. the achievable Δn as this enables significant enhancement in diffraction efficiency for a given thickness and number of recordable multiplexed holograms.[18] A higher Δn also enables the manufacture of gradient refractive index lenses with greater focusing power as well as having the capacity to record waveguides with tighter bend radii. In terms of device performance, this translates to improved specifications such as wider field of views, higher information densities, lower power read-out sources, etc.

Within the scope of formulating two-stage holographic photopolymers, the recordable Δn is a function of the difference in refractive index of the writing polymer and the matrix ($n_{oolymer}$ - n_{matrix}) as well as the volume fraction of the initial writing monomer present in the material (Ø).[19] However, effective high refractive index substituents (such as heavy halogens or aromatics)[20-22] have high molar refractions and low molar volumes, which are drastically different in structure to substituents of lower refractive index.[21-23] Therefore, for a given matrix, there is typically a significant trade-off between increasing the refractive index of the writing monomer and its reduced solubility in the underlying matrix.

Recently, sequential and orthogonal two-stage thiol-X click chemistry systems achieving high solubility have been successfully demonstrated with simple processability;[7, 8] however these formulations exhibited a low overall Δn ($\leq 4.0 \times 10^{-3}$) primarily due to the low refractive index difference ($n_{polymer}$ - n_{matrix}) associated with the presence of thiols in the stage 1 reactions. Similar issues of limited achievable Δn are encountered with alternative photopolymer systems involving acrylamide writing

monomers[24, 25] which have refractive indices similar to the binder, poly(vinyl alcohol).[9] Other groups have explored holographic composites such as nanoparticle-based photopolymers or liquid crystal photopolymers whereby the nanoparticles or liquid crystals,[26-29] acting as nonreactive higher refractive index species, migrate to the dark regions upon holographic exposure.[10, 30, 31] Notably, Tomita *et al.* reported a peak-to-mean Δn of 0.022 using high refractive index hyperbranched organic nanoparticles[30] (hitherto, the highest reported for materials in the academic literature). However, the intrinsic drawbacks of limited nanoparticle solubility and the slow reaction kinetics (> 1 minute for Δn development despite high recording intensities of 100-200 mW/cm^2) persist. The synthesis of high refractive index nanoparticles is also relatively cumbersome and arguably not a viable approach for mass use as recording materials in the aforementioned applications. Recently, Covestro AG have commercialized a product line of holographic photopolymer materials, Bayfol® HX, capable of high Δn values of up to 0.035 for reflection holograms at approximately 220 nm. However, at higher pitch recordings there is a noticeable decrease in Δn with a reported value of less than 0.01 for a 1 μm grating.[32]

Here, a stage 1 urethane and stage 2 acrylate formulation, similar to existing commercial materials,[32, 33] were combined to yield superior orthogonality and Δn recording performance relative to most other two-stage formulation systems. Focusing on maximizing the solubility of the writing monomer in a urethane matrix without sacrificing refractive index contrast, a colorless, low viscosity, high refractive index (n_D = 1.6) liquid acrylate monomer, 1,3-bis-(phenylthio)-2-propyl acrylate (BPTPA), was designed and synthesized using a facile synthetic route involving only two relatively

simple steps. Solubility and refractive index experiments were performed to evaluate viability as a two-stage holographic writing monomer against a reference, widely used high refractive index monomer, 2,4,6-tribromophenyl acrylate (TBPA).[1, 19] Monomer swelling studies of a urethane matrix showed a solubility improvement of around 50% as compared to TBPA in addition to a moderately higher refractive index increase per unit concentration of writing monomer. Crucially, we demonstrate optically clear films containing twice the amount of writing monomer are possible with BPTPA (60 wt%) when compared to TBPA, making peak-to-mean $\Delta n \sim 0.029$ accessible without any discernable optical deficiencies. To the best of our knowledge, this is the highest Δn for any reported holographic photopolymer within the peer-reviewed, i.e. non-patent, literature. The capabilities and versatility of BPTPA formulations are demonstrated through functional examples of refractive index structures at varying length scales through direct laser write (DLW) of an intricate pattern, projection mask lithography of a Fresnel lens, and transmission holograms.

1.7 Experimental

1.7.1 Materials

Commercially available reagents were used without further purification. Thiophenol, epichlorohydrin and butylated hydroxytoluene (BHT) free

radical stabilizer were purchased from Alfa Aesar. 1,8-Diazabicyclo[5.4.0]undec-7-ene (DBU) was purchased from Chem-Impex International. 4-dimethylaminopyridine (DMAP) was purchased from Oakwood Chemical. Reagent-grade triethylamine (Et_3N) was purchased from Fisher Scientific. Acryloyl chloride and polycaprolactone-block-polytetrahydrofuran-block-polycaprolactone, (average M_n 2000) were purchased from Sigma Aldrich. The photoinitiator, diphenyl(2,4,6-trimethylbenzoyl)phosphine oxide (TPO), was purchased from TCI America. Desmodur N3900 polyisocyanate was donated by Covestro AG (formerly Bayer MaterialScience).

Monomer Synthesis

Synthesis of 1,3-bis-(phenylthio)-2-propanol (BPTP): To a 250 mL round-bottomed flask equipped with a magnetic stir bar, 16 mL of thiophenol (157 mmol, 2.2 equiv.) was stirred with 23 mL of DBU (154 mmol, 2.2 equiv.) in 230 mL of toluene (0.3 M, w.r.t epichlorohydrin) for 10 minutes. Following this, 5.5 mL of epichlorohydrin (70.3 mmol, 1.0 equiv.) was added dropwise. The reaction vessel was allowed to stir at room temperature for 16 hrs. After this period, the volatiles were removed under reduced pressure and the residue was then diluted with DCM and washed with 1 M HCl (100 mL), distilled water (100 mL) and brine (50 mL). The combined organic extracts were dried over anhydrous Na_2SO_4, filtered and concentrated under reduced pressure. The crude product was purified by silica-gel column chromatography using 20% EtOAc in hexane as eluent to yield 17.1 g of a colorless, low viscosity liquid. (88% yield)
^1H NMR (400 MHz, $CDCl_3$) δ 7.36 – 7.33 (m, 4H), 7.29 – 7.24 (m, 4H), 7.22 – 7.18 (m, 2H), 3.86-3.79 (m, 1H), 3.20 (dd, *J* = 13.8, 5.0 Hz, 2H), 3.05 (dd, *J* = 13.8, 7.2 Hz, 2H);
^{13}C NMR (101 MHz, $CDCl_3$, 25°C): δ 135.1, 129.9, 129.1, 126.7, 68.2, 40.1;

Synthesis of acrylate writing monomer, 1,3-bis-(phenylthio)-2-propyl acrylate (BPTPA): To a 250 mL round-bottomed flask equipped with a magnetic stir bar, 10 g of BPTP (36.2 mmol, 1.0 equiv.), 25.2 mL of Et_3N (180.9 mmol, 5 equiv.), 0.4 g of BHT (1.81 mmol, 0.05 equiv.) were diluted with 120 mL of DCM (0.3 M w.r.t BPTP) and stirred for 10 minutes under Argon. The clear solution was cooled to 0˚C and 4.4 mL of acryloyl chloride (54.3 mmol, 2.2 equiv.) was added dropwise to the flask under Ar atmosphere followed by 0.4 g of DMAP (3.6 mmol, 0.1 equiv.). The reaction mixture was allowed to stir at room temperature for 16 hr. After this period, the volatiles were removed under reduced pressure and the residue was diluted with DCM (250 mL) and washed with 1 M HCl (100 mL), distilled water (100 mL) and brine (50 mL). The combined organic extracts were dried over anhydrous Na_2SO_4, filtered and concentrated under reduced pressure. The crude product was purified by silica-gel column chromatography using 20% EtOAc in hexane as eluent to yield the title compound BPTPA as a colorless, low viscosity liquid. (84% yield)

^{1}H NMR (400 MHz, $CDCl_3$) δ 7.38 – 7.35 (m, 4H), 7.28 – 7.24 (m, 4H), 7.20 – 7.16 (m, 2H), 6.27 (dd, *J* = 17.3, 1.4 Hz, 1H), 5.94 (dd, *J* = 17.3, 10.5 Hz, 1H), 5.76 (dd, *J* = 10.5, 1.4 Hz, 1H), 5.18 (p, *J* = 5.9 Hz, 1H), 3.29 (dd, *J* = 5.9, 3.3 Hz, 4H);

^{13}C NMR (101 MHz, $CDCl_3$, 25˚C): δ 165.3, 135.2, 131.4, 129.9, 129.0, 127.9, 126.6, 72.0, 36.3;

1.7.2 Methods

Nuclear Magnetic Resonance (NMR)

NMR spectra were recorded on a Bruker Avance-III 400 NMR spectrometer at 25 °C in chloroform-*d*. All chemical shifts are reported in ppm relative to chloroform solvent peak (δ = 7.26 ppm).

Refractive index measurements

The refractive indices of liquid samples were measured using an Abbe refractometer at the sodium-d line (589.3 nm) at room temperature. The refractive index of polymeric films was measured using a Metricon 2010/M prism coupler at a wavelength of 633 nm under ambient conditions.

Writing monomer swelling in urethane matrix

Half-inch diameter discs were punched out of 250 μm urethane films and their dry weights (w_i) measured. They were then individually placed in 4 mL vials containing either – a) 20 wt% TBPA in solvent, b) 20 wt% BPTPA in solvent or c) 100% solvent. The relatively nonvolatile solvents chosen were hexane and heavy mineral oil. After 1 week, the surface of each disc was patted dry with weighing paper and their equilibrium weights (w_f) measured.

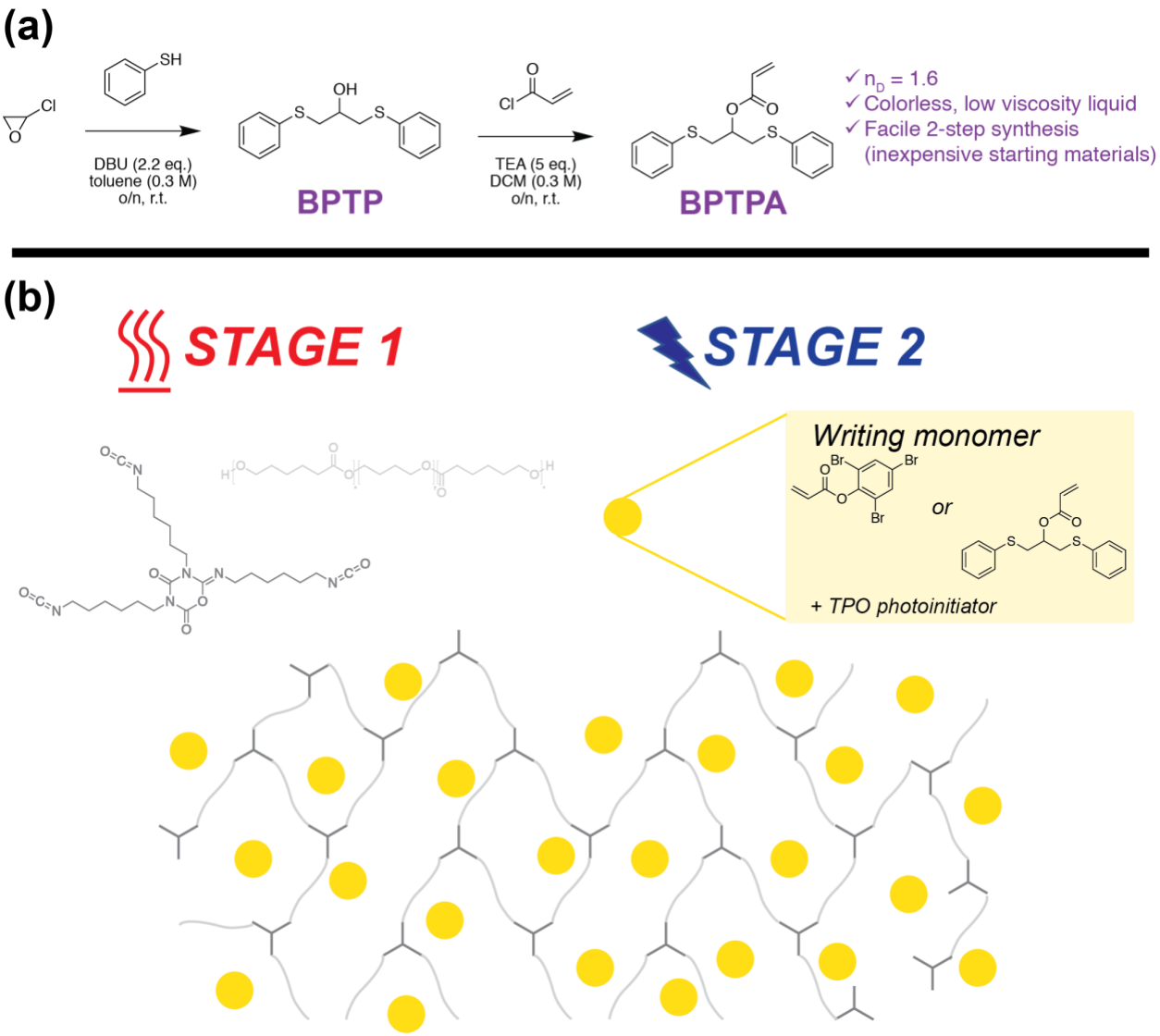

Scheme 0-1. (a) Overall synthetic route for novel acrylate writing monomer, BPTPA. The intermediate alcohol, 1,3-bis-(phenylthio)-2-propanol (BPTP), is synthesized by reaction with excess thiol under basic conditions to favor the bifunctional substitution after the thiol-epoxy ring opening reaction. (b) Schematic illustration for two-stage holographic photopolymer formulations. The stage 1 alcohol-isocyanate network is thermally cured at 70°C overnight with the dissolved writing chemistry (TPO photoinitiator with either TBPA or BPTPA) available for 405 nm recording.

Two-stage photopolymer recording film preparation

Two-stage photopolymer film samples were prepared by premixing the acrylate writing monomer (either TBPA or BPTPA) measured at a set weight percentage

(relative to the entire formulation) with 1-3 wt% TPO photoinitiator (based on writing monomer concentration) and the difunctional polyol in a 4 mL vial equipped with a magnetic stir bar until homogenous. A stoichiometric amount (OH:NCO = 1:1) of Desmodur N3900 trifunctional isocyanate was added to the vial and stirred. The resin was cast onto clean 1 x 1.5” glass slides and sandwiched with a corresponding glass slide or cover slip (Fisher Scientific) using binder clips with PET spacers of defined thicknesses (15, 25 & 250 μm) lining the perimeter to control the thickness. Samples were covered in aluminum foil and allowed to cure overnight in an oven at 70ºC. Acrylate reactivity was confirmed via FTIR to be negligible throughout this thermal process. A representation of the two-stage holographic photopolymers is illustrated in Scheme 0-1.

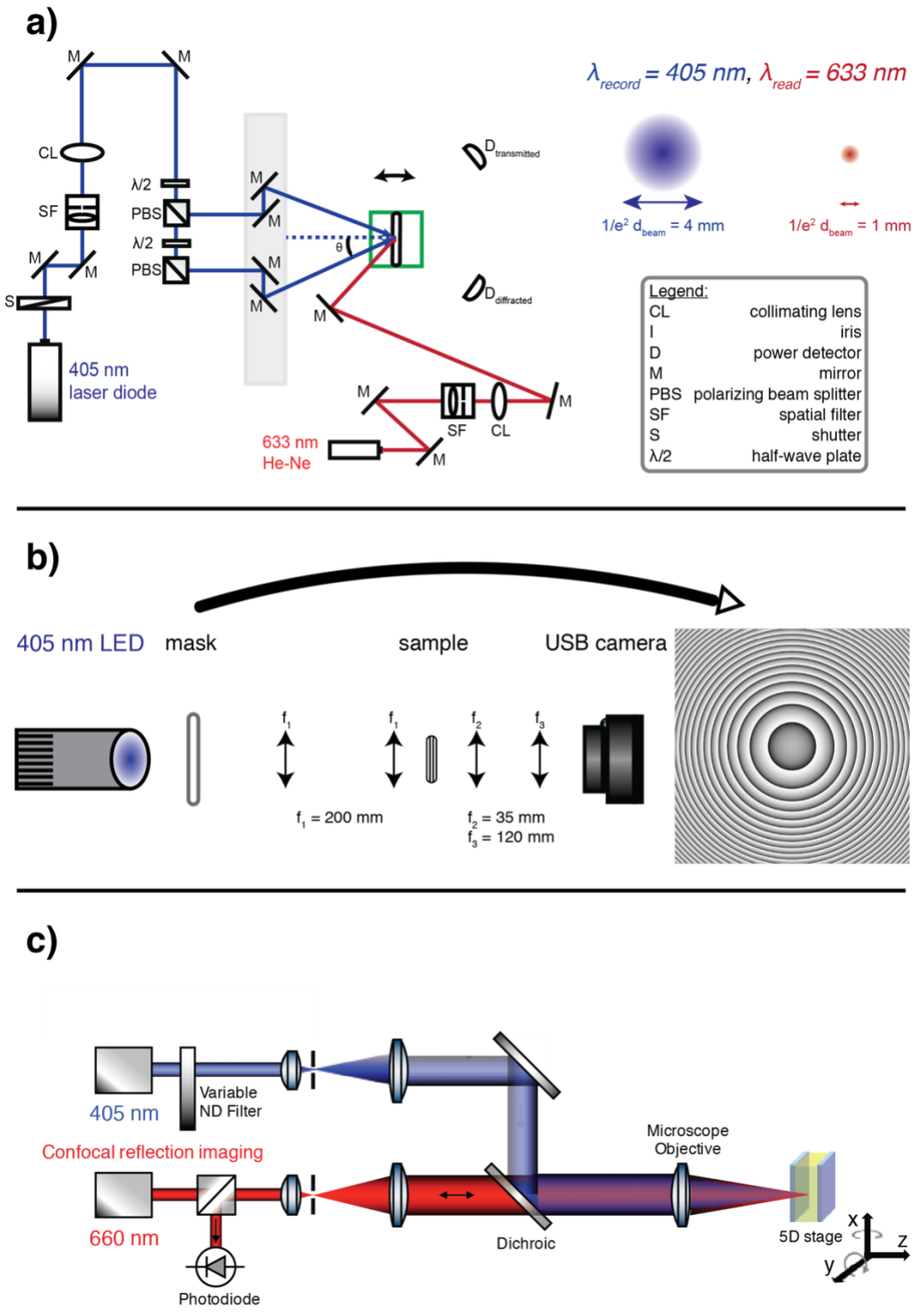

Figure 0-1. Optical recording schematics for systems used to record with 405 nm light: (a) volume transmission holograms recording sinusoidal diffraction gratings of 1 μm

fringe spacing with a peak recording intensity of 16 mW/cm^2 of a Gaussian laser beam with a 1/e^2 diameter of 4.3 mm, (b) photomask lithography using a 1" diameter Fresnel lens mask at an average recording intensity of 40 mW/cm^2, (c) direct laser write of an image pattern with a peak recording intensity of ~ 760 mW/cm^2 of a Gaussian beam with a 1/e^2 diameter of 10 μm.

Fourier Transform Infrared Spectroscopy (FTIR)

Fourier transform infrared spectroscopy was used to monitor the polymerization of the acrylate double bonds. A Thermo Scientific Nicolet 6700 FTIR spectrometer was electronically synchronized with a 405 nm LED source (Thorlabs) using a myDAQ device (National Instruments), allowing for monitoring of the acrylate peak at 814 cm^{-1} with a timed and defined illumination at 16 mW/cm^2. Optically thin samples were prepared between two salt (NaCl) plates using 15 μm spacers. The stage 1 to stage 2 acrylate conversion ($c_{acrylate}$) was monitored using a series scan, integrating over the range 790-830 cm^{-1} where $A_{initial}$ is the area of the unconsumed acrylate peak, and A_{final} is the area under the acrylate peak after the stage 2 reaction.

$$C_{acrylate} = (1 - \frac{A_{final}}{A_{initial}}) * 100\% \quad (1)$$

Holographic recording

A two-beam interference setup shown in Figure 0-1a was used to record volume transmission holograms with a spatially filtered wavelength stabilized 405 nm laser diode (Ondax, 40 mW). Both recording beams (1/e^2 intensity diameter of 4.3 mm) were power matched to give a total recording intensity of ~16 mW/cm^2. The beams were interfered at an external recording half-angle of 11.2° to produce a sinusoidal interference pattern with a fringe spacing of ~1 μm. A 633 nm He-Ne laser (Thorlabs), aligned approximately at the Bragg reconstruction angle, was used as a read beam to nondestructively probe the hologram formation throughout the recording process. Each

recording exposure is initially monitored for 300 s, then followed by a sample rotation from 15° to -15° at an angle increment of 0.05°. The optical power at both of the two detectors was measured throughout the experiment. The diffraction efficiency of each recorded hologram was calculated by taking the quotient of the diffracted power (P_d) to the total power (transmitted + diffracted), $DE = P_d/(P_d + P_t)$. The diffraction efficiency vs. angle profile was fitted to Kogelnik coupled wave theory[34] to obtain a peak-to-mean Δn and thickness (d).

Photolithography mask exposure

A projection lithography setup employing a 405 nm LED (Thorlabs – M405L3-C5) was used to expose a 1" diameter Fresnel lens (1.5 diopter) pattern on a greyscale halftone chrome mask (Toppan Mask) as illustrated in Figure 0-1b.

Direct laser write

A 405 nm continuous wave laser with a focused spot ($1/e^2$ intensity diameter of 13 μm) is used to record isolated or continuous refractive index structures. The sample is mounted on a 5-axis stage that controls both tip/tilt and xyz motion, while a co-aligned confocal reflection microscope operating at 660 nm is used to align the sample as shown in Figure 0-1c.

1.8 Results & Discussion

The goal of this work was to achieve a high Δn two-stage holographic material via an efficient writing monomer capable of a high refractive index after photopolymerization and significant loading into the matrix. The strategy to achieve this was through the design of a novel writing monomer capable of increased solubility in the urethane matrix without sacrificing refractive index. A typical approach is to incorporate high refractive

index groups via linker units to attach with the polymerizing functionality.[8] However, the linker units employed are usually alkyl chains which reduce the overall refractive index of the monomer and polymer. To achieve this structure synthetically without the typical drawback in refractive index, we employed a thiol-epoxy ring-opening reaction using a relatively high refractive index thiol, thiophenol (reported n_D = 1.588), and a substrate capable of further addition after the epoxide ring-opening, epichlorohydrin. With this in mind, the reaction was carried out with excess thiol under basic conditions so that after the initial ring opening reaction of the epichlorohydrin, the chloro-substituted alcohol intermediate (1-chloro-3-(phenylthio)-2-propanol) that formed was able to further react with thiophenol to yield the desired symmetric diphenylthio-substituted secondary alcohol, 1,3-bis(phenylthio)-2-propanol (BPTP), in a one-pot synthesis reaction. This molecular structure comprises advantageous characteristics for both refractive index and solubility. As outlined by the rearranged Lorentz-Lorenz equation,[35]

$$n = \sqrt{\frac{1 + 2\,(\frac{[R]}{V})}{1 - (\frac{[R]}{V})}}$$

where n is the refractive index, [R] is the molar refraction and V is the molar volume. In BPTPA, the phenyl (N_A = 25.463), sulfur and tertiary carbon moieties present are known high refractive index substituents with a high molar refraction relative to molar volume.[36]

In terms of solubility, the flexible thioether linkages are known to freely form random molecular orientations and thus suppress packing between polymer chains. This linker unit is also especially beneficial for imparting a high refractive index in terms of sulfur content (21% for BPTPA) as well as to improve the solubility of the writing

monomer/polymer within the polymer matrix. This behavior is evident by the measured refractive index of 1.62 (Abbe refractometer at 589.3 nm) for the colorless, low viscosity liquid BPTP precursor. Consistent properties are maintained even after the acylation reaction with acryloyl chloride which results in a colorless, low viscosity liquid with a refractive index of 1.6 (Abbe). The neat photopolymerized acrylate film using 1 mol% TPO registered a refractive index of 1.627 via prism coupler measurements at 633 nm.

To investigate further the viability and performance of BPTPA as a writing monomer, it was tested against a reference high refractive index writing monomer, TBPA. Given their comparable molecular weights, comparisons were done at equivalent weight percent compositions at 10 wt% increments. We encountered a solubility limitation at 50 wt% during formulation preparation whereby the monomer did not dissolve in the polyol to give a homogenous and transparent resin. In contrast, BPTPA formulations containing up to 60 wt% writing monomer was successfully prepared.

Solubility of writing monomer in urethane matrix

To assess the solubility capabilities of the writing monomer in a urethane matrix, we first determined the equilibrium mass uptake of monomer in a non-solvent (mineral oil) by the urethane matrix (Table 0-1) by measuring initial (W_i) and final weight (W_f). Approximately 50% more writing monomer (W_f/W_i) could be loaded into the matrix with BPTPA compared to TBPA. The quotient of the mass uptake of writing monomer ($W_f - W_i$) with the final weight of swollen matrix (W_f) was calculated to give a theoretical maximum loading of writing monomer (in wt%).

Table 0-1. Swelling – writing monomer mass uptake by the neat polymeric urethane matrix.

Neat matrix	W_f/W_i [a]	$\Phi_{theoretical}$ (wt%) [b]
TBPA	1.94 ± 0.07	45 ± 2
BPTPA	2.94 ± 0.06	63 ± 1
Control (no writing monomer)	1.03 ± 0.01	-

[a] The ratio of the measured final weight (W_f) of the sample to its initial weight (W_i) was calculated. [b] Theoretical maximum loading (in wt%) was calculated by taking the ratio of the amount of mass uptake to its final weight, i.e. $\phi = (W_f - W_i)/W_f * 100\%$

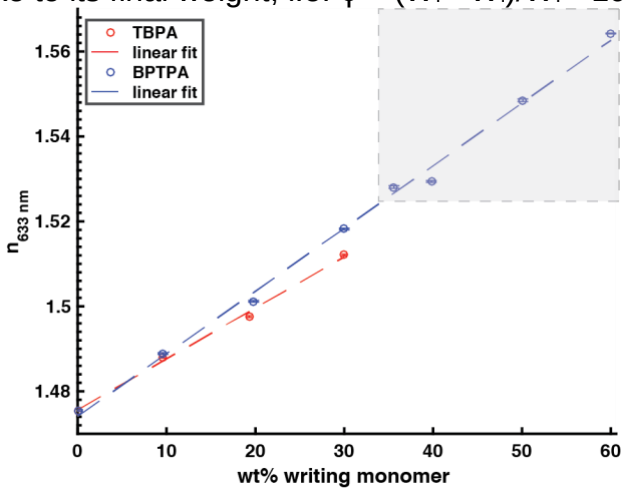

Figure 0-2. Final (stage 2) refractive indices of two-stage formulations for TBPA (red) and BPTPA (blue) as a function of writing monomer content in weight percent. The grey dashed-outline box in the upper right hand corner specifies the accessible region for refractive index increase due to a higher solubility writing monomer.

Refractive index of two-stage formulation

To determine the expected refractive index increase per unit of writing monomer present, the refractive indices of formulations containing varying amounts of writing monomer were measured in their stage 1 and stage 2 (after UV flood exposure) state as shown in Figure 0-2. As is evident from the gradients of the linear fits for both stage 1 and 2, BPTPA demonstrates a higher refractive index contrast increase per unit of writing monomer concentration (i.e. $\Delta n/[M]$). Using the gradient values for the linear fit equations, this $\Delta n/[M]$ increase is estimated to be approximately 20%. Therefore,

assuming both monomers react similarly in rate and final conversion, a marginally higher Δn structure would be expected at equivalent monomer concentrations. More crucially, the ability to increase writing monomer loading extends the refractive index contrast ($n_{photopolymer} - n_{matrix}$) as shown by the dashed grey box inset of Figure 0-2.

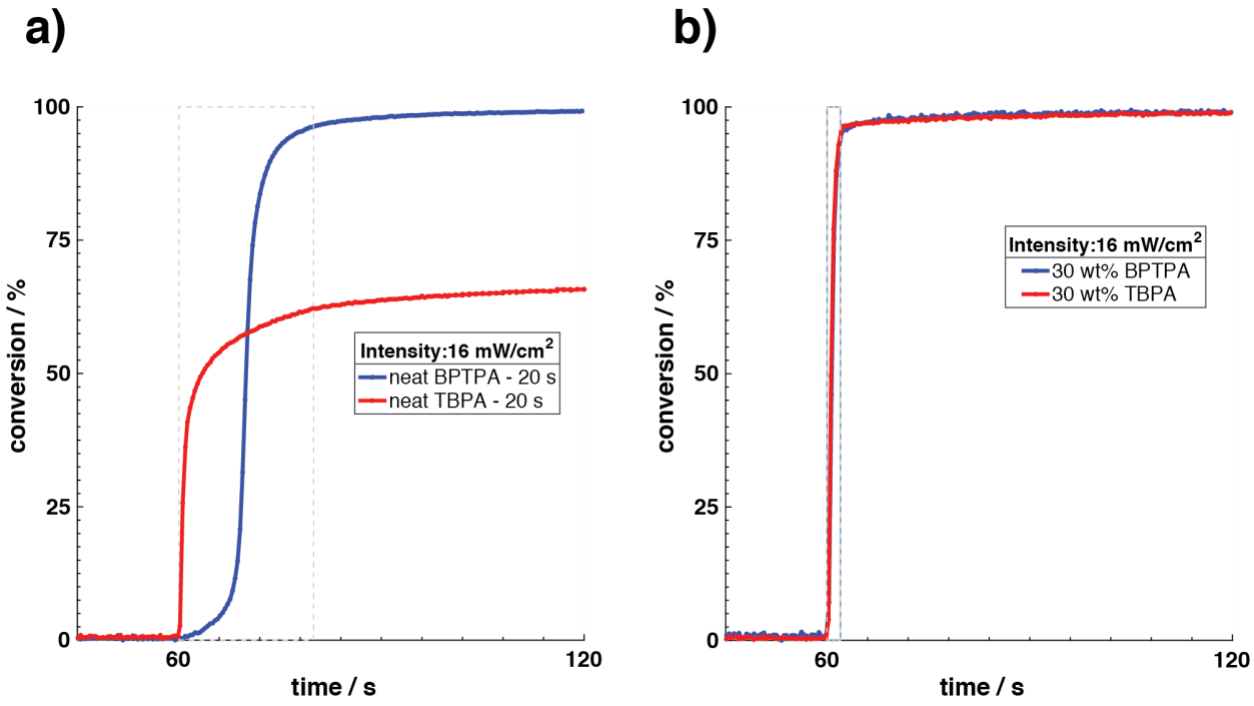

Figure 0-3. Real-time FTIR photopolymerization double bond conversion kinetics for the (a) neat acrylate (TBPA in red; BPTPA in blue) homopolymerization with 1 mol% TPO using triggered 405 nm LED irradiation (20 s at 16 mW/cm^2) at the 60 s mark, and (b) acrylate homopolymerization of 30 wt% writing monomer (TBPA in red; BPTPA in blue) formulation with 10 mol% TPO using triggered 405 nm LED irradiation (2 s at 16 mW/cm^2) at the 60 s mark.

Recording kinetics

The photopolymerization reactivity of BPTPA was assessed neat and as a stage 2 photopolymerization using 30 wt% writing monomer via real-time FTIR spectroscopy. Figure 0-3a shows that while TBPA has an almost instantaneous consumption of double

bonds upon irradiation, it distinctly reaches a plateau of around 65% conversion due to vitrification. In the case of neat BPTPA, however, it has a slower initial rate but does in fact reach quantitative conversion within the exposure time of 20 seconds. This distinct polymerization kinetics profile is attributed to the lower viscosities throughout the polymerization of BPTPA. When these writing monomers are used in two-stage formulations, it is clear from Figure 0-3b that they both are indistinguishable in reactivity rates or final conversion (both quantitative). Therefore, the FTIR data suggests that BPTPA is at least comparable if not preferred to TBPA for its ability to go to full conversion at higher writing monomer loadings.

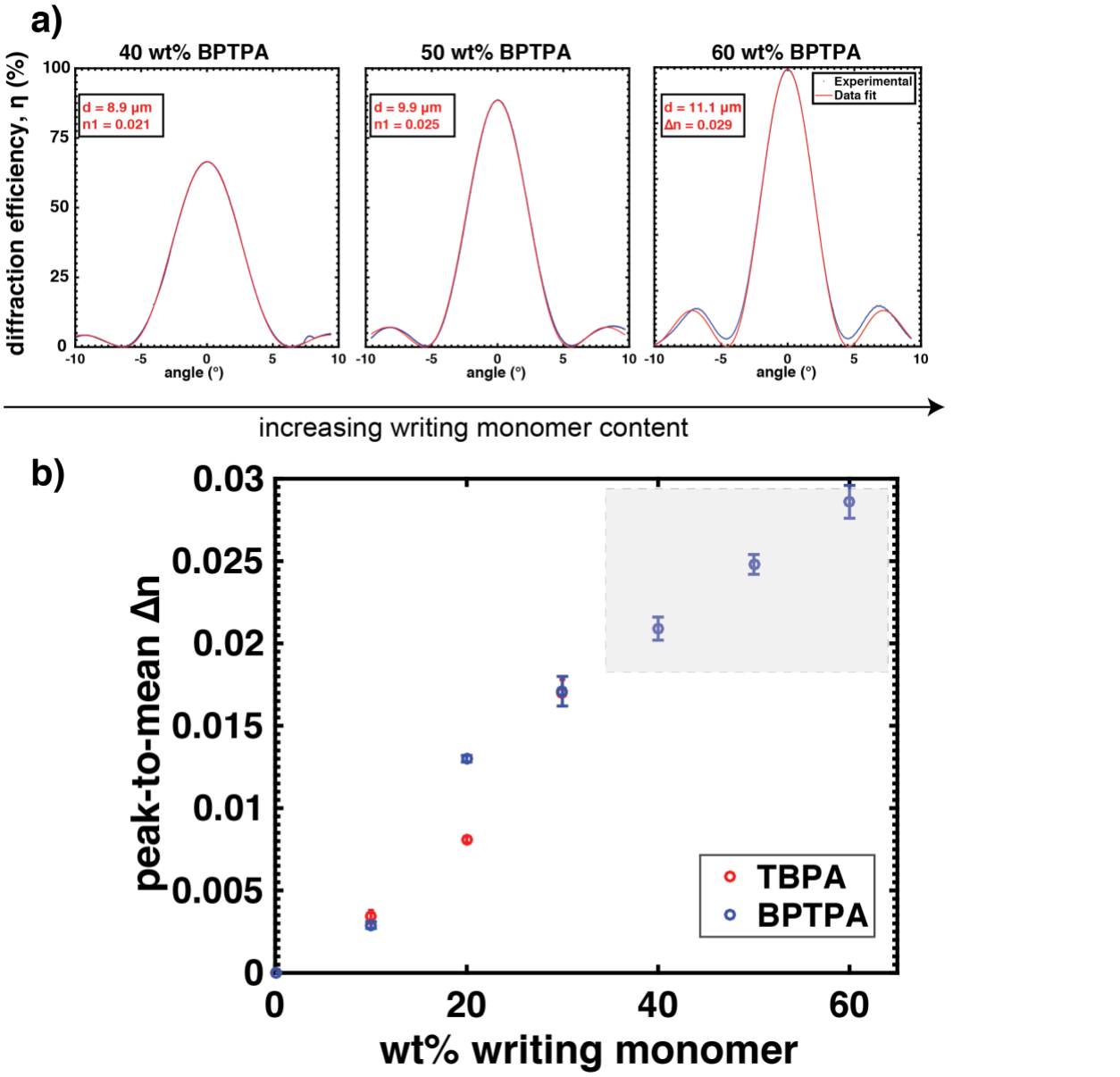

Figure 0-4. Transmission holography and Δn (peak-to-mean) values recorded with a pitch spacing of 1 μm at a recording intensity of 16 mW/cm^2 with exposure times of 1 s. (a) Representative diffraction efficiency vs. reconstruction angle scans for 40, 50 and 60 wt% BPTPA formulations (data points in blue) with the corresponding fits (in red) to classical Kogelnik Coupled Wave theory. (b) Comparison of peak-to-mean Δn performance of TBPA against BPTPA as a function of writing monomer content (TBPA in red; BPTPA in blue). The grey dashed-outline box in the upper right hand corner reveals the realized and achievable Δn increase from the higher solubility writing monomer BPTPA.

Holographic recording (transmission gratings)

Taking the solubility studies together with the refractive index measurements, we hypothesized a significant overall Δn recording improvement to be gained from enhancements in both Δn/[M] as well as the amount of monomer that can be loaded. As a demonstration, high diffraction efficiency transmission volume holograms (fringe spacing $\Lambda \approx 1$ μm) were recorded into the TBPA and BPTPA samples at varying monomer loadings in thin films (< 15 μm) to intentionally avoid over-modulation. Representative angular scans with good fits to Kogelnik coupled wave theory are shown in Figure 0-4a for samples containing 40, 50 and 60 wt% BPTPA with a peak-to-mean Δn of up to 0.029 demonstrated. Figure 0-4b shows the overall maximum achievable Δn for both writing monomers at increasing wt% loading. By increasing the writing monomer loading, we increase the observed Δn of a given material without a noticeable penalty in transparency or scatter. An additional advantage of the increased solubility of BPTPA is the boost in material sensitivity due to a concomitant increase in the polymerization rate that arises due to the higher monomer concentration.[37]

High sensitivity materials are especially critical for holography due to laser source limitations in power and overall setup stability time. This feature also extends to alternative photoinitiating systems which initiate at longer visible wavelengths but are less efficient.[9, 10, 31]

Bulk Δn vs. holographic Δn analysis

Achievable holographic Δn in two-stage materials from a sinusoidal exposure is a fraction of the maximum achievable index response from a uniform flood-cure. In fact, for a single holographic exposure (two-beam interference), it can be shown that the

highest achievable Δn of the first harmonic is approximately 88% of a material's maximum refractive index response (see Supporting Information). In Figure 0-5 the holographic Δn is plotted against the bulk Δn between stage 1 and 2 as measured using a prism coupler for both writing monomers. These results indicate that although BPTPA is able to achieve a higher holographic Δn through the increased solubility there is also a decrease in the "efficacy" of the increased index contrast at higher loadings.

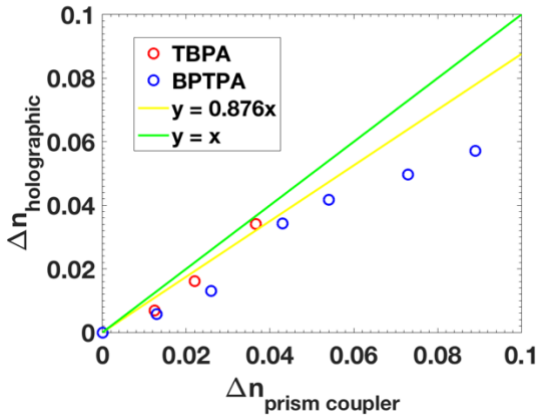

Figure 0-5. "Effective" refractive index contrast plot – achievable Δn with a sinusoidal intensity exposure measured via holography vs. the achievable Δn in bulk measured via prism coupler for TBPA (in red) and BPTPA (in blue) at varying writing monomer content. The green line specifies the ideal case for a perfect match between refractive index contrast in bulk and holographic materials. The yellow line indicates the actual theoretical maximum Δn (88%) to be expected from the holographic Δn measured which only measures the first harmonic.

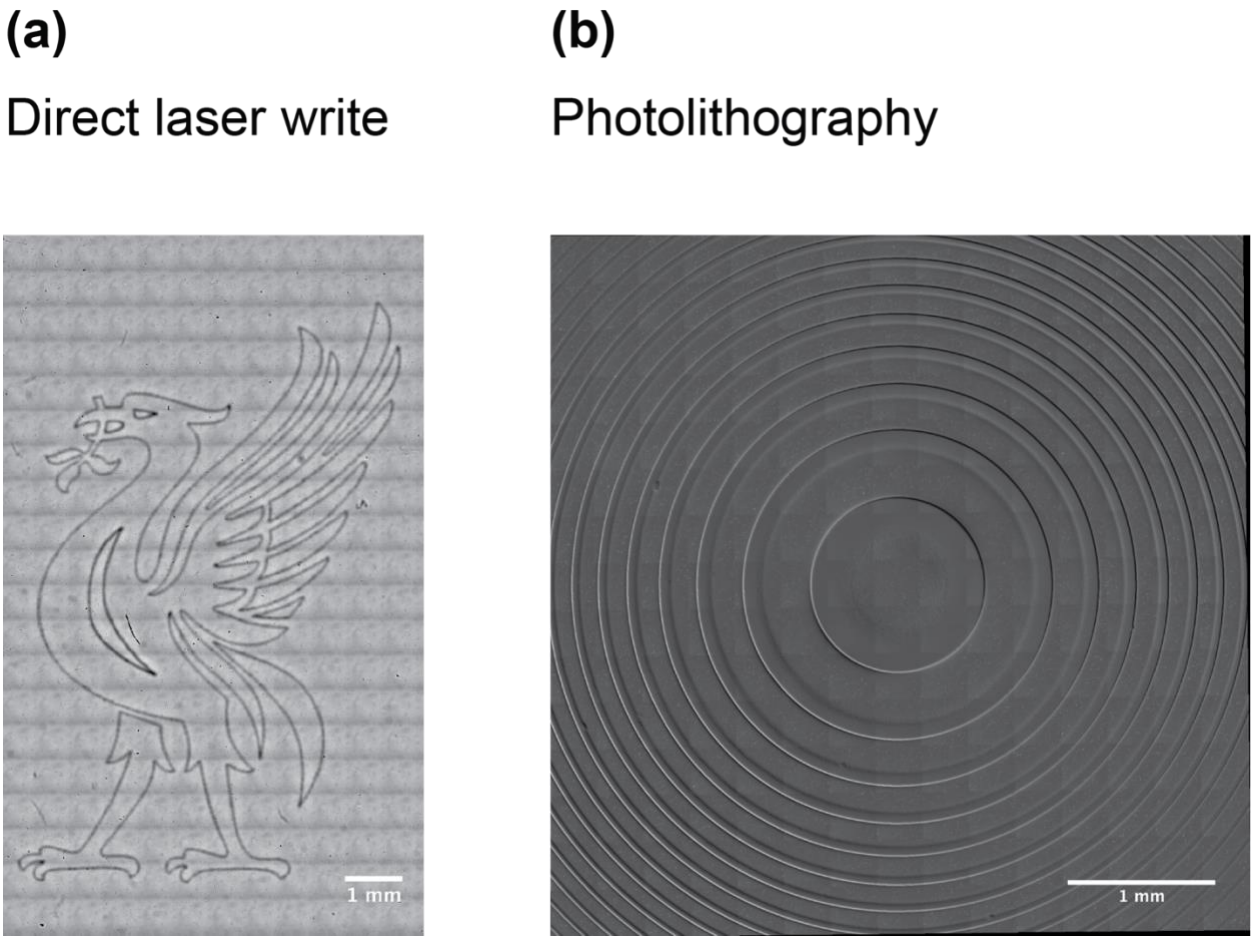

Figure 0-6. Demonstrative refractive index gradient examples. Stitched DIC microscope images of (a) direct laser write of a bird pattern, (b) projection mask lithography of a 1-inch diameter Fresnel lens.

Refractive index gradient demonstrations

Refractive index structures at low spatial frequencies are also demonstrated using DLW of an arbitrary pattern and projection lithography using a Fresnel lens etched chrome mask. The DLW example (Figure 0-6a) demonstrates distinct refractive index contrast between the photopolymer of BPTPA and the matrix whilst the Fresnel lens (Figure 0-6b) example validates the ability to record a structure with a fine gradient in refractive index. As evidenced by the stitched bright field DIC microscope (Nikon N-

STORM) images in Figure 0-6 the material was able to record distinct sub-micron to tens of microns-sized features with excellent fidelity in both cases.

1.9 Conclusions

We report a novel acrylate monomer, BPTPA, that exhibits excellent properties. It is a high refractive index, highly reactive, colorless, liquid monomer that is readily synthesized from economical starting materials. This monomer was assessed for its solubility and refractive index change upon polymerization in a urethane matrix for use as a writing monomer in a two-stage formulation. BPTPA excelled over a reference, widely used high refractive index monomer, TBPA, on both measures allowing for formulations containing up to 60 wt% loading of BPTPA which demonstrated a maximum $\Delta n \sim 0.029$ for volume transmission holograms. To the best of our knowledge, this value is the highest reported of any holographic photopolymer within the academic literature achieved with superior photosensitivity and simple synthetic preparation. This writing monomer and the synthetic protocol present promising avenues for the design of high refractive index writing monomers for high performance holographic photopolymers.

1.10 Supporting Information

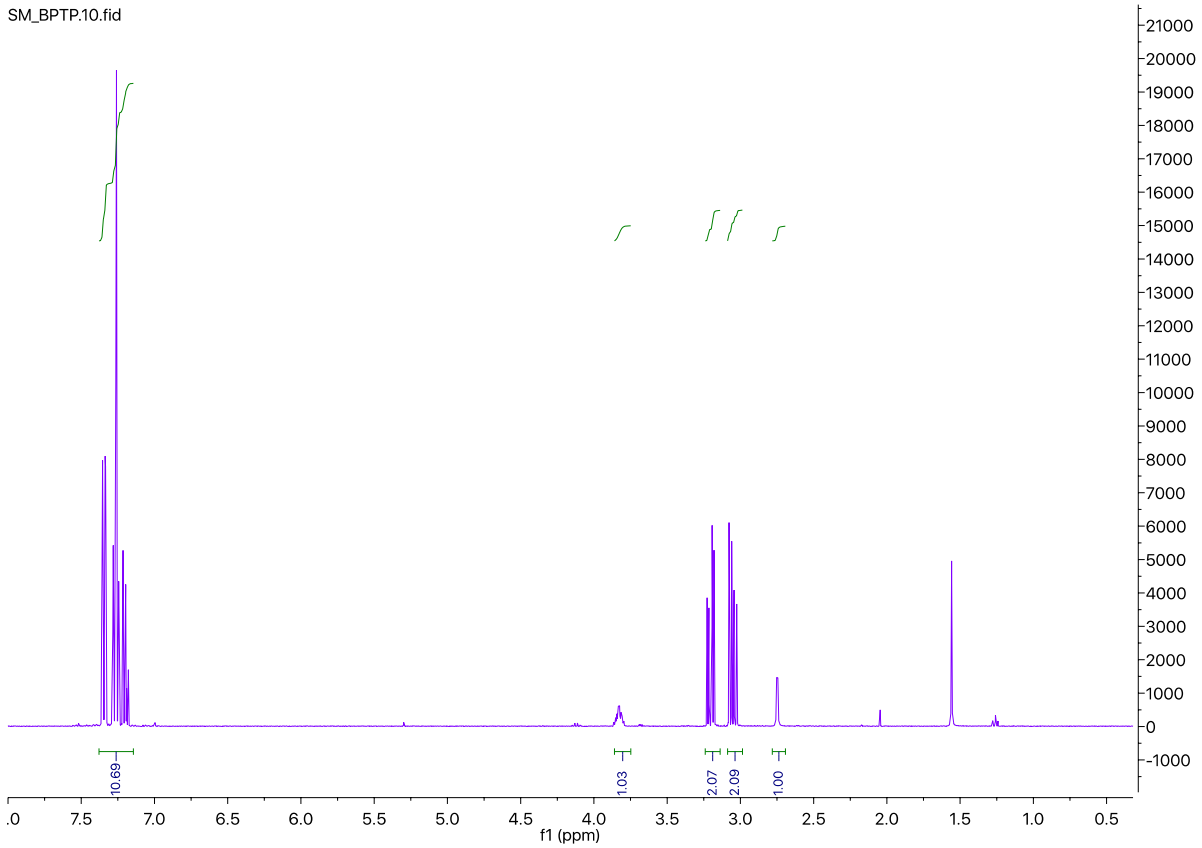

Figure S0-7. ^{1}H NMR spectra for synthesized BPTP after purification.

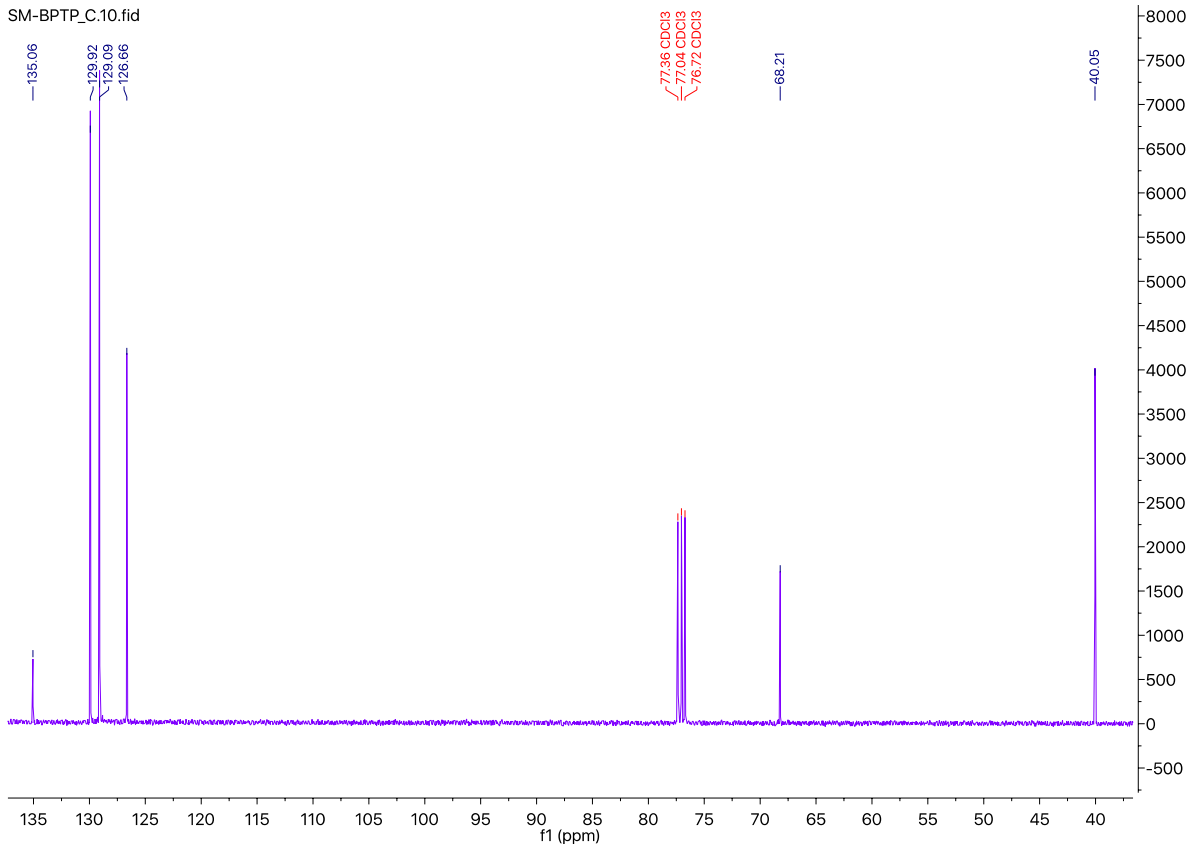

Figure S0-8. ^{13}C NMR spectra for synthesized BPTP after purification.

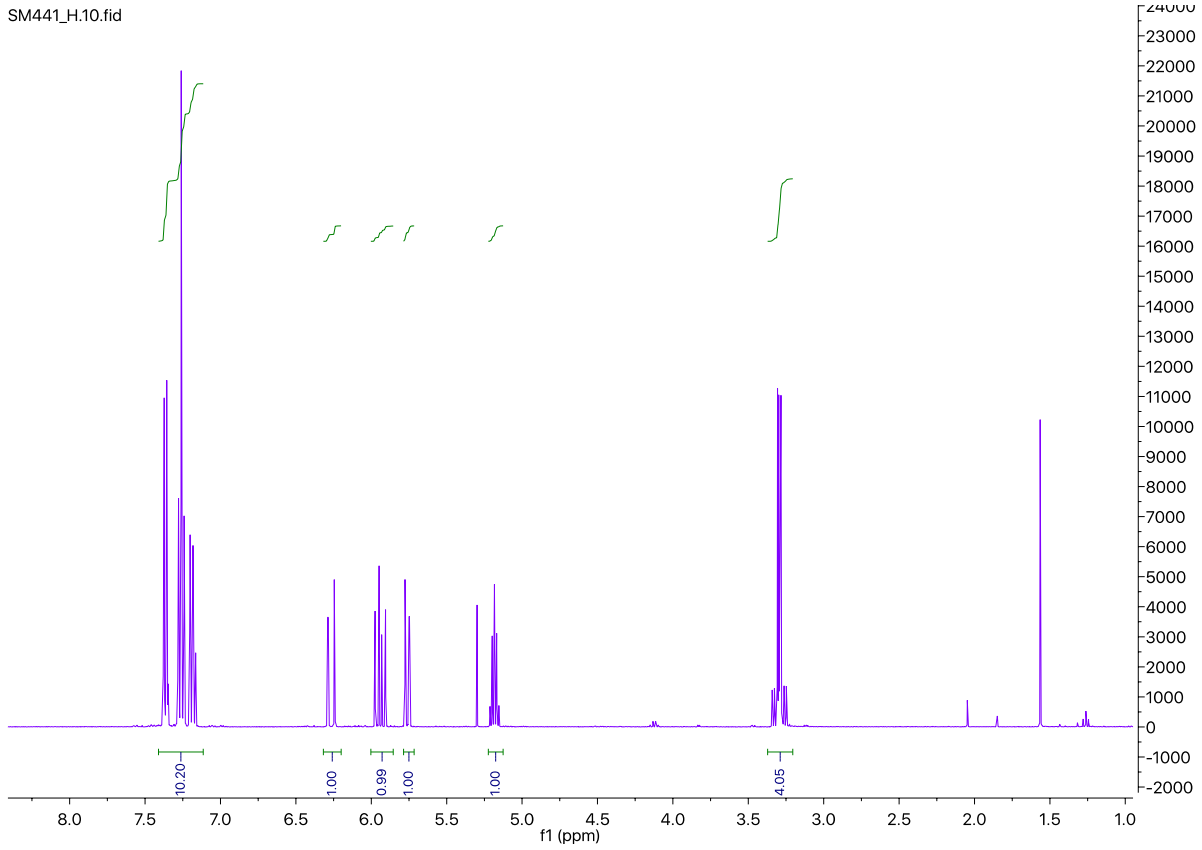

Figure S0-9. ^{1}H NMR spectra for synthesized BPTPA after purification.

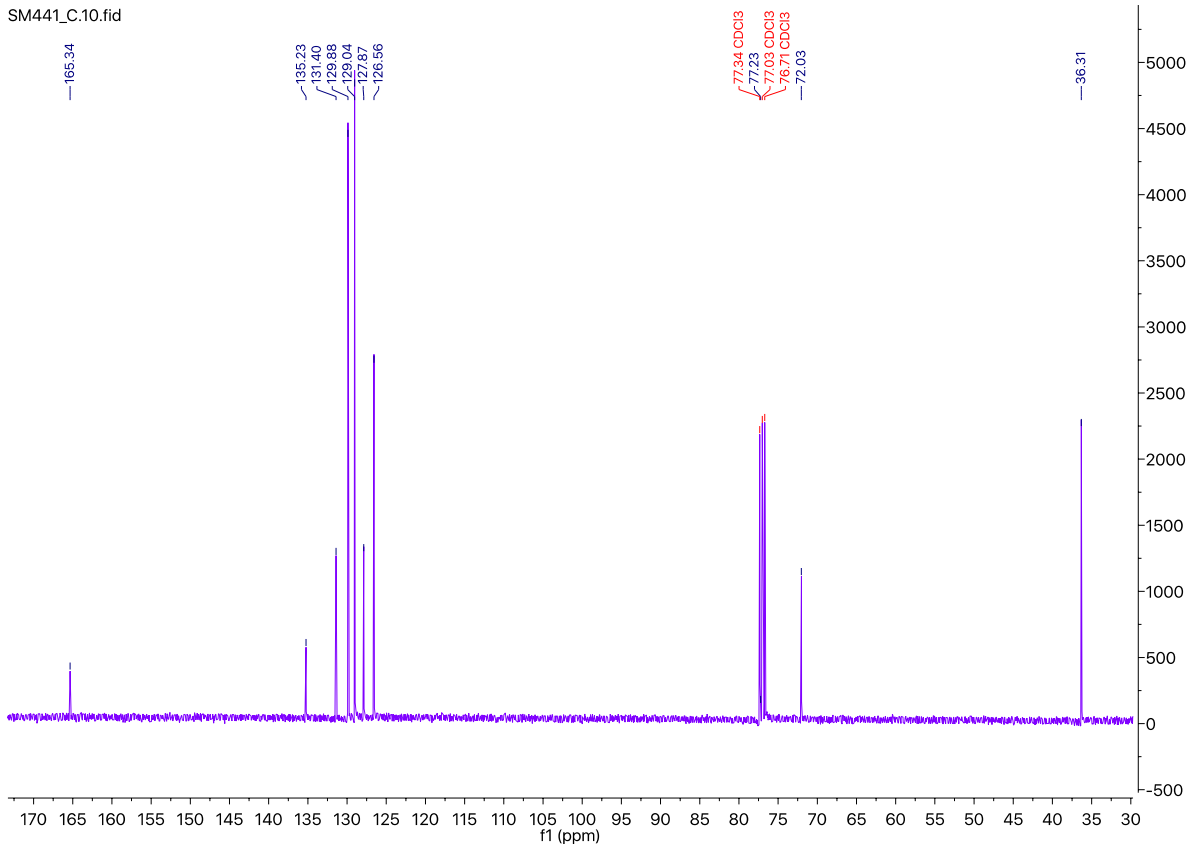

Figure S0-10. ^{13}C NMR spectra for synthesized BPTPA after purification.

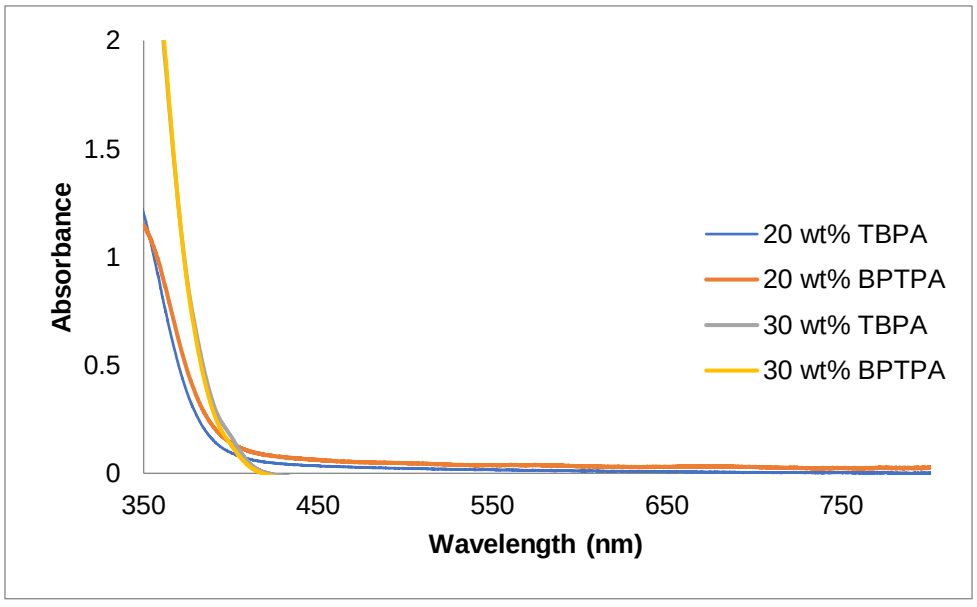

Figure S0-11. UV-vis absorption spectra of TBPA and BPTPA formulations before stage 2 polymerization.

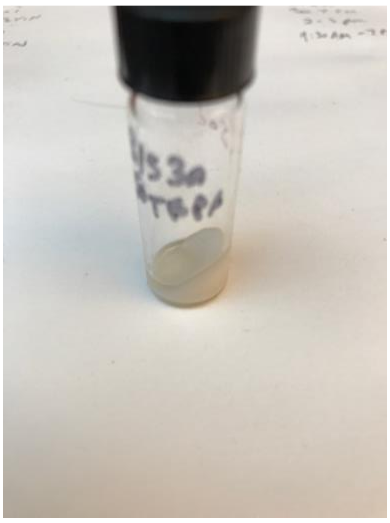

Figure S1. Loss of transparency of precursor resins at higher TBPA loadings (50 wt%)

Refractive index contrast measurable by a single Bragg hologram

The transmission Bragg hologram used to characterize material refractive index contrast is not a perfect measurement as the material saturates due to consumption of monomer. Specifically, consider the case in which the sinusoidal writing intensity consumes a significant fraction of the monomer species. As this first-order reaction proceeds, reduction of the monomer concentration proportionally reduces the propagation rate. The index of refraction thus saturates according to

$$\frac{\delta n(x)}{\Delta n} = 1 - e^{-E(x)/E_c}, \qquad \text{Eq. 1}$$

where δn is the local index change, Δn is the maximum index change that occurs upon full conversion, $E(x)$ is the local optical dose and E_c is the dose that consumes a fraction $1/e$ of the initial monomer concentration.

For two-beam interference writing, the local optical dose $E(x)$ is given by

$$E(x) = E_p \left[1 + \cos\left(2\pi \frac{x}{\Lambda}\right)\right]/2, \qquad \text{Eq. 2}$$

where $E_p$is the peak dose and Λ is the period of the writing sinusoid. As the peak dose E_p becomes significant in comparison to the dose that consumes $1/e$ of the concentration, the response saturates, resulting in flattened peaks as shown in Figure S0-12.

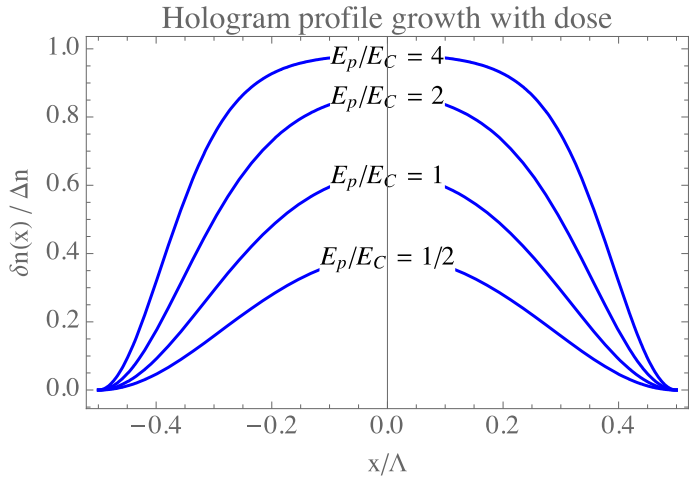

Figure S0-12. Index profiles δn normalized to the maximum index change Δn over one period of the interferogram, Λ. The sinusoidal response saturates as the peak dose, E_p, becomes large in comparison to the critical exposure dose E_C.

Diffraction off of such a phase structure will depend on the Fourier harmonics of the fundamental spatial frequency $1/\Lambda$. To obtain a quasi-closed form for the Fourier series $\delta n(x) = \sum_{m=0}^{\infty} n_m \cos\left(2\pi m \frac{x}{\Lambda}\right)$, we expand Eq. 1 in a power series in x, substitute in Eq. 2 and gather the coefficients of the m^{th} harmonic. The initial terms in this series for the first three harmonics are

$$\frac{n_1}{\Delta n} = \frac{1}{2}\left(\frac{E_p}{E_C}\right) - \frac{1}{2}\left(\frac{E_p}{E_C}\right)^2 + \frac{5}{64}\left(\frac{E_p}{E_C}\right)^3 - \frac{7}{384}\left(\frac{E_p}{E_C}\right)^4 + \frac{7}{2048}\left(\frac{E_p}{E_C}\right)^5 + O\left[\left(\frac{E_p}{E_C}\right)^6\right],$$

$$\frac{n_2}{\Delta n} = 0\left(\frac{E_p}{E_C}\right) - \frac{1}{16}\left(\frac{E_p}{E_C}\right)^2 + \frac{1}{32}\left(\frac{E_p}{E_C}\right)^3 - \frac{7}{768}\left(\frac{E_p}{E_C}\right)^4 + \frac{1}{512}\left(\frac{E_p}{E_C}\right)^5 + O\left[\left(\frac{E_p}{E_C}\right)^6\right], \qquad \text{Eq. 3}$$

$$\frac{n_3}{\Delta n} = 0\left(\frac{E_p}{E_C}\right) + 0\left(\frac{E_p}{E_C}\right)^2 + \frac{1}{192}\left(\frac{E_p}{E_C}\right)^3 - \frac{1}{384}\left(\frac{E_p}{E_C}\right)^4 + \frac{3}{4096}\left(\frac{E_p}{E_C}\right)^5 + O\left[\left(\frac{E_p}{E_C}\right)^6\right].$$

These reveal that, to lowest order, the m^{th} harmonic grows as the peak dose to the m^{th} power. These are plotted in Figure S0-13. The maximum of the first harmonic is $n_1 \approx 0.438$ at a peak dose of $E_p \approx 3.09E_C$, indicating that only 88% of the material maximum index response can be accessed with single-exposure two beam interference.

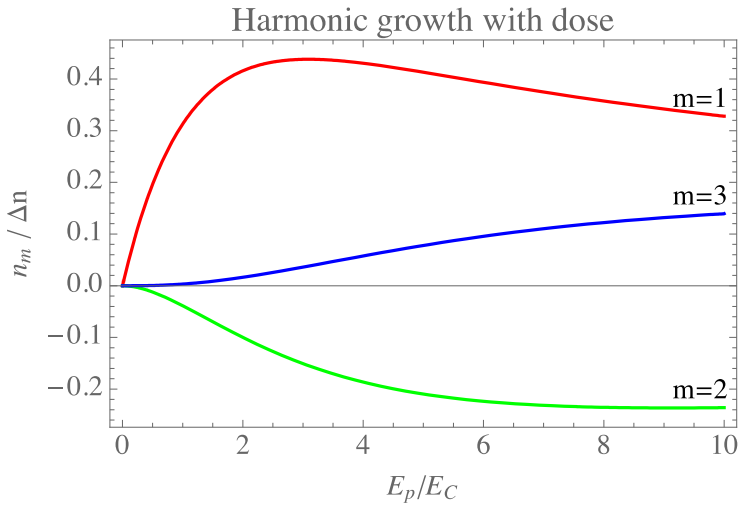

Figure S0-13. First through third harmonic of the recorded index change relative to the maximum index change Δn as a function of the peak dose, E_p relative to the critical exposure dose E_C. Note that n_m is the peak to mean amplitude and thus is bounded by $\pm\frac{1}{2}$. The functions plotted are given in Eq. 3 using the first 100 terms of the series.

1.11 Acknowledgements

The authors would like to thank Darren Forman, Jacob Friedlein and Maciej Podgorski for their help and advice throughout the preparation of this manuscript. The imaging work was performed at the BioFrontiers Institute Advanced Light Microscopy Core. Super resolution microscopy was performed on a Nikon N-STORM microscope supported by the Howard Hughes Medical Institute. This material is based upon work

supported by Konica Minolta and the National Science Foundation under Grant No. ECCS 1307918 and Grant No. DMR 1310528.

1.12 References

1. Nair, D. P.; Cramer, N. B.; Gaipa, J. C.; McBride, M. K.; Matherly, E. M.; McLeod, R. R.; Shandas, R.; Bowman, C. N., Two-Stage Reactive Polymer Network Forming Systems. *Adv. Funct. Mater.* **2012,** *22* (7), 1502-1510.

2. White, S. R.; Moore, J. S.; Sottos, N. R.; Krull, B. P.; Santa Cruz, W. A.; Gergely, R. C. R., Restoration of Large Damage Volumes in Polymers. *Science* **2014,** *344*, 620.

3. Podgorski, M.; Nair, D. P.; Chatani, S.; Berg, G.; Bowman, C. N., Programmable Mechanically Assisted Geometric Deformations of Glassy Two-Stage Reactive Polymeric Materials. *ACS Appl. Mater. Interfaces* **2014,** *6* (9), 6111-6119.

4. Toal, V., *Introduction to Holography*. 2012.

5. Kowalski, B. A.; McLeod, R. R., Design concepts for diffusive holographic photopolymers. *J. Polym. Sci. Part B: Polym. Phys.* **2016,** *54* (11), 1021-1035.

6. Dhar, L.; Hale, A.; Katz, H. E.; Schilling, M. L.; Schnoes, M. G.; Schilling, F. C., Recording Media That Exhibit High Dynamic Range for Digital Holographic Data Storage. *Opt. Lett.* **1999,** *24*, 487.

7. Peng, H. Y.; Nair, D. P.; Kowalski, B. A.; Xi, W. X.; Gong, T.; Wang, C.; Cole, M.; Cramer, N. B.; Xie, X. L.; McLeod, R. R.; Bowman, C. N., High Performance Graded Rainbow Holograms via Two-Stage Sequential Orthogonal Thiol-Click Chemistry. *Macromolecules* **2014,** *47* (7), 2306-2315.

8. Peng, H.; Wang, C.; Xi, W.; Kowalski, B. A.; Gong, T.; Xie, X.; Wang, W.; Nair, D. P.; McLeod, R. R.; Bowman, C. N., Facile Image Patterning via Sequential Thiol–Michael/Thiol–Yne Click Reactions. *Chem. Mater.* **2014,** *26*, 6819.

9. Cody, D.; Gribbin, S.; Mihaylova, E.; Naydenova, I., Low-Toxicity Photopolymer for Reflection Holography. *ACS Appl. Mater. Interfaces* **2016,** *8*, 18481.

10. Ni, M.; Peng, H.; Liao, Y.; Yang, Z.; Xue, Z.; Xie, X., 3D Image Storage in Photopolymer/ZnS Nanocomposites Tailored by “Photoinitibitor.”. *Macromolecules* **2015,** *48*, 2958.

11. Tomita, Y.; Urano, H.; Fukamizu, T. a.; Kametani, Y.; Nishimura, N.; Odoi, K., Nanoparticle-Polymer Composite Volume Holographic Gratings Dispersed with Ultrahigh-Refractive-Index Hyperbranched Polymer as Organic Nanoparticles. *Opt. Lett.* **2016,** *41*, 1281.

12. Peng, H.; Bi, S.; Ni, M.; Xie, X.; Liao, Y.; Zhou, X.; Xue, Z.; Zhu, J.; Wei, Y.; Bowman, C. N.; Mai, Y. W., Monochromatic Visible Light "Photoinitibitor": Janus-Faced Initiation and Inhibition for Storage of Colored 3D Images. *J. Am. Chem. Soc.* **2014,** *136*, 8855.

13. Choi, K.; Chon, J. W. M.; Gu, M.; Malic, N.; Evans, R. A., Low-Distortion Holographic Data Storage Media Using Free-Radical Ring-Opening Polymerization. *Adv. Funct. Mater.* **2009,** *19* (22), 3560-3566.

14. Urness, A. C.; Anderson, K.; Ye, C.; Wilson, W. L.; McLeod, R. R., Arbitrary GRIN Component Fabrication in Optically Driven Diffusive Photopolymers. *Opt. Express* **2015,** *23*, 264.

15. Sullivan, A. C.; Grabowski, M. W.; McLeod, R. R., Three-Dimensional Direct-Write Lithography into Photopolymer. *Appl. Opt.* **2007,** *46*, 295.

16. Yee, D. W.; Schulz, M. D.; Grubbs, R. H.; Greer, J. R., Functionalized 3D Architected Materials via Thiol-Michael Addition and Two-Photon Lithography. *Adv. Mater.* **2017,** *29*, 1605293.

17. Kress, B. C.; Gregory, G. G.; Davis, A. J.; Hahlweg, C. F., *Restocking the Optical Designers' Toolbox for Next-Generation Wearable Displays (Presentation Recording)*. 2015; p 957903.

18. Bruder, F.-K.; Hagen, R.; Rölle, T.; Weiser, M.-S.; Fäcke, T., From the Surface to Volume: Concepts for the Next Generation of Optical–Holographic Data-Storage Materials. *Angew. Chem.-Int. Edit.* **2011,** *50* (20), 4552-4573.

19. Kowalski, B. A.; Urness, A. C.; Baylor, M. E.; Cole, M. C.; Wilson, W. L.; McLeod, R. R., Quantitative Modeling of the Reaction/diffusion Kinetics of Two-Chemistry Diffusive Photopolymers. *Opt. Mater. Express* **2014,** *4*, 1668.

20. Liu, J. g.; Ueda, M., High Refractive Index Polymers: Fundamental Research and Practical Applications. *J. Mater. Chem.* **2009,** *19*, 8907.

21. Higashihara, T.; Ueda, M., Recent Progress in High Refractive Index Polymers. *Macromolecules* **2015,** *48* (7), 1915-1929.

22. Macdonald, E. K.; Shaver, M. P., Intrinsic High Refractive Index Polymers. *Polym. Int.* **2015,** *64*, 6.

23. Gharagheizi, F.; Ilani-Kashkouli, P.; Kamari, A.; Mohammadi, A. H.; Ramjugernath, D., Group Contribution Model for the Prediction of Refractive Indices of Organic Compounds. *Journal of Chemical & Engineering Data* **2014,** *59* (6), 1930-1943.

24. Meka, C.; Jallapuram, R.; Naydenova, I.; Martin, S.; Toal, V., Development of a Panchromatic Acrylamide-Based Photopolymer for Multicolor Reflection Holography. *Appl. Opt.* **2010,** *49*, 1400.

25. Liu, S.; Gleeson, M. R.; Guo, J.; Sheridan, J. T., High Intensity Response of Photopolymer Materials for Holographic Grating Formation. *Macromolecules* **2010,** *43*, 9462.

26. Bunning, T., The Morphology and Performance of Holographic Transmission Gratings Recorded in Polymer Dispersed Liquid Crystals. *Polymer* **1995,** *36*, 2699.

27. Bunning, T. J.; Natarajan, L. V.; and, V. P. T.; Sutherland, R. L., Holographic Polymer-Dispersed Liquid Crystals (H-PDLCs). *Annual Review of Materials Science* **2000,** *30* (1), 83-115.

28. Natarajan, L. V.; Shepherd, C. K.; Brandelik, D. M.; Sutherland, R. L.; Chandra, S.; Tondiglia, V. P.; Tomlin, D.; Bunning, T. J., Switchable Holographic Polymer-Dispersed Liquid Crystal Reflection Gratings Based on Thiol–Ene Photopolymerization. *Chem. Mater.* **2003,** *15*, 2477.

29. White, T. J.; Natarajan, L. V.; Tondiglia, V. P.; Lloyd, P. F.; Bunning, T. J.; Guymon, C. A., Monomer Functionality Effects in the Formation of Thiol–Ene Holographic Polymer Dispersed Liquid Crystals. *Macromolecules* **2007,** *40*, 1121.

30. Tomita, Y.; Urano, H.; Fukamizu, T.-a.; Kametani, Y.; Nishimura, N.; Odoi, K., Nanoparticle-polymer composite volume holographic gratings dispersed with ultrahigh-refractive-index hyperbranched polymer as organic nanoparticles. *Opt. Lett.* **2016,** *41* (6), 1281-1284.

31. Chen, G.; Ni, M.; Peng, H.; Huang, F.; Liao, Y.; Wang, M.; Zhu, J.; Roy, V. A. L.; Xie, X., Photoinitiation and Inhibition under Monochromatic Green Light for Storage of Colored 3D Images in Holographic Polymer-Dispersed Liquid Crystals. *ACS Appl. Mater. Interfaces* **2017,** *9*, 1810.

32. Bruder, F. K.; Fäcke, T.; Rölle, T., The Chemistry and Physics of Bayfol HX Film Holographic Photopolymer. *Polymers* **2017,** *9*, 472.

33. Ayres, M. R.; Anderson, K.; Askham, F.; Sissom, B.; Urness, A. C.; Bjelkhagen, H. I.; Bove, V. M., Holographic Data Storage at 2+ Tbit/in 2. *Proceedings of SPIE* **2015,** *9386*, 93860G.

34. Kogelnik, H., Coupled wave theory for thick hologram gratings. *The Bell System Technical Journal* **1969,** *48* (9), 2909-2947.

35. Heller, W., Remarks on Refractive Index Mixture Rules. *J. Phys. Chem.* **1965,** *69*, 1123.

36. Groh, W.; Zimmermann, A., What is the Lowest Refractive Index of an Organic Polymer? *Macromolecules* **1991,** *24*, 6660.

37. Odian, G. G., Principles of polymerization. **2004**.

Writing Monomer Design Considerations for High Δn Two-Stage Photopolymers and Their Novel Applications[1]

Two-stage photopolymers with high refractive index modulations (Δn > 0.015) were explored towards the one step fabrication of a quarter-pitch soft, flexible gradient refractive index (GRIN) lens with a 0.2 numerical aperture (NA). A mask projection lithography system operating at 430 nm was used to enable millimeter path lengths to circumvent absorption and non-uniform recordings. GRIN lenses up to 500 μm thick were successfully recorded with the expected phase delay corresponding to Δn of approximately 0.02; however, at higher path lengths significant haze was encountered. To address this, the design scope of writing monomers was systematically expanded to increase refractive index (n_D/20ºC: 1.60 – 1.66) and introduce carbamate moieties to improve solubility within stage I urethane matrices.

1.13 Introduction

Two-stage photopolymers have been shown to be exemplary recording materials for arbitrarily programming refractive index patterns throughout the volume of an otherwise transparent medium.[1-5] While these materials have recently been exploited for applications requiring relatively thin films (sub-200 μm), the ability to record in thicker media (1 – 5 mm) would expand on the multitude of accessible benefits as, for example, in the case of holography where the possible number of multiplexed holograms scales

[1] Contributing authors: Sudheendran Mavila, David B. Miller, Amy C. Sullivan, Christopher N. Bowman, and Robert R. McLeod

with the thickness of the media.[6-9] More crucially, the ability to record arbitrary phase structures in thick transparent two-stage photopolymer materials enables a facile route to new applications that cannot readily be realized with conventional techniques.

A prime example is the fabrication of gradient refractive index (GRIN) optics.[10-14] In contrast to existing GRIN lenses fabricated using techniques ranging from ion exchange[15] to direct laser writing[13] to partial polymerization-based approaches,[16] GRIN optics made with two-stage photopolymers are inherently soft and flexible. This characteristic makes them particularly attractive for biomedical-based applications such as a two-photon endoscopic imaging. Furthermore, two-stage photopolymers have the key advantage of not being limited by the recordable refractive index profiles unlike other techniques that rely on diffusion and symmetry.[12, 15] In fact, as the recorded GRIN profile relies fundamentally on the spatially modulated intensity pattern, the range of possible arbitrary gradient refractive index profiles[11] is extensive and probably second only to two-photon polymerization-based direct laser write[13] at fractions of the times required. This time requirement is especially significant when considering the fabrication of parts on the millimeter-scale or larger as the fabrication times needed scale dramatically.

Nevertheless, a significant hurdle to the realization of functional two-stage photopolymer-based GRIN optics is material performance, for which potential problems can be divided into two primary categories. First, at millimeter length scales there is significant Beer-Lambert absorption to consider that will result in a non-uniform intensity distribution along the optical/exposure axis. This gradient can be circumvented by using formulations with less photoinitiator although this reduction reduces the photosensitivity

and generally requires either longer exposure times or a higher intensity source to compensate. Second, there is the collective issue of achievable refractive index modulation (Δn) and the associated deficiencies incurred at higher Δn values. Previous reports have shown proof-of-concept demonstrations of recording a GRIN lens and lens array in two-stage photopolymers using a continuous wave (CW) 532 nm laser as well as arbitrary GRIN profiles using a digital micromirror device (DMD) with a narrowband incoherent UV LED to illuminate 8-bit grayscale intensity patterns. However, a major limitation in both instances was the maximum achievable Δn of the material ($< 5 \times 10^{-3}$) as shown by the weak phase function not exhibiting significant focusing. Functional GRIN lenses of moderate numerical aperture (NA) require Δn on the order of 10^{-2} to guide light. In this regard, recent advancements in the design of soluble, high refractive index writing monomers have begun to address this constraint on Δn. However these high Δn implementations were in thin films (sub-50 μm) where the tradeoff of absorption and photosensitivity are non-issues.[5] Herein, as shown in Scheme 0-1, we explore the feasibility of recording millimeter-scale GRIN optics in two-stage photopolymers using an inexpensive, off-the-shelf mask projection lithography system. The findings on optical deficiencies encountered in these thick GRIN materials were used to expand on an existing design scheme based on thiol-X ‘click’ chemistries[17, 18] for efficient high refractive index writing monomers.

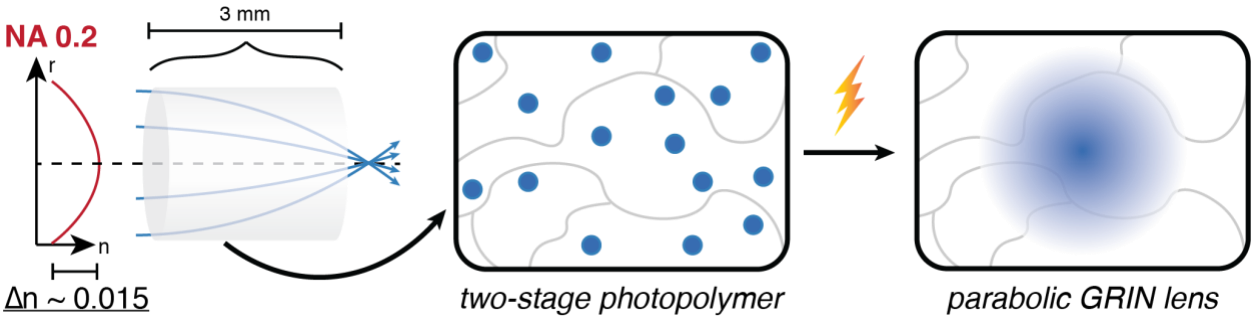

Scheme 0-1. Overview for the fabrication of high performance soft, flexible parabolic GRIN lenses via the optical patterning of high Δn two-stage photopolymers. A calculated refractive index profile for a 0.2 NA GRIN lens requires a material that is capable of a Δn of approximately 0.015 uniformly recorded over a 3 mm length.

1.14 Experimental

1.14.1 Materials

Generally, commercially available reagents were used without further purification. Thiophenol, 4-methyl thiophenol, 4-(methylsulfanyl) thiophenol, 2-naphthalene thiol, epichlorohydrin and butylated hydroxytoluene (BHT) free radical stabilizer were purchased from Alfa Aesar. 1,8-Diazabicyclo[5.4.0]undec-7-ene (DBU) was purchased from Chem-Impex International. 4-dimethylaminopyridine (DMAP) was purchased from Oakwood Chemical. Reagent-grade triethylamine (Et_3N) was purchased from Fisher Scientific. Acryloyl chloride and polycaprolactone-block-polytetrahydrofuran-block-polycaprolactone (average M_n 2000) were purchased from Sigma Aldrich. The photoinitiator, diphenyl(2,4,6-trimethylbenzoyl)phosphine oxide (TPO), was purchased from TCI America. Desmodur N3900 polyisocyanate was donated by Covestro AG (formerly Bayer MaterialScience).

Monomer Synthesis

Synthesis of di-substituted secondary alcohol

A previously reported procedure[5] was used for the combined thiol-epoxide ring-opening and thiol-halide substitution reactions between epichlorohydrin (1 equiv.) and a high refractive index monofunctional thiol (2.2 equiv.) to yield a secondary alcohol intermediate.

Synthesis of di-substituted acrylate

A previously reported procedure[5] was used for the synthesis of the acrylate from the secondary alcohol intermediate using acryloyl chloride.

Synthesis of BPTP-based urethane acrylate

To a 250 mL round-bottomed flask equipped with a magnetic stir bar, 6.05 g of BPTP (21.9 mmol, 1.0 equiv.), 3.33 g of 2-isocyanatoethyl acrylate (23.6 mmol, 1.08 equiv.), 0.487 g of BHT (2.21 mmol, 0.1 equiv.) were diluted with 23 mL of ethyl acetate (0.95 M w.r.t BPTP) and stirred under reflux overnight.

^{1}H NMR (400 MHz, Chloroform-*d*) δ 7.38 – 7.35 (m, 4H), 7.28 – 7.24 (m, 4H), 7.20 – 7.15 (m, 2H), 6.44 (dd, *J* = 17.3, 1.4 Hz, 1H), 6.13 (dd, *J* = 17.3, 10.4 Hz, 1H), 5.87 (dd, *J* = 10.4, 1.4 Hz, 1H), 5.03 (q, *J* = 5.9 Hz, 1H), 4.72 (t, *J* = 6.1 Hz, 1H), 4.18 (t, *J* = 5.3 Hz, 2H), 3.41 (q, *J* = 5.6 Hz, 2H), 3.27 (d, *J* = 5.9 Hz, 4H).

^{13}C NMR (101 MHz, $CDCl_3$) δ = 166.1, 155.5, 135.6, 131.6, 129.9, 129.1, 128.1, 126.6, 72.7, 63.6, 40.1, 36.6.

Two-stage photopolymer recording film preparation

Two-stage photopolymer film samples were prepared by premixing the acrylate writing monomer, 1,3-bis-(phenylthio)-2-propylacrylate (BPTPA), measured at 50 weight percentage (relative to the entire formulation) with 1 mol% TPO photoinitiator (based on writing monomer concentration) and the difunctional polyol in a 4 mL vial equipped with

a magnetic stir bar until homogenous. A stoichiometric amount (OH:NCO = 1:1) of Desmodur N3900 trifunctional isocyanate was added to the vial and stirred then degassed. The resin was deposited into custom-made cuvettes composed of a three component stack comprised of two outer 1" square glass slides with U-shaped cut glass spacers of defined thicknesses (1 & 3 mm) in the center. Each glass piece was bonded to the other with sodium silicate to form a single continuous piece.[19] Samples were covered in aluminum foil and allowed to cure overnight in an oven at 70ºC.

1.14.2 Methods

Nuclear Magnetic Resonance (NMR)

NMR spectra were recorded on a Bruker Avance-III 400 NMR spectrometer at 25 °C in chloroform-*d*. All chemical shifts are reported in ppm relative to chloroform solvent peak (δ = 7.26 ppm).

Refractive index measurements

A digital refractometer (Abbemat MW) was used to measure refractive index values at 20°C at the Fraunhofer lines – sodium-D (n_D, 589 nm), β hydrogen-F (n_F, 486 nm) and α hydrogen-C (n_C, 656 nm). Abbe number was calculated according to the equation, $V = (n_D-1)/(n_F-n_C)$.

Fourier Transform Infrared Spectroscopy (FTIR)

Fourier transform infrared spectroscopy was used to monitor the polymerization of the acrylate double bonds. A Thermo Scientific Nicolet 6700 FTIR spectrometer was used with a 405 nm LED source (Thorlabs) monitoring of the acrylate peak at 814 cm^{-1} with a timed illumination at 16 mW/cm^2. Optically thin samples were prepared between two salt (NaCl) plates using 15 μm spacers. The stage 1 to stage 2 acrylate conversion

($c_{acrylate}$) was monitored using a series scan, integrating over the range 790-830 cm^{-1} where $A_{initial}$ is the area of the unconsumed acrylate peak, and A_{final} is the area under the acrylate peak after the stage 2 reaction.

$$C_{acrylate} = (1 - \frac{A_{final}}{A_{initial}}) * 100\% \quad (1)$$

GRIN exposure and characterization system

The exposure system used to record GRIN structures is displayed in Scheme 0-2A. Briefly, an off-the-shelf 430 nm mounted LED source (Thorlabs M430L4) was homogenized using a combination of a square acrylic waveguide with a diffuser. A condenser lens then images the waveguide onto a grayscale photomask (Gamma Tech E6 slide film) to produce a defined intensity distribution. An OD4 425 nm longpass filter (Edmund Optics) was implemented to cut the undesired shorter wavelengths followed by an image-space telecentric lens to project the image of the mask with the appropriate demagnification and depth of focus for the desired beam diameter (ϕ = 1 mm) and working distance (approximately 3-4 mm) at the sample plane. The sample was placed on a mount attached to a three-axis stage synchronized to a computer for automated 2D grid exposures. A 633 nm He-Ne laser was co-aligned with the 430 nm beam for convenient exposure alignment and ensuring the sample was normal to the incident beam. After recording, the GRIN structure was analyzed by illuminating the sample with a flat phase, collimated 830 nm fiber-coupled laser diode. The wavefront immediately after the sample was magnified and imaged via a Keplerian telescope onto a Shack-Hartmann wavefront as shown in Scheme 0-2B. The measured phase delay relative to the incident flat phase is proportional to the Δn of the recorded GRIN.

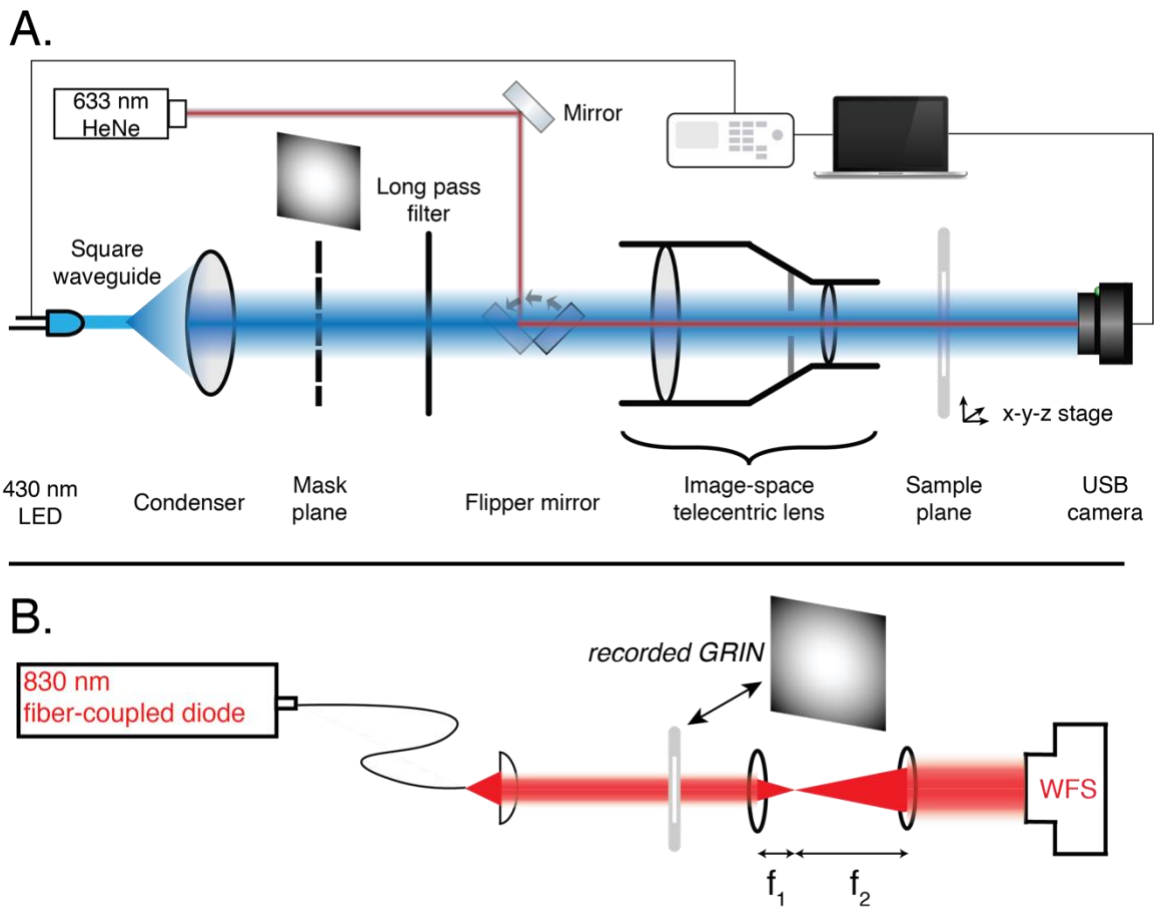

Scheme 0-2. Exposure system used to record and characterize GRIN structures. (A) Exposure system consists of a homogenized 430 nm LED and a 633 nm He-Ne laser for alignment purposes. The sample is situated on a mount connected to a three-axis stage that is computer-controlled to do 2D grid exposures. (B) Recorded GRIN samples are characterized using a fiber-coupled 830 nm laser diode with a Shack-Hartmann wavefront sensor.

1.15 Results & Discussion

A major goal of this work was to fabricate a quarter-pitch, soft and flexible parabolic GRIN lens with a NA of 0.2 using a high Δn two-stage material previously developed for holography. Based on the equation calculating the NA of a parabolic lens given by

$$NA = \sqrt{(n_0 + \Delta n)^2 - n_0^2} \quad (1)$$

where n_0 is the base refractive index, and Δn is the maximum refractive index modulation. Given that $n_0 = 1.47$ for the base urethane matrix with a desired NA of 0.2, a Δn just below 0.015 is required. This difference sets the minimum dynamic range requirements a material must achieve. Therefore, a two-stage formulation consisting of 50 wt% BPTPA was selected based on previously reported bulk refractive index change and holographic Δn results. For a 1 mm diameter lens, a length of approximately 3 mm was calculated to meet the quarter pitch specification.

At these length scales, absorption through the depth of the material becomes an important materials design consideration to ensure that the recorded refractive index profile is uniform in depth. To address this issue, exposure wavelengths were shifted beyond the typical absorption spectrum (i.e. $\lambda > 410$ nm) of the visible light photoinitiator used (TPO) allowing standard concentrations (1 mol% with respect to acrylate) to be used in the two-stage GRIN formulations. Specifically, calibration absorption curves were developed for TPO at the wavelength range of 410 to 450 nm before and after photolysis to obtain the logarithmic molar absorptivity spectrum shown in Figure 0-1. Evidently, a convenient wavelength of 430 nm, corresponding to an isosbestic point whereby absorption is invariant before and after photobleaching, was chosen for the GRIN exposure system using an inexpensive incoherent LED source. A drawback of this approach was the relatively broad bandwidth (15 nm FWHM) of the light source with significant amounts of power present at wavelengths down to 400 nm as shown by the dashed curve in Figure 0-2. Considering the orders of magnitude increase in molar absorptivity at these lower wavelengths, the designed material was evidently still optically thick. This issue was partially solved by the introduction of a commercial

longpass filter centered at 425 nm to cut off wavelengths below 420 nm as shown by the solid curve in Figure 0-2.

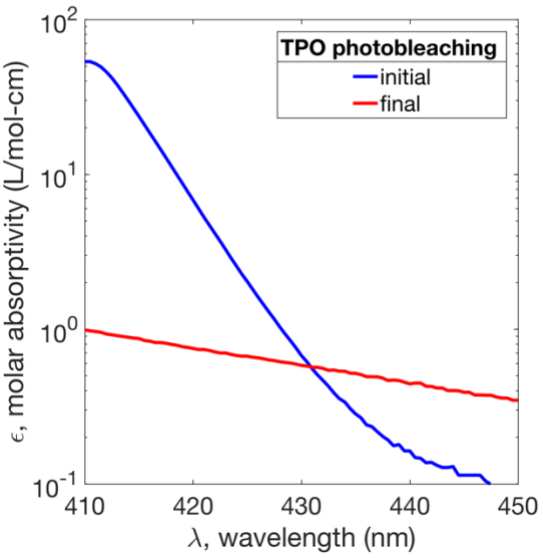

Figure 0-1. Molar absorptivity spectrum (logarithmic scale) of TPO before (in blue) and after (in red) after photolysis using a 10 mW/cm^2 405 nm LED irradiation for 10 minutes.

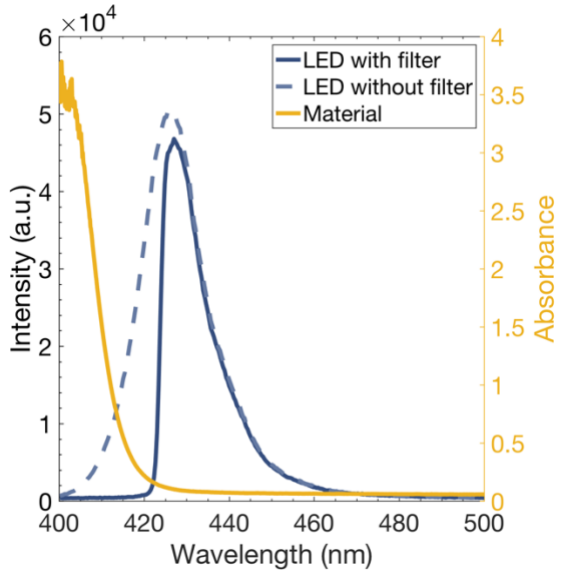

Figure 0-2. Overlay of the two-stage material absorption (1 cm thick) with the emission spectrum of a commercial 430 nm LED sources with (solid blue) and without (dashed blue) a 425 nm longpass filter.

The available intensity at the sample plane was measured to be approximately 40 μW/cm^2 requiring exposure times on the order of 60 minutes. Initial exposures in thin films ranging from 25 to 250 μm produced uniform phase structures. In particular, the measured phase delay of a 25 μm GRIN film corresponded faithfully with the expected Δn of ~0.02. However, at higher thicknesses (0.5 mm onwards) deleterious phase structures which scattered light were observed. These structures were collectively attributed as haze although they were distinguished as either forming within the exposure region or in the bulk after a flood exposure. The former appeared as long striations, and these undesired phase structures (present within the exposure regions) were imaged using differential interference contrast microscopy with typical images shown in Figure 0-3. Varying exposure times were used showing a sharp transition between faint but uniform phase structure (exposure 3) to a non-uniform, corrugated one (exposure 1).

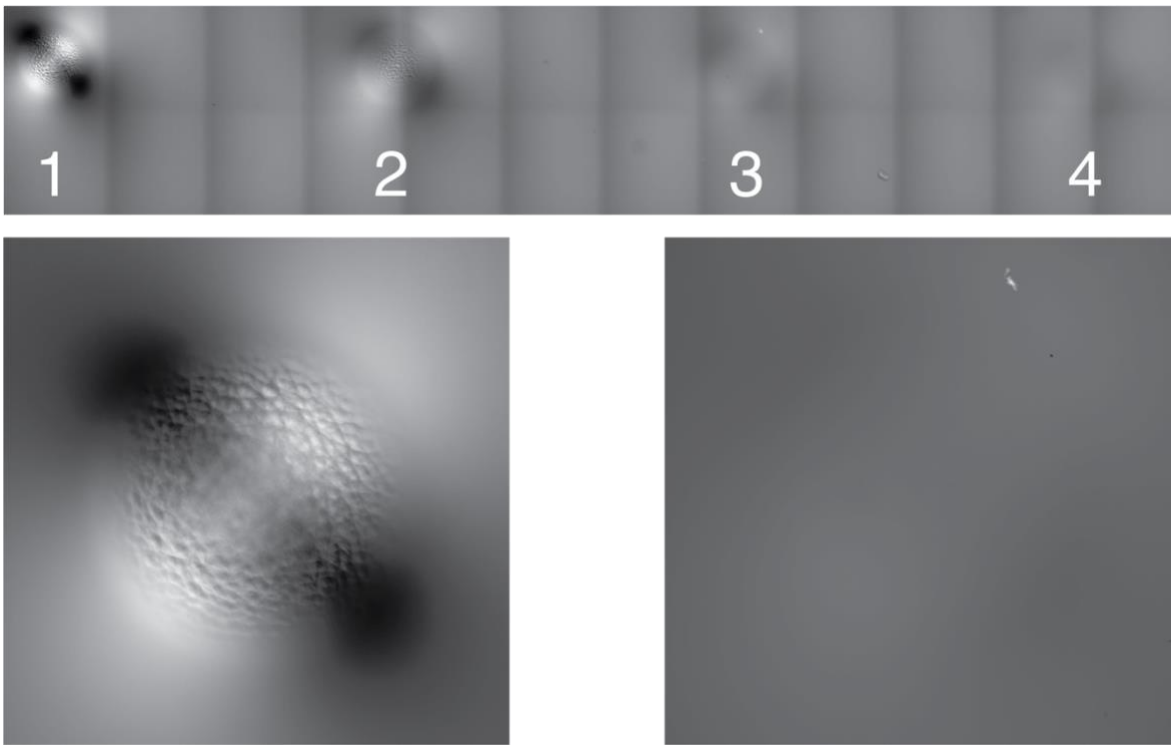

Figure 0-3. DIC images of a row of GRIN exposures of decreasing exposure times from left (1) to right (4). Close ups of exposure 1 and 3 are shown at the bottom. Phase irregularities are clearly evident on exposure 1 whereas exposure 3 looks faint but relatively uniform.

The second case of observed haze presented itself as a speckle pattern occurring throughout the bulk of the material as seen in Figure 0-4. Based on the undesirable amounts of haze observed in millimeter-thick BPTPA-based formulations, we hypothesized two possible explanations. First, the recording conditions were highly suboptimal due to the low absorption ($\epsilon < 10$ L/mol cm) at the recording wavelength coupled with the extremely low light intensity. This outcome has several implications including the low photoinitiator consumption causing significant non-linearities. Given that Δn development relies on reaction-diffusion, longer exposure times can be detrimental as polymerization and diffusion of multiple species (dissolved oxygen, monomer, oligomer, photoinitiator) occur on timescales that are inverted to what is

tested in holography. However, investigating this hypothesis essentially required a laser that could operate at 430 nm with moderate powers to achieve recording intensities on the order 1-20 mW/cm^2. This approach was outside the scope of this study.

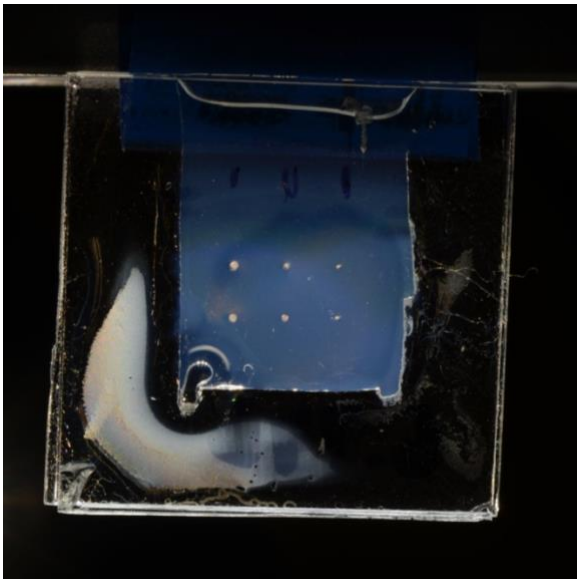

Figure 0-4. Photograph of a 3 mm thick two-stage formulation sample with a grid of GRIN exposures. The small individual exposure spots appear white and relatively opaque while the rest of the sample is translucent.

The alternative explanation considered was that writing chemistry solubility at high loadings (50 wt%) was the root cause. Phase separation or insolubility was not initially observed in thinner, holographic samples (≤ 250 μm thick) because any optical deficiencies present, such as haze/scatter, scale with the thickness of the material. Since lower loadings of BPTPA would not produce the required Δn, an alternative set of writing monomers with the following general characteristics were targeted: i) higher refractive index values to use at lower loading content, ii) moderately high refractive index with increased solubility, or ideally, iii) a combined improvement in both refractive index and solubility.

To achieve these aims, the conceived materials design strategy was reconsidered and expanded upon accordingly. To meet the first aim of primarily only increasing refractive index, we replaced the phenylthio substituent with higher refractive index groups by simply substituting in higher refractive index monothiols for the synthesis as shown in Scheme 0-3A. This substitution was conveniently achieved using derivatives of thiophenol (n_D/20°C = 1.588), namely 4-methylthiophenol, 4-(methylsulfanyl) thiophenol (n_D/20°C = 1.652) and 2-naphthalene thiol. The corresponding monofunctional acrylates were synthesized using the same procedure as BPTPA[5] to yield monomers with higher refractive indices (n_D/20°C) up to 1.6614 achieved for 1,3-bis-(naphthylthio)-2-propyl acrylate (BNTPA) and 1.6408 for 1,3-bis-(methylthiophenylthio)-2-propyl acrylate (BMTPTPA) although the 4-methylthiophenol analog, 1,3-bis-(methylphenylthio)-2-propyl acrylate (BMPTPA), had a moderately lower refractive index (n_D/20°C = 1.5921) in comparison to BPTPA (n_D/20°C = 1.6028). An alternative strategy explored was to use the high refractive index epoxide, 2-biphenylyl glycidyl ether, in a straightforward thiol-epoxide ring-opening reaction[17] to produce an asymmetric secondary alcohol that is then converted to a (meth)acrylate as shown in Scheme 0-3B. To demonstrate this modified approach, thiophenol was used to produce a viscous liquid monoacrylate (n_D/20°C = 1.6095).

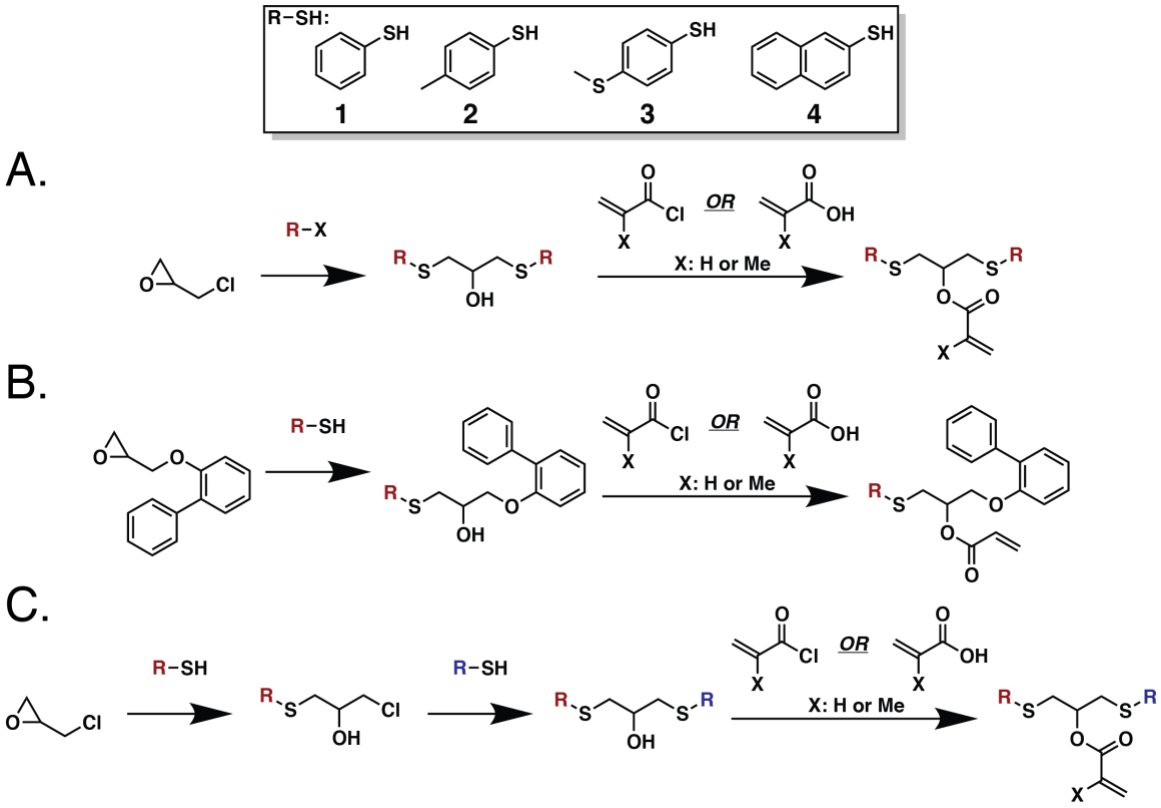

Scheme 0-3. Synthetic scheme for obtaining higher refractive index monofunctional acrylate writing monomers using high refractive index monofunctional thiols (R-SH). (a) The first strategy comprises the combined thiol-epoxide ring-opening and thiol-halide substitution reactions of epichlorohydrin with a high refractive index monothiol. (b) The second method involves the thiol-epoxide ring-opening of a high refractive index epoxide (here shown with 2-biphenylyl glycidyl ether) with a high refractive index monothiol. (c) The third approach combines the previous two in using two different high refractive index monothiols for the separate thiol-epoxide and thiol-halide reactions.

The series of writing monomers developed were tested in two-stage photopolymer formulations with 40 wt% writing monomer in the same urethane matrix used previously. Polymerization kinetics and final conversions assessments were performed using real-time FTIR with a timed 405 nm LED irradiation, and compared with BPTPA as the control at the same loading. As shown in Figure 0-5, all four of the acrylates achieve quantitative conversions with all the phenylthio-based derivatives (i.e. BPTPA, BMPTPA, and BMTPTPA) having nearly identical kinetic plots whereas the

dinaphthylthio-substituted monoacrylate, BNTPA, exhibited slightly slower kinetics. Overall, these results suggest a straightforward route to higher refractive index acrylate monomers than BPTPA with a majority of the desirable properties and characteristics intact such as the ability to dissolve 40 wt% of the writing monomer into the stage I urethane matrix.

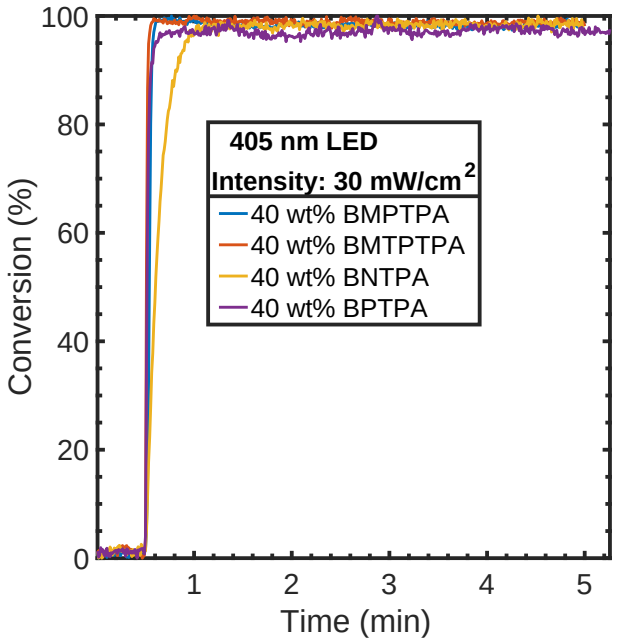

Figure 0-5. Real-time FTIR photopolymerization double bond conversion kinetics of 40 wt% loading of synthesized acrylate writing monomers in two-stage formulations. The 405 nm LED exposure (30 mW/cm^2) occurs at t = 0.5 min mark for 30 seconds.

To improve the writing monomer solubility, the overarching design approach taken was to incorporate urethane linkages, i.e. urethane (meth)acrylates, in the writing monomer via a straightforward and quantitative alcohol-isocyanate coupling reaction. Urethane acrylates are particularly appealing as they have been reported to exhibit enhanced propagation rates over their non-urethane containing counterparts.[20-22] Furthermore, urethane acrylates have been successfully employed in various two-stage

holographic photopolymer materials,[2, 23, 24] albeit in thin film applications. This approach allows for the use of a host of secondary alcohol intermediates generated from the earlier aim to be used to react with 2-isocyanatoethyl acrylate to yield the corresponding urethane acrylate as shown in Scheme 0-4A. This strategy was demonstrated using the precursor, 1,3-bis-(phenylthio)-2-propanol (BPTP), to get a highly viscous urethane acrylate (BPTPUA) with a measurably lower refractive index (n_D/20°C = 1.5782). An alternative approach to urethane (meth)acrylate monomers, shown in Scheme 0-4B is to instead use a high refractive index monofunctional isocyanate, such as 2-naphthyl isocyanate or 4-(methylthio)-phenyl isocyanate and functionalize it with 2-hydroxyethyl acrylate. However, this approach is limited to essentially only a single high refractive index substituent, and thus limits the range of achievable refractive index. This drawback is shown with the example using 4-(methylthio)-phenyl isocyanate to obtain a liquid urethane acrylate with a refractive index (n_D/20°C) of 1.5585, significantly lower than all the other monomers investigated. A full characterization of refractive index values and dispersion values (in terms of Abbe number) of synthesized monoacrylate writing monomers is presented in Table 0-1.

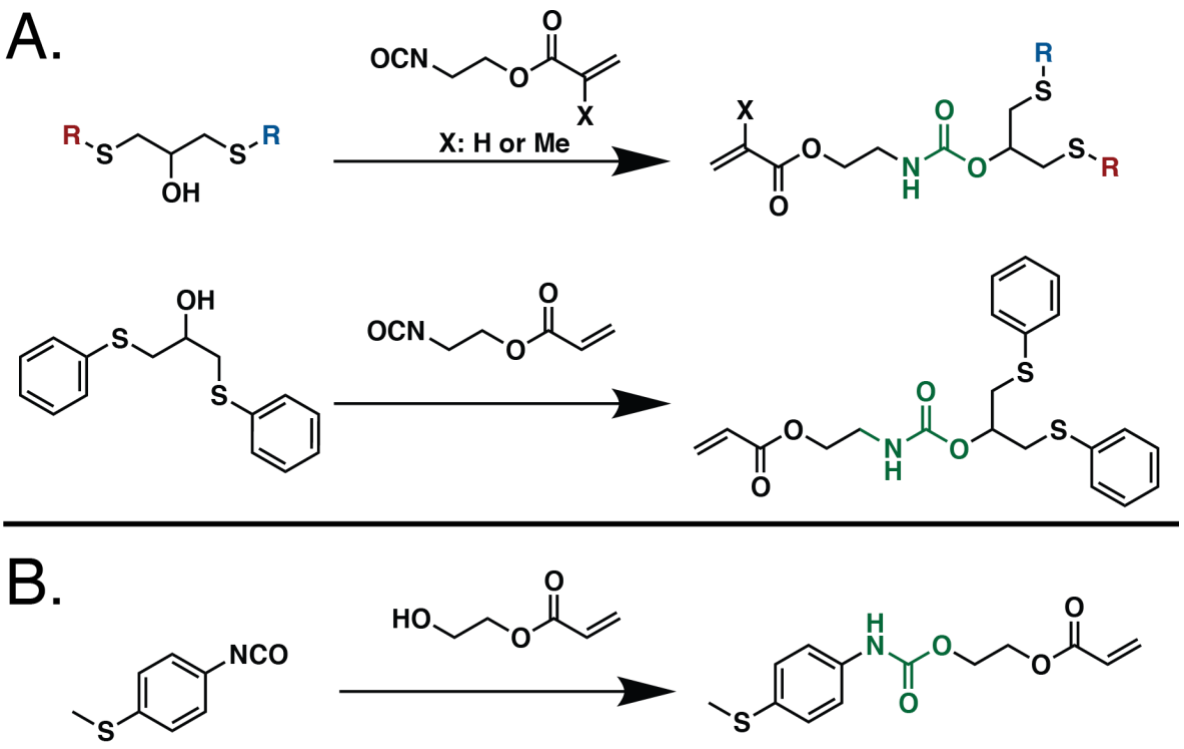

Scheme 0-4. Synthetic route for obtaining urethane acrylates. The urethane linkages present are expected to show improved solubility than their standard acrylate counterparts.

Table 0-1. Summary of synthesized high refractive index liquid acrylate writing monomers; n_D, n_F and n_C refers to the refractive index measured at λ = 589.3 nm, 486.2 nm, and 657.4 nm respectively. All refractive index measurements were taken at 20°C.

Compound	n_F	n_D	n_C	V
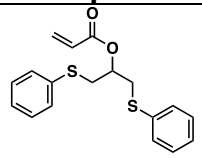 BPTPA	1.6188	1.6028	1.5967	27.3
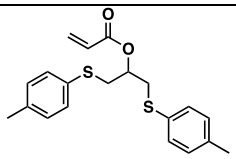 BMPTPA	1.6069	1.5921	1.5863	28.7
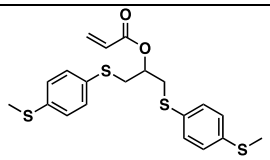 BMTPTPA	1.6615	1.6408	1.6291	19.8
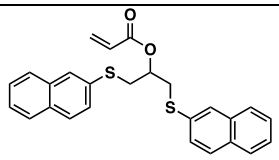 BNTPA	1.6859	1.6614	1.6524	19.7
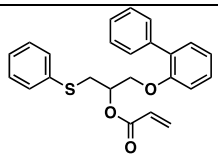	1.6269	1.6095	1.6028	25.3
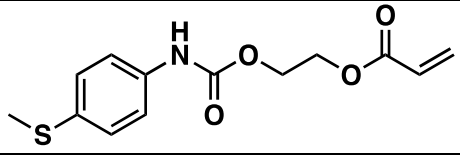	1.5734	1.5585	1.5532	27.7

To achieve writing monomers with a combined improvement in solubility and refractive index the idea of an asymmetric acrylate was explored. Here, as summarized in Scheme 0-3C, instead of the combined reactions of the thiol-epoxide ring-opening and the thiol-halide substitution, these reactions are separated and used with different monothiols to balance out a gain in refractive index with moieties that can aid in

solubility. This idea was preliminarily investigated using thiophenol and 4-(methylsulfanyl) thiophenol to yield an alcohol intermediate compound with a high refractive index value (n_D/20) of 1.6483. Further investigations along this path can incorporate a blend of the discussed strategies such as using multiple high refractive index substituents with a urethane bond present on a single writing monomer structure. These design strategies, though not explicitly investigated here, can also be extended to multifunctional systems to enable a more expansive set of writing chemistry formulations to tailor for specific application requirements in terms of film thickness, Δn, shrinkage, and haze/scatter etc.

1.16 Conclusions

The feasibility of employing high Δn two-stage photopolymer towards the fabrication of soft, flexible GRIN lenses was investigated. Using a simple and direct photomask projection lithography exposure system operating at 430 nm to achieve low absorptions, uniform phase structures were recorded in thin films (< 500 μm) realizing the expected Δn ~ 0.02. In thicker films, significant haze formation was encountered which prompted a thorough expansion of the writing monomer toolbox to optimize for Δn and haze. Liquid monomers with a refractive index increase of 0.0586 over the previously used BPTPA were achieved using a 2-naphthalene thiol derivative. In addition, facile routes to high refractive index urethane acrylate monomers were developed utilizing intermediates from previous methods. Overall, the extension of high refractive index writing monomers possessing a range of viscosities and structural moieties such as the carbamate linkage provides a critical foundation for specific

structure-property studies into the Δn-haze relationship for various applications involving the recording of phase structures in materials at varying thicknesses.

1.17 Supporting Information

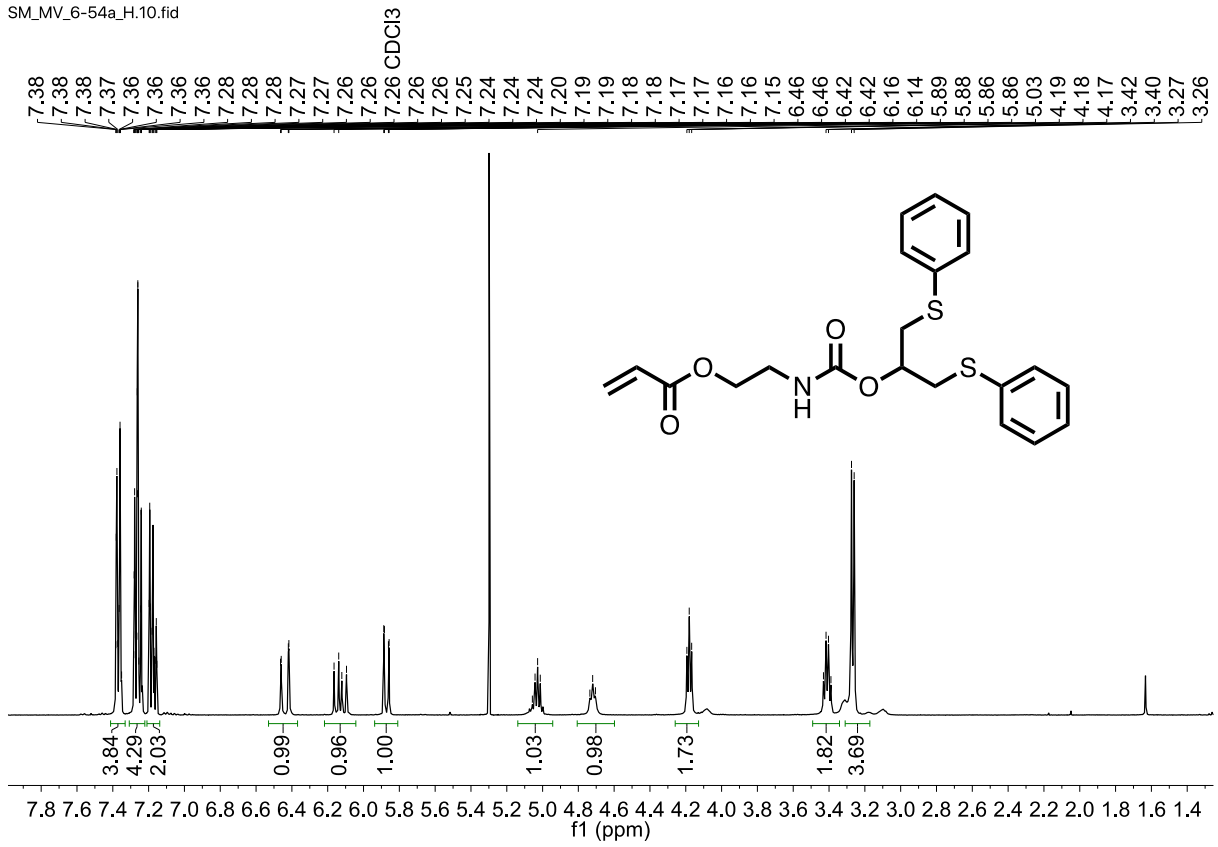

Figure S0-6. 1H NMR of BPTP-based urethane acrylate

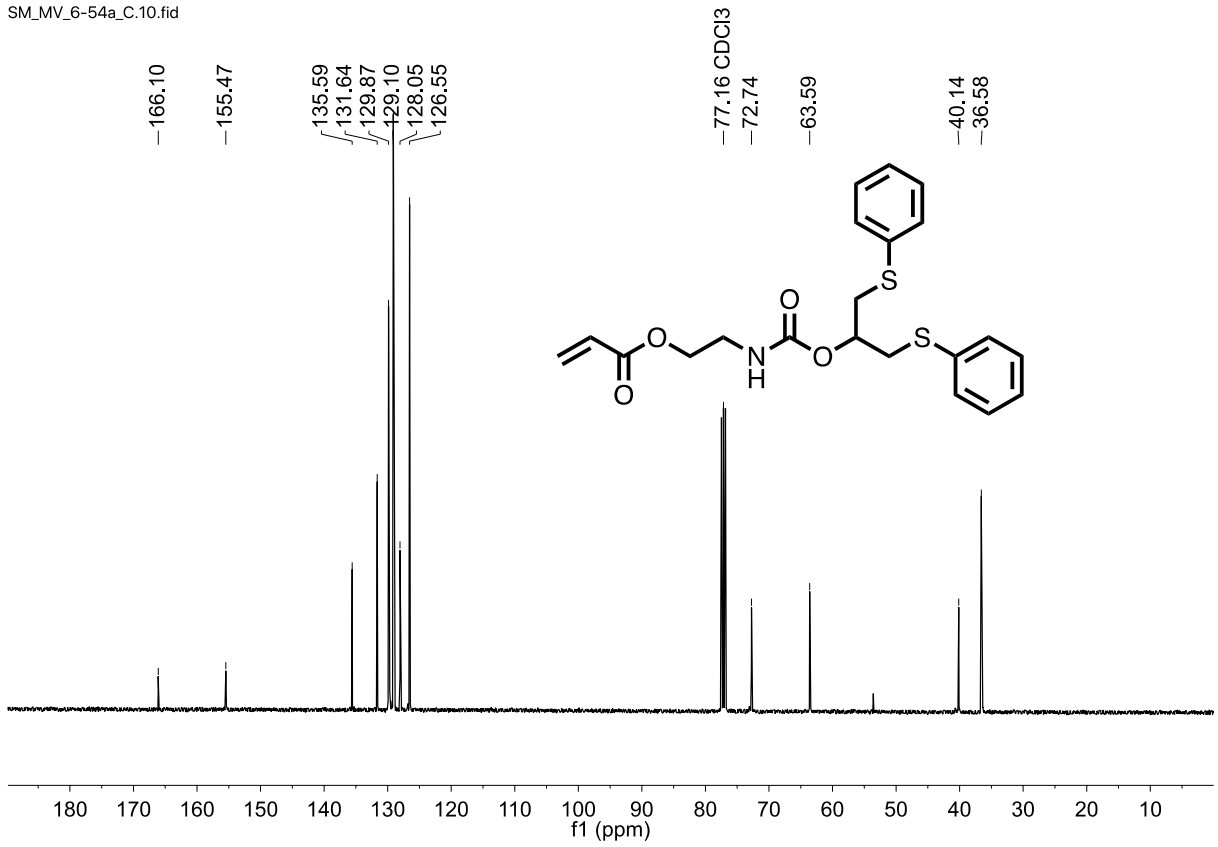

Figure S0-7. 13C NMR of BPTP-based urethane acrylate

1.18 Acknowledgements

This material is based upon work supported by Konica Minolta, the National Institute of Health, and the National Science Foundation under Grant No. ECCS 1307918 and Grant No. DMR 1310528.

1.19 References

1. Bruder, F. K.; Hagen, R.; Rölle, T.; Weiser, M. S.; Fäcke, T., From the Surface to Volume: Concepts for the Next Generation of Optical-Holographic Data-Storage Materials. *Angew. Chem., Int. Ed.* **2011,** *50*, 4552.

2. Bruder, F. K.; Fäcke, T.; Rölle, T., The Chemistry and Physics of Bayfol HX Film Holographic Photopolymer. *Polymers* **2017,** *9*, 472.

3. Peng, H.; Nair, D. P.; Kowalski, B. A.; Xi, W.; Gong, T.; Wang, C.; Cole, M.; Cramer, N. B.; Xie, X.; McLeod, R. R.; Bowman, C. N., High Performance Graded Rainbow Holograms via Two-Stage Sequential Orthogonal Thiol–Click Chemistry. *Macromolecules* **2014,** *47*, 2306.

4. Peng, H.; Wang, C.; Xi, W.; Kowalski, B. A.; Gong, T.; Xie, X.; Wang, W.; Nair, D. P.; McLeod, R. R.; Bowman, C. N., Facile Image Patterning via Sequential Thiol–Michael/Thiol–Yne Click Reactions. *Chem. Mater.* **2014,** *26*, 6819.

5. Alim, M. D.; Glugla, D. J.; Mavila, S.; Wang, C.; Nystrom, P. D.; Sullivan, A. C.; McLeod, R. R.; Bowman, C. N., High Dynamic Range (Δn) Two-Stage Photopolymers via Enhanced Solubility of a High Refractive Index Acrylate Writing Monomer. *ACS Applied Materials & Interfaces* **2018,** *10* (1), 1217-1224.

6. Coufal, H. J.; Psaltis, D.; Sincerbox, G. T., *Holographic data storage*. Springer: Berlin [etc.], 2000.

7. Hariharan, P., *Basics of holography*. Cambridge University Press: Cambridge, 2002.

8. Choi, K.; Chon, J. W. M.; Gu, M.; Malic, N.; Evans, R. A., Low-Distortion Holographic Data Storage Media Using Free-Radical Ring-Opening Polymerization. *Adv. Funct. Mater.* **2009,** *19* (22), 3560-3566.

9. Castagna, R.; Vita, F.; Lucchetta, D. E.; Criante, L.; Simoni, F., Superior-Performance Polymeric Composite Materials for High-Density Optical Data Storage. *Adv. Mater.* **2009,** *21* (5), 589-592.

10. Ye, C.; McLeod, R. R., GRIN lens and lens array fabrication with diffusion-driven photopolymer. *Opt. Lett.* **2008,** *33* (22), 2575-2577.

11. Urness, A. C.; Anderson, K.; Ye, C.; Wilson, W. L.; McLeod, R. R., Arbitrary GRIN Component Fabrication in Optically Driven Diffusive Photopolymers. *Opt. Express* **2015,** *23*, 264.

12. Moore, D. T., Gradient-index optics: a review. *Appl. Opt.* **1980,** *19* (7), 1035-1038.

13. Žukauskas, A.; Matulaitienė, I.; Paipulas, D.; Niaura, G.; Malinauskas, M.; Gadonas, R., Tuning the refractive index in 3D direct laser writing lithography: towards GRIN microoptics. *Laser & Photonics Reviews* **2015,** *9* (6), 706-712.

14. Kaehr, B.; Scrymgeour, D. A., Direct-write graded index materials realized in protein hydrogels. *Applied Physics Letters* **2016,** *109* (12), 123701.

15. Ohmi, S.; Sakai, H.; Asahara, Y.; Nakayama, S.; Yoneda, Y.; Izumitani, T., Gradient-index rod lens made by a double ion-exchange process. *Appl. Opt.* **1988,** *27* (3), 496-499.

16. Liu, J.-H.; Chiu, Y.-H., Process equipped with a sloped UV lamp for the fabrication of gradient-refractive-index lenses. *Opt. Lett.* **2009,** *34* (9), 1393-1395.

17. Brändle, A.; Khan, A., Thiol–epoxy 'click' polymerization: efficient construction of reactive and functional polymers. *Polymer Chemistry* **2012,** *3* (12), 3224-3227.

18. Lowe, A. B.; Bowman, C. N., *Thiol-X chemistries in polymer and materials science*. RSC Publishing: Cambridge, 2013; p xvii, 317 pages.

19. Observatory, L. I. G. W. Silicate Bonding Procedure (Hydroxide-Catalysis Bonding) https://dcc.ligo.org/public/0013/E050228/001/E050228-00_Silicate%20bonding%20procedure.pdf (accessed 3/21/19).

20. Cramer, N. B.; O'Brien, C. P.; Bowman, C. N., Mechanisms, polymerization rate scaling, and oxygen inhibition with an ultra-rapid monovinyl urethane acrylate. *Polymer* **2008,** *49* (22), 4756-4761.

21. Beckel, E. R.; Stansbury, J. W.; Bowman, C. N., Effect of Aliphatic Spacer Substitution on the Reactivity of Phenyl Carbamate Acrylate Monomers. *Macromolecules* **2005,** *38* (8), 3093-3098.

22. Barner-Kowollik, C.; Bennet, F.; Schneider-Baumann, M.; Voll, D.; Rölle, T.; Fäcke, T.; Weiser, M.-S.; Bruder, F.-K.; Junkers, T., Detailed investigation of the propagation rate of urethane acrylates. *Polymer Chemistry* **2010,** *1* (4), 470-479.

23. Glugla, D. J.; Chosy, M. B.; Alim, M. D.; Childress, K. K.; Sullivan, A. C.; McLeod, R. R., Multiple patterning of holographic photopolymers for increased refractive index contrast. *Opt. Lett.* **2018,** *43* (8), 1866-1869.

24. Bruder, F.-K.; Hagen, R.; Rölle, T.; Weiser, M.-S.; Fäcke, T., From the Surface to Volume: Concepts for the Next Generation of Optical–Holographic Data-Storage Materials. *Angew. Chem.-Int. Edit.* **2011,** *50* (20), 4552-4573.

Dynamic Networks in Two-Stage Holographic Photopolymers[1]

Dynamic networks in two-stage holographic photopolymers were investigated for the first time by incorporating allyl sulfides into the backbone of a polyurethane network. Systematic controlled studies were performed on the effects of allyl sulfide content in two-stage systems in terms of polymerization rate kinetics and conversion, base matrix refractive index increment as well as the associated stress relaxation kinetics and behavior. While the polymerization rates and final conversions remain unaffected by the presences of allyl sulfides, the base refractive index increment became substantial at higher allyl sulfide loadings (0.029 increase at 80 mol%). It was conclusively revealed that allyl sulfides effectively reduced the stresses induced from the acrylate photopolymerization. The introduction of thiols either by itself or with acrylates present were shown to noticeably increase the rate of stress relaxation compared to only having acrylates. Crucially, both reflection and transmission holograms were successfully recorded at a 135 and 1000 nm pitch respectively indicating a good spatial frequency response.

1.20 Introduction

Two-stage photopolymers are useful materials for optically recording refractive index structures in an otherwise transparent medium and have been used towards

[1] Contributing authors: Brady T. Worrell, Matthew K. McBride, Sudheendran Mavila, Maciej Podgórski, Amy C. Sullivan, Benjamin Kowalski, Robert R. McLeod, and Christopher N. Bowman

various holographic, gradient refractive index and diffractive optics applications. The primary constituents comprise a stage I matrix and stage II writing chemistry with preference for the two reaction stages to be orthogonal in nature. As refractive index structures are recorded via reaction-diffusion driven by the gradients in light intensity, most two-stage formulations entail a low crosslink density network with a low (typically sub-ambient) glass transition temperature (T_g) used to facilitate mass transport of the dissolved writing chemistry (i.e. monomer and photoinitiator). For this reason, stage I matrices are typically low in their refractive index ($n_D < 1.5$) while the incorporated writing monomers are preferably high refractive index ($n_D > 1.6$) to generate a high refractive index modulation (Δn). In this regard, multiple combinations of chemistries have been explored with the basic network structure of the stage I matrix formed thermally or spontaneously at ambient temperature.[1-4] Amongst the possible options, the polyurethane network has been recognized as a model stage I matrix when used in conjunction with rapidly photopolymerized acrylates as the high refractive index stage II writing monomers.[5-7]

Despite extensive research on the writing chemistry aspect of two-stage photopolymers, there has been a limited evaluation of the involvement of the stage 1 network beyond its simple role as a static host. While there has been previous work exploring the compatibility of writing monomers in a given urethane matrix through fundamental and functional solubility tests,[5] with the exception of a few approaches noted below, there is little to no information on the effects of the network with respect to recording refractive index structure. This shortage of information is because while the contributions and effects of the writing chemistry are direct and recognizable, studies on

modification to the host matrix are less straightforward to isolate as the direct cause. Furthermore, changing the network-forming monomers typically involves changing important factors such as: the base refractive index of the network, glass transition temperature of the network (T_g), molecular weight between crosslinks (M_c), and crosslink density (ρ_c). Such network modifications typically influence the reaction-diffusion properties of the writing step in a manner that makes direct comparisons between formulations with the same amount of writing chemistry difficult. This dissonance is exacerbated when trying to compare different network chemistries (e.g. alcohol-isocyanate[5, 6, 8, 9] vs. thiol-Michael[3, 10]) where, for example, the latter forms a relatively higher refractive index base network due to thioether formation at every network junction.

The prevailing concept on most two-stage holographic photopolymer systems is that the stage 1 matrix acts as a passive bystander throughout the recording process. Although there are undoubtedly mechanical, swelling and solubility effects of the network in response to the photopolymerization and mass transfer events occurring during and after recording, the network is not intentionally designed to actively participate. In fact, the involuntary effects of the network are presumed to be deleterious rather than being either beneficial or neutral due to the buildup of localized stresses imposed by the recording process. These highly localized mechanical stresses can result in mechanical warping birefringence (photoelasticity) that negatively impacts the final recording performance.

To address this deficiency, several network modification strategies have been considered to accommodate these limitations. In general, these approaches involve the

introduction of a chemical substituent attached to the network or within the backbone capable of actively participating during the photopolymerization process. These substituents are broadly categorized as being either ‘static’ or ‘dynamic’. Static implementations are network-bound groups that only participate with the polymerization in a single event and can include either the introduction of polymerizable groups (such as acrylates) or radical trap groups (such as 2,2,6,6-Tetramethyl-1-piperidinyloxy, TEMPO) as preferential termination sites. Notably, the latter has been reported in the patent literature to be a key component for increasing dynamic range (Δn) significantly in two-stage holographic photopolymers. On the other hand, dynamic network implementations involve the incorporation of dynamic covalent chemistry (DCC) groups within the network to enable dynamic bond exchange of the network. Unlike with static network approaches, dynamic networks have the advantage of being capable of multiple events and continuous participation, thus offering significantly more opportunities for overcoming the limitations of the network.

In recent years, multiple DCCs have been reported[11] and successfully implemented in a variety of crosslinked networks[12-16] as part of the Covalent Adaptable Networks (CANs) or vitrimers paradigm[17-19] whereby dynamic bond exchange occurs upon an applied stimulus or condition to enable ‘flow’ in covalently crosslinked systems. However, given the specific optical requirements of two-stage holographic photopolymers (such as having colorless and transparent films and short timescales) a majority of DCCs are not suitable for implementation for reasons including color,[15, 16, 20, 21] catalyst and temperature requirements,[14, 22] bond exchange rates and the mechanism of the dynamic exchange itself.[19, 23] An important consideration is also the synthetic

accessibility and ease of implementation into a two-stage photopolymer scheme bearing in mind the potential for undesired cross-reaction of multiple species. With this in mind, an appropriate choice of DCC for incorporation into existing high performance two-stage photopolymer systems is the allyl sulfide moiety, specifically, and addition-fragmentation chain transfer (AFT), generally. Being a radical-mediated process, AFT as a dynamic exchange reaction is readily photoinduced with conventional radical photoinitiators, a component already used in most two-stage holographic systems. Numerous reports have shown the efficacy of allyl sulfides in reducing shrinkage stress both during[24] and after[12, 25] network formation due to a bond rearrangement cascade whereby, under appropriate conditions, an active center effectively diffuses through the network[26] without altering its overall crosslink density. Furthermore, a previously reported allyl sulfide-containing diol[26] is readily synthesized in one step via a thiol-halide substitution reaction using commercially available 3-chloro-2-chloromethyl-1-propene and 2-mercaptoethanol.

Here, the first investigation of DCCs implemented into two-stage holographic photopolymers is presented with the goal of enabling active network participation during the optical recording process so as to alleviate recording-induced shrinkage stresses and modulate the photopolymerization favorably for increasing Δn. The radical-mediated allyl sulfide was selected as the DCC for implementation on the basis of optical material requirements as well as the exchange efficiency and suitability for implementation. Fundamental studies on polymerization rate kinetics and refractive index contributions were studied to understand the impact of allyl sulfide contributions at varying concentrations. Using a standard, though unoptimized, writing chemistry we

demonstrate the ability to record uniform, high quality holograms in both transmission and reflection geometries covering a wide pitch range of approximately 135 to 1000 nm using mild exposure conditions of 10 seconds or less at 10 mW/cm^2.

1.21 Experimental

1.21.1 Materials

Commercially available reagents were used without further purification. Dibromopropane and 2-mercaptoethanol were purchased from Alfa Aesar. Sodium methoxide and 3-chloro-2-chloromethyl-1-propene were purchased from Sigma-Aldrich. Absolute ethanol, dichloromethane (DCM) and methanol (MeOH) were purchased from Fisher Scientific.

Synthesis of allyl sulfide diol (AS-diol)

A previously reported procedure was followed.[26] Briefly, 3-chloro-2-chloromethyl-1-propene was reacted with a slight excess of 2-mercaptoethanol using sodium methoxide as the base in MeOH.

Synthesis of control diol (C-diol)

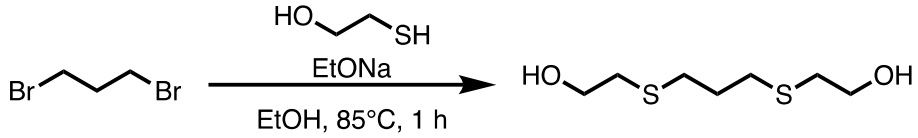

To a 500 mL round-bottomed flask equipped with a magnetic stir bar was added 7.73 g (6.94 mL, 99.0 mmol, 2.00 equiv) of 2-mercatoethanol was diluted with 150 mL (0.30 M, w.r.t dibromopropane) of absolute ethanol. To this solution, 6.74 g (99.0 mmol, 2.00 equiv) of sodium ethoxide was added portion-wise at room temperature. The flask was refluxed for 30 min under nitrogen atmosphere. After this period, 10 g (49.5 mmol, 2.00 equiv) of 1,3-dibromopropane was added dropwise to the reaction mixture to form a

yellow precipitate. The reaction mixture was refluxed for another 1 h. After this period, the reaction mixture was cooled to room temperature. The precipitate was filtered off through a short pad celite. The filtrate was evaporated to remove the volatiles. The crude product was purified by silica-gel column chromatography using 5% MeOH in DCM as eluent to give pale yellow liquid. The product was dissolved in EtOH (50 mL) and activated charcoal was added. After stirring overnight at room temperature the charcoal was filtered off through a short pad of celite and the filtrate was evaporated to give 7.0 g (72%) of the title compound as a colorless liquid.

C-diol: colorless liquid; 72 % yield; R_f = 0.28 (TLC conditions: 5 % MeOH/DCM); NMR (400 MHz, $CDCl3_6$) δ = 3.76 (t, 4H), 2.75 (t, 4H), 2.67 (t, 4H), 2.23 (s, 2H), 1.92 (q, 2H).

1.21.2 Methods

Fourier Transform Infrared Spectroscopy (FTIR)

Fourier transform infrared spectroscopy was used to monitor the polymerization of the acrylate double bonds. A Thermo Scientific Nicolet 6700 FTIR spectrometer was used with a 405 nm LED source (Thorlabs) monitoring of the C=C peak at ~6170 cm^{-1} with a timed illumination at 10 mW/cm^2. Two-stage photopolymer films approximately 250 μm thick were analyzed in the near-infrared region. The stage 1 to stage 2 acrylate conversion ($c_{acrylate}$) was monitored using a series scan, integrating over the range 6150-6200 cm^{-1} where $A_{initial}$ is the area of the unconsumed acrylate peak, and A_{final} is the area under the acrylate peak after the stage 2 reaction.

$$C_{acrylate} = (1 - \frac{A_{final}}{A_{initial}}) * 100\% \quad (1)$$

In-situ stress relaxation

A RSA-G2 dynamic mechanical analyzer (TA Instruments) was used to perform stress relaxation experiments using the built-in stress relaxation mode with a 5% strain applied at ambient temperature. Films were cut into rectangular strips and measured with calipers prior to instrument loading.

Holographic recording

A two-beam interference setup was used to record volume transmission holograms with a spatially filtered wavelength stabilized 405 nm laser diode (Ondax, 40 mW). Both recording beams ($1/e^2$ intensity diameter of 4.3 mm) were power matched to give a total recording intensity of ~10 mW/cm^2. The beams were interfered at an external recording half-angle of 11.7° to produce a sinusoidal interference pattern with a fringe spacing of ~1 μm. A 633 nm He-Ne laser (Thorlabs), aligned approximately at the Bragg reconstruction angle, was used as a read beam to nondestructively probe the hologram formation throughout the recording process. Each recording exposure was initially monitored for 300 s, then followed by a sample rotation from 10° to -10° at an angle increment of 0.05°. The optical power at both of the two detectors was measured throughout the experiment. The diffraction efficiency of each recorded hologram was calculated by taking the quotient of the diffracted power (P_d) to the total power (transmitted + diffracted), $DE = I_d/(I_d + I_t)$. The diffraction efficiency vs. angle profile was fitted to Kogelnik coupled wave theory[27] to obtain a peak-to-mean Δn and thickness (d).

A one beam reflection setup was used to record volume reflection holograms with a spatially filtered wavelength stabilized 405 nm laser diode (Ondax, 40 mW). A collimated 1” diameter beam was redirected towards the optical table with a periscope

mirror. A coupon consisting of the sample and a mirror were placed on the table with index matching fluid (water or xylene) in between.

1.22 Results & Discussion

The introduction of DCCs in a network fundamentally deviates from the classical concept of orthogonality between the two stages, i.e. network and writing chemistries. As illustrated in Scheme 0-1, while the writing chemistry remains unperturbed (i.e. does not react) during the stage I network formation, the same is not true during the stage II recording. The key distinction of a two-stage system with a DCC-containing network is that, instead, stage I and II interactions are critically enabled by the DCC moiety. Specifically, dynamic exchange allows for bond rearrangement, via bond-breaking and bond-forming, to occur during and after the stage II acrylate homopolymerization. Therefore, network stress relaxation occurs to accommodate the shrinkage stresses developed by the patterning exposure. In the case of the AFT-based allyl sulfide, any radical species will add to the double bond to form a radical intermediate that results in a fragmentation. However, depending on the radical species adding to the allyl sulfide, the AFT exchange may either be reversible when the same thiyl radical species is being added and fragmented, or irreversible if a carbon-centered radical, such as the acrylic radical, is involved.

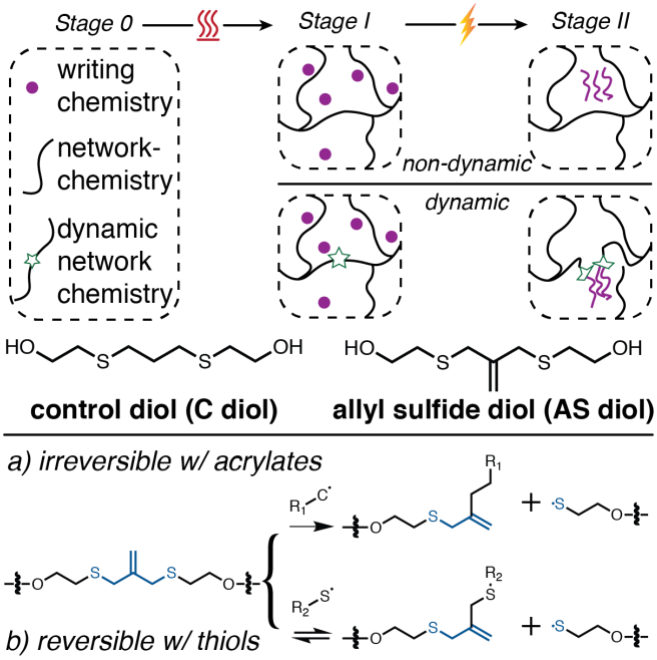

Scheme 0-1. Schematic illustration of how two-stage systems with DCC-containing networks fundamentally differ from the conventional two-stage systems without DCC. In the former case, during the photopatterning step the stage I network is capable of interacting with the stage II writing chemistry via the DCC moiety. In the case of allyl sulfides, if a) acrylic radicals are solely involved, the exchange is irreversible. However, when b) thiyl radicals are present, the AFT mechanism instead becomes reversible.

To control for the effects of network crosslinking density, resins for the investigation of allyl sulfide were formulated by substituting either an allyl sulfide diol (AS-diol) or control diol (C-diol) for the high molecular weight polyol in an otherwise standardized two-stage formulation as described in the experimental section. Both AS-diol and C-diol have close to identical molecular weights (same M_c and ρ_c) and both contain two sulfur atoms (similar base refractive index) with the only major difference being that C-diol does not have a carbon-carbon double bond located at the central carbon atom of the symmetric molecule. This distinction means that C-diol is incapable of undergoing AFT and thus forms ‘non-dynamic’ materials. Two loadings of each diol at 20 and 80 mol% were designed to give four formulations corresponding to a low and

high network crosslink density respectively. Details of each of the four formulations are listed in Table 0-1.

Table 0-1. Composition for each tested formulation for allyl sulfide-containing dynamic matrices study. A stoichiometric stage I polyurethane network is formed whereby either C diol or AS diol is incorporated at 20 or 80 mol%. The stage II writing chemistry is maintained at 30 wt% TBPA of the overall formulation with TPO set at 1 mol% with respect to the writing monomer.

Formulation	**AS diol**	**Polyol**	**Desmodur N3900**	**TBPA**	**TPO**
C20	20	80	100	30 wt%	1 mol%
C80	80	20	100	30 wt%	1 mol%
AS20	20	80	100	30 wt%	1 mol%
AS80	80	20	100	30 wt%	1 mol%

Previous investigations into radical photopolymerizations in the presence of allyl sulfides were shown to retard the polymerization rate due to the competition of radicals.[24] The allyl sulfide moiety acts as a chain-transfer agent that can transiently sequester a propagating radical to reduce the overall polymerization rate. In the case of an acrylate photopolymerization system, propagation rates are expected to be fast enough to not be able to notice any difference in polymerization kinetics. A preliminary investigation into this involved a real-time FTIR study whereby the AS diol was substituted at varying loadings (inequivalent M_c and ρ_c) and compared. As shown in Figure 0-1, dramatically different polymerization rates were observed using the same irradiation conditions.

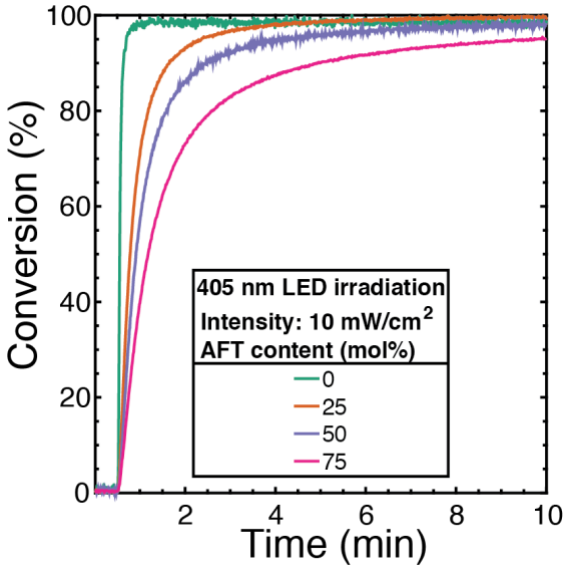

Figure 0-1. FTIR reaction kinetics in two-stage formulations with increasing amounts of AS diol in replacement of the polyol resulting in increasing crosslinking density. A continuous 405 nm LED irradiation of 10 mW/cm^2 was turned on 30 s after the start of the run.

However, when formulations were adjusted to account for the differences in network parameters, i.e. maintaining constant M_c and ρ_c, identical reaction kinetics were observed as shown by the overlapping plots in Figure 0-2. This set of FTIR results clearly demonstrate the importance of controlling the network configuration for correct DCC incorporation to enhance rather than diminish recording performance. Another consideration is the relative concentration of the allyl sulfide moieties present in the network relative to the writing chemistry. In this respect, although not investigated, higher molecular weight polyols containing multiple allyl sulfide moieties can be readily obtained by a simple alcohol-isocyanate oligomerization of the studied allyl sulfide diol with non-allyl sulfide diols and diisocyanates. This approach is analogous to a previously reported method of obtaining allyl sulfide-containing diacrylate liquid crystal oligomers via the thiol-Michael reaction.[25]

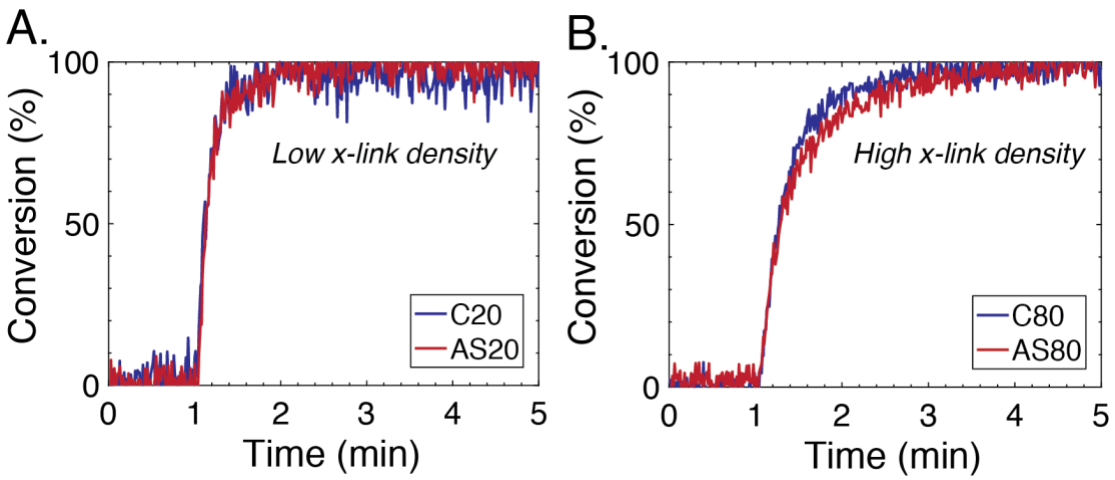

Figure 0-2. FTIR reaction kinetics in two-stage formulations with either C diol or AS diol in replacement of the polyol at (A) 20 mol% diol relative to the polyol or (B) 80 mol% diol relative to the polyol. A continuous 405 nm LED irradiation of 10 mW/cm^2 was turned on 1 min after the start of the run. While the allyl sulfide moiety itself does not noticeably impact the polymerization kinetics, a higher stage I crosslink density does reduce the conversion rate marginally presumably due to the lower diffusion rate of the writing chemistry in a stiffer, higher T_g matrix.

An important consideration of introducing sulfur-containing allyl sulfides, especially at high concentration loadings, is the impact on Δn due to the increase of the base network's refractive index. To verify this impact, we measured the refractive index at 20°C for the three visible wavelengths used for the Abbe number calculation for two-stage formulations without TBPA writing monomer (i.e. stage 0), with 30 wt% TBPA writing monomer unpolymerized (i.e. stage I), and 30 wt% TBPA writing monomer polymerized (i.e. stage II) as well as the base matrix only as listed in Table 0-2. Comparing the various base matrices (i.e. no writing monomer present), it is evident that 20 mol% of either AS-diol or C-diol has a minimal effect on increasing refractive index with a marginal increase of 0.0021 and 0.0025 respectively. However, at 80 mol% loading of either diol the refractive index increment is 0.0298 and 0.0291 for AS-diol and C-diol respectively. This disproportionate increase in refractive index can be partially

explained by the concomitant increase in crosslink density due to the higher proportion of low molecular weight diols; although these results indicate the relative tradeoff faced in considering between improving the dynamic AFT exchange versus lowering the overall Δn due to the increase of the base refractive index.

Table 0-2. Stage 0, I and II refractive index values and Abbe number values for two-stage films containing allyl sulfide and control diols (20 & 80 mol% loading).

Formulation	**n_D**	**n_F**	**n_C**	**V**
Matrix only	1.4808	1.4870	1.4783	55.3
C20 – stage 0	1.4833	1.4897	1.4808	54.4
C20 – stage I	1.5077	1.5159	1.5045	44.5
C20 – stage II	1.5142	1.5223	1.5111	45.8
C80 – stage 0	1.5099	1.5171	1.5070	50.2
C80 – stage I	1.5310	1.5400	1.5275	42.2
C80 – stage II	1.5383	1.5472	1.5348	43.5
AS20 – stage 0	1.4829	1.4893	1.4804	54.4
AS20 – stage I	1.5077	1.5159	1.5045	44.6
AS20 – stage II	1.5151	1.5232	1.5119	45.7
AS80 – stage 0	1.5106	1.5181	1.5077	49.1
AS80 – stage I	1.5319	1.5411	1.5283	41.5
AS80 – stage II	1.5399	1.5490	1.5363	42.5

Stress relaxation kinetics in two-stage formulations

As a proof-of-concept experiment, in-situ stress relaxation experiments were performed with a 405 nm LED irradiation (10 mW/cm^2) to confirm whether the allyl sulfide was contributing effectively within the system. Two systems were investigated, a control without any allyl sulfide and a system with 50 mol% AS-diol substituted for the polyol were chosen to conduct a baseline assessment of the efficacy of allyl sulfide units. Therefore, it is important to note that, as with the initial set of FTIR results, the

crosslinking densities of these two systems were not the same or normalized. Nevertheless, this crosslink density dependence does not change the DMA results shown in Figure 0-3 whereby photopolymerization-induced stresses manifested in an increase in the overall modulus of the material (E), which was clearly observed in both systems (with and without allyl sulfide) upon irradiation from the increase in the normalized modulus (E/E_0) plot on the secondary y-axis. In the case of the control system without allyl sulfides present, the acrylate photopolymerization resulted in a permanent increase in E. However, with allyl sulfide present, the initial increase in stress is noticeably reduced throughout the irradiation. This conclusively showed that the propagating radicals formed were able to add to the allyl sulfide units present in the network backbone and effectively incorporate the acrylate homopolymer into the network. This network rearrangement caused a dissipation of the polymerization-induced stresses during the irradiation.

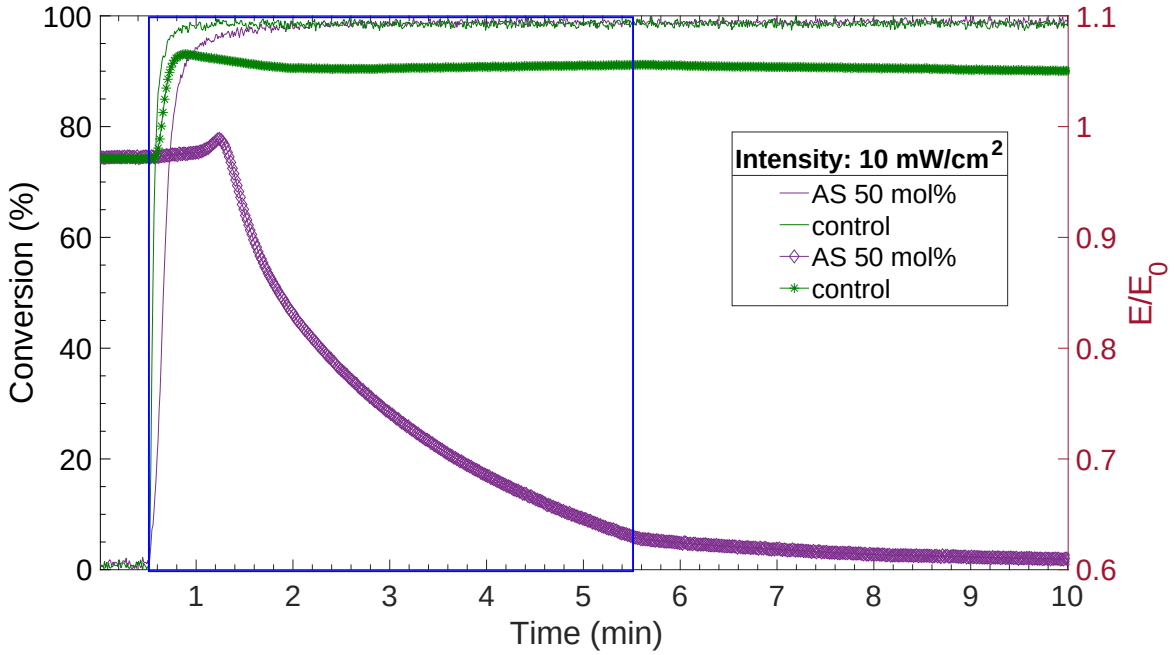

Figure 0-3. Overlaid plot of FTIR photopolymerization kinetics (primary y-axis) and stress relaxation kinetics (secondary y-axis) due to photopolymerization-induced stress from a uniform 405 nm LED irradiation (10 mW/cm^2, represented by the blue box from t = 0.5 min for 5 min) of a two-stage formulation with either 50 mol% allyl sulfide (purple) or no allyl sulfide (green). An increase in modulus results from the acrylate homopolymerization. Part of this modulus increase is attributable to the shrinkage stresses that developed due to the polymerization. With allyl sulfides present, the propagating carbon-centered radical was able to add to the network backbone to partially reduce the polymerization-induced stresses.

However, it is notable that the relaxation of the stresses in Figure 0-3 did not decrease all the way. Further investigation on why this stress relaxation was limited revealed that the carbon-centered acrylic radicals irreversibly added to the allyl sulfides and thus resulted in termination rather than fragmentation which effectively consumes the available allyl sulfides.[24] In contrast, introducing thiols into the system leads to the formation of thiyl radicals that can add reversibly to the allyl sulfide via RAFT, form a tris(methyl sulfide) radical intermediate and then fragment to regenerate another allyl sulfide and thiyl radical. Thus, the propensity of a cascading AFT mechanism is

significantly increased with thiol radicals present instead of acrylic radicals. This hypothesis was verified with the same stress relaxation experiments performed using systems containing either acrylate writing monomer only (40 wt% TBPA), thiol only (20 wt% HDT), or both species present together (10 wt% HDT and 20 wt% TBPA) as displayed in Figure 0-4. Evidently, the system with both thiol and acrylate present displayed the most rapid and complete stress relaxation as the acrylates presumably polymerized with significant amounts of chain transfer with the free thiols present to form thiyl radical that were then able to undergo AFT reversibly with the allyl sulfides.

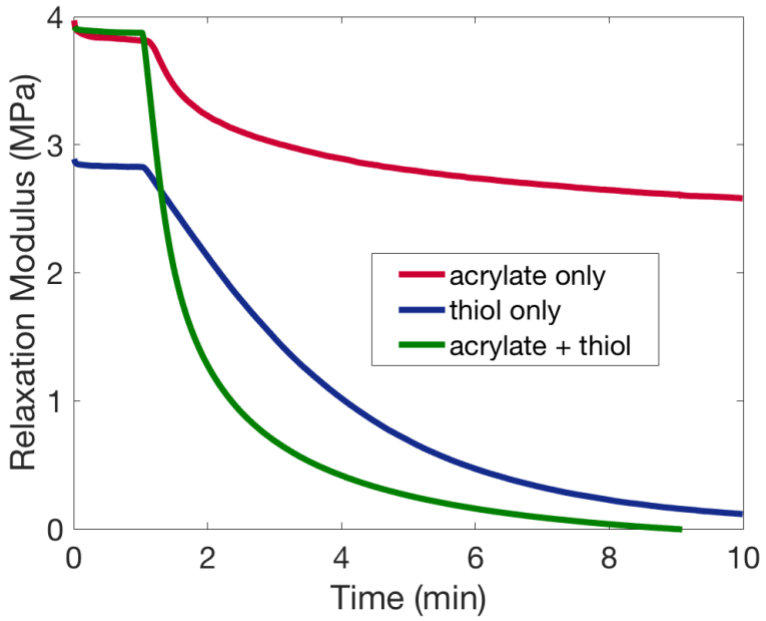

Figure 0-4. Stress relaxation kinetics due to photopolymerization-induced stress from a uniform 405 nm LED irradiation for systems containing i) 40 wt% TBPA writing monomer only, ii) 20 wt% hexane dithiol only, and iii) 20 wt% TBPA writing monomer and 10 wt% hexane dithiol present.

Holographic recording

Proof-of-concept holography experiments were performed on allyl sulfide-containing two-stage formulations alongside the corresponding control formulations.

Transmission holograms with a 1 μm pitch were successfully recorded at 405 nm using 10 mW/cm^2 with exposure times of 10 seconds or less. As shown by the representative diffraction efficiency-angle scans shown in Figure 0-5 and Figure 0-6, well-defined angular selectivity profiles are produced that can be fitted to Kogelnik coupled wave theory to determine thickness (d) and Δn. A major takeaway from this set of holography data is that the presence of allyl sulfides can achieve uniform holograms at comparable Δn values in materials that have a significant majority of the induced stresses dissipated due to AFT. In particular with the case of the high crosslinking density formulations shown in Figure 0-6, we can see that uniform holograms with higher Δn can be achieved with the AS80 samples compared to the corresponding control (C80).

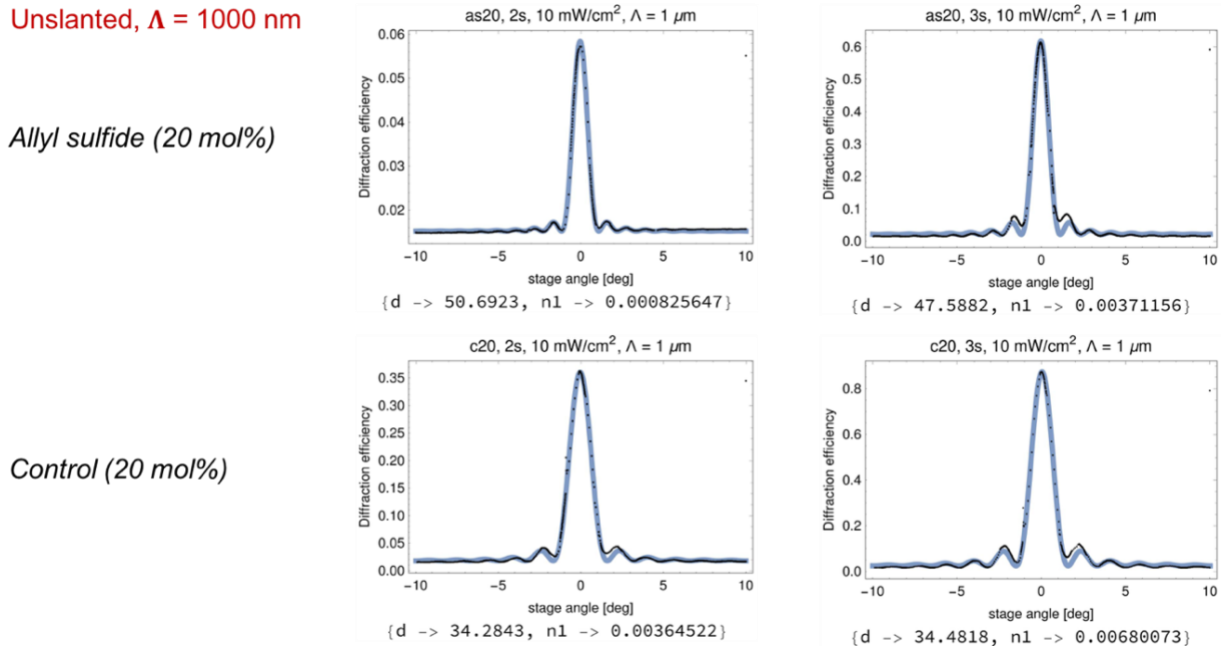

Figure 0-5. Representative transmission holography diffraction efficiency vs. angle scans for low crosslink density formulations comprising 20 mol% of AS-diol or C-diol recorded at a pitch spacing of 1000 nm using short exposure times (1 – 3 seconds) at a recording intensity of 10 mW/cm^2.

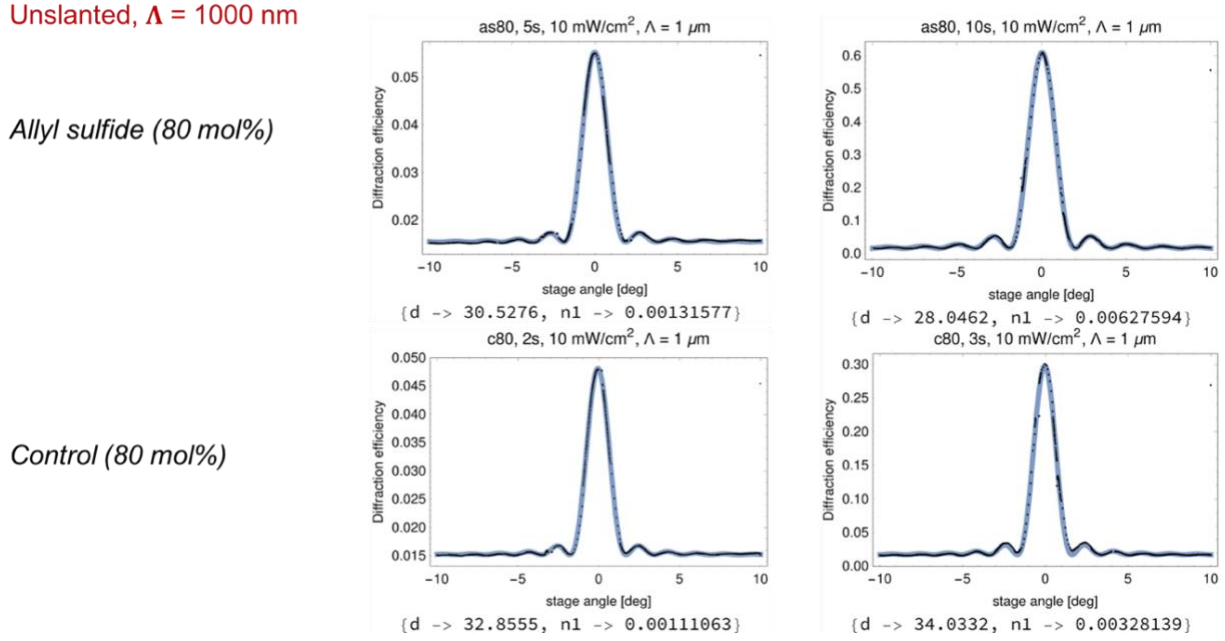

Figure 0-6. Representative transmission holography diffraction efficiency vs. angle scans for low crosslink density formulations comprising 80 mol% of AS-diol or C-diol recorded at a pitch spacing of 1000 nm using short exposure times (1 – 10 seconds) at a recording intensity of 10 mW/cm^2.

A preliminary set of reflection holograms was also recorded with formulations using a simple single beam reflection setup at 405 nm to record gratings with a pitch spacing of approximately 135 nm. While a consistent and conclusive set of data could not be obtained to discern between the effects of allyl sulfides, clear and distinct reflection notches shown in Figure 0-7 do conclusively show that high spatial frequencies are supported by materials with allyl sulfides present. Possible reasons for the inconsistent results include the stability of the exposure setup relative to the exposure time or possibly the long exposure durations activating the dynamic exchange in a manner that negatively influenced the recording of the reflection hologram. Further research on this in the presence of thiols for a more optimized AFT mechanism would be required.

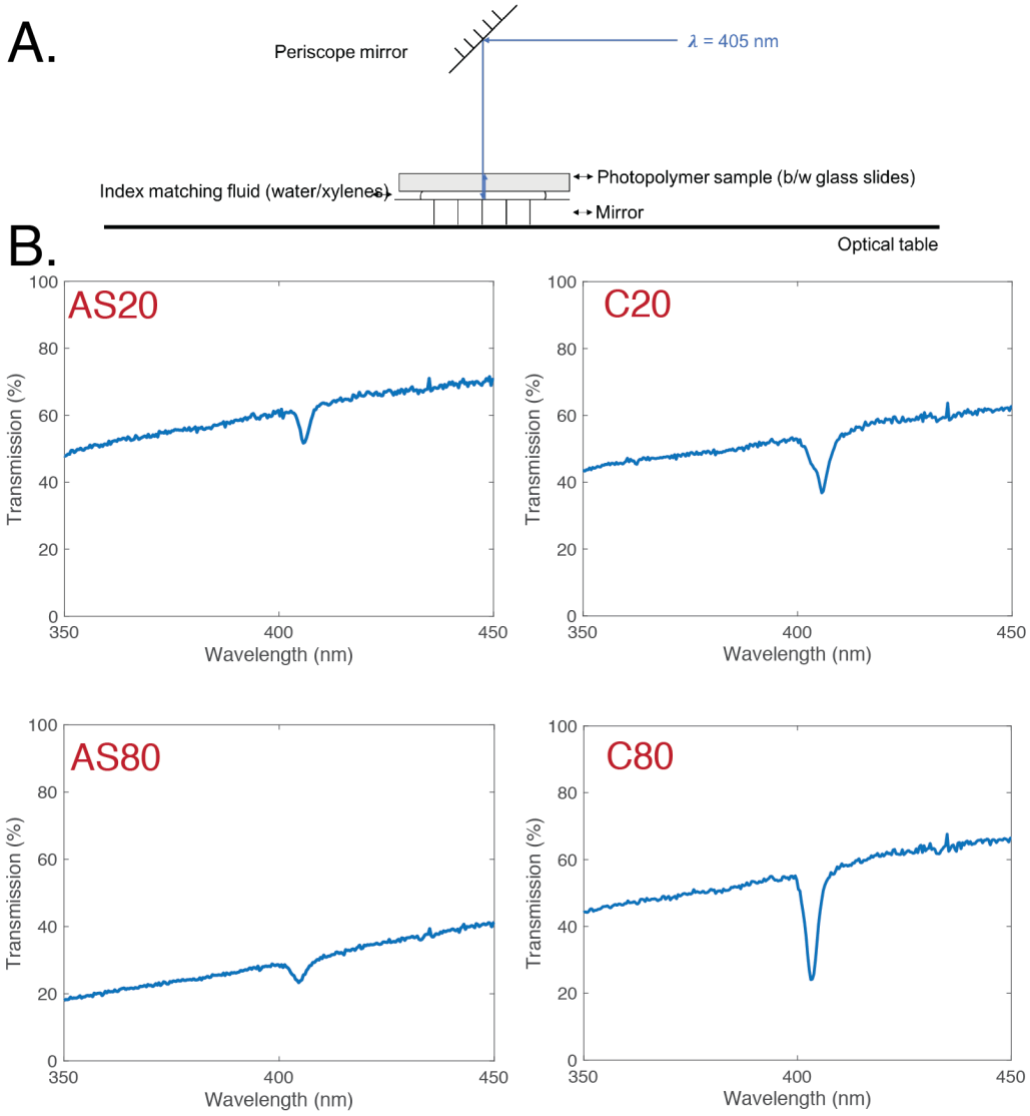

Figure 0-7. Single beam reflection holography recordings on allyl sulfide formulations. (A) A simplified diagram showing the final section of the one-beam recording of normally incident reflection gratings with 405 nm using a beam sent down to an optical table using a periscope mirror with a mirror and an index matching fluid (either water or xylenes) between the holographic sample. (B) Representative transmittance spectrum of recorded reflection holograms for 20 (top) and 80 mol% (bottom) AS diol (left) and C diol (right) containing two-stage formulations.

Despite the numerous benefits of allyl sulfides, a noticeable shortcoming common to any AFT-based DCC is the reliance on a radical source (i.e. photoinitiator), which is typically finite in its concentration and thus in its effects.[12] Additionally, it may be beneficial to have independent control over the photopolymerization and stress relaxation.

However, in the allyl sulfide-based systems these processes are inherently coupled. In this respect, alternative DCCs that are not radical-mediated and capable of long-lived exchange are advantageous. Thus, based on the same general holographic materials criteria discussed above, transthioesterification exchange of thioester and thiol groups represents an ideal anionic-mediated alternative DCC for deployment in two-stage holographic photopolymers. Thioester exchange in crosslinked polymers has been recently developed[13] and studied extensively[28-30] showing that ambient temperature thiol-thioester exchange occurs rapidly over several minutes and continuously with control over the choice in stimulus on/off requirement.[13] In this regard, thioesters offer the distinct advantage over allyl sulfides (or any radical-mediated DCC for that matter) of being completely decoupled from light exposure as a stimulus for bond exchange. This orthogonality is especially significant because the timescales for holographic exposures typically need to be short (< 5 seconds ideally) for stability reasons. One caveat of employing thioesters, however, is the requirement of thiol to generate thiolate anions for exchange to occur. Generally speaking, thiols are not orthogonal to the alcohol-isocyanate reaction and can interfere with polyurethane formation via a thiol-isocyanate reaction.[31]

Preliminary investigation of incorporating thioesters was undertaken using an alternative two-stage system comprising a stage I network formed via a thiol-Michael addition with a stage II methacrylate homopolymerization.[32] However, preparation of a one-pot system required excess thiol as well as a relatively strong base[13, 29, 30] to be present for the exchange to occur. However, this requirement meant that the thiol-Michael network gelation occurred too rapidly to properly cast optical quality films for further

testing. Unfortunately, using minimal amounts of thiol and/or base meant that the system would effectively not be dynamic as the stage II methacrylate homopolymerization would consume any small concentration of excess thiol. Thus, alternative routes to employing thioesters would open avenues towards a continuously dynamic holographic recording material and could lead to interesting performance enhancements.

1.23 Conclusions

A first foundational investigation of DCC in two-stage holographic photopolymers was undertaken using radical-mediated allyl sulfides to produce optically transparent films indistinguishable to standard, non-dynamic ones. Compared to a suitable control formulation, the presence of allyl sulfides were confirmed to not affect the polymerization rate kinetics but did result in stress relaxation as radicals were produced. When only acrylates were used, stress relaxation was noticeable but incomplete however introducing thiols to the system improved the stress relaxation noticeably due to the reversible exchange of the thiyl radicals with allyl sulfides. Both transmission and reflection holograms were successfully recorded revealing a good spatial frequency range. A preliminary exploration of formulating thioesters in two-stage formulations was also done with limited success due to the fundamental requirements of thiol and base/nucleophile for exchange. Potentially, the combination of both DCCs are possible and this work sets the preliminary foundation on these two orthogonal DCC approaches to dynamic two-stage holographic photopolymers.

1.24 Acknowledgements

This material is based upon work supported by the National Science Foundation.

1.25 References

1. Cho, Y. H.; Shin, C. W.; Kim, N.; Kim, B. K.; Kawakami, Y., High-Performance Transmission Holographic Gratings via Different Polymerization Rates of Dipentaerythritol Acrylates and Siloxane-Containing Epoxides. *Chem. Mat.* **2005,** *17* (25), 6263-6271.

2. Peng, H. Y.; Nair, D. P.; Kowalski, B. A.; Xi, W. X.; Gong, T.; Wang, C.; Cole, M.; Cramer, N. B.; Xie, X. L.; McLeod, R. R.; Bowman, C. N., High Performance Graded Rainbow Holograms via Two-Stage Sequential Orthogonal Thiol-Click Chemistry. *Macromolecules* **2014,** *47* (7), 2306-2315.

3. Peng, H.; Wang, C.; Xi, W.; Kowalski, B. A.; Gong, T.; Xie, X.; Wang, W.; Nair, D. P.; McLeod, R. R.; Bowman, C. N., Facile Image Patterning via Sequential Thiol–Michael/Thiol–Yne Click Reactions. *Chem. Mater.* **2014,** *26*, 6819.

4. Dhar, L.; Hale, A.; Katz, H. E.; Schilling, M. L.; Schnoes, M. G.; Schilling, F. C., Recording Media That Exhibit High Dynamic Range for Digital Holographic Data Storage. *Opt. Lett.* **1999,** *24*, 487.

5. Alim, M. D.; Glugla, D. J.; Mavila, S.; Wang, C.; Nystrom, P. D.; Sullivan, A. C.; McLeod, R. R.; Bowman, C. N., High Dynamic Range (Deltan) Two-Stage Photopolymers via Enhanced Solubility of a High Refractive Index Acrylate Writing Monomer. *ACS Appl Mater Interfaces* **2018,** *10* (1), 1217-1224.

6. Glugla, D. J.; Chosy, M. B.; Alim, M. D.; Childress, K. K.; Sullivan, A. C.; McLeod, R. R., Multiple patterning of holographic photopolymers for increased refractive index contrast. *Opt. Lett.* **2018,** *43* (8), 1866-1869.

7. Bruder, F.-K.; Hagen, R.; Rölle, T.; Weiser, M.-S.; Fäcke, T., From the Surface to Volume: Concepts for the Next Generation of Optical–Holographic Data-Storage Materials. *Angew. Chem.-Int. Edit.* **2011,** *50* (20), 4552-4573.

8. Bruder, F. K.; Hagen, R.; Rölle, T.; Weiser, M. S.; Fäcke, T., From the Surface to Volume: Concepts for the Next Generation of Optical-Holographic Data-Storage Materials. *Angew. Chem., Int. Ed.* **2011,** *50*, 4552.

9. Bruder, F. K.; Fäcke, T.; Rölle, T., The Chemistry and Physics of Bayfol HX Film Holographic Photopolymer. *Polymers* **2017,** *9*, 472.

10. Peng, H.; Nair, D. P.; Kowalski, B. A.; Xi, W.; Gong, T.; Wang, C.; Cole, M.; Cramer, N. B.; Xie, X.; McLeod, R. R.; Bowman, C. N., High Performance Graded Rainbow Holograms via Two-Stage Sequential Orthogonal Thiol–Click Chemistry. *Macromolecules* **2014,** *47*, 2306.

11. Rowan, S. J.; Cantrill, S. J.; Cousins, G. R. L.; Sanders, J. K. M.; Stoddart, J. F., Dynamic Covalent Chemistry. **2002,** *41* (6), 898-952.

12. Scott, T. F.; Schneider, A. D.; Cook, W. D.; Bowman, C. N., Photoinduced plasticity in cross-linked polymers. *Science* **2005,** *308* (5728), 1615-1617.

13. Worrell, B. T.; McBride, M. K.; Lyon, G. B.; Cox, L. M.; Wang, C.; Mavila, S.; Lim, C. H.; Coley, H. M.; Musgrave, C. B.; Ding, Y. F.; Bowman, C. N., Bistable and photoswitchable states of matter. *Nat. Commun.* **2018,** *9*, 7.

14. Montarnal, D.; Capelot, M.; Tournilhac, F.; Leibler, L., Silica-Like Malleable Materials from Permanent Organic Networks. *Science* **2011,** *334* (6058), 965-968.

15. Otsuka, H.; Nagano, S.; Kobashi, Y.; Maeda, T.; Takahara, A., A dynamic covalent polymer driven by disulfide metathesis under photoirradiation. *Chem. Commun.* **2010,** *46* (7), 1150-1152.

16. Rekondo, A.; Martin, R.; Ruiz de Luzuriaga, A.; Cabañero, G.; Grande, H. J.; Odriozola, I., Catalyst-free room-temperature self-healing elastomers based on aromatic disulfide metathesis. *Mater. Horizons* **2014,** *1* (2), 237-240.

17. Kloxin, C. J.; Scott, T. F.; Adzima, B. J.; Bowman, C. N., Covalent Adaptable Networks (CANs): A Unique Paradigm in Cross-Linked Polymers. *Macromolecules* **2010,** *43* (6), 2643-2653.

18. Bowman, C. N.; Kloxin, C. J. J. A. C. I. E., Covalent adaptable networks: reversible bond structures incorporated in polymer networks. **2012,** *51* (18), 4272-4274.

19. Kloxin, C. J.; Bowman, C. N., Covalent adaptable networks: smart, reconfigurable and responsive network systems. *Chem. Soc. Rev.* **2013,** *42* (17), 7161-7173.

20. Amamoto, Y.; Otsuka, H.; Takahara, A.; Matyjaszewski, K., Self-healing of covalently cross-linked polymers by reshuffling thiuram disulfide moieties in air under visible light. *Adv Mater* **2012,** *24* (29), 3975-80.

21. Fenoli, C. R.; Bowman, C. N., Synthesis of novel trithiocarbonate and allyl sulfide containing monomers. *Polymer Chemistry* **2014,** *5* (1), 62-68.

22. Denissen, W.; Winne, J. M.; Du Prez, F. E., Vitrimers: permanent organic networks with glass-like fluidity. *Chem. Sci.* **2016,** *7* (1), 30-38.

23. Chen, X.; Dam, M. A.; Ono, K.; Mal, A.; Shen, H.; Nutt, S. R.; Sheran, K.; Wudl, F., A Thermally Re-mendable Cross-Linked Polymeric Material. **2002,** *295* (5560), 1698-1702.

24. Kloxin, C. J.; Scott, T. F.; Bowman, C. N., Stress Relaxation via Addition−Fragmentation Chain Transfer in a Thiol-ene Photopolymerization. *Macromolecules* **2009,** *42* (7), 2551-2556.

25. McBride, M. K.; Hendrikx, M.; Liu, D. Q.; Worrell, B. T.; Broer, D. J.; Bowman, C. N., Photoinduced Plasticity in Cross-Linked Liquid Crystalline Networks. *Adv. Mater.* **2017,** *29* (17), 6.

26. Meng, Y.; Fenoli, C. R.; Aguirre-Soto, A.; Bowman, C. N.; Anthamatten, M., Photoinduced Diffusion Through Polymer Networks. *Adv. Mater.* **2014,** *26* (37), 6497-6502.

27. Kogelnik, H., Coupled wave theory for thick hologram gratings. *The Bell System Technical Journal* **1969,** *48* (9), 2909-2947.

28. Wang, C.; Mavila, S.; Worrell, B. T.; Xi, W. X.; Goldman, T. M.; Bowman, C. N., Productive Exchange of Thiols and Thioesters to Form Dynamic Polythioester-Based Polymers. *ACS Macro Lett.* **2018,** *7* (11), 1312-1316.

29. Wang, C.; Goldman, T. M.; Worrell, B. T.; McBride, M. K.; Alim, M. D.; Bowman, C. N., Recyclable and repolymerizable thiol-X photopolymers. *Mater. Horizons* **2018,** *5* (6), 1042-1046.

30. Worrell, B. T.; Mavila, S.; Wang, C.; Kontour, T. M.; Lim, C. H.; McBride, M. K.; Musgrave, C. B.; Shoemaker, R.; Bowman, C. N., A user's guide to the thiol-thioester exchange in organic media: scope, limitations, and applications in material science. *Polymer Chemistry* **2018,** *9* (36), 4523-4534.

31. Chatani, S.; Sheridan, R. J.; Podgorski, M.; Nair, D. P.; Bowman, C. N., Temporal Control of Thiol-Click Chemistry. *Chem. Mat.* **2013,** *25* (19), 3897-3901.

32. Chatani, S.; Nair, D. P.; Bowman, C. N., Relative reactivity and selectivity of vinyl sulfones and acrylates towards the thiol-Michael addition reaction and polymerization. *Polymer Chemistry* **2013,** *4* (4), 1048-1055.

Realizing High Refractive Index Thiol-X Materials: A General and Scalable Synthetic Approach[1]

Photopolymers formed from the family of thiol-X ‘click’ reactions notably form sulfur-containing thioether linkages. While sulfur-containing materials are conventionally expected to result in high refractive index (n_D/20°C > 1.6) materials, this is rarely realized with thiol-X photopolymers due to the lack of sufficiently high refractive index monomers. Here, an efficient and highly modular synthetic strategy to obtain high refractive index thiol-X monomers is presented. The efficacy of the overall approach is demonstrated using only commercially available starting compounds to yield low viscosity (< 1000 cP) liquid multi-thiol and diallyl ether monomers with high refractive indices (n_D/20°C > 1.64). These synthesized monomers underwent thiol-ene photopolymerizations rapidly to high conversions (> 85%) achieving refractive index values (n_D/20°C) up to 1.665 with typical narrow and well-defined tan δ peaks. The convenience of the low viscosity resins and their excellent optical quality was demonstrated in a facile replication overmolding procedure to aspherize a commercial spherical lens using a negative PDMS mold. An optically clear aspherized lens was reliably obtained showing an expected increase in optical power and numerical aperture (NA) due to the higher refractive index photopolymer overmold.

[1] Contributing authors: Sudheendran Mavila, David Miller, Sijia Huang, Maciej Podgórski, Lewis M. Cox, Amy C. Sullivan, Robert R. McLeod, and Christopher N. Bowman

1.26 Introduction

Polymers are important alternative optical materials to inorganic glass due to their superiorities in ease of processing, weight, impact resistance, and versatility in controlling other material properties of interest. Despite the excellent high refractive indices and low dispersions available with glass, polymers have effectively replaced them in several consumer applications such as lenses for eyeglasses, cameras, and various consumer electronics.[1]

Photopolymers extend the advantages of polymers further by offering on-demand speed of cure at ambient temperatures and low energy consumptions.[2] Crucially, photopolymerizations offer spatial and temporal control that are leveraged to control degree of polymerization and thus material properties such as refractive index. The pairing of precision optics with high performance photopolymers has led to a plethora of advanced applications including optical adhesives, replication molding of complex optical surfaces,[3] nanoimprint lithography,[4, 5] gradient refractive index (GRIN) optics,[6] holographic optical elements (HOEs),[7-9] and vat photopolymerization additive manufacturing.[10, 11] Similar to other optical materials, high refractive index values (defined here as $n_D > 1.6$) are desirable to achieve superior performance for a number of these applications.

However, while significant progress has been made in the concerted pursuit of high refractive index polymers,[12-14] a majority of these strategies have come at the expense of other important considerations such as color[15], processability or synthetic accessibility. Significantly, amongst the body of work in high refractive index polymers only a small subset is applicable towards photopolymerizations. This discrepancy is

because most approaches involve a thermally driven polymerization reaction (such as polycondensation[16-18] or inverse vulcanization[15]) to produce the high refractive index polymer. In this regard, it is perhaps more appropriate to consider high refractive index polymers in terms of their scope of applicability and possible implementations.

Therefore, while the overall field of high refractive index polymers is reasonably advanced, there has been limited work on the rational design of customizable monomers capable of achieving high refractive index photopolymers. To address this gap, we were interested in devising photopolymerizable monomers suited for step-growth based thiol-X polymerizations. The rationale being that in contrast to conventional chain-growth (meth)acrylate photopolymers,[19-21] thiol-X step-growth polymerizations exhibit significantly reduced polymerization stresses due to their step-growth development. Lower stresses mean polymer optics with less birefringence or aberrations and better uniformity overall.

Another key advantage of thiol-X polymers is their intrinsic incorporation of sulfur at every formed thioether linkage to form materials with high sulfur content as shown in Scheme 0-1. Due to their high atomic refraction values, sulfur-containing compounds are well known to be effective substituents for increasing refractive index materials.[8, 13, 14, 19-27] However, with a few notable exceptions that involved using inorganic thiol-ene monomers,[24, 26] achieving high refractive index values has been relatively unrealized in organic thiol-X polymers[27] due to a deficiency of adequately high refractive index monomers. Commercially available thiols with functionalities of three or greater are predominantly either alkyl-based, mercaptopropionates or mercaptoacetates. These compounds consist of organic atoms (such as oxygen, hydrogen and carbon) that,

unlike sulfur, do not contribute to refractive index due to their low atomic refractions.[13, 23] To illustrate this point, a commonly used tetrathiol, pentaerythritol tetrakis(3-mercaptopropionate) (PETMP), has a quoted literature refractive index value (at 20°C) of only 1.531 due to the presence of the ester groups.[27] A similar situation can be found with multifunctional ene monomers. To this end, we were motivated to develop a synthetic strategy to enable the judicious design of high refractive index monomers for use in thiol-X (photo)polymerizations. We validate this synthetic framework by utilizing predominantly inexpensive and widely available starting materials to produce in scale (10s of grams) a set of multifunctional thiol and ene monomers that are low viscosity liquids (< 500 cP) with relatively high refractive index (n_D > 1.6) and exhibit excellent resin solubility.

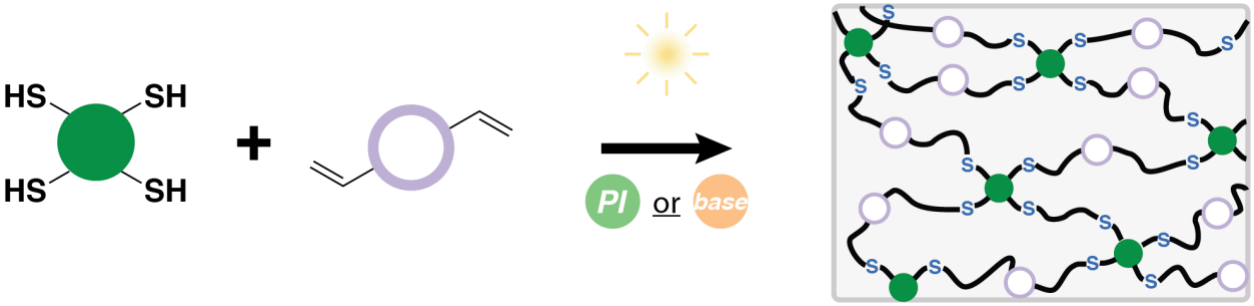

Scheme 0-1. Multifunctional thiols and enes are photopolymerized via a variety of thiol-X 'click' reactions to obtain crosslinked, sulfur-rich polymers. Thiol-X 'click' reactions can be either radical-mediated (using photoinitiators) or anionic-mediated (using a photobase) typically achieving quantitative conversions using appropriate conditions.

1.27 Experimental

1.27.1 Materials

Commercially available reagents were used without further purification. Thiophenol, epichlorohydrin, 2-mercaptoethanol and butylated hydroxytoluene (BHT) free radical stabilizer were purchased from Alfa Aesar. 1,8-

Diazabicyclo[5.4.0]undec-7-ene (DBU) was purchased from Chem-Impex International. 4-(methylsulfanyl)thiophenol was purchased from TCI America. Thiourea was purchased from Sigma-Aldrich. Reagent-grade triethylamine (Et_3N) and sodium hydroxide (NaOH) were purchased from Fisher Scientific. Absolute ethanol (200 proof) ethanol was purchased from Decon Labs Inc.

Synthesis of 1-chloro-3-(phenylthio)-2-propanol (CPTP)

CPTP was prepared according to a previously reported procedure.[28] Briefly, to a dry 500 g round-bottomed flask equipped with a magnetic stir bar was added 50 mL (640 mmol, 1 eq) of epichlorohydrin and 24.4 g (64 mmol, 0.1 eq) of borax to 320 mL (2 M) of deionized water. 65 mL (635 mmol, 1 eq) of thiophenol was added dropwise to the stirring solution using an addition funnel over 1 hour. The reaction was allowed to proceed at room temperature for 4 hours. Subsequently the mixture was extracted with CH_2Cl_2 (3 x 100 mL) then washed with water (200 mL) and brine (50 mL). The combined extracts were dried with Na_2SO_4 and concentrated in vacuo. No further purification was performed and the compound was used as is.

CPTP: ^{1}H NMR (400 MHz, $CDCl_3$) δ = 7.42-7.39 (m, 2H), 7.33-7.29 (m, 2H), 7.26-7.22 (m, 1H), 3.97-3.90 (m, 1H), 3.72-3.64 (m, 2H), 3.20-3.06 (m, 2H), 2.62 (d, 1H); ^{13}C NMR (101 MHz, $CDCl_3$) δ = 134.7, 130.3, 130.1, 129.4, 127.1, 69.7, 48.1, 38.4.

General procedure for the synthesis of intermediate X-diol – 1,2-ethanedithiol-based intermediate diol (EDT-OH) and 4,4'-thiobisbenzenethiol-based intermediate diol (TBT-OH)

To a 250 mL round-bottomed flask equipped with a magnetic stir bar was added 2.50 g (9.98 mmol) of 4,4'-thiobisbenzenethiol and was diluted with 100 mLs of toluene.

To this mixture, 3.8 g (25.0 mmol) of DBU was added. After stirring at room temperature for 10 min, 4.5 g (22.0 mmol) of **CPTP** was added. The resulting suspension was heated to 90 °C for 16 h. After this period, the flask was cooled to room temperature and the toluene was removed under reduced pressure to afford a crude residue which was diluted with EtOAc (~200 mLs), washed with 1N HCl (~150 mLs, 2X), water (~150 mLs, 1X), and brine (~150 mLs, 1X). The combined organics were dried over Na_2SO_4, filtered, and concentrated under reduced pressure to yield 5.6 g (96%) of the title compound (**TBT-OH**) as yellow viscous liquid.

EDT-OH: ^{1}H NMR (400 MHz, $CDCl_3$) δ = 7.40-7.38 (m, 4H), 7.32-7.28 (m, 4H), 7.24-7.20 (m, 2H), 3.84-3.77 (m, 2H), 3.16-3.12 (m, 2H), 3.06-3.00 (m, 2H), 2.84-2.78 (m, 2H), 2.75 (m, 4H), 2.67-2.62(m, 2H), 1.64 (bs, 2H).; ^{13}C NMR (101 MHz, $CDCl_3$) δ = 135.1, 130.1, 129.3, 127.1, 126.8, 126.5, 69.1, 40.3, 38.8, 32.9.

TBT-OH: ^{1}H NMR (400 MHz, $CDCl_3$) δ = 7.39-7.36 (m, 4H), 7.31-7.27 (m, 8H), 7.24-7.20 (m, 6H), 3.89-3.83 (m, 2H), 3.24-3.18 (m, 4H), 3.13-3.04 (m, 4H), 2.75 (bs, 2H).; ^{13}C NMR (101 MHz, $CDCl_3$) δ = 135.0, 134.6, 133.8, 131.5, 130.3, 130.0, 129.2, 126.8, 68.1, 40.1, 39.8.

General procedure for the synthesis of X-diallyl ether – 1,2-ethanedithiol-based diallyl ether (EDTDAE) and 4,4'-thiobisbenzenethiol-based diallyl ether (TBTDAE)

To a 250 mL round-bottomed flask equipped with a magnetic stir bar was added 5.6 g (9.60 mmol) of **TBT-OH** and was diluted with 100 mLs of anhydrous THF. The flask was cooled to 0 °C and 1.15 g (28.8 mmol) of 60% NaH in mineral oil was added. After stirring at room temperature for 1 h, 3.5 g (28.8 mmol) of allyl bromide was added followed by 0.16 g (0.96 mmol) of potassium iodide. The resulting solution was stirred at

room temperature for 16 h. After this period, the reaction mixture was diluted with EtOAc (~200 mLs), washed with 1N HCl (~150 mLs, 2X), water (~150 mLs, 1X), and brine (~150 mLs, 1X). The combined organics were dried over Na_2SO_4, filtered, and concentrated under reduced pressure reduced pressure to yield the crude as pale yellow liquid which was purified by column chromatography eluting with (30% EtOAc/hexanes). Evaporation of the fractions under reduced pressure yielded 4.2 g (67%) of the title compound (**TBTDAE**) as colorless viscous liquid.

EDTDAE: ^{1}H NMR (400 MHz, $CDCl_3$) δ = 7.39-7.36 (m, 4H), 7.31-7.26 (m, 4H), 7.21-7.17 (m, 2H), 5.99-5.83 (m, 2H), 5.25-5.13 (m, 4H), 4.09-4.00 (m, 4H), 3.67-3.61 (m, 2H), 3.18-3.16 (m, 4H), 2.87-2.73 (m, 8H); ^{13}C NMR (101 MHz, $CDCl_3$) δ = 136.2, 134.7, 129.6, 129.1, 126.4, 117.6, 77.8, 71.2, 37.0, 35.6, 33.2, 33.1.

TBTDAE: ^{1}H NMR (400 MHz, $CDCl_3$) δ = 7.37-7.34 (m, 4H), 7.30-7.26 (m, 8H), 7.23-7.17 (m, 6H), 5.90-5.80 (m, 2H), 5.20-5.11 (m, 4H), 4.04-4.01 (m, 4H), 3.70-3.64 (m, 2H), 3.27-3.14 (m, 8H); ^{13}C NMR (101 MHz, $CDCl_3$) δ = 136.0, 135.7, 134.5, 133.4, 131.6, 130.0, 129.7, 129.1, 126.5, 117.8, 76.7, 71.3, 37.4.

Synthesis of 1,3-bis-(hydroxyethylthio)-2-propanol (BHETP)

To a dry 250 g round-bottomed flask equipped with a magnetic stir bar was added 10 mL (128 mmol, 1 eq) of epichlorohydrin and 10.9 g (273 mmol, 2.13 eq) of sodium hydroxide to 125 mL (1 M) of 200 proof absolute ethanol. 19 mL (270 mmol, 2.11 eq) of 2-mercaptoethanol was added dropwise to the stirring solution using an addition funnel over 1 hour. The reaction was heated to 50°C and stirred for 1 hour. The reaction mixture was then cooled to room temperature and 13.5 mL (159 mmol, 0.58 eq) of 36% concentrated hydrochloric acid were added to form a precipitate. The

precipitate was filtered off through a short pad of celite. The filtrate was then concentrated under reduced pressure.

BHETP: ^{1}H NMR (400 MHz, $CDCl_3$) δ = 5.05(d, 1H), 4.77(t, 2H), 3.72-3.67(m, 1H), 3.55-3.50(m,4H), 2.70-.55 (m, 8H); ^{13}C NMR (101 MHz, $CDCl_3$) δ = 70.9, 61.4, 38.2, 35.2.

Synthesis of trithiol 1

The synthesis of trithiol **1** was adapted from a procedure reported in the patent literature.[29] Briefly, to a dry 500 g round-bottomed flask equipped with a reflux condenser and magnetic stir bar was added 22 g of BHETP (104 mmol, 1 equiv.) and 28.9 g (379 mmol, 3.66 equiv.) of thiourea, and was dissolved in 63.3 g (1.58 M) of 36% aqueous hydrochloric acid solution and homogenized. This solution was heated to 110 °C and stirred for 1 hr. After this period, the reaction was cooled to room temperature and 61.5 g (762 mmol, 7.35 equiv.) of 50% aqueous NaOH solution was added under N_2 atmosphere. The suspension was then allowed to stir at room temperature for 24 hr. After this period, 200 mL of toluene was added and the mixture was filtered via suction then transferred to a separatory funnel. The organic layer was washed with 1 M hydrochloric acid solution, water and brine then dried over sodium sulfate. The solution was filtered and concentrated under reduced pressure to yield 25.2 g (93%) of the title compound as a colorless liquid which was used as is without further purification.

Trithiol 1: ^{1}H NMR (400 MHz, $CDCl_3$) δ = 2.95-2.71(m, 15H), 1.79-1.72 (m, 3H); ^{13}C NMR (101 MHz, $CDCl_3$) δ = 49.0, 37.2, 36.2, 35.8, 28.8, 25.1, 24.9.

Synthesis of 1-chloro-3-(hydroxyethylthio)-2-propanol (CHTEP)

To a dry 250 mL round-bottomed flask equipped with a magnetic stir bar was added 25 mL (320 mmol, 1 eq) of epichlorohydrin and 12.2 g (32 mmol, 0.1 eq) of borax to 160 mL (2 M) of deionized water. 50 mL (710 mmol, 2.22 eq) of 2-mercaptoethanol was added dropwise to the stirring solution using an addition funnel over 1 hour. The reaction was allowed to proceed for 16 hours.

CHETP: ^{1}H NMR (400 MHz, $CDCl_3$) δ = 3.99-3.95(m, 1H), 3.81-3.77(m, 2H), 3.69-3.61(m, 2H), 2.87-2.68(m, 4H); ^{13}C NMR (101 MHz, $CDCl_3$) δ = 70.7, 61.3, 48.0, 36.4, 36.1.

Synthesis of tetrafunctional alcohol 1

To a dry 250 g mL round-bottomed flask equipped with a magnetic stir bar was added 4 mL (47.7 mmol, 1 eq) of 1,2-ethanedithiol, 16.6 g (97.3 mmol, 2.04 eq) of CHETP, 4.23 g (106 mmol, 2.22 eq) in 100 mL (0.48 M) of absolute ethanol. The mixture was heated to 50°C and stirred for one hour. The reaction mixture was then cooled at room temperature and 1.5 mL of hydrochloric acid (36%) was added to form a precipitate. The salt precipitate was separated by filtration and the filtrate was concentrated under reduced pressure.

Tetra-alcohol 1: ^{1}H NMR (400 MHz, DMSO-d_6) δ = 4.78 (bs, 4H), 3.73-3.67(m, 2H), 3.35 (t, 4H), 2.74-2.54 (m, 6H); ^{13}C NMR (101 MHz, DMSO-d_6) δ = 70.4, 60.91, 37.7, 37.2, 34.8, 32.3.

Synthesis of tetrathiol 1

To a dry 100 mL round-bottomed flask equipped with a magnetic stir bar was added 17 g (46.9 mmol, 1 eq) of tetrafunctional alcohol 1 and 17.1 g (225 mmol, 4.8 eq) in 20 mL of 36% concentrated HCl (2.34 M). The solution was heated and stirred for six

hours at 110°C. Following this the solution was cooled to room temperature and 12.1 g of sodium hydroxide 50% aqueous solution were added while keeping at 20°C, then heated and stirred for 30 minutes at 110°C. The solution was then cooled to room temperature and 40 mL of toluene was added for separatory extraction. The organic phase was washed with 1 M HCl solution then with water three times. The organic phase was dried by anhydrous sodium sulfate then concentrated in vacuo.

Tetra-thiol 1: ^{1}H NMR (400 MHz, $CDCl_3$) δ = 2.96-2.86 (m, 9H), 2.85-2.79 (m, 7H), 2.77-2.69 (m, 6H), 1.81-1.69 (m, 4H); ^{13}C NMR (101 MHz, DMSO-d_6) δ = 51.6, 48.9, 37.1, 36.1, 35.7, 28.8, 28.7, 28.2, 25.1, 24.9.

1.27.2 Methods

Refractive index and dispersion measurements

A digital refractometer (Abbemat MW) was used to measure refractive index values at 20°C at the Fraunhofer lines –β hydrogen-F (n_F, 486 nm), sodium-D (n_D, 589 nm), and α hydrogen-C (n_C, 656 nm). Abbe number was calculated according to the equation, $V = (n_D-1)/(n_F-n_C)$.

Viscosity measurement

A rotational rheometer (ARES-G2, TA Instruments) with a parallel plate geometry was used to measure the viscosity of the liquid monomers using a 0.4 mm gap with a shear rate of 10-500 s^{-1} using 20 mm diameter quartz plates at ambient temperature. All resins showed Newtonian fluid behavior.

Dynamic Mechanical Analysis (DMA)

A DMA (Q800, TA Instruments) was used to conduct temperature sweep experiments on rectangular photopolymer films with an applied oscillatory strain of

0.1%. Sample dimensions were approximately 10 x 5 x 0.5 mm. A temperature ramp rate of 3°C/min was used from -60 to 60°C at a frequency of 1 Hz. The glass transition temperature (T_g) was taken as the peak of the tan δ curve. The rubbery modulus was measured at 40°C for rubbery samples.

Aspherizing lens via overmolding

The negative mold was made by casting degassed PDMS (Sylgard 184, Dow Corning), mixed at a standard 10:1 weight ratio, around a commercial aspheric lens (ACL1210U, Thorlabs) that was anchored to a round petri dish (Pyrex) with blocking wax. The PDMS was cured overnight in an oven at 60°C then subsequently released from the petri dish and lens package to get the negative asphere PDMS mold as shown in Scheme 0-2A. Approximately 100 µL of thiol-ene resin was dispensed into the cavity of the PDMS mold followed by careful placement of the spherical lens (LA1540, Thorlabs). A broad spectrum UV lamp (Acticure 4000, EXFO) was used to cure for 150 seconds on each side to obtain the aspherized lens as illustrated in Scheme 0-2B.

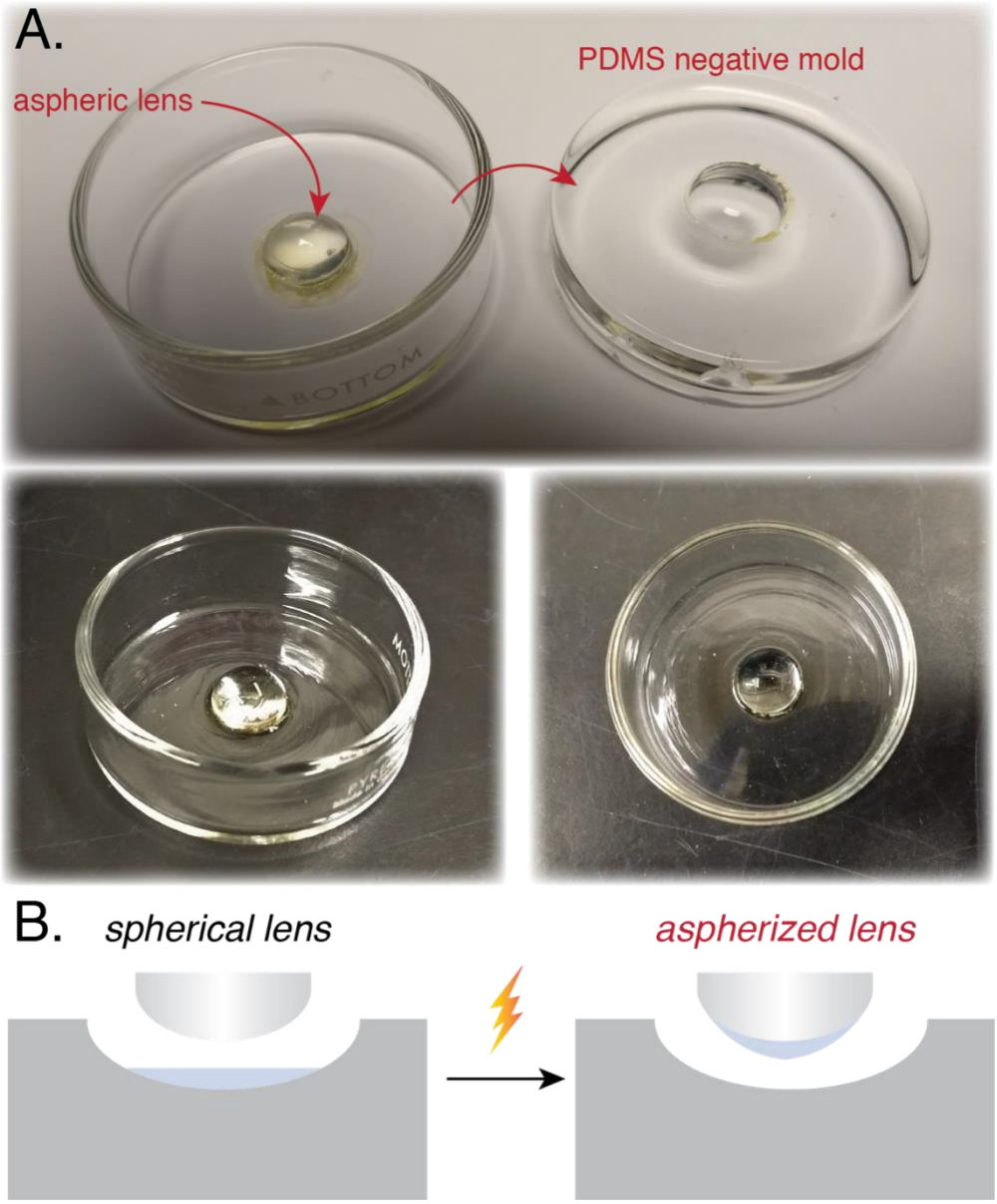

Scheme 0-2. Aspherizing a spherical lens by overmolding with photopolymer resin. (A) A commercial aspheric lens was affixed to the bottom of a petri dish with blocking wax and PDMS resin was cast over and allowed to cure overnight at 60°C. After curing, the negative PDMS mold was freed from the petri dish and lens. (B) Approximately 100 µL of thiol-ene resin was placed in the well of the negative mold followed by a commercial spherical lens. This package was cured with a UV lamp on both sides for 150 seconds each. The aspherized lens was then removed from the PDMS mold.

1.28 Results & Discussion

The synthetic strategy shown in Figure 0-1

Figure 0-1. Synthetic strategy developed to obtain high refractive index multifunctional enes and thiols. (A) Multifunctional enes are synthesized in three steps. The first step involves the generation of a Cl-linker from the thiol-epoxide ring-opening reaction of epichlorohydrin with a monothiol. This Cl-linker is used to couple on to a multithiol to produce a multifunctional hydroxyl intermediate which is then converted to a number of polymerizable groups including alkynes, allyl ethers, (meth)acrylates, norbornenes and urethane (meth)acrylates. (B) Multifunctional thiols are synthesized with an analogous procedure using a chlorinated diol for the Cl-linker instead. (C) Example high refractive index monothiol and multithiol substrates applicable for use as the Cl-linker and the high refractive index core respectively.

is generally outlined for thiol- and ene- functional molecules separately with both routes sharing similarities in the thiol substrates. Overall, a set of thiol-X ‘click’ reactions[30, 31] (i.e. thiol-epoxide and thiol-halide) were used to generate the desired multifunctional monomers with good overall efficiencies. The high degree of customizability is a salient feature of this synthetic approach to achieve monomers with tunable material specifications.[32] In particular with the route to multifunctional enes shown in Figure 0-1, a wide range of (photo)polymerizable monomers possessing useful properties are obtained from three relatively simple steps.

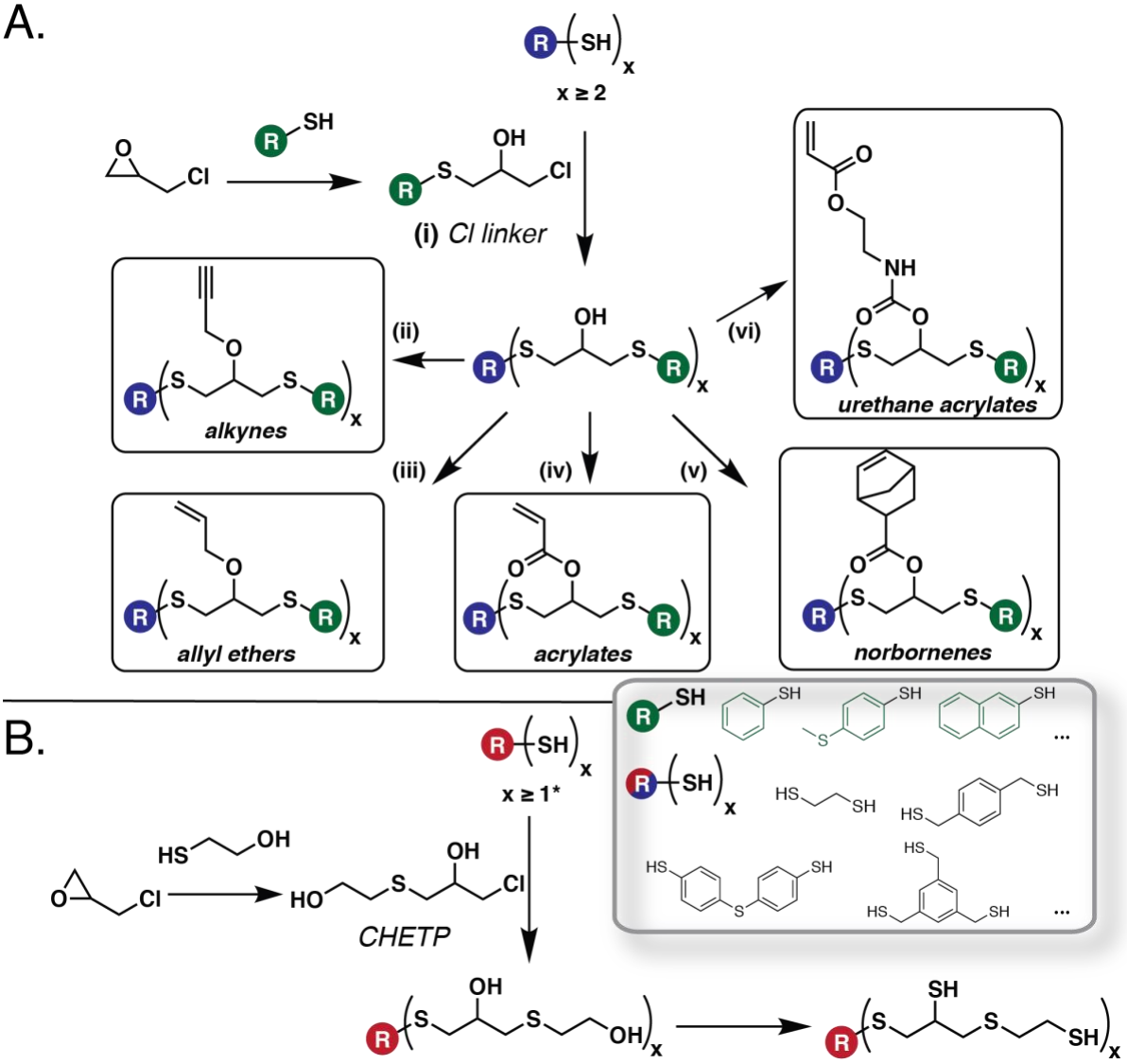

Figure 0-1. Synthetic strategy developed to obtain high refractive index multifunctional enes and thiols. (A) Multifunctional enes are synthesized in three steps. The first step involves the generation of a Cl-linker from the thiol-epoxide ring-opening reaction of epichlorohydrin with a monothiol. This Cl-linker is used to couple on to a multithiol to produce a multifunctional hydroxyl intermediate which is then converted to a number of polymerizable groups including alkynes, allyl ethers, (meth)acrylates, norbornenes and urethane (meth)acrylates. (B) Multifunctional thiols are synthesized with an analogous procedure using a chlorinated diol for the Cl-linker instead. (C) Example high refractive index monothiol and multithiol substrates applicable for use as the Cl-linker and the high refractive index core respectively.

In the first step, a high refractive index chlorinated linker (Cl-linker) intermediate is produced by the efficient thiol-epoxide ring-opening reaction with a monofunctional

thiol such as thiophenol. While a number of good approaches exist for the selective thiol-epoxide reaction without any thiol-halide side reaction occurring, we found a previously reported borax-catalyzed procedure[28] to be convenient for large scale (> 50 grams) synthesis. Using thiophenol (n_D/20°C = 1.588), we synthesized 1-chloro-3-(phenylthio)-2-proponal (CPTP) as well as a significantly higher refractive index analog using 4-(methylsulfanyl)thiophenol to produce a 1-chloro-3-(methylthiophenylthio)-2-propanol (CMTPTP) to demonstrate the range of high refractive index Cl-linkers possible with this facile and efficient reaction as listed in Table 0-1.[33]

The second step involves the selection of a multi-thiol ‘core’ which reacts with the *Cl*-linker via a thiol-halide nucleophilic substitution reaction under basic conditions. This thiol-halide step produces a compound with secondary hydroxyl groups equivalent in functionality to the multi-thiol ‘core’, which is the most influential component for controlling the final properties and characteristics of the final monomer. While fewer choices are commercially available for multi-thiols (especially for functionalities greater than two), there are a number of high refractive index multifunctional thiols previously reported in the literature that can be utilized.[22, 25, 34, 35] Nevertheless we used commercially available 1,2-ethane dithiol (EDT) and 4,4’-thiobisbenzenethiol (TBT) as the ‘cores’ for demonstrative example compounds. Notably, multi-thiols such as TBT that are typically insoluble in neat thiol-ene resins are readily incorporated to generate the desired hydroxy compound.

Table 0-1. Refractive index and dispersion values (measured at 20°C) of compounds synthesized including the Cl-linker precursors, diallyl ethers and multifunctional thiols including the measured viscosities of diallyl ether monomers at ambient temperature.

Compound	Structure	n_F	n_D	n_C	V	η (cP)
Chlorinated linker						
CPTP	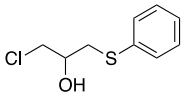	1.6027	1.5887	1.5833	30.4	-
CMTPTP	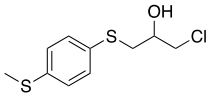	1.6522	1.6332	1.6261	24.2	-
Diallyl ethers (DAEs)						
EDTDAE	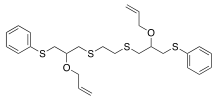	1.6094	1.5954	1.5900	30.7	88
TBTDAE	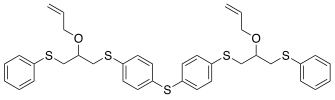	1.6647	1.6440	1.6362	22.6	560
Multi-thiols						
trithiol **1**	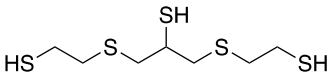	1.6592	1.6457	1.6405	34.5	43
tetrathiol **1**	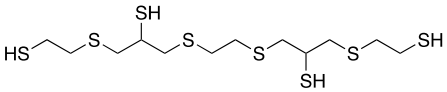	1.6533	1.6403	1.6352	35.3	189

In the final step, a range of polymerizable groups are attached to the hydroxyl groups using established procedures to generate allyl ethers, alkynes, (meth)acrylates, norbornenes, and urethane (meth)acrylates. Here, we primarily validate the overall strategy with diallyl ether (DAE) monomers using a standard procedure involving allyl bromide in THF under basic conditions (NaH).

For high refractive index multi-thiols, the desired goal was to obtain a set of sulfur-rich alkyl structures without any other heteroatoms or aromatic groups present. The primary intention behind this approach was to primarily achieve low viscosity liquid monomers that could achieve high refractive index values without being significantly absorptive or dispersive.[13, 23, 36] Given this preference, we were inspired by patents from Mitsui Chemicals disclosing a scalable route to a sulfur-containing alkyl trithiol using

epichlorohydrin and 2-mercaptoethanol as the starting materials.[29] However, to obtain higher functionality (greater than three) thiols the aforementioned approach of using a Cl-linker for the ene monomers was employed as presented in Figure 0-1B. Here, the required Cl-linker was instead a diol synthesized by the exclusive thiol-epoxide ring-opening of epichlorohydrin with 2-mercaptoethanol using the same borax-catalyzed procedure[28] to produce the colorless liquid, 1-chloro-3-(hydroxyethylthio)-2-propanol (CHETP). This compound can then be reacted with a multi-thiol under basic conditions via a thiol-halide substitution to obtain a higher functionality hydroxyl compound as shown in Figure 0-1. Similar to the synthetic route for the multifunctional ene monomers, the multi-thiol forms the core of the molecule and can be chosen to tune material properties as needed. The intermediate hydroxy compounds are finally converted to the corresponding multi-thiol with thiourea followed by acid hydrolysis. Although this synthetic route involves three steps overall, greater flexibility in formulation design is achieved in being able to use higher functionality thiols in terms of controlling gel point conversion,[37] and/or refractive index. Furthermore, compared to other synthetic routes to multi-thiols presented in the literature, the reactions are higher yielding and require significantly less expensive reactants for the same number of steps.[22, 25]

The strategies laid out for both multifunctional thiols and enes critically involve a thiol-epoxide ring-opening reaction to form sulfur-rich alkyl chains to give relatively low viscosity liquid monomers. As such, both sets of monomers share the same underlying structure and thus exhibit good solubility with each other in neat thiol-ene resins due to their mutual compatibility (‘like dissolves like’). Resin solubility without the use of solvents is a key trait desired for almost all photopolymerization systems and is

especially valuable for high volume applications such as vat photopolymerization 3D printing.

To establish a baseline level for this overall synthetic approach and validate its efficacy, we opted to use only commercially available and preferably inexpensive starting materials to show accessibility. We selected thiophenol (lit. n_D/20°C = 1.588) to form the high refractive index Cl-linker, CPTP, and chose EDT (alkyl) and TBT (aromatic) as the two dithiol cores to be converted using allyl bromide to the corresponding diallyl ethers, EDTDAE and TBTDAE respectively. Both monomers were liquids with n_D/20°C values of 1.5954 and 1.6440 respectively and Abbe numbers of 30.7 and 22.6 respectively. In addition, a new tetrathiol was synthesized using EDT as the dithiol core with BHETP to form the tetra-alcohol that was then converted to tetrathiol 1. These synthesized monomers were used with commercially available PETMP to form 4 distinct sets of thiol-ene networks as illustrated in Figure 0-2.

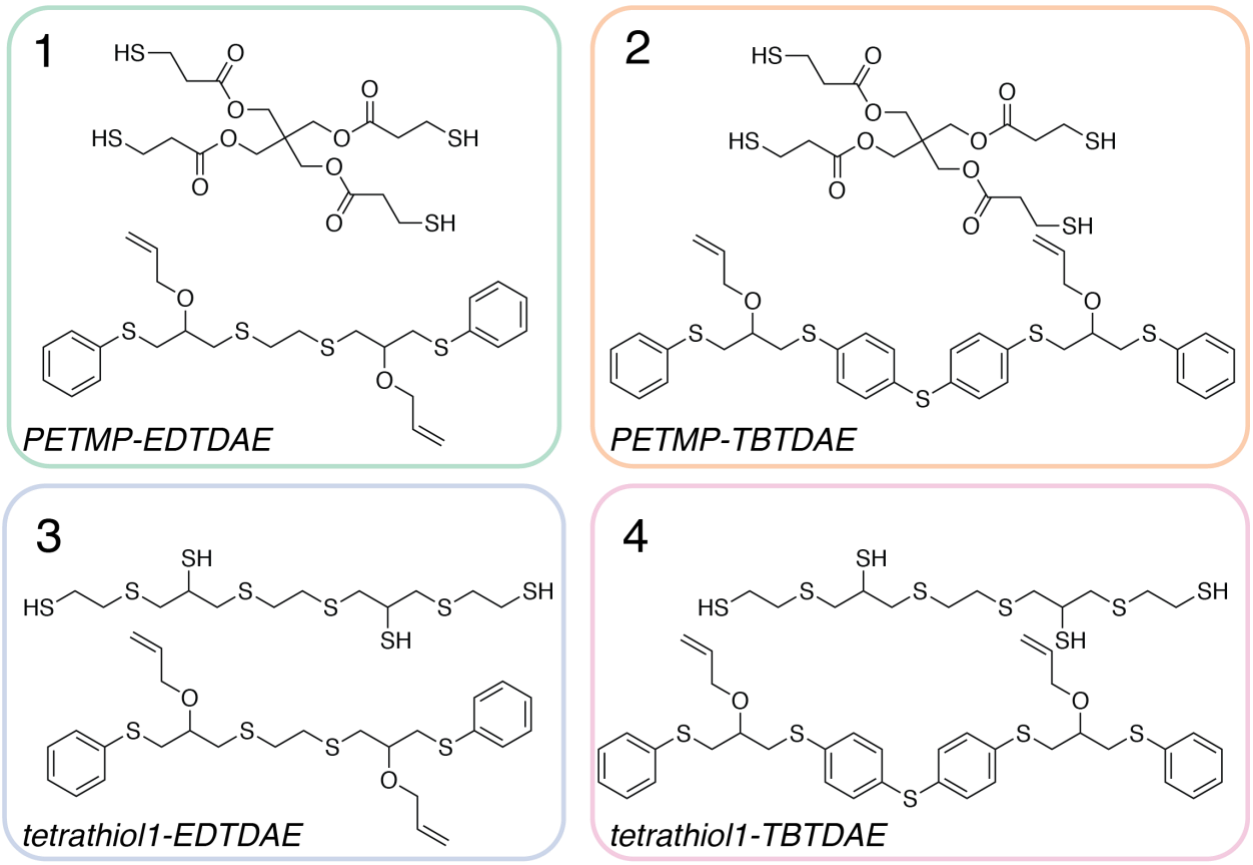

Figure 0-2. Demonstrative stoichiometric thiol-ene systems using PETMP, tetrathiol 1 and the dienes EDTDAE and TBTDAE with 0.5 wt% DMPA present in each formulation. Formulation 1 is PETMP-EDTDAE. Formulation 2 is PETMP-TBTDAE. Formulation 3 is tetrathiol1-EDTDAE. Formulation 4 is tetrathiol1-TBTDAE.

The reaction kinetics and conversion of these four thiol-ene formulations were studied using real-time FTIR with a 365 nm exposure at 20 mW/cm^2. Figure 0-3 shows the rapid reaction kinetics typical of a thiol-ene reaction with conversions well past the conversion required for gelation. It is notable that both formulations containing TBTDAE do go to high conversions of at least 80% although they clearly are slower in their reactions than the corresponding alkyl-based EDTDAE. This difference is likely due to the more viscous nature of TBTDAE compared to EDTDAE. Another prominent feature is that the thiol conversion for the tetrathiol 1 containing systems were both higher with

both diallyl ethers. We hypothesize this outcome was due to the insufficient purity (~90%) of the synthesized tetrathiol causing the disparity between thiol and ene conversions.

More crucially, photopolymerizing the EDTDAE and TBTDAE with the commercial tetrathiol, PETMP, via a photoinitiated thiol-ene reaction yielded a colorless crosslinked polymer network with a n_D/20°C of 1.6029 and 1.6335 and Abbe numbers of 34.4 and 26.4 respectively. As expected, the aromatic dithiol core present in TBTDAE efficiently enhances refractive index by 0.03, although this comes at the expense of increased dispersion (i.e. reduced Abbe number). To achieve a balanced increase in refractive index and dispersion, further investigation into suitable substituents for the core and the Cl-linker is required. Typically these are synthesized structures that incorporate sulfur in an aliphatic,[21, 38] cyclic,[25, 35] or acyclic[21] structure over an aromatic one.[16-19, 39, 40] To validate this idea, the synthesized tetrathiol 1 was photopolymerized separately with the same set of diallyl ethers using the same conditions as before to obtain n_D^{20} values of 1.6330 and 1.6651 and Abbe numbers of 32.2 and 25.0 respectively. A complete set of refractive index and dispersion values for the crosslinked thiol-ene systems is listed in Table 0-2. With a higher purity tetrathiol 1, it would be reasonable to expect these numbers to be even higher with increased thiol and ene conversions.

Overall through judicious choice of substrates, the presented synthetic strategy permits the balancing of traditionally competing optical property requirements such as absorption, color, dispersion against refractive index in addition to other non-optical property considerations such as monomer viscosity, solubility, or polymer glass

transition temperatures. In this regard, the presented methodology provides extensive opportunities for a systematic and tailored approach to materials design beyond just high refractive index optical applications.

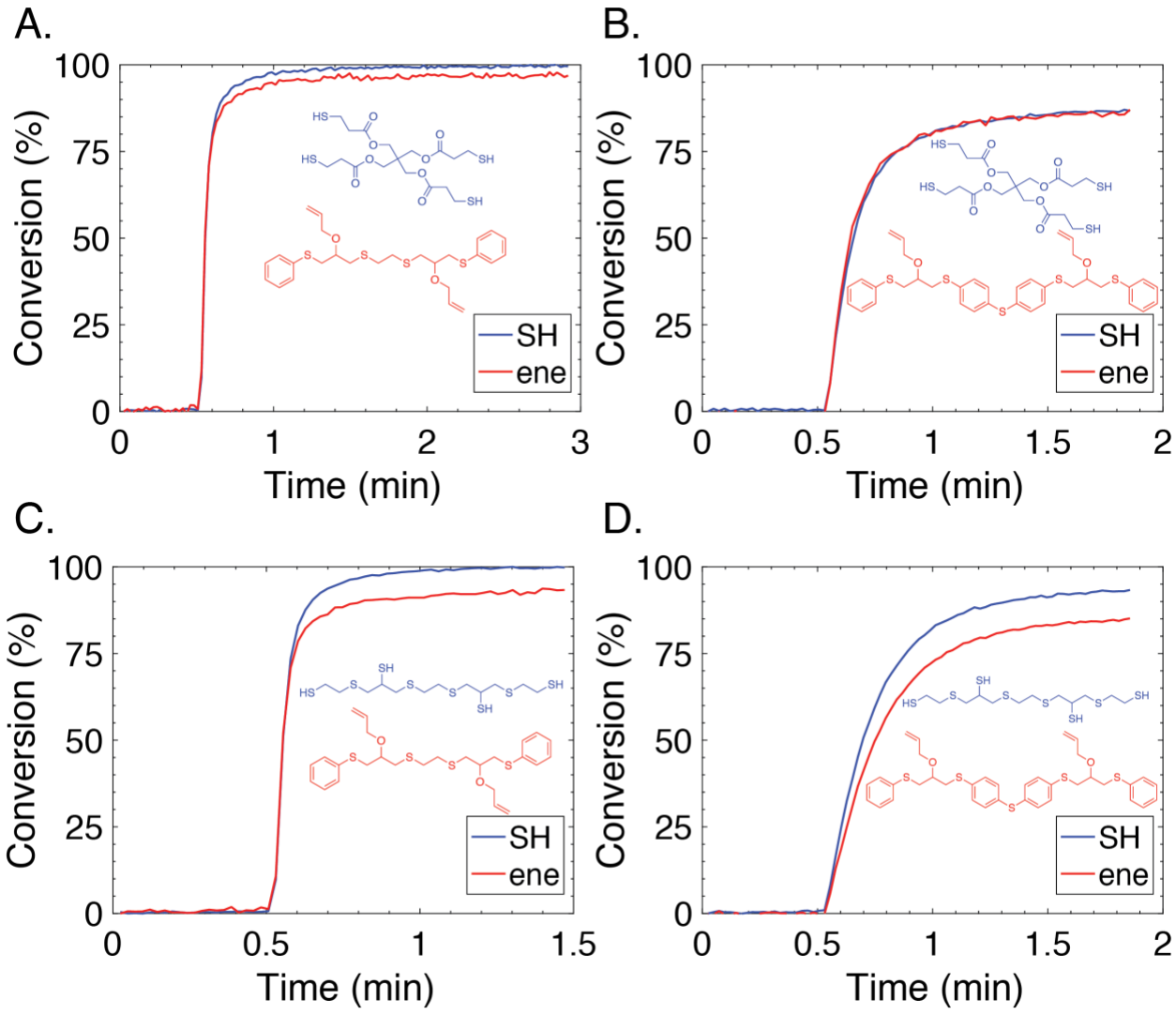

Figure 0-3. FTIR reaction kinetics and conversions with neat stoichiometric thiol-ene resins using either commercially available PETMP or synthesized tetrathiol 1 as the thiol, and either the synthesized EDTDAE or TBTDAE as the dienes with 0.5 wt% DMPA and 365 nm irradiation at 20 mW/cm^2. (A) PETMP-EDTDAE system. (B) PETMP-TBTDAE system. (C) tetrathiol1-EDTDAE system. (D) tetrathiol1-TBTDAE system.

Table 0-2. Refractive index and dispersion values (measured at 20°C) of photopolymerized stoichiometric thiol-ene networks with the measured viscosities of initial, unreacted resins at ambient temperature. A continuous 365 nm irradiation at 20 mW/cm^2 was used to polymerize each liquid resin for 5 minutes.

Thiol-ene structures	n_F	n_D	n_C	V	η (cP)
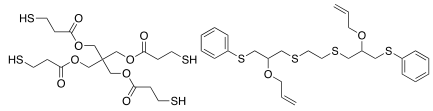	1.6155	1.6029	1.5979	34.4	117
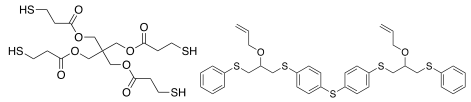	1.6509	1.6335	1.6269	26.4	340
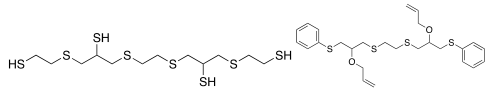	1.6471	1.6330	1.6275	32.2	73
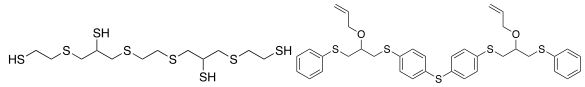	1.6844	1.6651	1.6578	25.0	167

Aside from achieving high refractive index values at relatively high Abbe numbers, as shown in Figure 0-4, a broad range of thermomechanical properties were accessed from the four example systems with T_g values between -18 to 16°C and rubbery moduli (at 40°C) between 0.9 and 4.8 MPa. The step-growth nature of the thiol-ene polymerization characteristically produced uniform networks with a narrow glass transition regime.[30, 31] This is evident in Figure 0-4B by the distinct and relatively narrow tan δ curves for each thiol-ene system. These specific thiol-ene systems also exhibited elevated tan δ values (2.2 – 2.5) compared to other thiol-ene systems[41] signifying good damping and energy dissipating qualities.[41]

Photocurable liquid monomers are commercially used as optical adhesives or to fabricate replication optics thus typically requiring good optical transmittance and clarity across the designed wavelengths as well as a match in refractive index.[3, 42] While a number of resins exist for the refractive index range below 1.6, higher refractive index glasses (or other media) ideally require a closely matched value (± 0.1 or less). However, the associated advantages of using photocurable optical-grade resins, such as the ease of production and high throughput, can be severely limited by prohibitively viscous resins. In this respect, the set of monomers prepared (resin viscosity range: 73 – 340 cP) are far superior to existing high refractive index commercial resins such as NOA 170 which has a quoted viscosity range of 4400 – 5500 cP.[43] Using the highest refractive index example system, i.e. tetrathiol1-TBTDAE, this facile overmolding procedure was employed to aspherize a spherical lens using a PDMS negative mold.[3] As seen in Figure 0-5, the optical clarity and surface finish of the thiol-ene photopolymer overmold (left side) is of high enough quality that the 1 mm spaced vertical lines look indistinguishably clear with either lens. However, as expected, the high refractive index overmold increased the optical power and numerical aperture (NA) of the lens, resulting in a greater magnification (approximately 1.5x) of the lens.

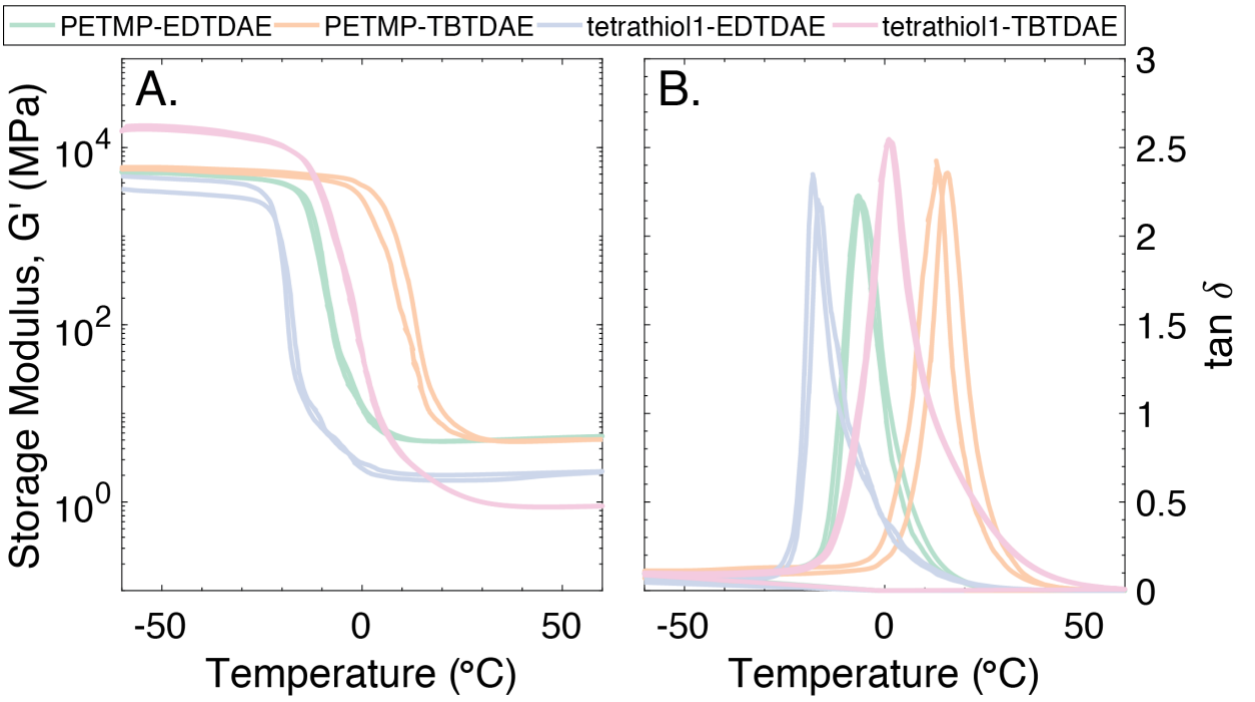

Figure 0-4. Thermomechanical properties of the photopolymerized thiol-ene networks measured at a frequency of 1 Hz with an applied oscillatory strain of 0.1%. A temperature sweep was conducted from -60 to 60°C at a ramp rate of 3 °C/min. (A) Storage modulus (G') vs. temperature plots for all four systems. (B) tan δ vs. temperature plots for all four systems showing well-defined and relatively narrow peaks. Crosslinked networks with a T_g range of -18 to 16°C, and a rubbery modulus range of 0.9 to 4.8 MPa at 40°C was obtained for the four example thiol-ene systems.

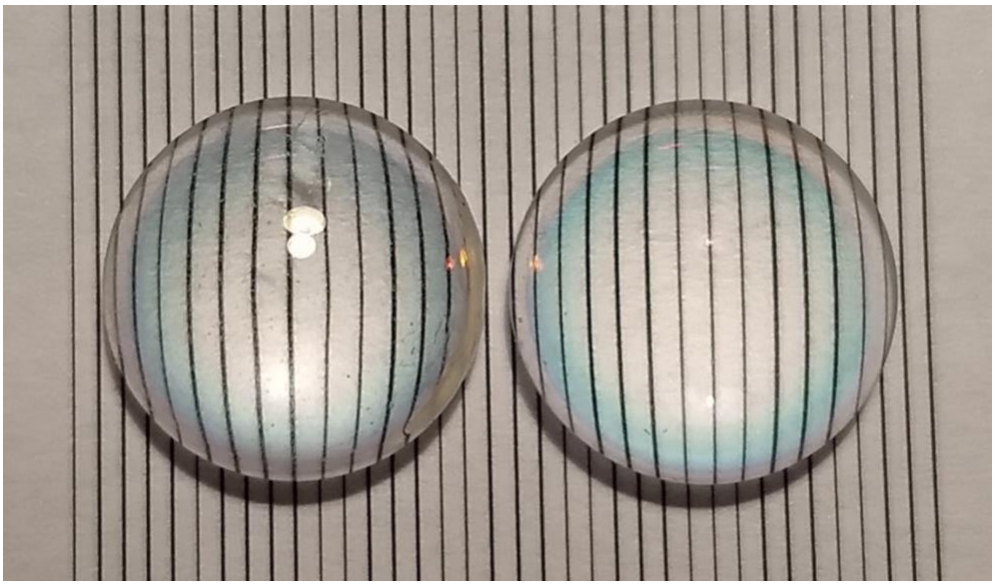

Figure 0-5. Side-by-side view of an overmolded aspherized lens (left) and the pristine spherical lens (right) over an array of lines spaced 1 mm apart. The higher refractive index overmold increases the optical power and NA of the lens as shown by the larger magnification.

1.29 Conclusions

To summarize, we present a general and efficient synthetic strategy based on efficient thiol-X ‘click’ chemistries for the facile and modular synthesis of a vast range of high refractive index monomers. This strategy is compatible with existing approaches to high refractive index thiols but greatly expands on the scope of monomer design for both thiols and enes. A defining feature of the presented approach is the precise, multi-faceted control over the final monomer structure to enable rational materials design of final properties. We validated this strategy at each synthetic step by selecting only commercially available substrates to produce a representative set of liquid thiol-X monomers with refractive indices exceeding 1.6. These monomers were polymerized neat via a standard thiol-ene photopolymerization achieving rapid and high conversions of both thiol and ene groups. These photopolymerizations produced homogeneous

networks with narrow glass transition regimes, in addition to clear and transparent polymer films with a valuable refractive index range between 1.6 and 1.7 with Abbe numbers in excess of 25. The utility of the prepared low viscosity monomers was successfully demonstrated with a simple overmolding procedure to aspherize a base spherical lens. Excellent optical properties were demonstrated with the polymer overmold showing the expected increase in optical power and NA.

1.30 Supporting Information

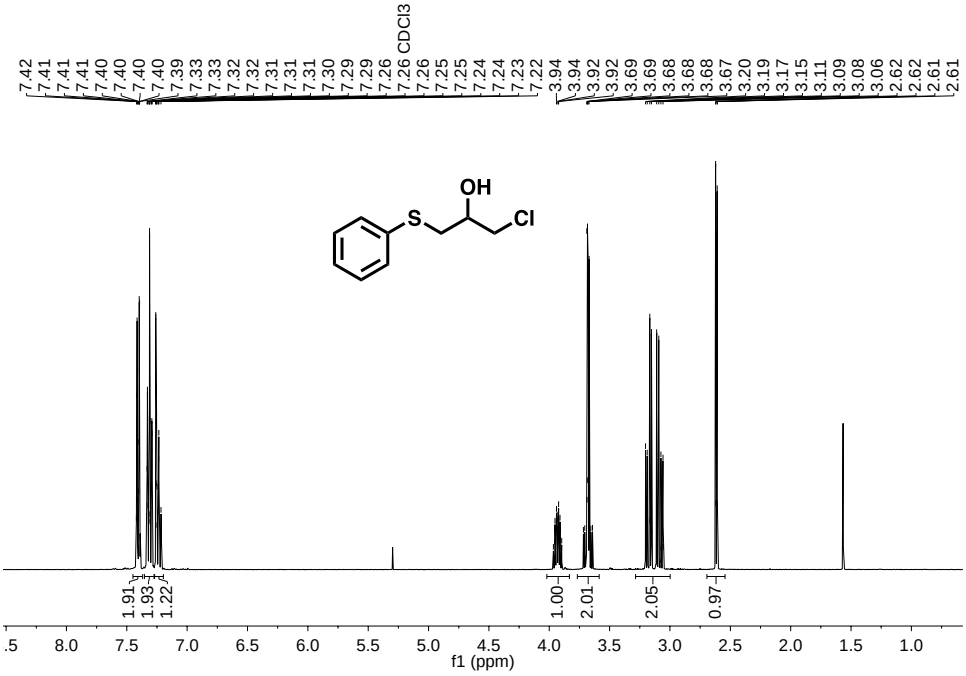

Figure S0-6. ^{1}H NMR spectra for CPTP.

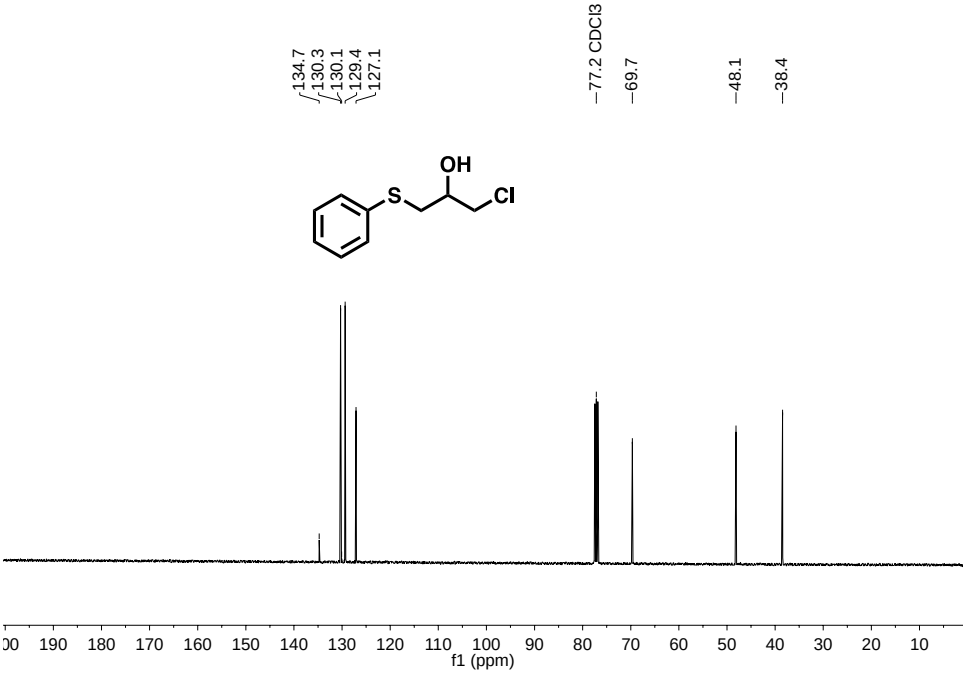

Figure S0-7. ^{13}C NMR spectra for CPTP.

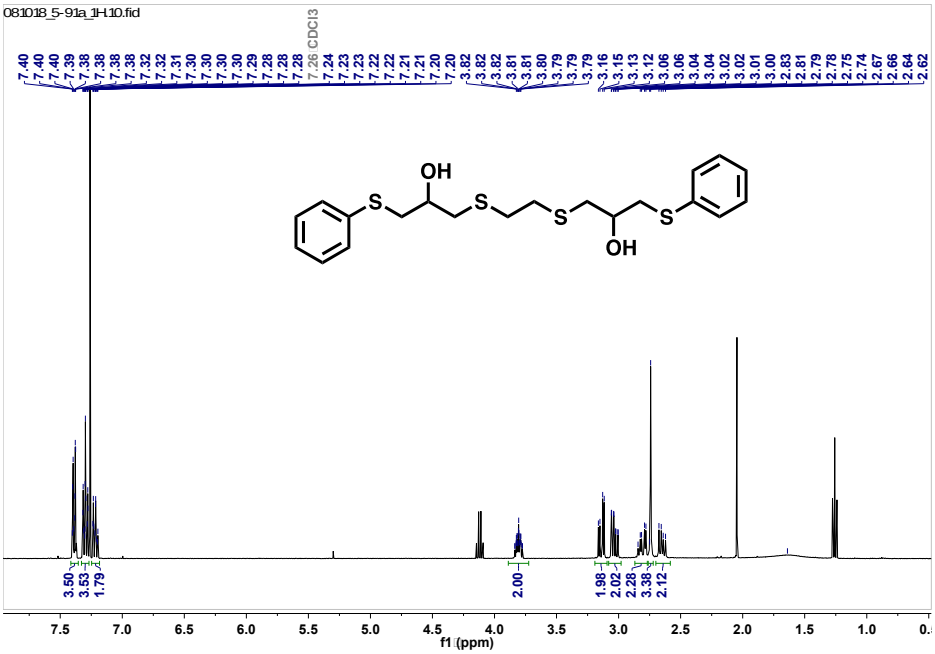

Figure S0-8. ^{1}H NMR spectra for EDT-OH.

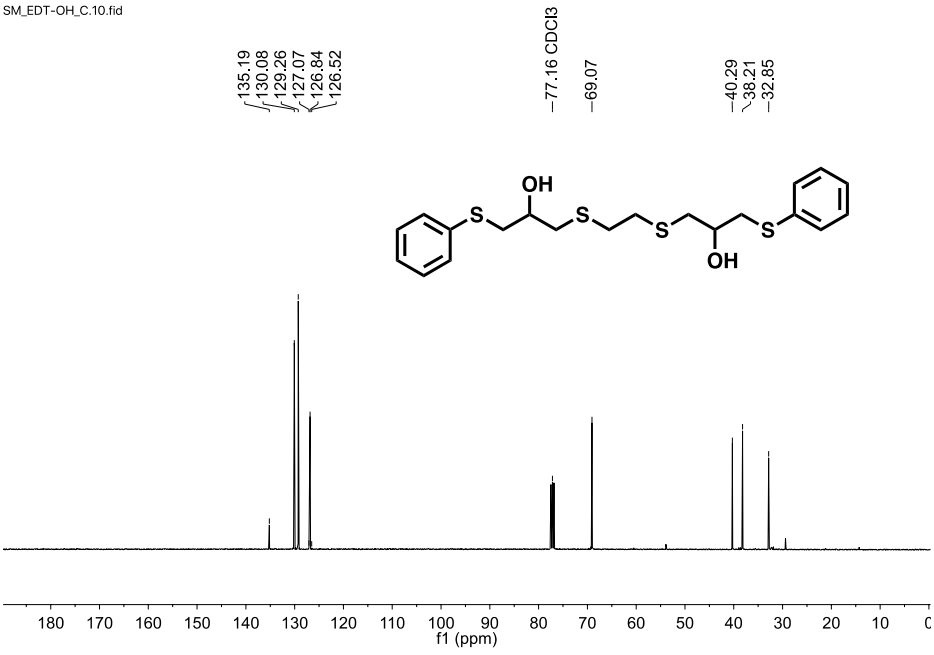

Figure S0-9. ^{13}C NMR spectra for EDT-OH.

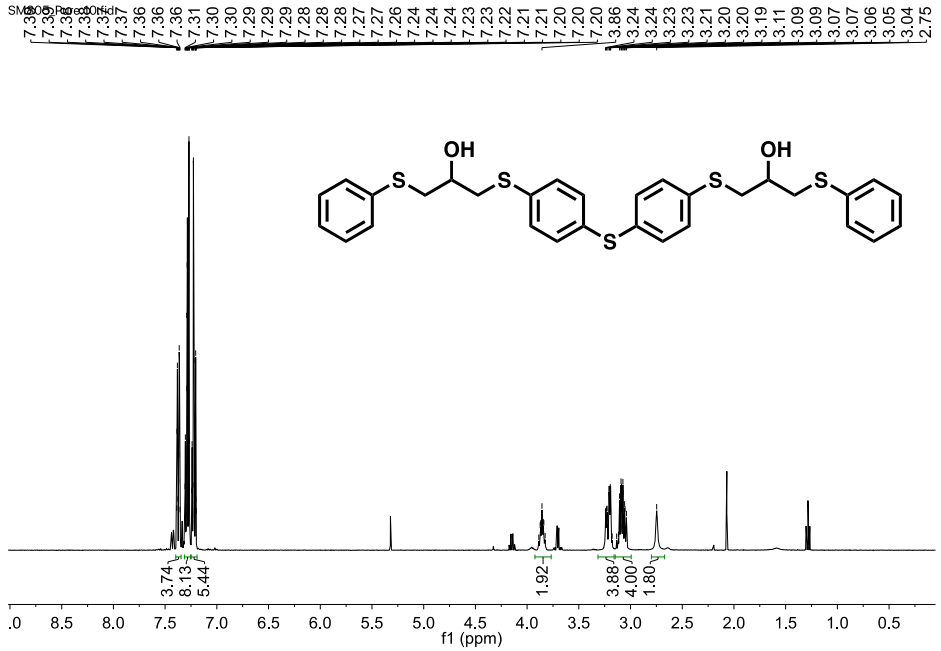

Figure S0-10. ^{1}H NMR spectra for TBT-OH.

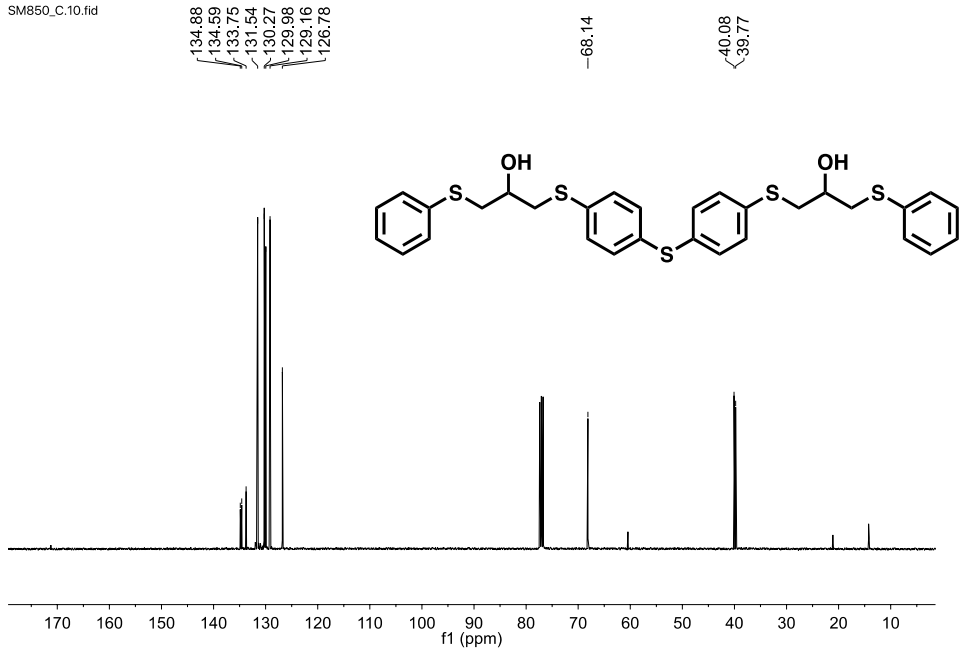

Figure S0-11. ^{13}C NMR spectra for TBT-OH.

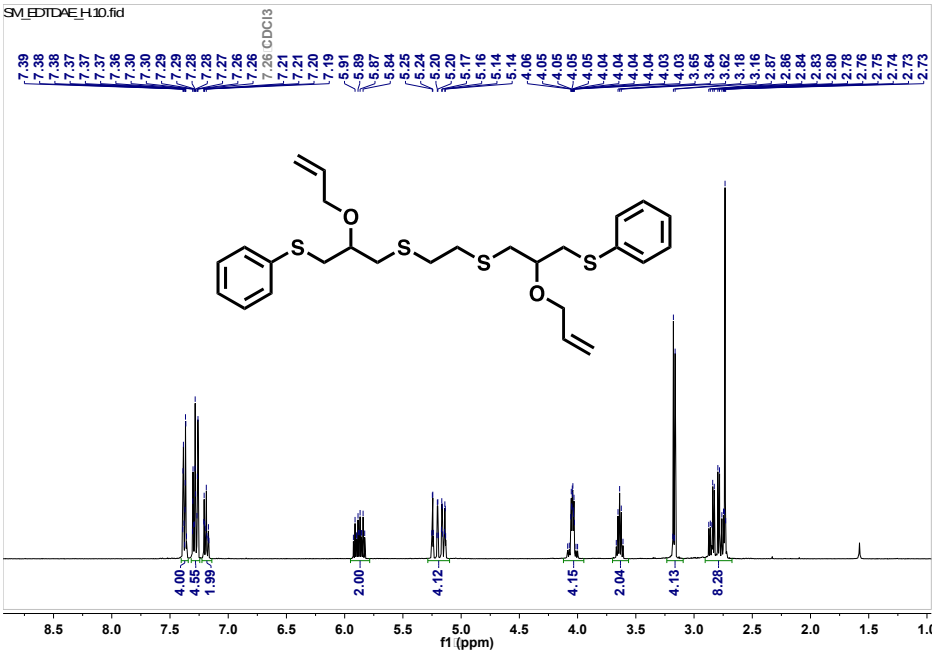

Figure S0-12. ^{1}H NMR spectra for EDTDAE.

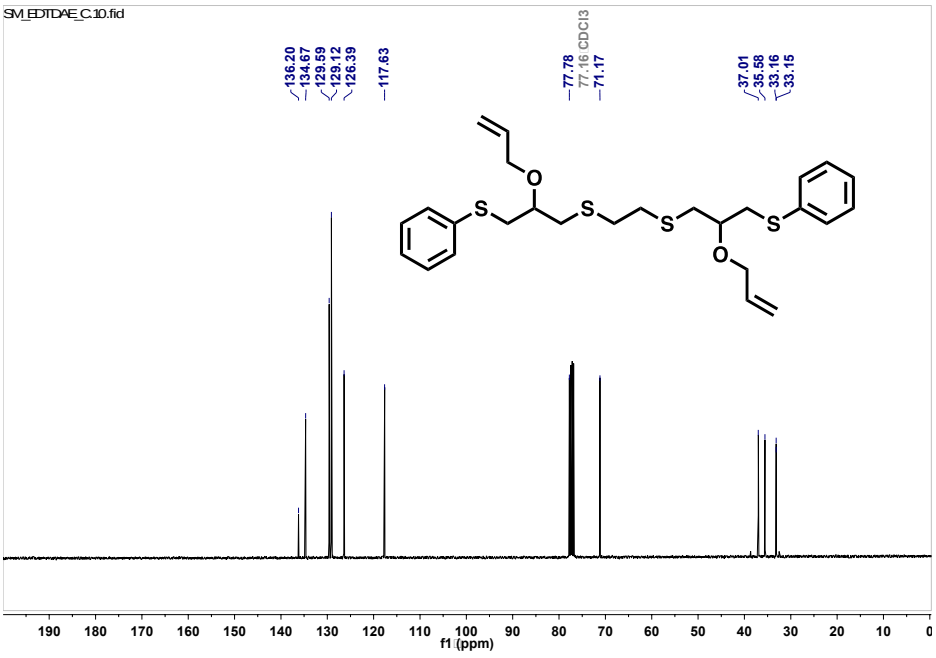

Figure S0-13. ^{13}C NMR spectra for EDTDAE.

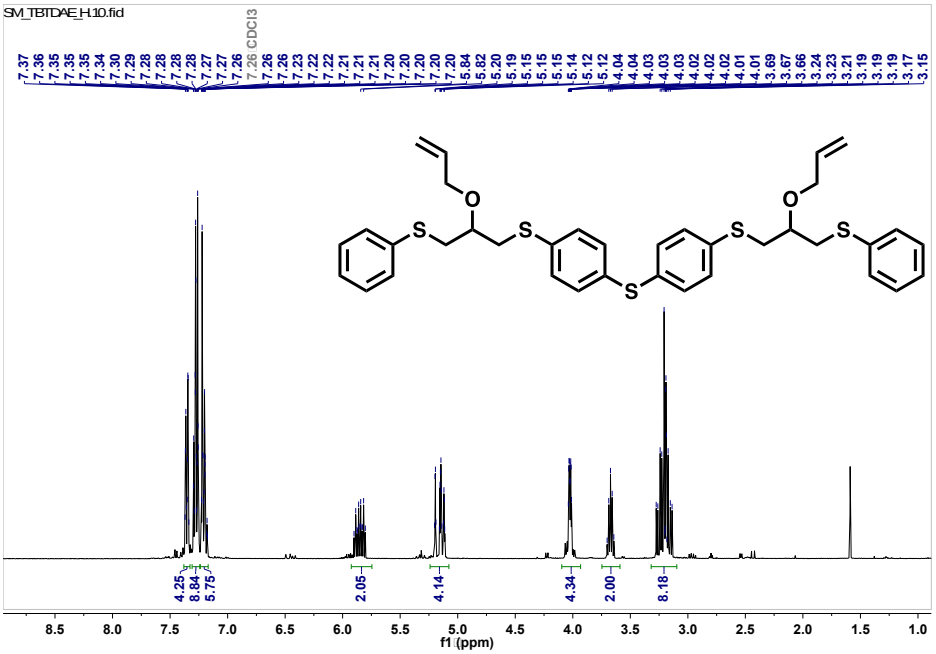

Figure S0-14. ^{1}H NMR spectra for TBTDAE.

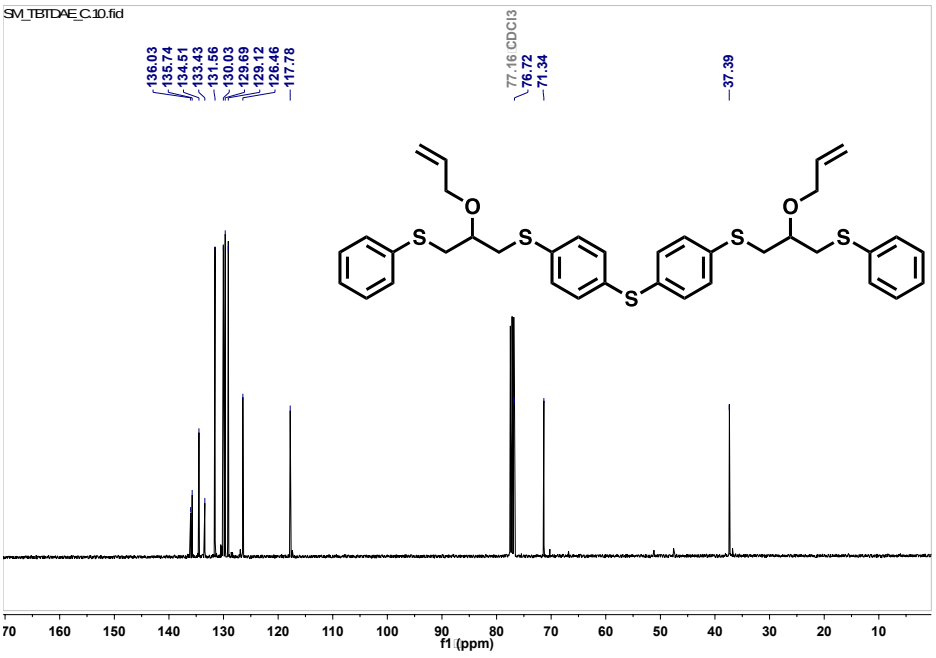

Figure S0-15. ^{13}C NMR spectra for TBTDAE.

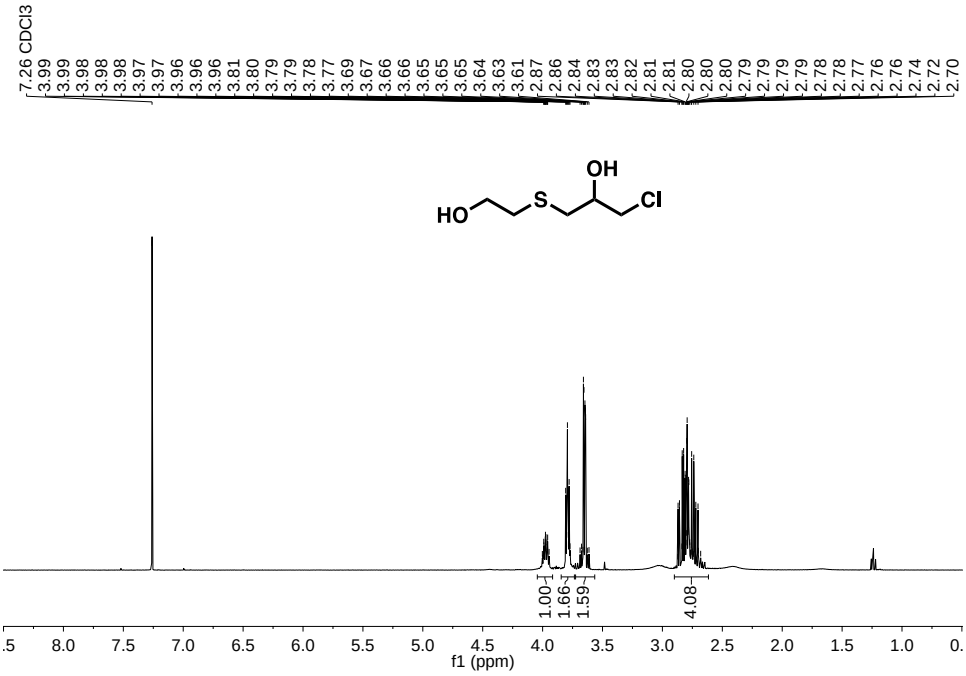

Figure S0-16. ^{1}H NMR spectra for CHETP.

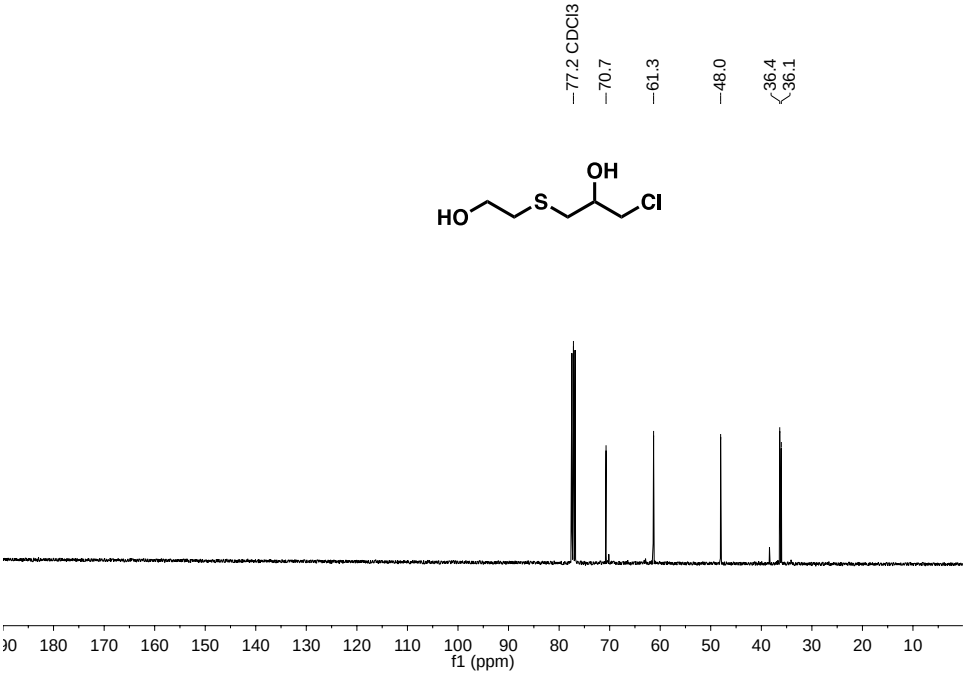

Figure S0-17. ^{13}C NMR spectra for CHETP.

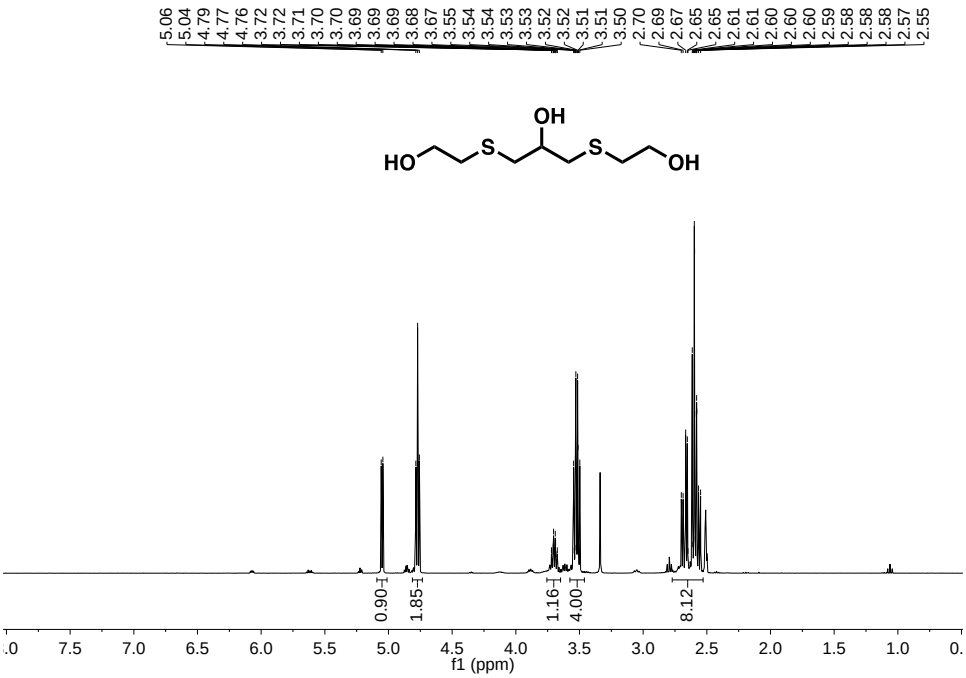

Figure S0-18. ^{1}H NMR spectra for BHETP.

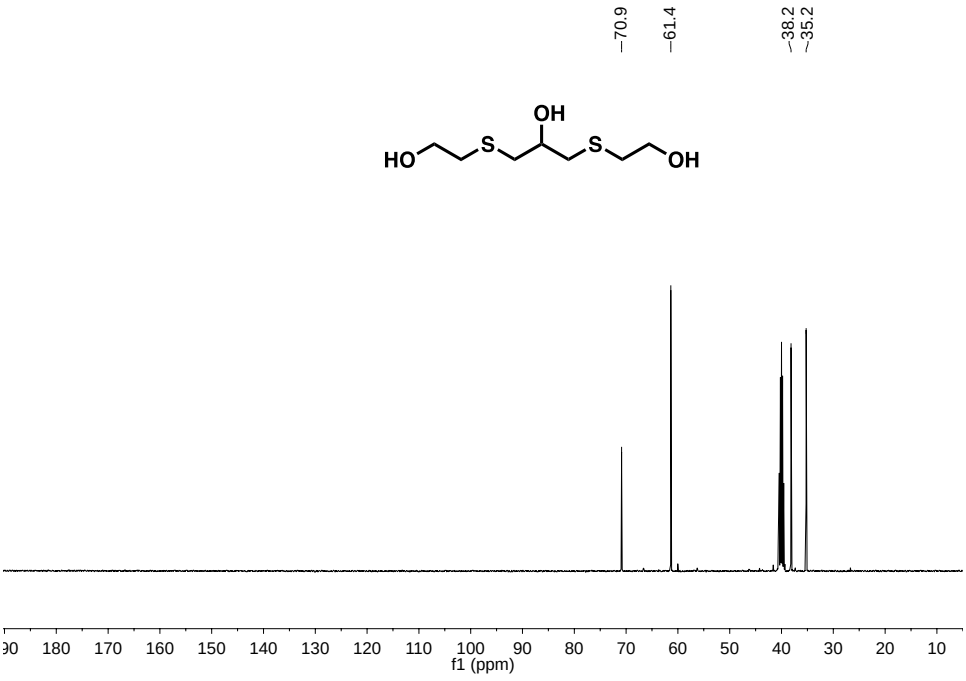

Figure S0-19. ^{13}C NMR spectra for BHETP.

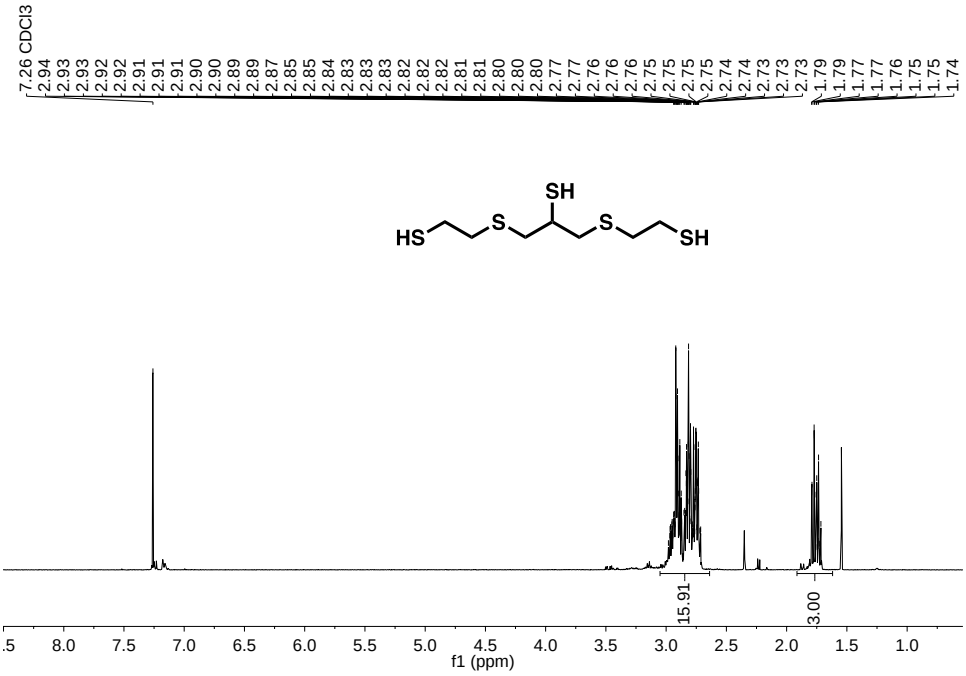

Figure S0-20. ^{1}H NMR spectra for trithiol 1.

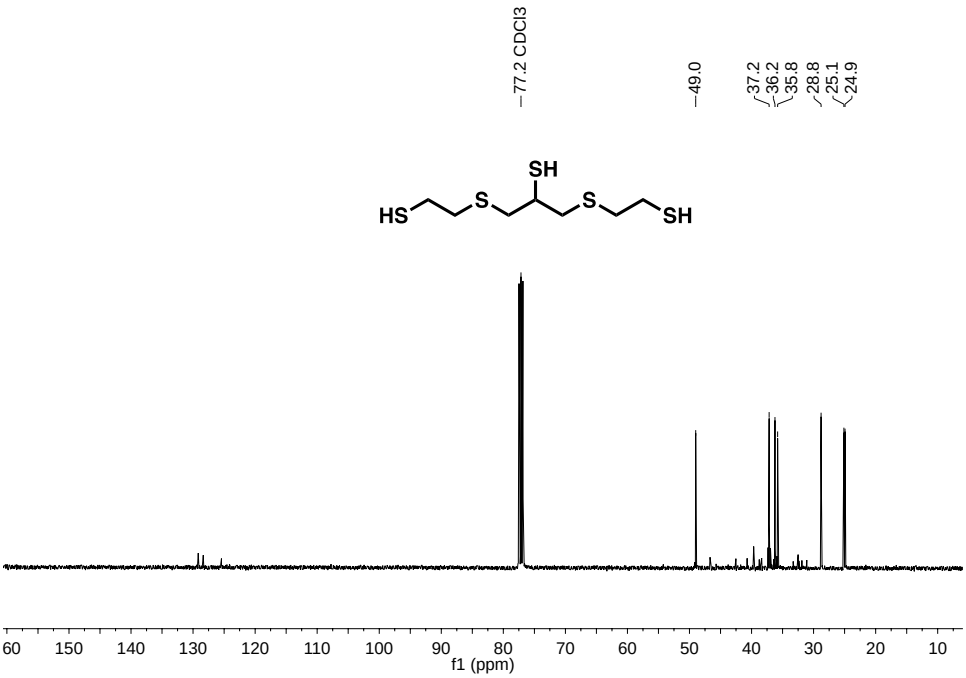

Figure 0-21. ^{13}C NMR spectra for trithiol 1.

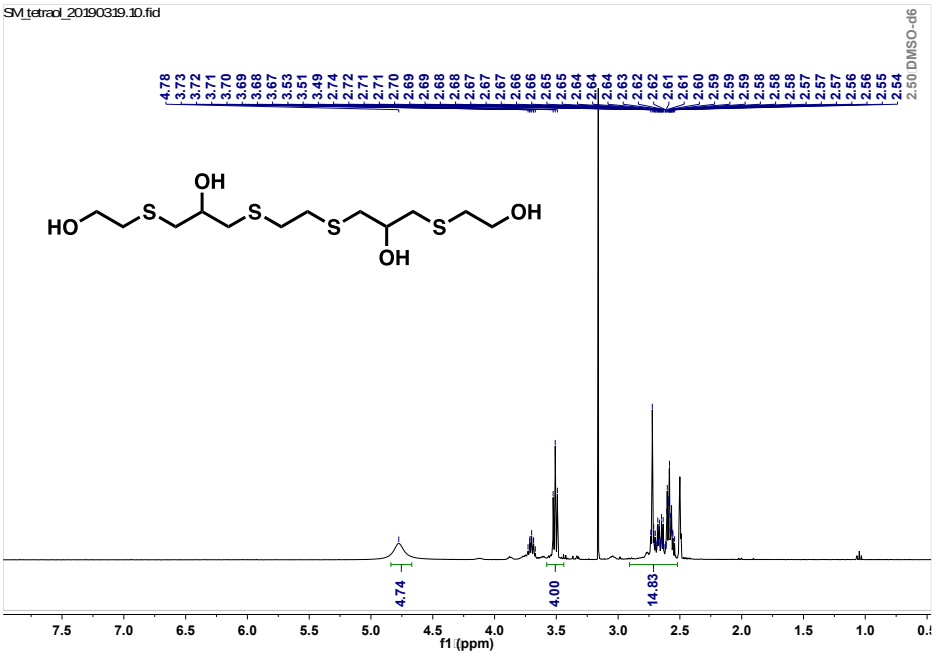

Figure S0-22. ^{1}H NMR spectra for tetra-alcohol 1.

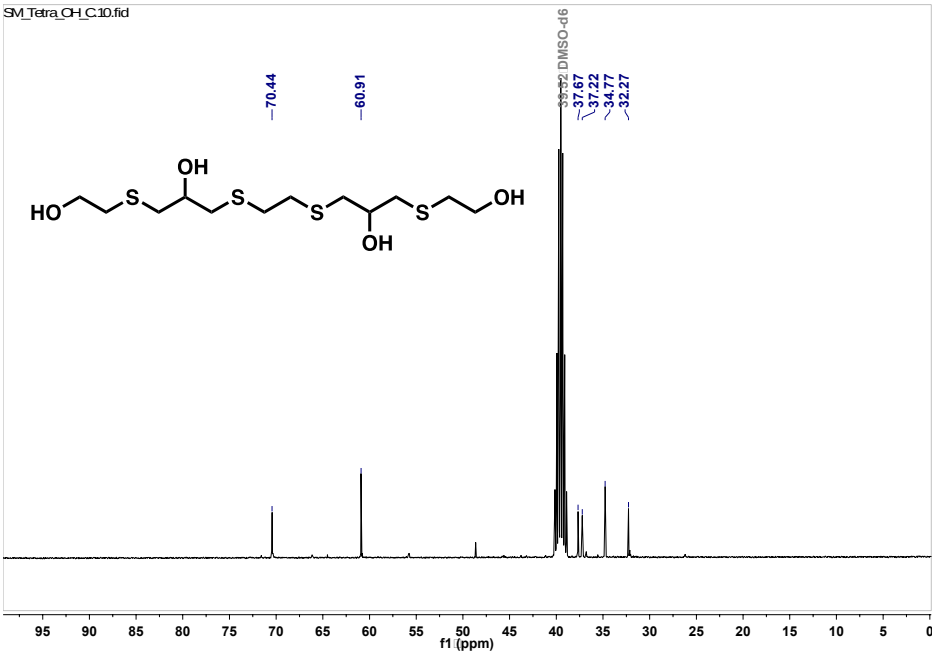

Figure S0-23. ^{13}C NMR spectra for tetra-alcohol 1.

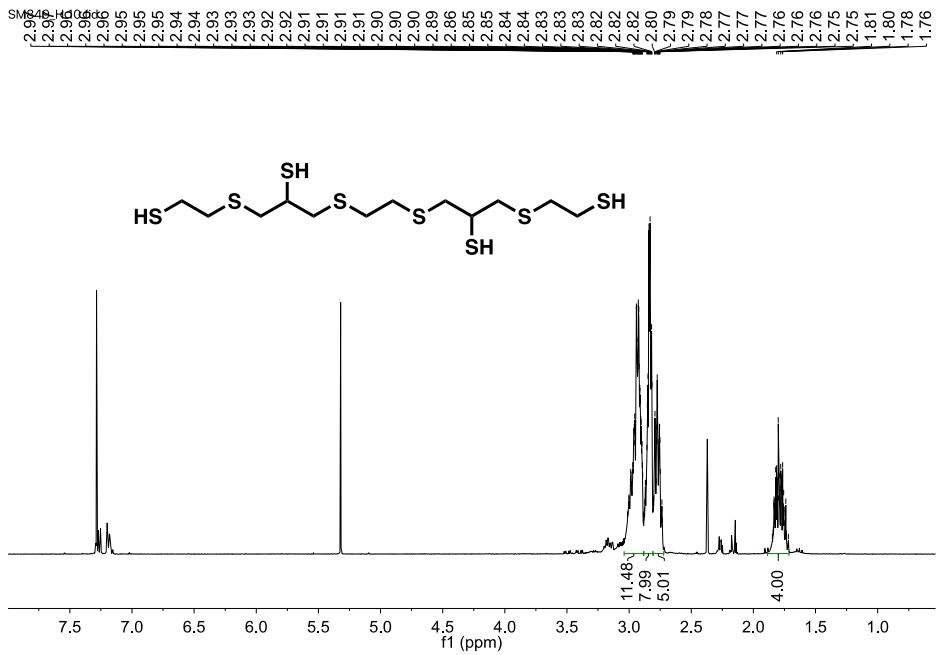

Figure S0-24. ^{1}H NMR spectra for tetra-thiol 1.

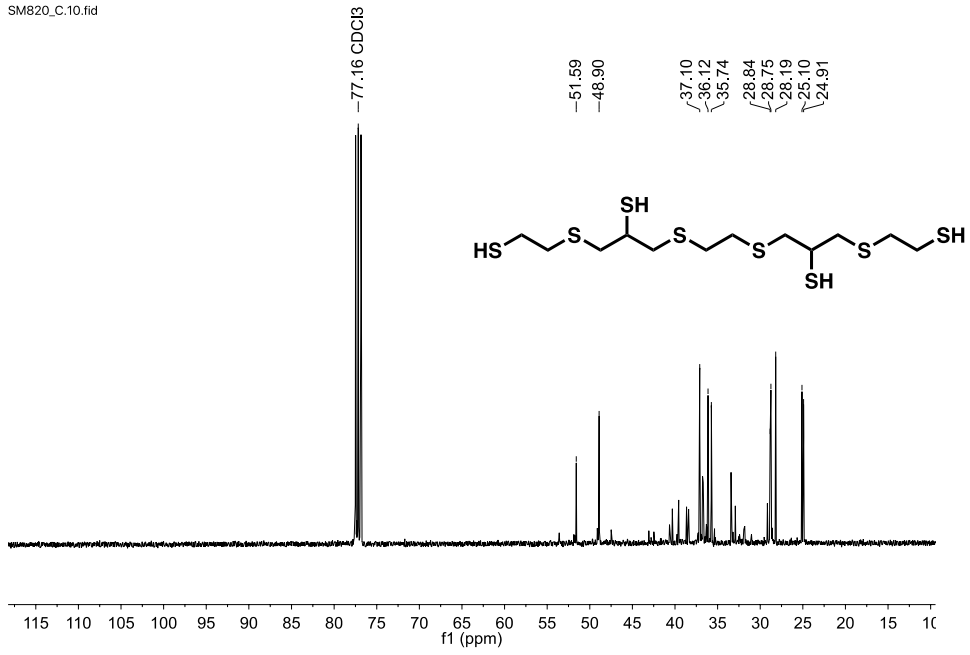

Figure S0-25. ^{13}C NMR spectra for tetra-thiol 1.

1.31 Acknowledgements

This material is based upon work supported by the National Science Foundation and Facebook.

1.32 References

1. Dislich, H., Plastics as Optical Materials. *Angew. Chem.-Int. Edit.* **1979,** *18* (1), 49-59.

2. Decker, C., Light-induced crosslinking polymerization. *Polymer International* **2002,** *51* (11), 1141-1150.

3. Xia, Y.; Kim, E.; Zhao, X.-M.; Rogers, J. A.; Prentiss, M.; Whitesides, G. M., Complex Optical Surfaces Formed by Replica Molding Against Elastomeric Masters. *Science* **1996,** *273* (5273), 347-349.

4. Calafiore, G.; Fillot, Q.; Dhuey, S.; Sassolini, S.; Salvadori, F.; Mejia, C. A.; Munechika, K.; Peroz, C.; Cabrini, S.; Piña-Hernandez, C., Printable photonic crystals with high refractive index for applications in visible light. *Nanotechnology* **2016,** *27* (11), 115303.

5. Pina-Hernandez, C.; Koshelev, A.; Digianantonio, L.; Dhuey, S.; Polyakov, A.; Calafiore, G.; Goltsov, A.; Yankov, V.; Babin, S.; Cabrini, S.; Peroz, C., Printable planar lightwave circuits with a high refractive index. *Nanotechnology* **2014,** *25* (32), 325302.

6. Beadie, G.; Shirk, J. S.; Rosenberg, A.; Lane, P. A.; Fleet, E.; Kamdar, A.; Jin, Y.; Ponting, M.; Kazmierczak, T.; Yang, Y., Optical properties of a bio-inspired gradient refractive index polymer lens. *Opt. Express* **2008,** *16* (15), 11540-11547.

7. Bruder, F. K.; Fäcke, T.; Rölle, T., The Chemistry and Physics of Bayfol HX Film Holographic Photopolymer. *Polymers* **2017,** *9*, 472.

8. Alim, M. D.; Glugla, D. J.; Mavila, S.; Wang, C.; Nystrom, P. D.; Sullivan, A. C.; McLeod, R. R.; Bowman, C. N., High Dynamic Range (Deltan) Two-Stage Photopolymers via Enhanced Solubility of a High Refractive Index Acrylate Writing Monomer. *ACS Appl Mater Interfaces* **2018,** *10* (1), 1217-1224.

9. Fernández, R.; Bleda, S.; Gallego, S.; Neipp, C.; Márquez, A.; Tomita, Y.; Pascual, I.; Beléndez, A., Holographic waveguides in photopolymers. *Opt. Express* **2019,** *27* (2), 827-840.

10. Chen, X.; Liu, W.; Dong, B.; Lee, J.; Ware, H. O. T.; Zhang, H. F.; Sun, C., High-Speed 3D Printing of Millimeter-Size Customized Aspheric Imaging Lenses with Sub 7 nm Surface Roughness. *Adv. Mater.* **2018,** *30* (18), 1705683.

11. Gissibl, T.; Thiele, S.; Herkommer, A.; Giessen, H., Two-photon direct laser writing of ultracompact multi-lens objectives. *Nature Photonics* **2016,** *10*, 554.

12. Liu, J.-g.; Ueda, M., High refractive index polymers: fundamental research and practical applications. *Journal of Materials Chemistry* **2009,** *19* (47), 8907-8919.

13. Higashihara, T.; Ueda, M., Recent Progress in High Refractive Index Polymers. *Macromolecules* **2015,** *48* (7), 1915-1929.

14. Macdonald, E. K.; Shaver, M. P., Intrinsic High Refractive Index Polymers. *Polym. Int.* **2015,** *64*, 6.

15. Griebel, J. J.; Namnabat, S.; Kim, E. T.; Himmelhuber, R.; Moronta, D. H.; Chung, W. J.; Simmonds, A. G.; Kim, K.-J.; van der Laan, J.; Nguyen, N. A.; Dereniak, E. L.; Mackay, M. E.; Char, K.; Glass, R. S.; Norwood, R. A.; Pyun, J., New Infrared Transmitting Material via Inverse Vulcanization of Elemental Sulfur to Prepare High Refractive Index Polymers. *Adv. Mater.* **2014,** *26* (19), 3014-3018.

16. Liu, J.-g.; Nakamura, Y.; Shibasaki, Y.; Ando, S.; Ueda, M., High Refractive Index Polyimides Derived from 2,7-Bis(4-aminophenylenesulfanyl)thianthrene and Aromatic Dianhydrides. *Macromolecules* **2007,** *40* (13), 4614-4620.

17. Fukuzaki, N.; Higashihara, T.; Ando, S.; Ueda, M., Synthesis and Characterization of Highly Refractive Polyimides Derived from Thiophene-Containing Aromatic Diamines and Aromatic Dianhydrides. *Macromolecules* **2010,** *43* (4), 1836-1843.

18. Tapaswi, P. K.; Choi, M.-C.; Jeong, K.-M.; Ando, S.; Ha, C.-S., Transparent Aromatic Polyimides Derived from Thiophenyl-Substituted Benzidines with High Refractive Index and Small Birefringence. *Macromolecules* **2015,** *48* (11), 3462-3474.

19. Matsuda, T.; Funae, Y.; Yoshida, M.; Yamamoto, T.; Takaya, T., Optical material of high refractive index resin composed of sulfur-containing aromatic methacrylates. **2000,** *76* (1), 50-54.

20. Okutsu, R.; Ando, S.; Ueda, M., Sulfur-Containing Poly(meth)acrylates with High Refractive Indices and High Abbe's Numbers. *Chem. Mat.* **2008,** *20* (12), 4017-4023.

21. Matsuda, T.; Funae, Y.; Yoshida, M.; Yamamoto, T.; Takaya, T., Optical material of high refractive index resin composed of sulfur-containing aliphatic and alicyclic methacrylates. *Journal of Applied Polymer Science* **2000,** *76* (1), 45-49.

22. Okutsu, R.; Suzuki, Y.; Ando, S.; Ueda, M., Poly(thioether sulfone) with High Refractive Index and High Abbe's Number. *Macromolecules* **2008,** *41* (16), 6165-6168.

23. Liu, J. g.; Ueda, M., High Refractive Index Polymers: Fundamental Research and Practical Applications. *J. Mater. Chem.* **2009,** *19*, 8907.

24. Bhagat, S. D.; Chatterjee, J.; Chen, B.; Stiegman, A. E., High Refractive Index Polymers Based on Thiol–Ene Cross-Linking Using Polarizable Inorganic/Organic Monomers. *Macromolecules* **2012,** *45* (3), 1174-1181.

25. Suzuki, Y.; Higashihara, T.; Ando, S.; Ueda, M., Synthesis and Characterization of High Refractive Index and High Abbe's Number Poly(thioether sulfone)s based on Tricyclo[5.2.1.02,6]decane Moiety. *Macromolecules* **2012,** *45* (8), 3402-3408.

26. Chen, X.; Fang, L.; Wang, J.; He, F.; Chen, X.; Wang, Y.; Zhou, J.; Tao, Y.; Sun, J.; Fang, Q., Intrinsic High Refractive Index Siloxane–Sulfide Polymer Networks Having High Thermostability and Transmittance via Thiol–Ene Cross-Linking Reaction. *Macromolecules* **2018,** *51* (19), 7567-7573.

27. Chan, J. W.; Zhou, H.; Hoyle, C. E.; Lowe, A. B., Photopolymerization of Thiol-Alkynes: Polysulfide Networks. *Chem. Mat.* **2009,** *21* (8), 1579-1585.

28. Gao, P.; Xu, P.-F.; Zhai, H., Borax-catalyzed thiolysis of 1,2-epoxides in aqueous medium. *Tetrahedron Letters* **2008,** *49* (46), 6536-6538.

29. Suzuki, Y. K. S. I. Mercapto compound, a high refractive index resin and lens and a process for preparing them
. 1992.

30. Hoyle, C. E.; Bowman, C. N., Thiol–Ene Click Chemistry. *Angew. Chem.-Int. Edit.* **2010,** *49* (9), 1540-1573.

31. Hoyle, C. E.; Lowe, A. B.; Bowman, C. N., Thiol-click chemistry: a multifaceted toolbox for small molecule and polymer synthesis. *Chem. Soc. Rev.* **2010,** *39* (4), 1355-1387.

32. Hawker, C. J.; Wooley, K. L., The Convergence of Synthetic Organic and Polymer Chemistries. *Science* **2005,** *309* (5738), 1200-1205.

33. Nebioglu, A.; Leon, J. A.; Khudyakov, I. V., New UV-Curable High Refractive Index Oligomers. *Industrial & Engineering Chemistry Research* **2008,** *47* (7), 2155-2159.

34. Okubo, T.; Kohmoto, S.; Yamamoto, M., Synthesis, characterization, and optical properties of polymers comprising 1,4-dithiane-2,5-bis(thiomethyl) group. **1998,** *68* (11), 1791-1799.

35. Okubo, T.; Kohmoto, S.; Yamamoto, M., Synthesis, characterization, and optical properties of polymers comprising 1,4-dithiane-2,5-bis(thiomethyl) group. *Journal of Applied Polymer Science* **1998,** *68* (11), 1791-1799.

36. Matsumoto, K.; Costner, E. A.; Nishimura, I.; Ueda, M.; Willson, C. G., High Index Resist for 193 nm Immersion Lithography. *Macromolecules* **2008,** *41* (15), 5674-5680.

37. Stockmayer, W. H., Theory of Molecular Size Distribution and Gel Formation in Branched Polymers II. General Cross Linking. **1944,** *12* (4), 125-131.

38. Maheswara, M.; Oh, S.-H.; Ju, J.-J.; Park, S. K.; Park, S.; Do, J. Y., High refractive index of transparent acrylate polymers functionalized with alkyl sulfur groups. *Polymer Journal* **2009,** *42*, 249.

39. Nakagawa, Y.; Suzuki, Y.; Higashihara, T.; Ando, S.; Ueda, M., Synthesis of Highly Refractive Poly(phenylene thioether) Derived from 2,4-Dichloro-6-alkylthio-1,3,5-triazines and Aromatic Dithiols. *Macromolecules* **2011,** *44* (23), 9180-9186.

40. Nakabayashi, K.; Imai, T.; Fu, M.-C.; Ando, S.; Higashihara, T.; Ueda, M., Poly(phenylene thioether)s with Fluorene-Based Cardo Structure toward High Transparency, High Refractive Index, and Low Birefringence. *Macromolecules* **2016,** *49* (16), 5849-5856.

41. McNair, O. D.; Janisse, A. P.; Krzeminski, D. E.; Brent, D. E.; Gould, T. E.; Rawlins, J. W.; Savin, D. A., Impact Properties of Thiol–Ene Networks. *ACS Appl. Mater. Interfaces* **2013,** *5* (21), 11004-11013.

42. Zwiers, R. J. M.; Dortant, G. C. M., Aspherical lenses produced by a fast high-precision replication process using UV-curable coatings. *Appl. Opt.* **1985,** *24* (24), 4483-4488.

43. Norland Optical Adhesive 170. https://www.norlandprod.com/adhesives/NOA170.html (accessed 3/26/19).

Fundamentals of Photopolymerizable Thermoplastics[1]

Thermoplastics, such as poly(ethylene) and poly(ethylene terephthalate), are high molecular weight linear polymers that have become the preeminent synthetic materials of modern society. Photopolymers are crosslinked materials conveniently fabricated from low viscosity liquid resins in a matter of seconds using light. Thermoplastics formed from photopolymerizations, however, do not develop sufficiently useful material properties compared to traditional methods such as injection molding or extrusion. Here, a set of photopolymerizable systems capable of forming semicrystalline high molecular weight polymers in seconds at ambient temperature using visible light at low intensities (1 mW/cm^2) is presented. This new paradigm of photopolymers enables access to an extraordinary set of mechanical properties (such as elongations to break of around 800% strain, and toughness values of around 100 MJ/m^3) and capabilities (melt and reprocess) not achievable with existing photopolymers.

1.33 Introduction

Thermoplastics, more universally known as ‘plastics’, are the defining synthetic materials of modern society based on their unmatched versatility and utility. While thermoplastics, such as poly(ethylene terephthalate) (PET),[1, 2] are ubiquitous and produced globally on a massive industrial scale there remains no way of producing

[1] Contributing authors: Kimberly K. Childress, Neil J. Baugh, Alina M. Martinez, Benjamin D. Fairbanks, Matthew K. McBride, Brady T. Worrell, Jeffrey W. Stansbury, Robert R. McLeod, and Christopher N. Bowman

thermoplastic materials, or even close mimics, via photopolymerization. This disparity is because the polymerization kinetics of linear polymers are inherently slow which limits the molecular weights achieved and the conversion which ultimately severely limits the mechanical properties.

Here, as shown in Figure 0-1, the distinct virtues of both thermoplastics and photopolymers are combined into a single materials platform, extending thermoplastic materials to be photopolymerizable. Utilizing a unique subset of dithiol and divinyl monomers, we demonstrate that semicrystalline high molecular weight polymers are rapidly produced under neat conditions at ambient temperature using mild irradiation and dose conditions. Owing to the high molecular weights and extent of crystallinity quickly achieved in these photopolymerizable thermoplastic systems, impressively strong and tough materials closely resembling important thermoplastics, such as PET, are formed. A systematic study of the structure-property relationships were investigated with varying alkyl dithiol lengths with the model diallyl ester monomer.

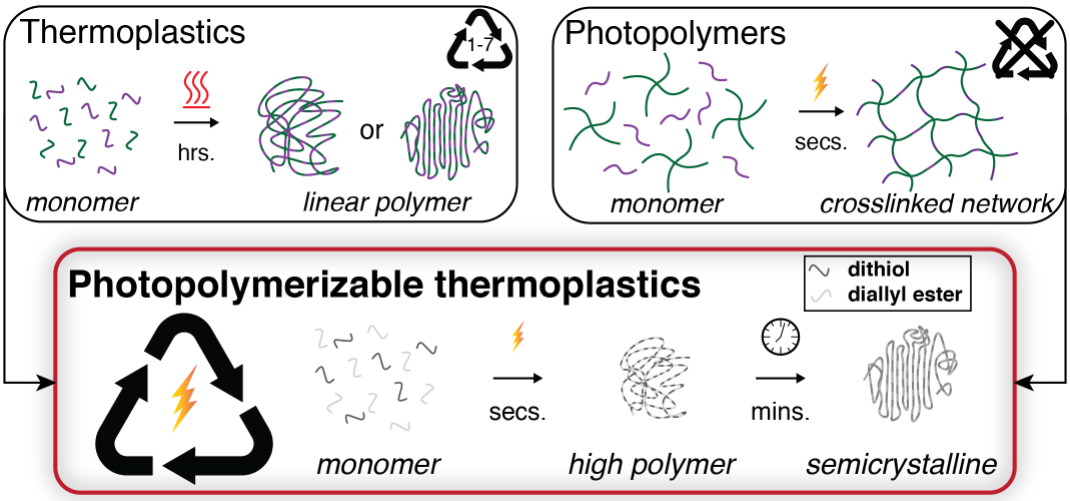

Figure 0-1. Overview of photopolymerizable thermoplastics. (a) Schemes of traditional thermoplastics and photopolymers. The former typically involve thermally-driven

polymerizations forming polymers that vary in degree of branching and range from being completely amorphous to semicrystalline. In contrast, photopolymers generally comprise the light-induced formation of permanent, crosslinked networks that are amorphous. The presented system, photopolymerizable thermoplastics, harnesses the thiol-ene reaction to combine the key characteristics (i.e. light-induced formation of robust, linear polymers) of both systems. Specifically, a stoichiometric ratio of alkyl dithiol and diallyl ester monomers were studied.

1.34 Experimental

1.34.1 Materials

Commercially available photoinitiator and monomers were used as received without further purification. Alkyl dithiols 1,2-ethane dithiol (EDT), 1,3-propane dithiol (PDT), and 1,8-octane dithiol (ODT) were purchased from Acros while 1,4-butane dithiol (BDT), 1,5-pentane dithiol (PDT), and 1,6-hexane dithiol (HDT), 1,9-nonane dithiol (NDT), and 1,10-decane dithiol (DDT) were purchased from Alfa Aesar and Sigma-Aldrich. Diallyl terephthalate (DAT), diallyl isophthalate (DAI), diallyl phthalate (DAP), and photoinitiator, diphenyl(2,4,6-trimethylbezoyl)phosphine oxide (TPO), were purchased from TCI America.

1.34.2 Methods

Thiol-ene formulation preparation and photopolymerization

A stoichiometric ratio of dithiol and diallyl monomers were well mixed in a 20 mL scintillation vial (VWR) with TPO photoinitiator set at 1 mol% to either functional group (corresponding to 0.87 wt% of the total formulation). Films were prepared between glass plates with 250 μm plastic shims (Precision Brand) lining the perimeter to control the thickness with binder clips used to clamp the slides together. A broadband LED source (ECO UV Bar) was used to irradiate the samples at an intensity of approximately 7 mW/cm^2 at 405 nm for 5 – 10 minutes.

Fourier Transform Infrared Spectroscopy (FTIR)

Fourier transform infrared spectroscopy was used to monitor the polymerization of the thiol and carbon-carbon double bonds. A Thermo Scientific Nicolet 6700 FTIR spectrometer was used with a 405 nm LED source (Thorlabs) using a myDAQ device (National Instruments) synchronized to a computer for timed and defined illuminations at 1-10 mW/cm^2. Optically thin samples were prepared between two salt (NaCl) plates using 15 μ m spacers. Thiol conversion (c_{thiol}) and vinyl conversion (c_{vinyl}) were monitored using a series scan, integrating over the ranges 2550-2600 cm^{-1} and 1778-1650 cm^{-1} respectively. Conversion of functional groups (c) was calculated with the equation,

$$c = (1 - \frac{A_{final}}{A_{initial}}) * 100\% \quad (1)$$

where $A_{initial}$ is the area of the unconsumed functional group peak, and A_{final} is the area under the thiol or C=C peak after the thiol-ene reaction.

Photo-rheology

A rotational rheometer (ARES-G2, TA Instruments) with a parallel plate geometry using a photocuring geometry equipped with mirrors and a 20 mm diameter quartz plate for in-situ irradiation using a 405 nm LED (Thorlabs) with an intensity of 10 mW/cm^2.

Polarized optical imaging

A Nikon Eclipse Ci optical microscope equipped with a commercial DLP (Mightex Polygon 400) and visible LED source control module (Mightex BioLED) was used to image the photopolymerization and subsequent crystallization of thiol-ene resins

between two glass slides. An analyzer was inserted after irradiation to take cross polarized images of the crystallization events.

Differential scanning calorimetry (DSC)

Differential scanning calorimetry (DSC) was conducted with a TA Instruments DSC2500 at a heating and cooling rate of 2°C/min under a N_2 atmosphere. Approximately 5-7 mg of sample was measured in a hermetically sealed aluminum pan. The melting temperature (T_m) was taken as the peak of the melting endotherm, the glass transition temperature (T_g) was taken as the midpoint of the heat capacity change, and the cold crystallization temperature (T_c) was taken as the peak of the exotherm. The heat of fusion (ΔH_f) was taken as the area of the melting endotherm.

Size exclusion chromatography with multi-angle light scattering and viscometry (SEC-MALS-IV)

A size-exclusion chromatography equipped with a UV and differential refractive index detector (Tosoh EcoSEC) was used with a multi-angle light scattering detector (Wyatt Treos II) and an online viscometer (Wyatt Viscostar).

Mechanical tensile testing

A uniaxial tensile tester (Exceed Model E42 – MTS) was used on thiol-ene films cut into ASTM D368 Type V dogbones ranging in thickness (120 – 250 μm) and tested with a strain rate of 5 mm/min at ambient temperature.

1.35 Results & Discussion

A series of in-situ experiments were conducted to gain fundamental insight on the various processes occurring in these photopolymerizable thermoplastic systems. The studied systems comprised a stoichiometric ratio of alkyl dithiol (collectively

referred to as ‘xDT’) and diallyl terephthalate (DAT) with the 1,6-hexane dithiol (HDT) used as a representative system unless otherwise stated (hereon referred to as the ‘HDT-DAT’ system). The structures used are shown in Figure 0-2.

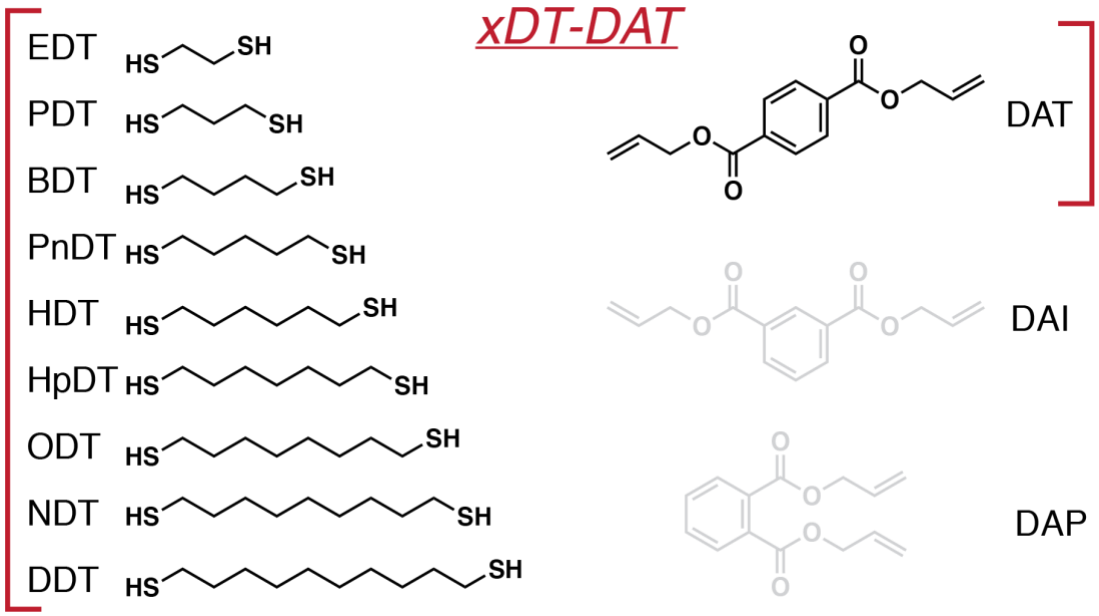

Figure 0-2. Chemical structures of alkyl dithiols (xDT) and the diallyl esters monomers used. Primarily, systems comprising xDT and DAT were investigated.

First and foremost, achieving sufficiently high molecular weights in linear step-growth photopolymerizations requires rapid reaction kinetics to near quantitative conversions. As shown in Figure 0-3, this condition was confirmed using real-time Fourier transform infrared spectroscopy (FTIR) for each xDT-DAT system (except NDT-DAT) by monitoring the swift disappearance of both characteristic SH and C=C peaks upon 405 nm LED irradiation using modest exposure intensities (1-10 mW/cm^2). Furthermore, as evident in Figure 0-3, with the exception of the EDT-DAT system the effectively identical kinetic profiles of both thiol and ene groups for every system suggests an archetypal step growth process with minimal to no vinyl homopolymerization observed. The rapid and selective thiol-ene kinetics observed are

consistent with recent reports by the Liska group where they observed preferential as well as enhanced reactivities of vinyl esters (highly similar to the allyl ester groups in DAT) with thiols compared to just the vinyl homopolymerization. The outlying ene conversion of the EDT-DAT system is most likely due to the incorrect integration of the C=C peak and/or a limitation of infrared spectroscopy sensitivity rather than an incomplete conversion. This notion is supported by the fact that the conversion profiles of thiol and ene were essentially indistinguishable except for the conversion plateau values. An alternative look at the respective thiol and ene reactivity for each system is presented in Figure 0-4 showing that the thiols are indistinguishable in their reactivity and final conversions. The same can be said of the ene conversion except for the EDT-DAT.

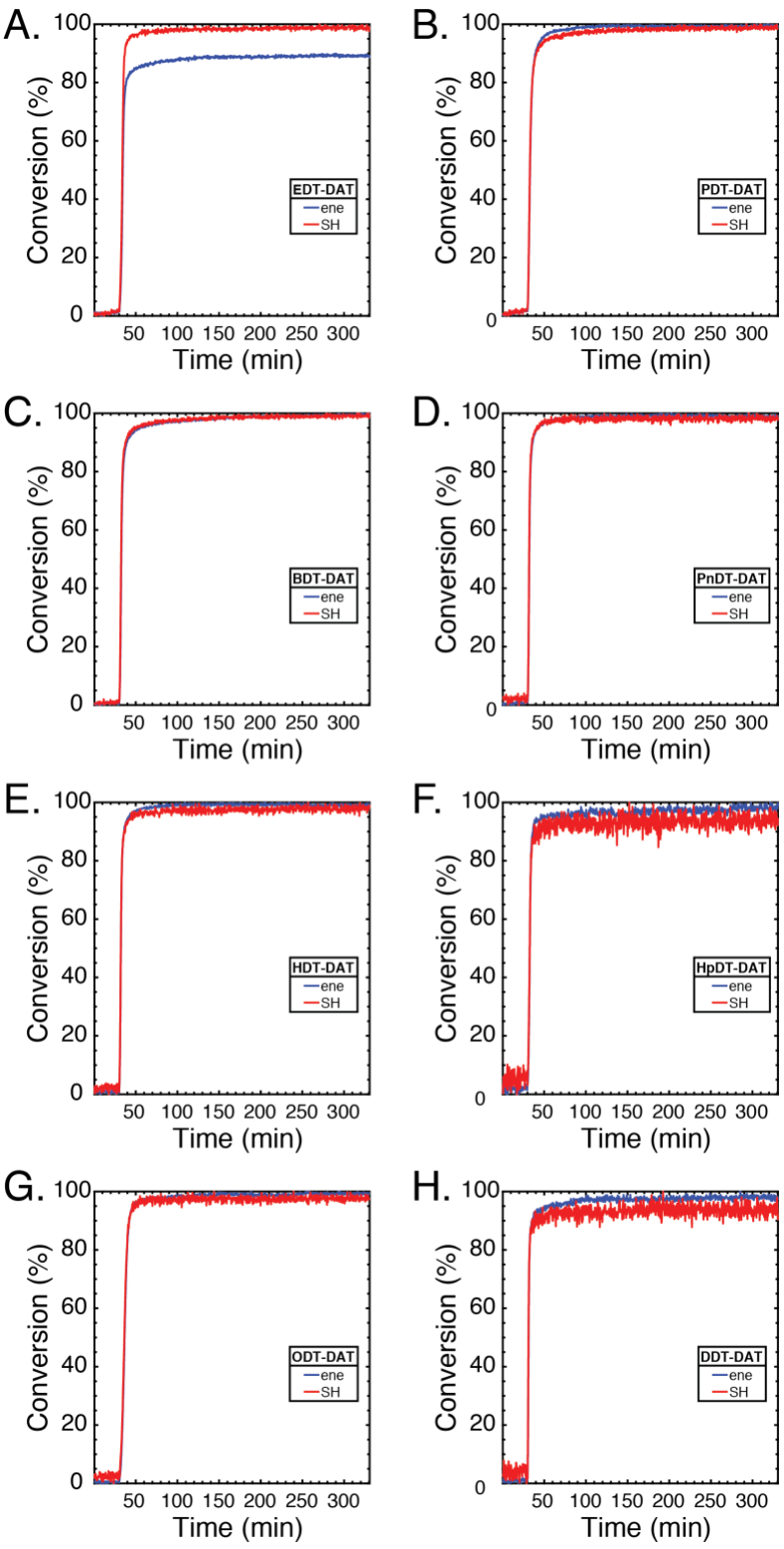

Figure 0-3. Polymerization kinetics obtained via real-time FTIR of the thiol-ene photopolymerization using a continuous irradiation turned on at t = 30 s (405 nm LED, 1

mW/cm^2) for each xDT-DAT system. (A) EDT-DAT system. (B) PDT-DAT system. (C) BDT-DAT system. (D) PnDT-DAT system. (E) HDT-DAT system. (F) HpDT-DAT system. (G) ODT-DAT system. (H) DDT-DAT system.

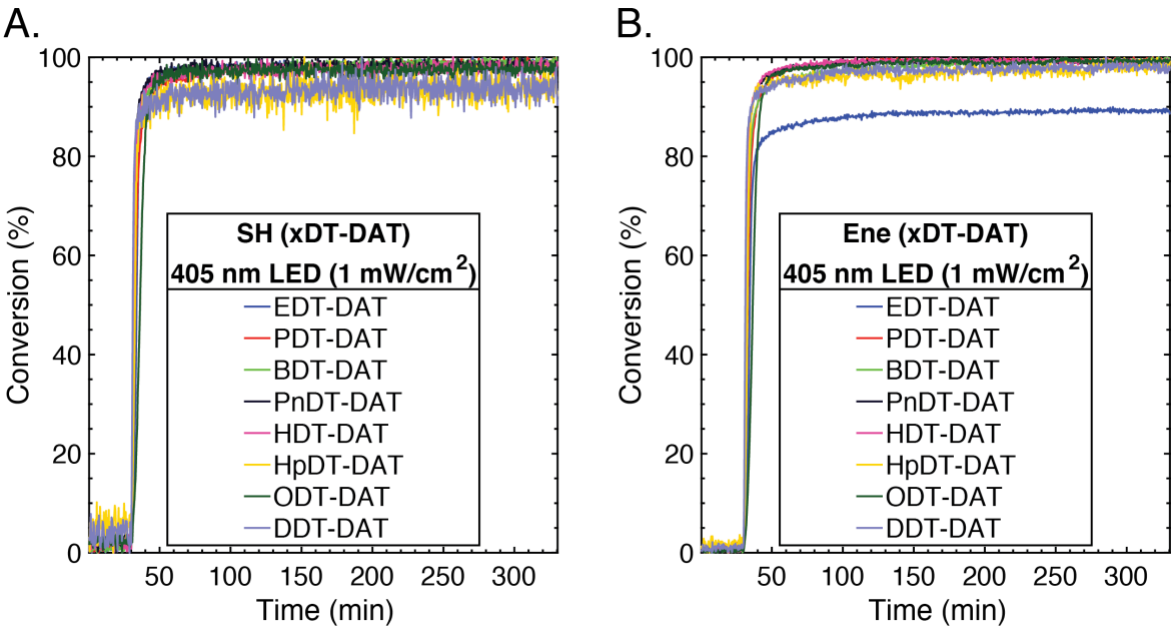

Figure 0-4. Polymerization kinetics obtained via real-time FTIR of the thiol-ene photopolymerization using a continuous irradiation turned on at t = 30 s (405 nm LED, 1 mW/cm^2) for each xDT-DAT system. (A) All thiol conversions for xDT-DAT. (B) All ene conversions for xDT-DAT.

Next, the HDT-DAT system was used as a representative system to investigate the modulus development of the thermoplastic photopolymer systems upon similar 405 nm irradiation conditions using real-time photo-rheology to measure both storage (G') and loss moduli (G''). As shown in Figure 0-5, moduli increased dramatically due to the photopolymerization with a rapid G'-G'' crossover (indicative of solid-like behavior) observed. However, storage modulus continued to increase further well after the polymerization timescale before eventually plateauing. This phenomenon was also reflected in a dramatic concurrent increase in the complex viscosity of the system as shown on the secondary y-axis of Figure 0-5. Based on this rheological data and the

independent observation of changes in the physical appearance of the formed polymer, i.e. going from transparent to translucent to white, it was hypothesized that crystallization was occurring.

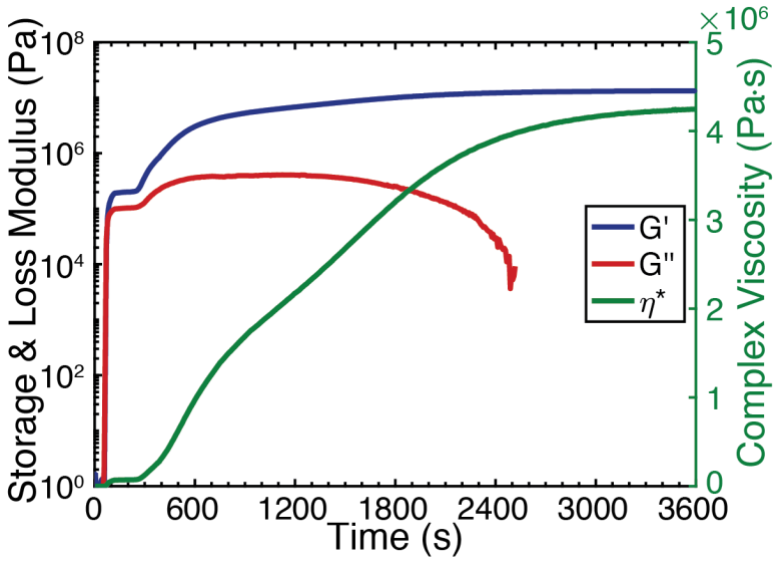

Figure 0-5. Real-time modulus development of HDT-DAT obtained via photo-rheology revealing a sharp increase in both storage (G') and loss (G'') modulus due to the photopolymerization with an eventual decrease in G'' below the instrumental detection limits. Critically, G' continues to increase well after the polymerization before eventually hitting a plateau due to crystallization. This phenomenon is also revealed in the concomitant increase in the complex viscosity.

To directly confirm crystallization, *in-situ* polarized microscopy imaging of the photopolymerization and crystallization processes were conducted with a series of representative time points presented in Figure 0-6 showing the development of characteristic spherulites[3, 4] over several minutes – well after the polymerization timescale as determined from real-time FTIR. Curiously, when a uniform circular illumination was used, spherulites were observed to grow preferentially first at the exposure interface presumably due to favorable heterogenous nucleation as shown by the sequence of differential interference contrast (DIC) images in Figure 0-7. After this

initial growth, spherulites coalesce inwards until they impinge on each other with the inner centroid developing at a much later time point.

The ability and propensity for crystallization in these particular thiol-ene systems is explained by the fast reaction kinetics and quantitative conversions that result in long polymer chains with high degrees of linear symmetry.[5] Thus, produced polymers are expected to be minimally branched with high degrees of stereoregularity and a regular step-growth configuration (i.e. marginal homopolymerization). Furthermore, in an analogy to PET, crystallization is promoted by the combination of the flexible alkyl chains to organize,[5] the intermolecular dipole-dipole interactions between the polar carbonyl groups[6] as well as the regular π-π stacking of the benzene rings present along the main chain. Systems that used the 1,2-substituted (diallyl phthalate) and 1,3-substituted (diallyl isophthalate) structural isomers instead of DAT were not observed to be crystalline. Classically, spherulite formation (crystallization) in polymers has been observed from melts or solutions with a large degree of undercooling ($\Delta T = T_m - T_c$, the difference between melting and crystallization temperatures).[3, 4, 7-10] However, here crystallization occurs from a polymer formed and kept at ambient temperature.

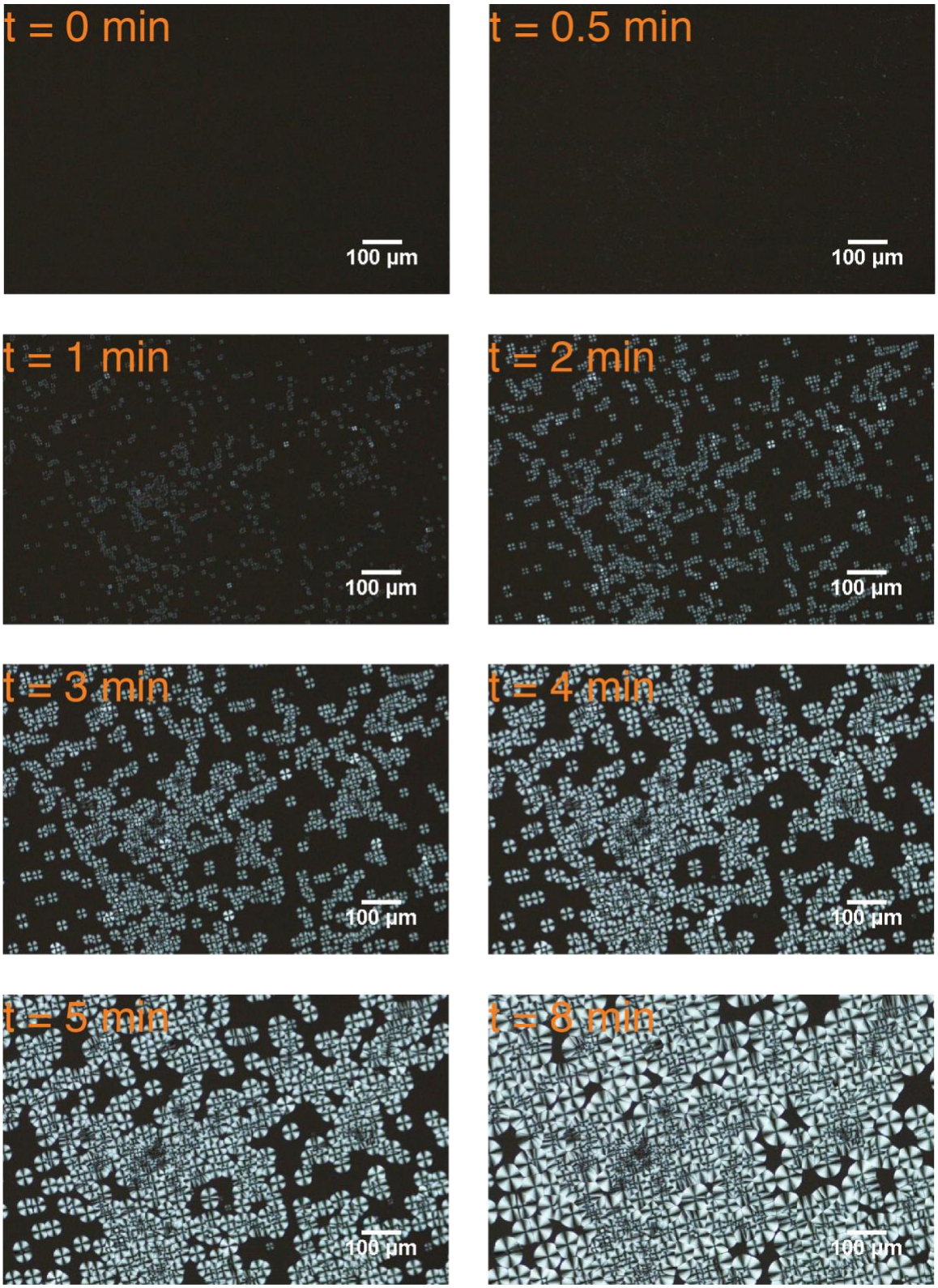
t = 0 min
100 µm
t = 0.5 min
100 µm
t = 1 min
100 µm
t = 2 min
100 µm
t = 3 min
100 µm
t = 4 min
100 µm
t = 5 min
100 µm
t = 8 min
100 µm

Figure 0-6. A series of images at representative time points viewed through crossed polarizers of the crystallization observed in the form of characteristic spherulite formation after the photopolymerization of HDT-DAT using a uniform 400 nm flood illumination.

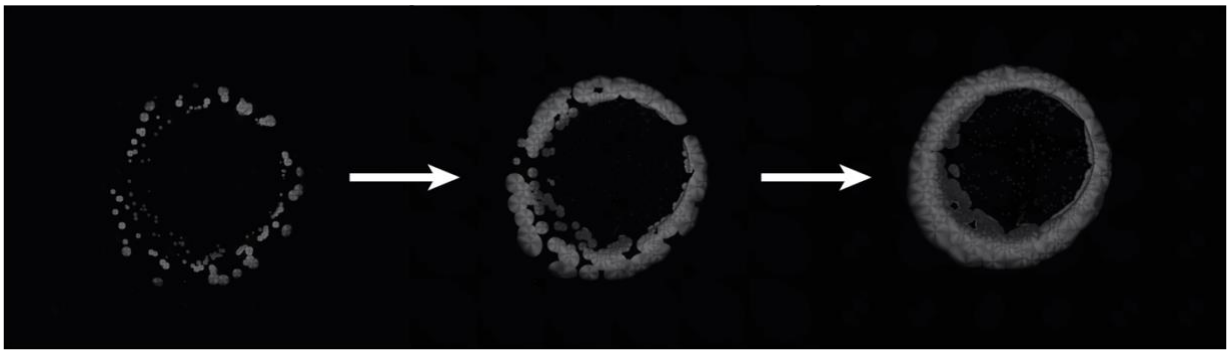

Figure 0-7. A series of large DIC images taken at representative time points after a circular 405 nm LED beam was irradiated on a neat HDT-DAT resin.

While the presence of crystallinity in the HDT-DAT polymers are generally indicative of linear polymers, the formation of a non-crosslinked polymer can be unequivocally confirmed by either its ability to melt, flow, or be dissolved in a suitable solvent. First, differential scanning calorimetry (DSC) was used with standard heat-cool-heat ramp cycles with distinct first-order phase transitions observed in the form of relatively sharp melting endotherms with a typically broader exothermic exotherm (Figure S0-18 – Figure S0-26, Supporting Information). Certainly, the detection of distinct first-order phase transitions (i.e. melting and crystallization) strongly supports the notion of semicrystalline linear polymers being produced from these rapid thiol-ene photopolymerizations. Solubility tests were also conducted separately in both THF and DCM at a concentration of 1 mg/mL for each xDT-DAT system at ambient temperature as summarized in Table 0-1. The systems with the four lowest molecular weight alkyl dithiols, i.e. EDT, PDT, BDT, and PnDT, did not exhibit any solubility of the polymer in either solvent except for PDT-DAT in DCM. All the other systems dissolved easily in

both solvents. The insolubility of the lower molecular weight alkyl dithiols is not unsurprising given their structural resemblance to the commercial polyesters, PET and poly(butylene terephthalate). These commercial polymers are known to not be soluble in either DCM or THF, and instead require highly polar fluorinated solvents such as hexafluoroisopropanol (HFIP) or trifluoroethanol (TFE) to dissolve them. However, testing the solubilities of the xDT-DAT systems in these polar solvents was beyond the scope of this study.

Table 0-1. Summary of solubilities of xDT-DAT polymers in either THF or DCM tested at a concentration of 1 mg/mL at ambient temperature.

xDT-DAT	Solubility (1 mg/mL)	
	THF	DCM
EDT-DAT	No	No
PDT-DAT	No	Yes
BDT-DAT	No	No
PnDT-DAT	Yes	Yes
HDT-DAT	Yes	Yes
HpDT-DAT	Yes	Yes
ODT-DAT	Yes	Yes
NDT-DAT	Yes	Yes
DDT-DAT	Yes	Yes

Next, as high molecular weights are the defining characteristic for functionally useful thermoplastics,[5, 6] absolute molecular weights (MW), dispersity and chain morphology (degree of branching) of photopolymerized thermoplastics were determined using size-exclusion chromatography with multi-angle light scattering and differential viscometry (SEC-MALS-IV) in tetrahydrofuran (THF). A summary of the results are

listed in Table 0-2. Evidently, high average molecular weights on the order 10^4 g/mol are achieved in all the tested xDT-DAT systems with polydispersity values close to 2 suggesting the formation of a step-growth polymer.[5, 11, 12] Furthermore, individual intrinsic viscosity vs. molecular weight plots (Mark-Houwink-Sakurada plots) were fitted to reveal exponent **a** values between 0.46 and 0.56 which is indicative of a random coil morphology; these results are consistent with the observed tendency towards crystallization.

Table 0-2. Summarized SEC-MALS-IV results for xDT-DAT covering average number molecular weight (M_n), average weight molecular weight (M_w), polydispersity index (M_w/M_n), and the Mark-Houwink-Sakurada parameters a and K.

xDT-DAT	M_n [10^4 g/mol]	M_w [10^4 g/mol]	M_w/M_n	a	K [mL/g]
HDT-DAT	7.12	18.8	2.65	0.46	0.373
HpDT-DAT	4.8	9.51	1.98	0.546	0.165
ODT-DAT	4.92	8.96	1.82	0.542	0.185
NDT-DAT	4.14	8.37	2.02	0.521	0.238
DDT-DAT	4.24	7.41	1.75	0.557	0.178

According to the Carothers equation,[12] achieving these molecular weights in a linear step-growth system (corresponding to degree of polymerizations approaching 100) would entail near-perfect stoichiometric balance (r = 1) and conversions of about 99% or greater. Generally speaking, these requirements are unattainable for most polymerization methods, let alone photopolymerizations that occur in seconds. Possible explanations of these molecular weight results are limited to either: i) a pure thiol-ene step-growth polymerization, ii) a predominantly thiol-ene with a minor contribution from homopolymerization of the diallyl ester, or iii) significant ene homopolymerization. The former is unlikely because commercial monomers were used as received without further

purification and would result in a stoichiometric imbalance between thiol and ene, even if the monomers were weighed out perfectly (which they certainly were not). The latter explanation is also effectively ruled out by the solubility of the polymer in organic solvent as a diallyl homopolymerization would produce intractable covalently crosslinked networks. Therefore, we deduced that it is most probable that a thiol-ene step-growth is the predominant polymerization mechanism with further increases in molecular weight supported by small amounts of homopolymerization of any residual ene groups to produce linear polymers with low degrees of branching.

This premise is supported by recent studies by the Liska group where they investigated the reactivity of vinyl esters (close analogs to the allyl esters used in these studies) with thiols against their (meth)acrylate(s) structural counterparts.[13] Their seminal studies revealed thiol-vinyl ester photopolymerizations proceeded significantly faster than the vinyl ester homopolymerization and could even match the reactivity kinetics of acrylates. This behavior was attributed to the differences in resonance stabilizations of the acrylate and vinyl ester radicals leading to different monomer and radical reactivities.[14] Vinyl ester radicals, as opposed to acrylate (α-carbonyl) radicals, lack significant resonance stabilization and are thus prone to hydrogen abstraction making them relatively poor chain-growth monomers but excellent thiol-ene step-growth monomers. Based on our set of results, we observe the allyl esters to behave similarly. However, unlike vinyl esters, allyl esters have the advantage of being more widely available commercially due to their synthetic accessibility. In this regard, it is also foreseeable that additional photopolymerizable thermoplastic systems analogous to other high performance polyesters such as poly(ethylene naphthalate) or poly(butylene

succinate) can be arrived at in scale. Therefore, while relatively less studied than other vinyls (such as allyl ethers, vinyl ethers and norbornenes),[15] both allyl and vinyl esters represent highly promising ene groups that deserve greater attention for broader thiol-ene applications.

It is well established that thermoplastic polymers only develop useful mechanical properties at critical molecular weight values.[12] To verify the molecular weights measured via SEC-MALS-IV were sufficiently high for practical use, uniaxial tensile testing of 120 – 250 μm thick dogbones (ASTM Type V) for the range of xDT-DAT systems were conducted with multiple repeats. The key mechanical properties are summarized in Table 0-3 with the stress-strain plots for each xDT-DAT system shown in order from Figure 0-8 (EDT-DAT) to Figure 0-16 (DDT-DAT). As shown in these engineering stress-strain plots, characteristic necking followed by significant amounts of strain hardening was observed to occur at elastomeric-like elongations suggesting significant amounts of entanglements of the amorphous phase. Interestingly, a few of these systems, such as HDT-DAT, exhibited a peculiar plastic deformation mechanism consisting of periodic reductions in stress at elevated strains evident by the jagged features on the stress-strain plots from Figure 0-8 to Figure 0-16. This behavior was physically observed on the deformed sample as intermittent striations with alternating lines of white, opaque regions and transparent regions as shown in Figure 0-17. Overall, these semicrystalline linear polymers exhibited extremely ductile behavior achieving ultimate tensile strengths between 15 to 24 MPa at failure strains ranging from 300% to 800%. These simple xDT-DAT systems thus cover a useful range of mechanical properties not encountered with the existing classes of polymers. In this

respect, photopolymerizable thermoplastics can be considered to represent their own unique class of polymeric materials.

Table 0-3. Summarized mechanical properties of xDT-DAT systems from the stress-strain plots due to a uniaxial tensile deformation at 5 mm/min at ambient temperature using photopolymer films (thickness: 0.12 – 0.25 mm) cut into ASTM D368 Type V dogbones.

xDT-DAT	Young's modulus (MPa)	Yield strength (MPa)	Ultimate tensile strength (MPa)	Failure strain (%)	Toughness (MJ/m^3)
EDT-DAT	183 ± 12	14.6 ± 0.9	18.0 ± 2.6	320 ± 66	44.1 ± 10.7
PDT-DAT	104 ± 7	9.37 ± 0.38	16.4 ± 2.9	558 ± 138	61.5 ± 20.2
BDT-DAT	85 ± 6	8.65 ± 0.44	24.5 ± 3.0	669 ± 104	94.9 ± 21.5
PnDT-DAT	70 ± 3	6.19 ± 0.29	15.6 ± 1.0	702 ± 60	63.7 ± 6.9
HDT-DAT	74.6 ± 5.2	7.17 ± 0.57	24.4 ± 1.6	793 ± 25	102 ± 9
HpDT-DAT	89.5 ± 3.3	7.39 ± 0.27	22.2 ± 2.7	825 ± 81	102 ± 19
ODT-DAT	68.6 ± 4.6	7.33 ± 0.27	27.2 ± 3.1	809 ± 67	119 ± 20
NDT-DAT	104.5 ± 7.3	8.87 ± 0.45	19.6 ± 3.1	697 ± 107	85.8 ± 20.5
DDT-DAT	79.8 ± 4.0	8.59 ± 0.34	23.7 ± 1.9	696 ± 57	97.7 ± 13.2

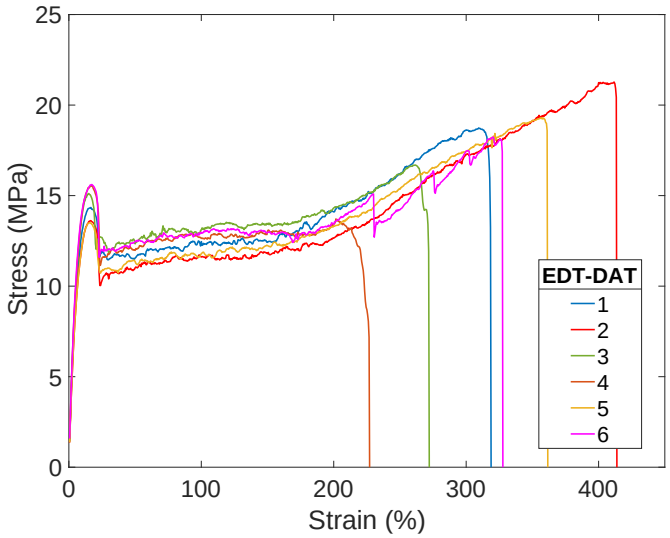

Figure 0-8. Engineering stress-strain plot for EDT-DAT using ASTM D368 Type V dogbones (0.12 – 0.13 mm thick) at a strain rate of 5 mm/min. (n = 6)

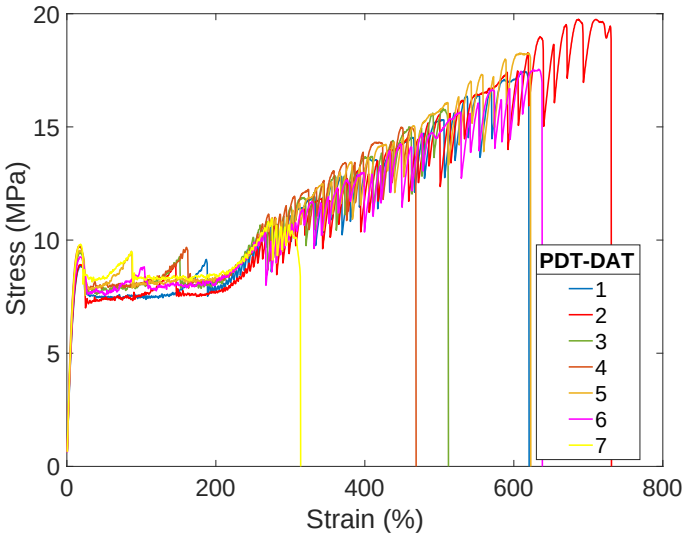

Figure 0-9. Engineering stress-strain plot for PDT-DAT using ASTM D368 Type V dogbones (0.13 – 0.19 mm thick) at a strain rate of 5 mm/min. (n = 7)

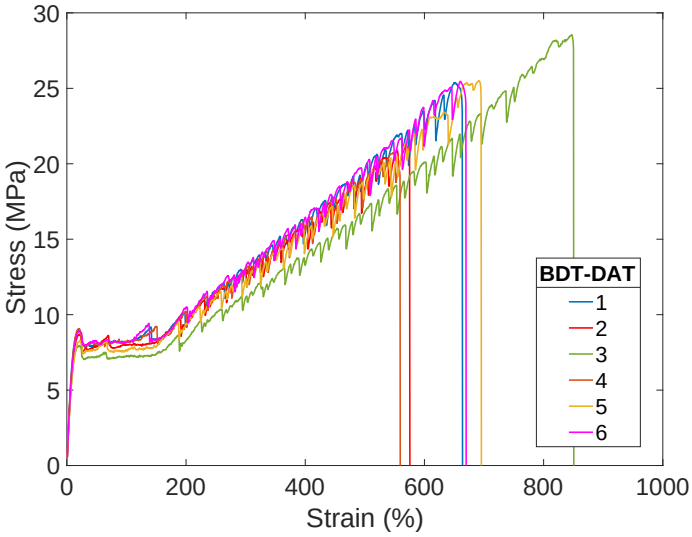

Figure 0-10. Engineering stress-strain plot for BDT-DAT using ASTM D368 Type V dogbones (0.14 – 0.17 mm thick) at a strain rate of 5 mm/min. (n = 6)

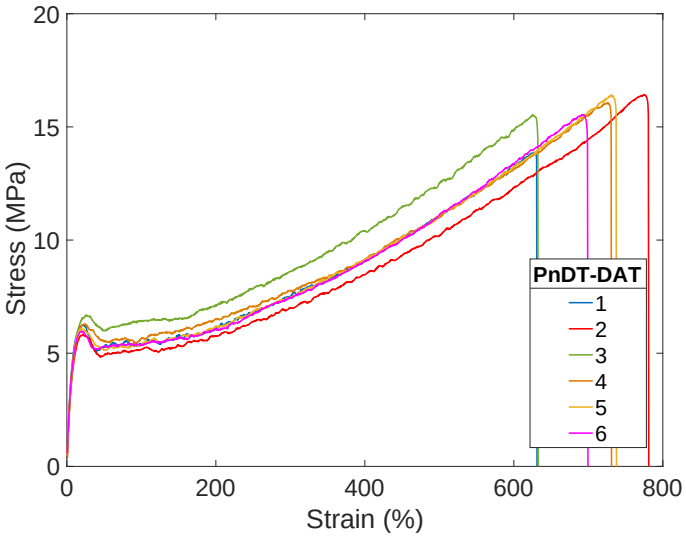

Figure 0-11. Engineering stress-strain plot for PnDT-DAT using ASTM D368 Type V dogbones (0.15 – 0.21 mm thick) at a strain rate of 5 mm/min. (n = 6)

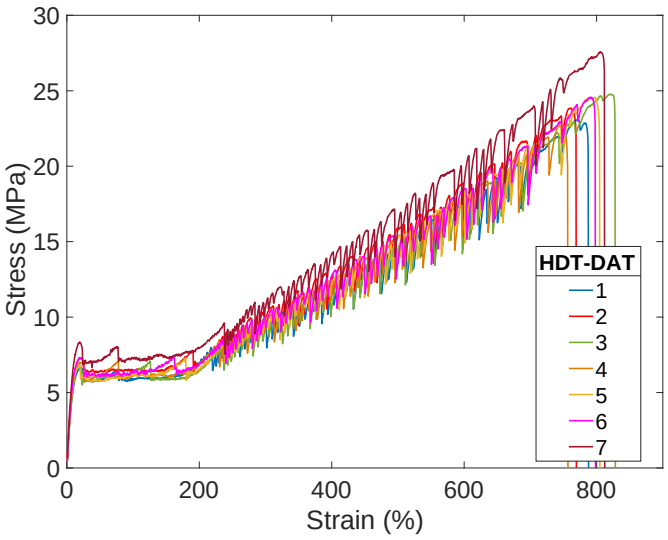

Figure 0-12. Engineering stress-strain plot for HDT-DAT using ASTM D368 Type V dogbones (0.12 – 0.18 mm thick) at a strain rate of 5 mm/min. (n = 7)

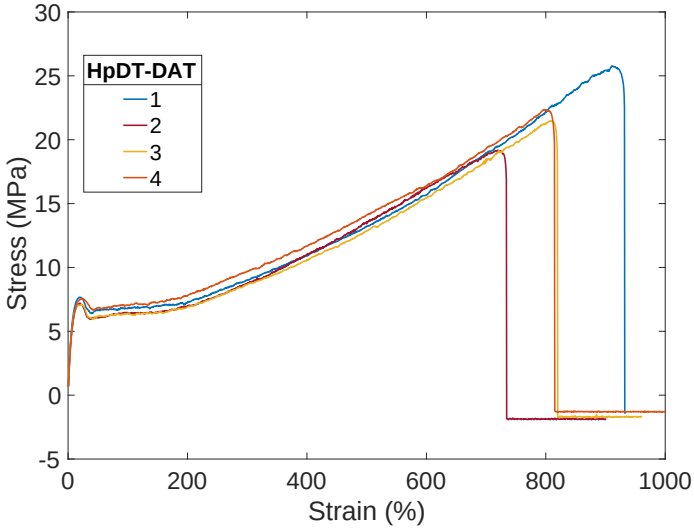

Figure 0-13. Engineering stress-strain plot for HpDT-DAT using ASTM D368 Type V dogbones (0.22 – 0.24 mm thick) at a strain rate of 5 mm/min. (n = 4)

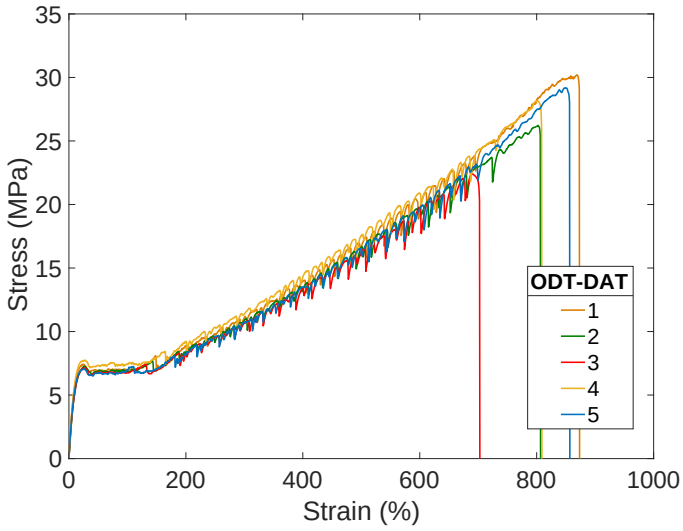

Figure 0-14. Engineering stress-strain plot for ODT-DAT using ASTM D368 Type V dogbones (0.15 – 0.2 mm thick) at a strain rate of 5 mm/min. (n = 5)

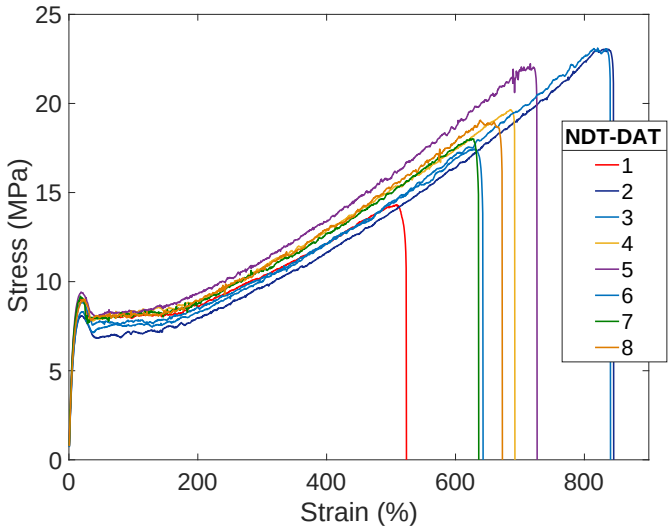

Figure 0-15. Engineering stress-strain plot for NDT-DAT using ASTM D368 Type V dogbones (0.13 – 0.22 mm thick) at a strain rate of 5 mm/min. (n = 8)

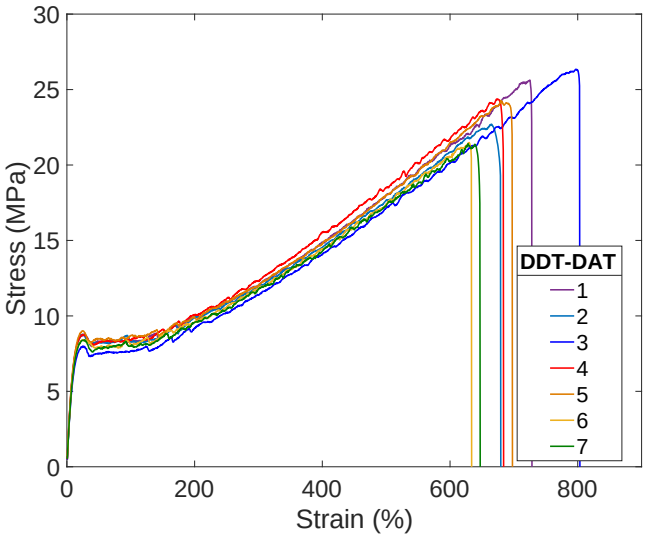

Figure 0-16. Engineering stress-strain plot for DDT-DAT using ASTM D368 Type V dogbones (0.15 – 0.2 mm thick) at a strain rate of 5 mm/min. (n = 7)

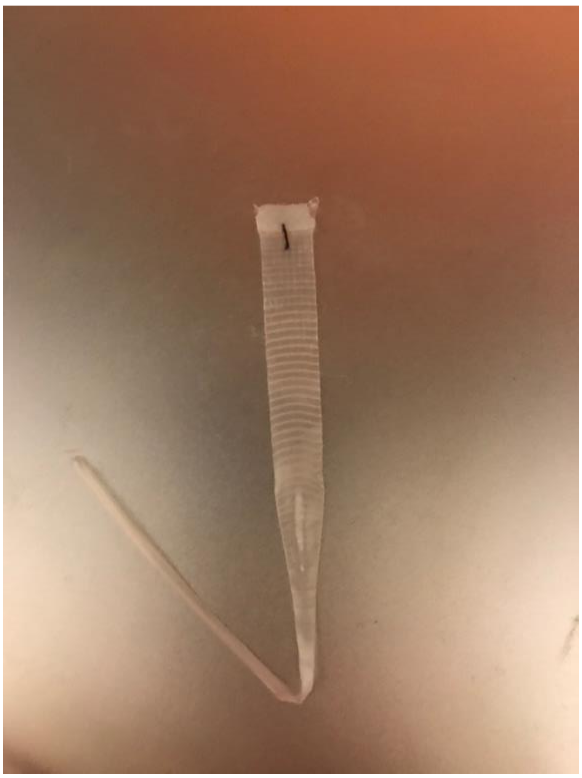

Figure 0-17. Photograph of one end of a HDT-DAT ASTM D368 Type V dogbone strained to failure with visible periodic striations of opaque and translucent regions.

1.36 Conclusions

Photopolymerizable thermoplastic systems are reported and studied for the first time. These interesting systems are enabled via the rapid thiol-ene ‘click’ reaction for a subset of difunctional thiol and ene monomers to produce semicrystalline high polymers capable of unique mechanical properties not easily achieved with existing methods. A thorough investigation revealed that the rapid thiol-ene polymerization produces high average molecular weight polymers on the order of 10^4 g/mol with the narrow polydispersity values expected of step-growth polymers (approximately 2). These formed polymers were confirmed to rearrange and organize at ambient temperature to form crystalline domains over a timescale of several minutes to hours. A systematic structure-properties relationship study was done investigating the effects of the chain

length of the alkyl dithiols on mechanical properties revealing a valuable range of properties intermediate of current elastomers (extensibilities of around 800%) and thermoplastics (ultimate tensile strengths: 15 – 25 MPa and toughness values: 45 – 120 MJ/m^3) used commercially. The findings here greatly expand on the material properties accessible with photopolymers.

1.37 Supporting Information

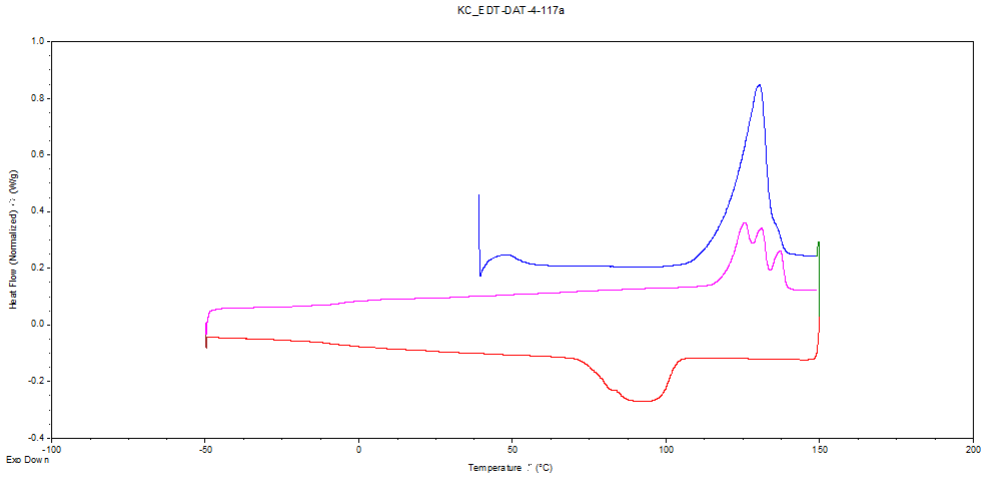

Figure S0-18. DSC trace of EDT-DAT system.

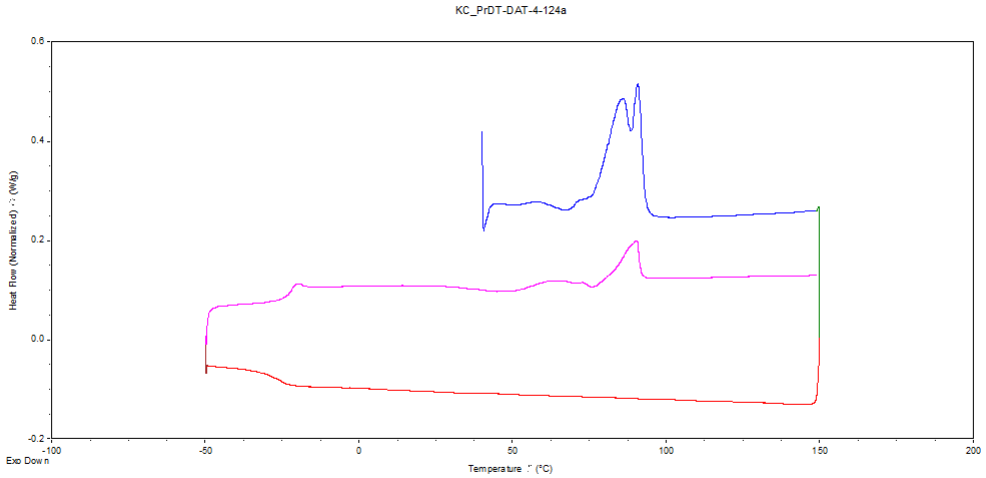

Figure S0-19. DSC trace of PDT-DAT system.

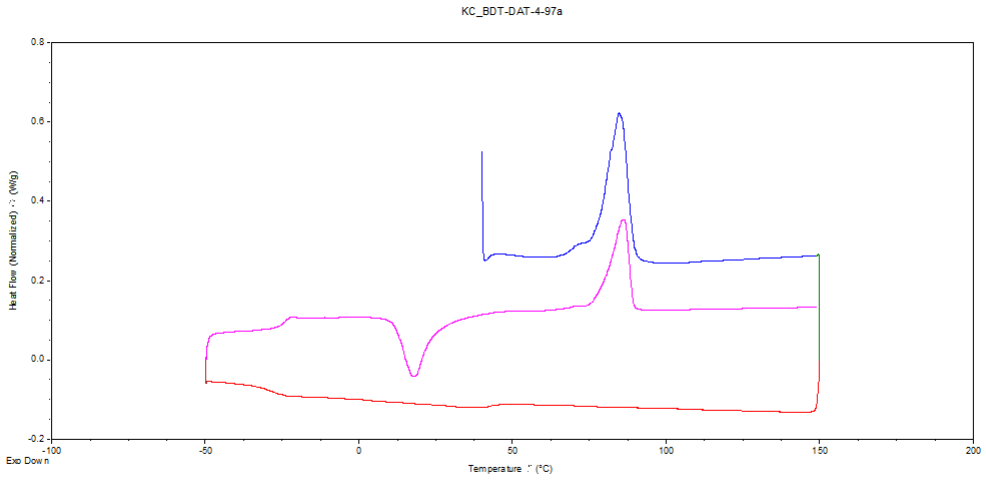

Figure S0-20. DSC trace of BDT-DAT system.

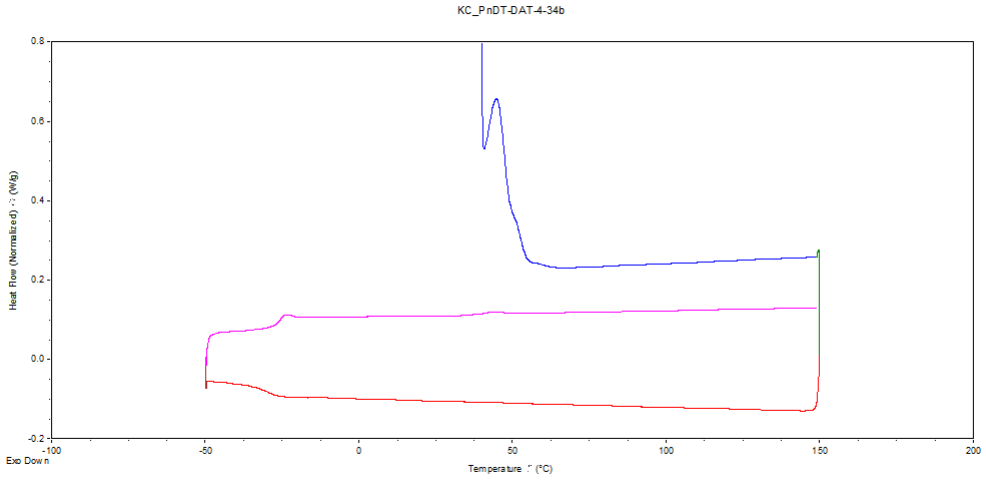

Figure S0-21. DSC trace of PnDT-DAT system.

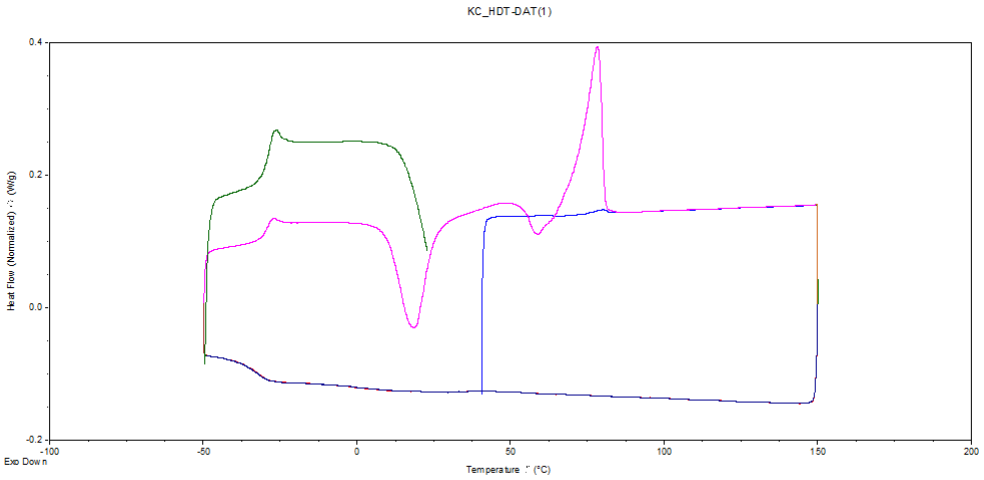

Figure S0-22. DSC trace of HDT-DAT system.

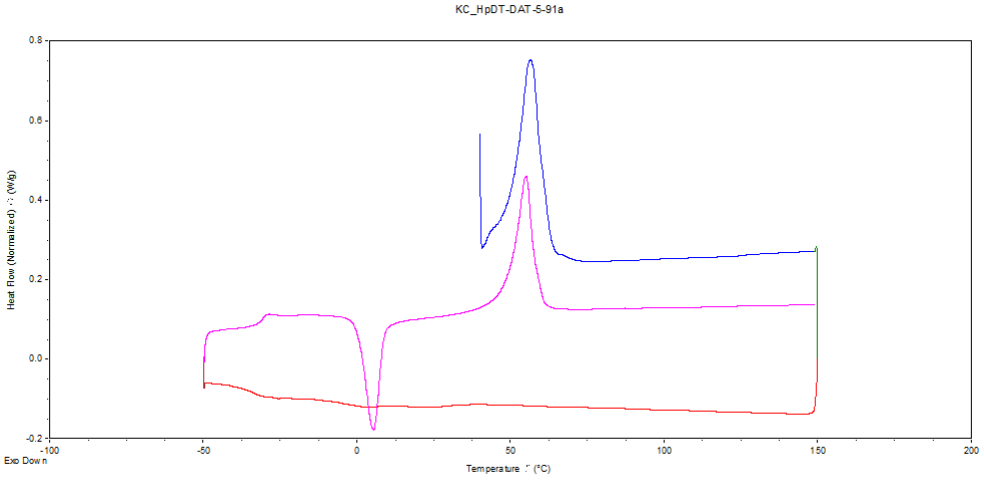

Figure S0-23. DSC trace of HpDT-DAT system.

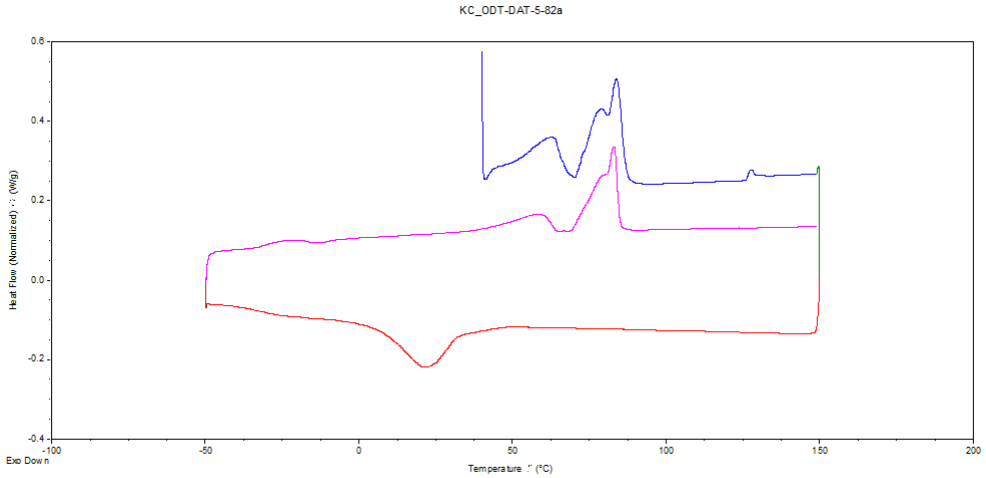

Figure S0-24. DSC trace of ODT-DAT system.

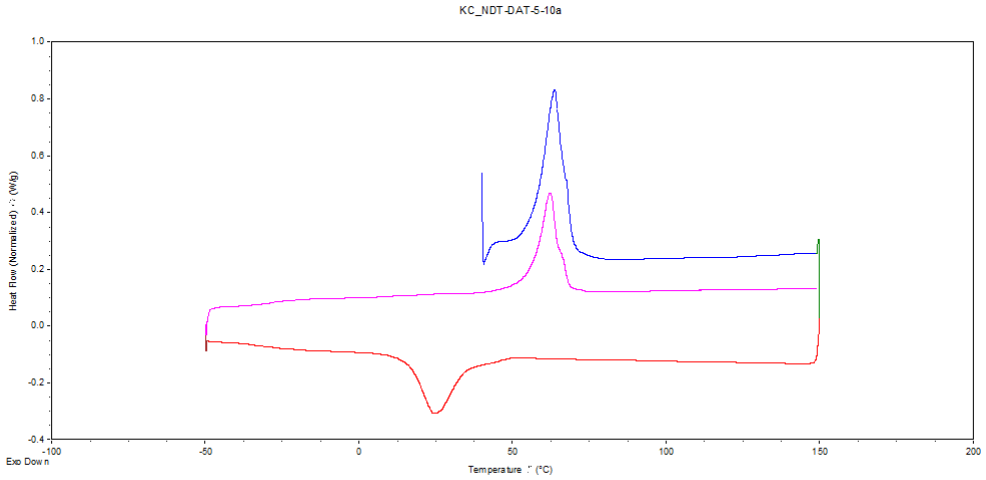

Figure S0-25. DSC trace of NDT-DAT system.

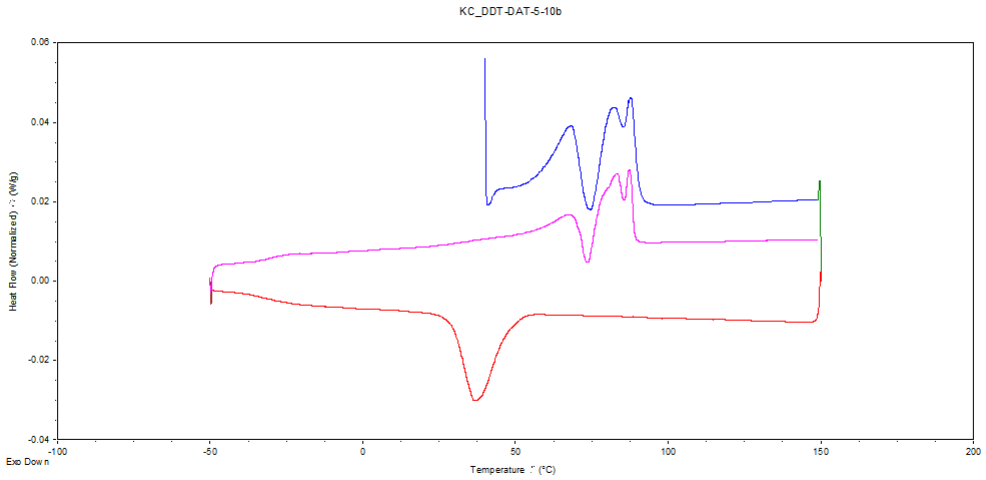

Figure S0-26. DSC trace of DDT-DAT system.

1.38 Acknowledgements

The imaging work was performed at the BioFrontiers Institute Advanced Light Microscopy Core. Super resolution microscopy was performed on a Nikon N-STORM microscope supported by the Howard Hughes Medical Institute. This material is based upon work supported by the Patten Chair endowment.

1.39 References

1. Rahimi, A.; García, J. M., Chemical recycling of waste plastics for new materials production. *Nature Reviews Chemistry* **2017,** *1*, 0046.

2. Garcia, J. M.; Robertson, M. L., The future of plastics recycling. **2017,** *358* (6365), 870-872.

3. Shtukenberg, A. G.; Punin, Y. O.; Gunn, E.; Kahr, B., Spherulites. *Chem. Rev.* **2012,** *112* (3), 1805-1838.

4. Crist, B.; Schultz, J. M., Polymer spherulites: A critical review. *Prog. Polym. Sci.* **2016,** *56*, 1-63.

5. Carothers, W. H., Polymerization. *Chem. Rev.* **1931,** *8* (3), 353-426.

6. Mark, H., Intermolecular Forces and Mechanical Behavior of High Polymers. *Industrial & Engineering Chemistry* **1942,** *34* (11), 1343-1348.

7. Ozawa, T., Kinetics of non-isothermal crystallization. *Polymer* **1971,** *12* (3), 150-158.

8. Jeziorny, A., Parameters characterizing the kinetics of the non-isothermal crystallization of poly (ethylene terephthalate) determined by DSC. *Polymer* **1978,** *19* (10), 1142-1144.

9. Strobl, G., From the melt via mesomorphic and granular crystalline layers to lamellar crystallites: A major route followed in polymer crystallization? *The European Physical Journal* **2000,** *3* (2), 165-183.

10. Mandelkern, L., *Crystallization of polymers*. Cambridge Univ Press: [Place of publication not identified], 2010.

11. Carothers, W. H., Polymers and polyfunctionality. *Transactions of the Faraday Society* **1936,** *32* (0), 39-49.

12. Odian, G. G., Principles of polymerization. **2004**.

13. Mautner, A.; Qin, X.; Wutzel, H.; Ligon, S. C.; Kapeller, B.; Moser, D.; Russmueller, G.; Stampfl, J.; Liska, R., Thiol-ene photopolymerization for efficient curing of vinyl esters. *J. Polym. Sci. Part A: Polym. Chem.* **2013,** *51* (1), 203-212.

14. Alfrey, T.; Price, C. C., Relative reactivities in vinyl copolymerization. *J. Polym. Sci.* **1947,** *2* (1), 101-106.

15. Northrop, B. H.; Coffey, R. N., Thiol–Ene Click Chemistry: Computational and Kinetic Analysis of the Influence of Alkene Functionality. *J. Am. Chem. Soc.* **2012,** *134* (33), 13804-13817.

Vat Photopolymerization Additive Manufacturing of Photopolymerizable Thermoplastics[1]

Materials used for vat photopolymerization additive manufacturing exclusively form crosslinked polymers. This generally means they cannot be reprocessed or recycled. Furthermore, an overwhelming majority of the resins used in vat photopolymerization 3D printing are (meth)acrylate-based which inherently has its limitations. Here, the recently developed photopolymerizable thermoplastics paradigm is explored towards additive manufacturing using a model thiol-ene system. The ability to 3D print with excellent spatial resolutions and small feature sizes (several microns) at standard print times (≤ 10 s per layer) was demonstrated using commercial SLA 3D printers for a number of example prints with a relatively unoptimized resin. Critically, printed objects were melted and reprocessed enabling a new class of sustainable, reprocessable photopolymer materials for light-based 3D printing.

1.40 Introduction

Additive manufacturing (3D printing), widely regarded as the next frontier in prototyping, production and manufacturing,[1-3] is a rapidly evolving technology for highly complex and customized materials fabrication.[3] In particular, light-based 3D printing, or stereolithography (SLA), is arguably one of the most promising technologies for 3D

[1] Contributing authors: Kimberly K. Childress, Neil J. Baugh, Alina M. Martinez, Amelia Davenport, Matthew K. McBride, Brady T. Worrell, Jeffrey W. Stansbury, Robert R. McLeod, and Christopher N. Bowman

printing polymers,[4, 5] offering a superior combination of cost, throughput, versatility and resolution. While significant progress has been made with respect to SLA printing technologies in terms of print speed,[6, 7] methodology,[7-9] multi-material printing,[10] and achievable resolutions,[6-10] the absence of key enabling material characteristics remains a persistent barrier inhibiting significant progress in key fields. One such unrealized material class is the ability to photopolymerize linear polymers rapidly that resemble conventional thermoplastics with their enhanced toughness, extensibility and semicrystalline character. This has limited the 3D printing of thermoplastics to fused deposition modeling (FDM) and selective laser sintering (SLS), which is generally regarded as an inferior technique to vat photopolymerization in terms of minimum feature size, resolution, layer-to-layer adhesion, and finishing quality.

On a basic level, SLA-suitable photopolymers need to be: i) sufficiently reactive to enable rapid polymerization, ii) capable of high spatial resolutions, iii) mechanically strong, and iv) economical. For these reasons, the majority of SLA 3D printing resins are effectively restricted to radical chain-growth polymerizations of multi(meth)acrylates.[3, 4, 6, 7, 10-16] Further, they almost exclusively involve the use of multifunctional monomers that lead to highly crosslinked networks.[3] While a diverse and valuable array of material properties have been achieved through extensive formulation engineering (comprising monomers and oligomers of varying molecular weights, reactive/unreactive diluents, additives, stabilizers), there are fundamental limitations intrinsic to all chain growth multi(meth)acrylate systems such as low pre-gel conversions and significant shrinkage stresses. Given these inherent constraints, achieving an encompassing range of properties for 3D printing with (meth)acrylate photopolymers

alone is intractable. In light of this shortcoming, multiple researchers have explored strategies to extend the useful but limited material property space of standard (meth)acrylates towards the ultimate goal of high performance, functional SLA 3D prints[4, 10-19] that can match or even enhance the library of properties offered by existing manufacturing methods such as injection molding or extrusion. While significant progress[4] has been made towards achieving elastomeric-like materials,[11, 12, 17-19] reprocessability,[15] enhanced toughness,[16, 17] and even multi-material printing,[10, 20] there has been limited work[13, 14] on the vat photopolymerization of thermoplastic polymers. Important work from the Long group introduced novel strategies to 3D print all-aromatic polyimides comparable to commercial Kapton[13, 14]. However the final polyimide was arrived at via thermal post-processing that required high resin viscosities and involved significant shrinkage of the final part due to the removal of solvent. Outside the scope of (meth)acrylate-based systems, the thiol-ene reaction has been recently investigated as an alternative SLA resin chemistry[17, 21-23] offering competitive reactivities to acrylates with the additional benefits of generally higher conversions and reduced polymerization shrinkage stresses. Notably, the Gall group reported on tough, semicrystalline thiol-ene photopolymers using a rigid, crystalline spiroacetal di-alkene monomer[24] in a loosely crosslinked formulation containing 7.5 mol% trithiol crosslinker for 3D printing showing high extensibility and moderate strengths.[17]

All these approaches fundamentally involve the fabrication of an insoluble, crosslinked photopolymer and to the best of our knowledge, no prior work on SLA-based 3D printing of linear polymers has been reported. Here, we validate the applicability of the photopolymerizable thermoplastics materials platform towards

additive manufacturing to enable a new class of SLA-printed thermoplastic materials. Crucially, using a model photopolymerizable thermoplastic thiol-ene system consisting of 1,6-hexane dithiol and diallyl terephthalate (HDT-DAT), we demonstrate the vat photopolymerization-based 3D printing of high resolution thermoplastics objects that are subsequently melted and/or reprocessed.

1.41 Experimental

1.41.1 Materials

Commercially available photoinitiator and monomers were used as received without further purification. 1,6-hexane dithiol (HDT) was purchased from Sigma-Aldrich. Diallyl terephthalate (DAT) and diphenyl(2,4,6-trimethylbezoyl)phosphine oxide (TPO) photoinitiator were purchased from TCI America. TPO-L photoinitiator was kindly donated by IGM Resins.

Printing resin formulation

A stoichiometric mix of HDT DAT was mixed with 4 wt% TPO-L photoinitiator, 0.07 wt% carbon black with 1 wt% of a proprietary surfactant additive.

1.41.2 Methods

Polarized optical imaging with DLP patterning

A Nikon Eclipse Ci optical microscope equipped with a commercial DLP (Mightex Polygon 400) and visible LED source control module (Mightex BioLED) was used to image the photopolymerization and subsequent crystallization of thiol-ene resins between two glass slides. An analyzer was inserted after irradiation to take cross polarized images of the crystallization events.

SLA 3D printing

A commercial DLP printer (Origin) with an intensity of approximately 7 mW/cm^2 at 385 nm was used. All prints used an initial exposure time of 10 – 20 seconds for 3-5 layers with exposure times of 4 – 10 seconds per layer.

1.42 Results & Discussion

Given the interesting set of mechanical properties displayed, the HDT-DAT system was used as the test formulation to assess the viability of photopolymerizable thermoplastics as SLA 3D printing resins. The ability to pattern simple 2D patterns was first done using a commercial digital light processing (DLP) as well as a scanning laser microscope on a neat HDT-DAT system to validate the viability of patterning and the extent to which it could be done.

With DLP patterning, a well resolved CU buffalo was successfully patterned using a commercial DLP system with a low intensity 400 nm LED (power ~ 40 μW) as evident in Figure 0-1. The overall pattern is discernable with features on the order of several microns observable although there is a noticeable halo surrounding the overall buffalo indicating that there is some degree of over-cure due to reaction-diffusion. Nevertheless, this simple DLP experiment showed that 2D photopatterning was possible without features getting washed out during or after the exposure.

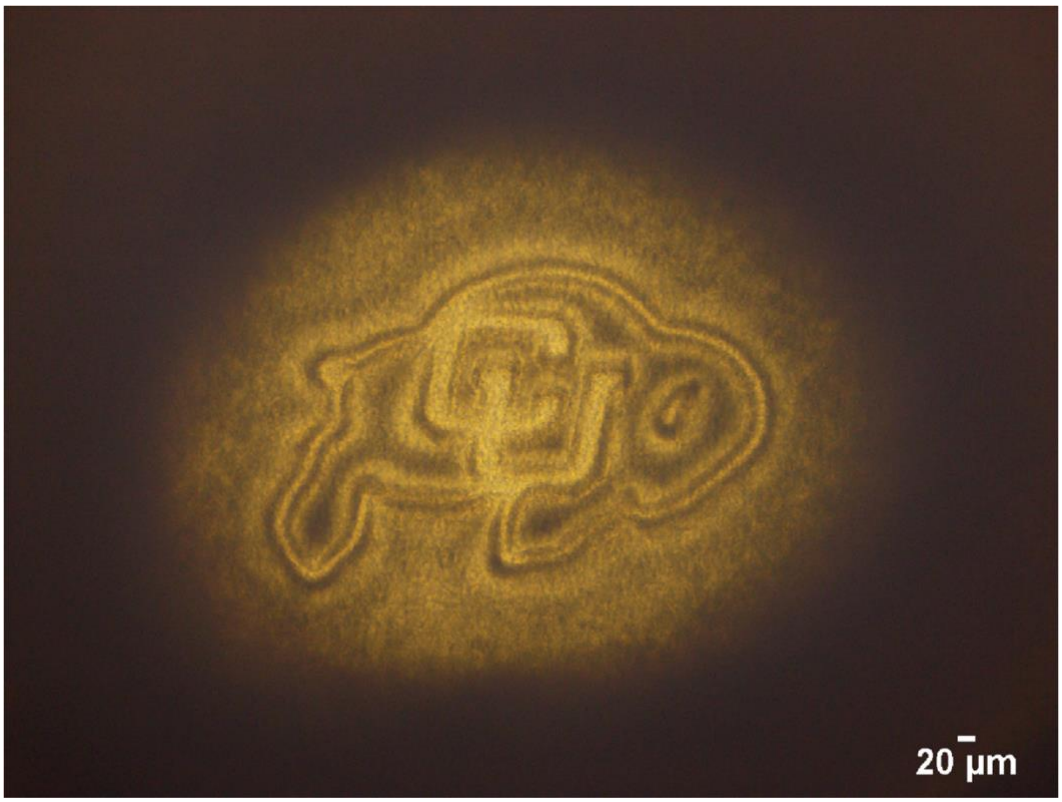

Figure 0-1. A CU buffalo is imaged patterned on a neat HDT-DAT thiol-ene resin using a commercial DLP attached to a polarized microscope. Feature sizes on the order of several microns can be discerned with some over-cure observed.

In the case of patterning with a high intensity scanning laser, a noticeable ‘over-cure’ was observed as seen in the differential interference contrast image in Figure 0-2 whereby spherulites were observed to form within tens of seconds of irradiation outside the intended red shaded square irradiation pattern. Peculiarly, a symmetric square pattern consistently produced an asymmetric crystallized pattern. This preferential directionality could have been induced by the manner in which the scanning laser exposes as well as the relative spot size. The high intensity of the exposure could also be a contributor as this leads to rapid polymerization within a low viscosity medium without any significant inhibiting species to confine reaction-diffusion. Overall, these set of photopatterning results suggest that spatial resolution control (i.e. control over the

crystallization) in photopolymerizable thermoplastics is highly dependent on the exposure intensity.

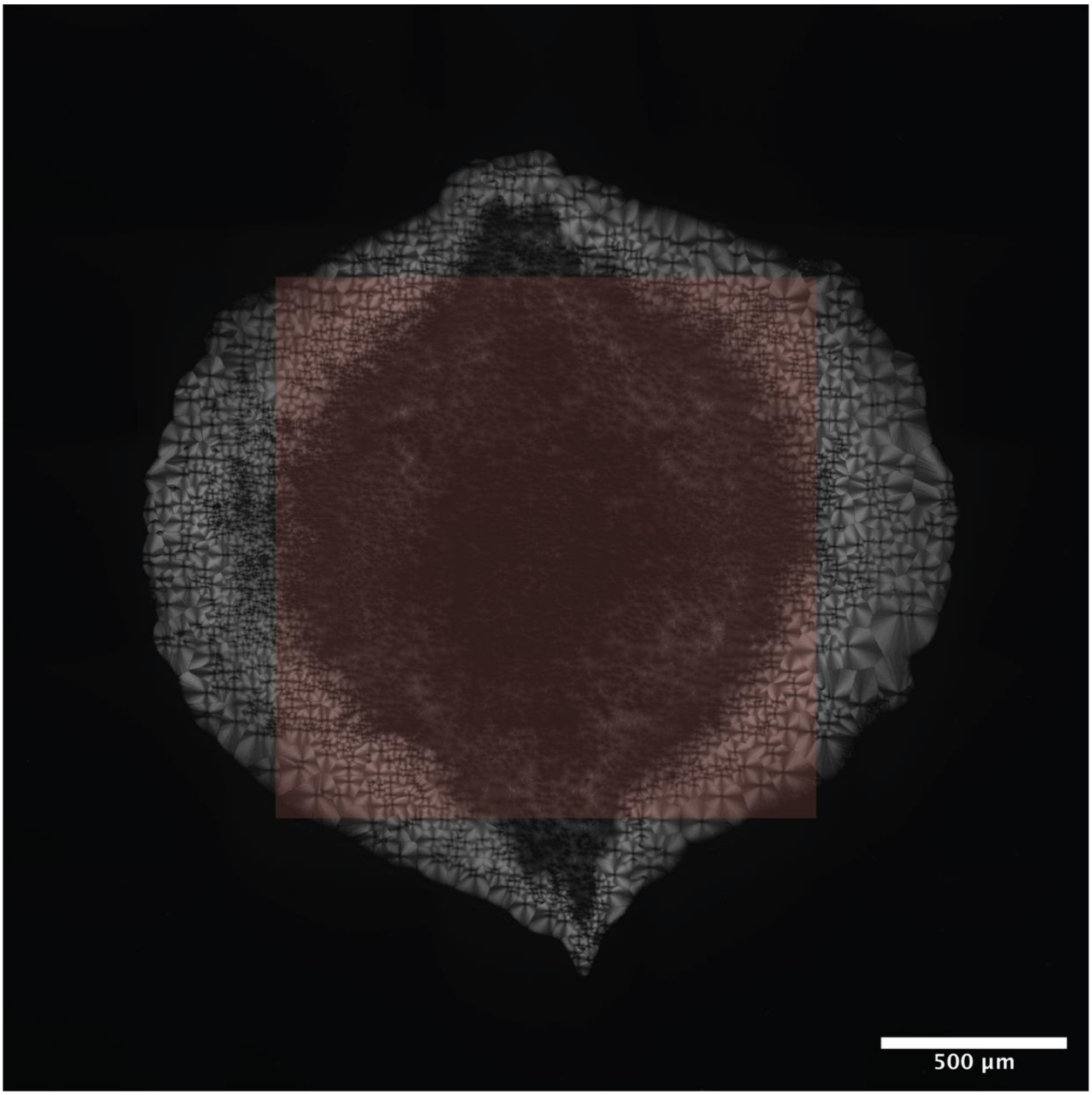

Figure 0-2. A DIC image of the resulting pattern produced from a square irradiation (in red) using a high intensity 405 nm scanning laser. Significant over-curing is observed with crystallization occurring unexpectedly in a preferentially non-isotropic manner.

Based on the previous set of 2D photopatterning experiment, an experimental thiol-ene 3D printing resin was formulated using carbon black as the photoabsorber in

an otherwise unoptimized 3D printing formulation. Generally speaking, the lack of oxygen inhibition in addition to the rapid reactivities makes SLA 3D printing of thiol-ene resins more challenging than conventional (meth)acrylate systems with additional considerations over the crystallization process. As shown in Figure 0-3, using a commercial production-grade DLP-based 3D printer, appropriate spatial resolutions were obtained for a standard quality control (QC) test print. In addition, other simple objects ranging from a batarang to a ring from Lord of the Rings were also successfully printed as shown in Figure 0-4. In particular, the fine details of the Elvish inscription was accurately printed as shown in Figure 0-5.

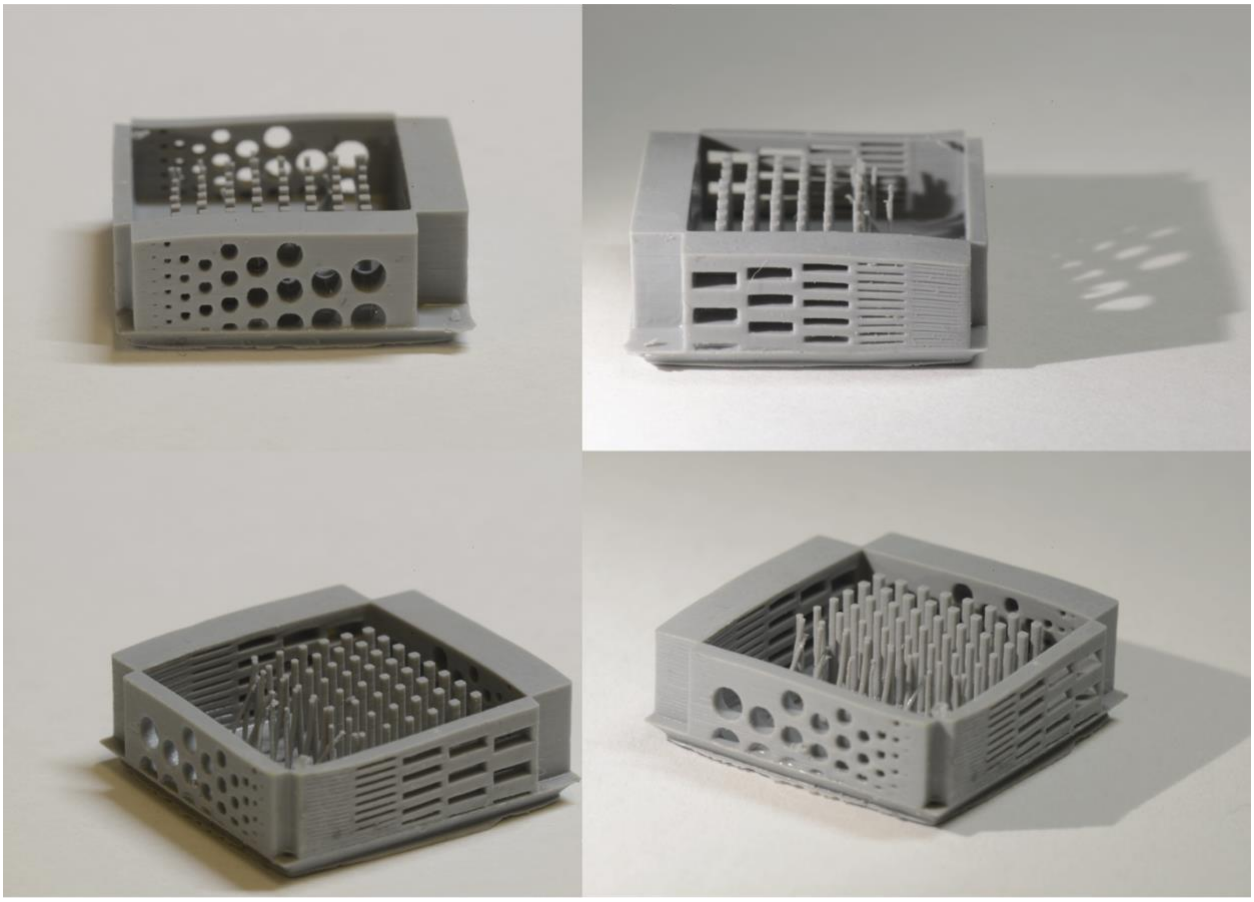

Figure 0-3. Photographs of a QC 3D print at multiple angles showing the high spatial resolutions achieved with both positive and negative features.

Figure 0-4. Photograph of a 3D printed batarang sitting on top of an oversized ring with Elvish inscription on the outer face of the ring.

Figure 0-5. Close-up photograph of the ring showing the Elvish inscription was faithfully captured during the 3D print of the thiol-ene HDT-DAT thermoplastic resin.

The viability of 3D printing photopolymerizable thermoplastics was further validated with the same resin formulation on a commercial projector-based desktop 3D printer (Solus) using modified print parameters. As shown in Figure 0-6 and , a diverse

Figure 0-6. 3D prints of a House Stark direwolf sigil, an amulet, and a House Targaryen three-headed dragon sigilbreathing flames sigil.

The high levels of intricacy and customization offered by 3D printing offers tremendous potential for a variety of use cases for meltable additive manufacturing resins. Specifically, with respect to jewelry investment casting, current 3D printing approaches involve printing the positive of a ring, or set of rings, that eventually serve as a sacrifice after casting in gypsum. Since all existing resins form crosslinked polymers, the embedded prints within the set gypsum need to be burnt off at polymer decomposition temperatures (in excess of 500°C) for removal. This process is tedious and ultimately imperfect as residual ash and/or residue can limit final resolutions of the mold quality, particularly for jewelry and other high-value products. This same concept of decomposing a sacrificial printed photopolymer is also employed for 3D printing ceramics.[25] In these instances, the ability to simply melt an embedded print and flow out

the polymer represents an enabling advancement over current methods. This is demonstrated as a proof-of-concept with photopolymerizable thermoplastics by removing a fractional portion of a QC print consisting of a base with 4 pillars. This object was placed on a glass slide such that the pillars were standing upright as shown in Figure 0-7. The slide was then placed on a hotplate operating at 90°C (slightly above the melting temperature of HDT-DAT at 87°C). Within 30 seconds, the base in direct contact with the glass slide melted causing the upright pillars to wilt and eventually fall over. This caused the rest of the print to melt and form a puddle. In the last image (far right) a glass pipette tip was used to manipulate the melt into an arbitrary design. This experiment clearly demonstrated the ability to heat a 3D printed object into a melt that could then be reprocessed.

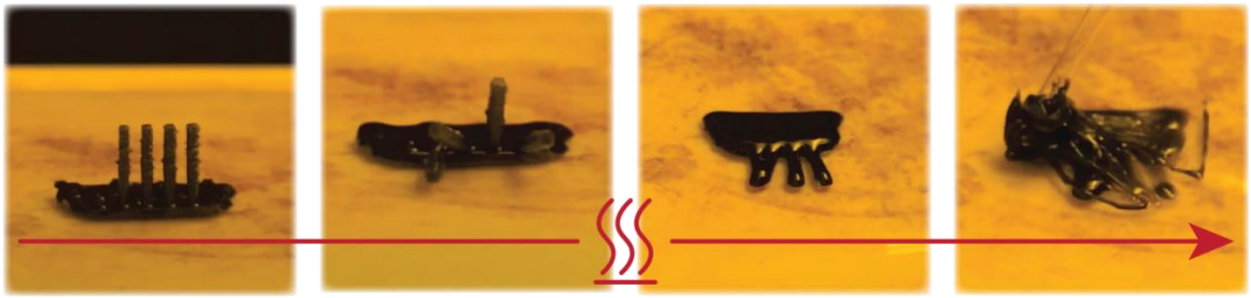

Figure 0-7. A time series of images showing the progression (from left to right) of a 3D printed object consisting of 4 pillars on a base that was situated on a glass slide and placed on a hotplate set at 90°C. As heat conducts from the glass slide to the object, the base melted causing the standing pillars to wilt and fall before eventually melting themselves. In the last image a glass pipette tip was used to rearrange the melt to an arbitrary design.

While essentially all thermoplastics are inherently recyclable, the unfortunate reality is that less than 10% of all plastics get recycled[26, 27] with PET being the most recycled polymer. A major reason is the relatively low cost of production for low value end uses in contrast to the steep costs of sorting and recycling. Unlike conventional

thermoplastics, photopolymerizable thermoplastics are likely to only be economically feasible for high value applications such as 3D printing. Hence, they are less likely to be used for short single-use (typically low value) applications and more likely to be recycled and sustainable, possibly alleviating the issue of 3D printing exacerbating the plastics waste problem with permanent crosslinked polymers.[28] In fact, a valuable feature of photopolymerizable thermoplastics is its intrinsic reprocessability. This feature lends to the concept of being able to reuse a SLA printed object (or cured resin) as a feedstock for one of the alternative 3D printing methods such as fused deposition modeling (FDM) and material jetting. As these additive manufacturing techniques fundamentally rely on the deposition of melted materials, printed photopolymerizable thermoplastics at the end of their SLA lifetime can be recycled for use as ‘new’ resins for FDM. A preliminary demonstration of this was

The practical factors that may limit viability of the thiol-ene chemistry as 3D printing resins are primarily shelf-life resin stability and the unpleasant odor. In the former case, it has been well established that thiol-ene resin stability can vary widely from a few hours to multiple months with multiple strategies reported to effectively address this.[29] Within the scope of the studied photopolymerizable thermoplastic thiol-ene systems, a limited stability of a few days was observed with 1,2-ethane dithiol-based (EDT) systems. Given the low starting viscosities of these thiol-ene systems, the finite stability of the resin can actually be considered useful in the slow and gradual generation of low molecular weight oligomers for reducing odor (primarily due to low molecular weight thiols) without dramatically compromising print quality. Furthermore, as mentioned earlier, any reacted photopolymerizable thermoplastics resin can simply

be repurposed instead of discarded. While the issue of odor is more of an inconvenience issue than of toxicity (unlike with many acrylates), several measures can be taken to mitigate the overall smell. One simple chemical approach would be to pre-oligomerize the resin to form higher molecular weight species while more direct strategies such as printing in a fume hood or employing a vapor extraction system could also be considered.

1.43 Conclusions

Here, the first instance of the vat photopolymerization 3D printing of mechanically robust linear polymers was disclosed using photopolymerizable thermoplastics. A model system, HDT-DAT, was used with carbon black in an otherwise unoptimized resin formulation to produce high quality 3D prints that displayed excellent positive and negative resolutions using a commercial 3D printer at standard print times (< 10 seconds per layer). Critically, the intrinsic ability to melt at accessible temperatures (~80°C) and reprocess these otherwise tough materials lends itself to a variety of new uses not achievable with current photopolymers.

1.44 Acknowledgements

The authors would like to thank Charlie Rackson for photographing the 3D printed objects. The imaging work was performed at the BioFrontiers Institute Advanced Light Microscopy Core. Super resolution microscopy was performed on a Nikon N-STORM microscope supported by the Howard Hughes Medical Institute. This material is based upon work supported by the Patten Chair endowment.

1.45 References

1. Gibson, I., *Additive Manufacturing Technologies*. Springer: New York, 2014.

2. Ngo, T. D.; Kashani, A.; Imbalzano, G.; Nguyen, K. T. Q.; Hui, D., Additive manufacturing (3D printing): A review of materials, methods, applications and challenges. *Composites Part B: Engineering* **2018,** *143*, 172-196.

3. Ligon, S. C.; Liska, R.; Stampfl, J.; Gurr, M.; Mulhaupt, R., Polymers for 3D Printing and Customized Additive Manufacturing. *Chem. Rev.* **2017,** *117* (15), 10212-10290.

4. Layani, M.; Wang, X. F.; Magdassi, S., Novel Materials for 3D Printing by Photopolymerization. *Adv. Mater.* **2018,** *30* (41), 7.

5. Stansbury, J. W.; Idacavage, M. J., 3D printing with polymers: Challenges among expanding options and opportunities. *Dent. Mater.* **2016,** *32* (1), 54-64.

6. de Beer, M. P.; van der Laan, H. L.; Cole, M. A.; Whelan, R. J.; Burns, M. A.; Scott, T. F., Rapid, continuous additive manufacturing by volumetric polymerization inhibition patterning. *Sci. Adv.* **2019,** *5* (1), eaau8723.

7. Tumbleston, J. R.; Shirvanyants, D.; Ermoshkin, N.; Janusziewicz, R.; Johnson, A. R.; Kelly, D.; Chen, K.; Pinschmidt, R.; Rolland, J. P.; Ermoshkin, A.; Samulski, E. T.; DeSimone, J. M., Continuous liquid interface production of 3D objects. **2015,** *347* (6228), 1349-1352.

8. Shusteff, M.; Browar, A. E. M.; Kelly, B. E.; Henriksson, J.; Weisgraber, T. H.; Panas, R. M.; Fang, N. X.; Spadaccini, C. M., One-step volumetric additive manufacturing of complex polymer structures. *Sci. Adv.* **2017,** *3* (12), eaao5496.

9. Kelly, B. E.; Bhattacharya, I.; Heidari, H.; Shusteff, M.; Spadaccini, C. M.; Taylor, H. K., Volumetric additive manufacturing via tomographic reconstruction. *Science* **2019**, eaau7114.

10. Schwartz, J. J.; Boydston, A. J., Multimaterial actinic spatial control 3D and 4D printing. *Nat. Commun.* **2019,** *10* (1), 791.

11. Poelma, J.; Rolland, J., Rethinking digital manufacturing with polymers. *Science* **2017,** *358* (6369), 1384-1385.

12. Patel, D. K.; Sakhaei, A. H.; Layani, M.; Zhang, B.; Ge, Q.; Magdassi, S., Highly Stretchable and UV Curable Elastomers for Digital Light Processing Based 3D Printing. *Adv. Mater.* **2017,** *29* (15), 1606000.

13. Hegde, M.; Meenakshisundaram, V.; Chartrain, N.; Sekhar, S.; Tafti, D.; Williams, C. B.; Long, T. E., 3D Printing All-Aromatic Polyimides using Mask-Projection Stereolithography: Processing the Nonprocessable. *Adv. Mater.* **2017,** *29* (31), 1701240.

14. Herzberger, J.; Meenakshisundaram, V.; Williams, C. B.; Long, T. E., 3D Printing All-Aromatic Polyimides Using Stereolithographic 3D Printing of Polyamic Acid Salts. *ACS Macro Lett.* **2018,** *7* (4), 493-497.

15. Zhang, B.; Kowsari, K.; Serjouei, A.; Dunn, M. L.; Ge, Q., Reprocessable thermosets for sustainable three-dimensional printing. *Nat. Commun.* **2018,** *9* (1), 1831.

16. Seidler, K.; Griesser, M.; Kury, M.; Harikrishna, R.; Dorfinger, P.; Koch, T.; Svirkova, A.; Marchetti-Deschmann, M.; Stampfl, J.; Moszner, N.; Gorsche, C.; Liska, R., Vinyl Sulfonate Esters: Efficient Chain Transfer Agents for the 3D Printing of Tough Photopolymers without Retardation. *Angew Chem Int Ed Engl* **2018,** *57* (29), 9165-9169.

17. Sycks, D. G.; Wu, T.; Park, H. S.; Gall, K., Tough, stable spiroacetal thiol-ene resin for 3D printing. *Journal of Applied Polymer Science* **2018,** *135* (22), 46259.

18. Bhattacharjee, N.; Parra-Cabrera, C.; Kim, Y. T.; Kuo, A. P.; Folch, A., Desktop-Stereolithography 3D-Printing of a Poly(dimethylsiloxane)-Based Material with Sylgard-184 Properties. *Adv. Mater.* **2018,** *30* (22), 1800001.

19. Thrasher, C. J.; Schwartz, J. J.; Boydston, A. J., Modular Elastomer Photoresins for Digital Light Processing Additive Manufacturing. *ACS Appl. Mater. Interfaces* **2017,** *9* (45), 39708-39716.

20. Dolinski, N. D.; Page, Z. A.; Callaway, E. B.; Eisenreich, F.; Garcia, R. V.; Chavez, R.; Bothman, D. P.; Hecht, S.; Zok, F. W.; Hawker, C. J., Solution Mask

Liquid Lithography (SMaLL) for One-Step, Multimaterial 3D Printing. *Adv. Mater.* **2018,** *30* (31), 1800364.

21. Leonards, H.; Engelhardt, S.; Hoffmann, A.; Pongratz, L.; Schriever, S.; Bläsius, J.; Wehner, M. M.; Gillner, A., Advantages and drawbacks of Thiol-ene based resins for 3D-printing. *Proceedings of SPIE* **2015,** *9353*, 7.

22. Chen, L.; Wu, Q.; Wei, G.; Liu, R.; Li, Z., Highly stable thiol–ene systems: from their structure–property relationship to DLP 3D printing. *Journal of Materials Chemistry C* **2018,** *6* (43), 11561-11568.

23. Wallin, T. J.; Pikul, J. H.; Bodkhe, S.; Peele, B. N.; Mac Murray, B. C.; Therriault, D.; McEnerney, B. W.; Dillon, R. P.; Giannelis, E. P.; Shepherd, R. F., Click chemistry stereolithography for soft robots that self-heal. *Journal of Materials Chemistry B* **2017,** *5* (31), 6249-6255.

24. Sycks, D. G.; Safranski, D. L.; Reddy, N. B.; Sun, E.; Gall, K., Tough Semicrystalline Thiol–Ene Photopolymers Incorporating Spiroacetal Alkenes. *Macromolecules* **2017,** *50* (11), 4281-4291.

25. Halloran, J. W., Ceramic Stereolithography: Additive Manufacturing for Ceramics by Photopolymerization. *Annual Review of Materials Research* **2016,** *46* (1), 19-40.

26. Rahimi, A.; García, J. M., Chemical recycling of waste plastics for new materials production. *Nature Reviews Chemistry* **2017,** *1*, 0046.

27. Garcia, J. M.; Robertson, M. L., The future of plastics recycling. **2017,** *358* (6365), 870-872.

28. Fortman, D. J.; Brutman, J. P.; De Hoe, G. X.; Snyder, R. L.; Dichtel, W. R.; Hillmyer, M. A., Approaches to Sustainable and Continually Recyclable Cross-Linked Polymers. *ACS Sustain. Chem. Eng.* **2018,** *6* (9), 11145-11159.

29. Ligon, S. C.; Husár, B.; Wutzel, H.; Holman, R.; Liska, R., Strategies to Reduce Oxygen Inhibition in Photoinduced Polymerization. *Chem. Rev.* **2014,** *114* (1), 557-589.

Bibliography

1. Odian, G. G., Principles of polymerization. **2004**.

2. Young, R. J.; Lovell, P. A., Introduction to polymers. **2011**.

3. Flory, P. J., Molecular Size Distribution in Three Dimensional Polymers. I. Gelation1. *J. Am. Chem. Soc.* **1941,** *63* (11), 3083-3090.

4. Mandelkern, L., *Crystallization of polymers*. Cambridge Univ Press: [Place of publication not identified], 2010.

5. Nogales, A.; Hsiao, B. S.; Somani, R. H.; Srinivas, S.; Tsou, A. H.; Balta-Calleja, F. J.; Ezquerra, T. A., Shear-induced crystallization of isotactic polypropylene with different molecular weight distributions: in situ small-and wide-angle X-ray scattering studies. *Polymer* **2001,** *42* (12), 5247-5256.

6. Sarasua, J.-R.; Rodríguez, N. L.; Arraiza, A. L.; Meaurio, E., Stereoselective Crystallization and Specific Interactions in Polylactides. *Macromolecules* **2005,** *38* (20), 8362-8371.

7. Flory, P. J., Constitution of Three-dimensional Polymers and the Theory of Gelation. *The Journal of Physical Chemistry* **1942,** *46* (1), 132-140.

8. Decker, C., Light-induced crosslinking polymerization. *Polymer International* **2002,** *51* (11), 1141-1150.

9. Allen, N. S., Photoinitiators for UV and visible curing of coatings: Mechanisms and properties. *Journal of Photochemistry and Photobiology A: Chemistry* **1996,** *100* (1-3), 101-107.

10. Fouassier, J. P.; LalevÈe, J., Photoinitiators for Polymer Synthesis : Scope, Reactivity, and Efficiency. **2013**.

11. Eibel, A.; Fast, D. E.; Gescheidt, G., Choosing the ideal photoinitiator for free radical photopolymerizations: predictions based on simulations using established data. *Polymer Chemistry* **2018,** *9* (41), 5107-5115.

12. Decker, C.; Jenkins, A. D., Kinetic approach of oxygen inhibition in ultraviolet- and laser-induced polymerizations. *Macromolecules* **1985,** *18* (6), 1241-1244.

13. Chatani, S.; Kloxin, C. J.; Bowman, C. N., The power of light in polymer science: photochemical processes to manipulate polymer formation, structure, and properties. *Polymer Chemistry* **2014,** *5* (7), 2187-2201.

14. Park, H. Y.; Kloxin, C. J.; Scott, T. F.; Bowman, C. N., Covalent adaptable networks as dental restorative resins: Stress relaxation by addition–fragmentation chain transfer in allyl sulfide-containing resins. *Dent. Mater.* **2010,** *26* (10), 1010-1016.

15. Park, H. Y.; Kloxin, C. J.; Abuelyaman, A. S.; Oxman, J. D.; Bowman, C. N., Novel dental restorative materials having low polymerization shrinkage stress via stress relaxation by addition-fragmentation chain transfer. *Dent. Mater.* **2012,** *28* (11), 3-9.

16. Podgorski, M.; Becka, E.; Claudino, M.; Flores, A.; Shah, P. K.; Stansbury, J. W.; Bowman, C. N., Ester-free thiol-ene dental restoratives-Part A: Resin development. *Dent. Mater.* **2015,** *31* (11), 1255-1262.

17. Tumbleston, J. R.; Shirvanyants, D.; Ermoshkin, N.; Janusziewicz, R.; Johnson, A. R.; Kelly, D.; Chen, K.; Pinschmidt, R.; Rolland, J. P.; Ermoshkin, A.; Samulski, E. T.; DeSimone, J. M., Continuous liquid interface production of 3D objects. **2015,** *347* (6228), 1349-1352.

18. Stansbury, J. W.; Idacavage, M. J., 3D printing with polymers: Challenges among expanding options and opportunities. *Dent. Mater.* **2016,** *32* (1), 54-64.

19. Ligon, S. C.; Liska, R.; Stampfl, J.; Gurr, M.; Mulhaupt, R., Polymers for 3D Printing and Customized Additive Manufacturing. *Chem. Rev.* **2017,** *117* (15), 10212-10290.

20. Shusteff, M.; Browar, A. E. M.; Kelly, B. E.; Henriksson, J.; Weisgraber, T. H.; Panas, R. M.; Fang, N. X.; Spadaccini, C. M., One-step volumetric additive manufacturing of complex polymer structures. *Sci. Adv.* **2017,** *3* (12), eaao5496.

21. Layani, M.; Wang, X. F.; Magdassi, S., Novel Materials for 3D Printing by Photopolymerization. *Adv. Mater.* **2018,** *30* (41), 7.

22. Stockmayer, W. H., Theory of Molecular Size Distribution and Gel Formation in Branched Polymers II. General Cross Linking. **1944,** *12* (4), 125-131.

23. Hawker, C. J.; Wooley, K. L., The Convergence of Synthetic Organic and Polymer Chemistries. *Science* **2005,** *309* (5738), 1200-1205.

24. Kolb, H. C.; Finn, M. G.; Sharpless, K. B., Click Chemistry: Diverse Chemical Function from a Few Good Reactions. *Angew. Chem.-Int. Edit.* **2001,** *40* (11), 2004-2021.

25. Hoyle, C. E.; Bowman, C. N., Thiol–Ene Click Chemistry. *Angew. Chem.-Int. Edit.* **2010,** *49* (9), 1540-1573.

26. Lowe, A. B.; Bowman, C. N., *Thiol-X chemistries in polymer and materials science*. RSC Publishing: Cambridge, 2013; p xvii, 317 pages.

27. Kade, M. J.; Burke, D. J.; Hawker, C. J., The power of thiol-ene chemistry. *J. Polym. Sci. A Polym. Chem.* **2010,** *48* (4), 743-750.

28. Lowe, A. B., Thiol-ene “click” reactions and recent applications in polymer and materials synthesis. *Polymer Chemistry* **2010,** *1* (1), 17-36.

29. Hoyle, C. E.; Lowe, A. B.; Bowman, C. N., Thiol-click chemistry: a multifaceted toolbox for small molecule and polymer synthesis. *Chem. Soc. Rev.* **2010,** *39* (4), 1355-1387.

30. Nair, D. P.; Podgorski, M.; Chatani, S.; Gong, T.; Xi, W. X.; Fenoli, C. R.; Bowman, C. N., The Thiol-Michael Addition Click Reaction: A Powerful and Widely Used Tool in Materials Chemistry. *Chem. Mat.* **2014,** *26* (1), 724-744.

31. Brändle, A.; Khan, A., Thiol–epoxy ‘click’ polymerization: efficient construction of reactive and functional polymers. *Polymer Chemistry* **2012,** *3* (12), 3224-3227.

32. Stuparu, M. C.; Khan, A., Thiol-epoxy “click” chemistry: Application in preparation and postpolymerization modification of polymers. *J. Polym. Sci. Part A: Polym. Chem.* **2016,** *54* (19), 3057-3070.

33. Fernández-Rodríguez, M. A.; Shen, Q.; Hartwig, J. F., A General and Long-Lived Catalyst for the Palladium-Catalyzed Coupling of Aryl Halides with Thiols. *J. Am. Chem. Soc.* **2006,** *128* (7), 2180-2181.

34. Lowe, A. B., Thiol–ene “click” reactions and recent applications in polymer and materials synthesis: a first update. *Polymer Chemistry* **2014,** *5* (17), 4820-4870.

35. Xi, W. X.; Scott, T. F.; Kloxin, C. J.; Bowman, C. N., Click Chemistry in Materials Science. *Adv. Funct. Mater.* **2014,** *24* (18), 2572-2590.

36. Ligon, S. C.; Husár, B.; Wutzel, H.; Holman, R.; Liska, R., Strategies to Reduce Oxygen Inhibition in Photoinduced Polymerization. *Chem. Rev.* **2014,** *114* (1), 557-589.

37. O'Brien, A. K.; Bowman, C. N., Impact of Oxygen on Photopolymerization Kinetics and Polymer Structure. *Macromolecules* **2006,** *39* (7), 2501-2506.

38. Goodner, M. D.; Bowman, C. N., Development of a comprehensive free radical photopolymerization model incorporating heat and mass transfer effects in thick films. *Chemical Engineering Science* **2002,** *57* (5), 887-900.

39. O'Brien, A. K.; Cramer, N. B.; Bowman, C. N., Oxygen inhibition in thiol–acrylate photopolymerizations. **2006,** *44* (6), 2007-2014.

40. Chatani, S.; Nair, D. P.; Bowman, C. N., Relative reactivity and selectivity of vinyl sulfones and acrylates towards the thiol-Michael addition reaction and polymerization. *Polymer Chemistry* **2013,** *4* (4), 1048-1055.

41. Chatani, S.; Sheridan, R. J.; Podgorski, M.; Nair, D. P.; Bowman, C. N., Temporal Control of Thiol-Click Chemistry. *Chem. Mat.* **2013,** *25* (19), 3897-3901.

42. Xi, W. X.; Krieger, M.; Kloxin, C. J.; Bowman, C. N., A new photoclick reaction strategy: photo-induced catalysis of the thiol-Michael addition via a caged primary amine. *Chem. Commun.* **2013,** *49* (40), 4504-4506.

43. Chan, J. W.; Hoyle, C. E.; Lowe, A. B.; Bowman, M., Nucleophile-Initiated Thiol-Michael Reactions: Effect of Organocatalyst, Thiol, and Ene. *Macromolecules* **2010,** *43* (15), 6381-6388.

44. Dislich, H., Plastics as Optical Materials. *Angew. Chem.-Int. Edit.* **1979,** *18* (1), 49-59.

45. Born, M.; Wolf, E.; Bhatia, A. B., *Principles of optics electromagnetic theory of propagation, interference and diffraction of light*. Cambridge Univ. Press: Cambridge, 2016.

46. Gharagheizi, F.; Ilani-Kashkouli, P.; Kamari, A.; Mohammadi, A. H.; Ramjugernath, D., Group Contribution Model for the Prediction of Refractive Indices of Organic Compounds. *Journal of Chemical & Engineering Data* **2014,** *59* (6), 1930-1943.

47. Liu, J.-g.; Ueda, M., High refractive index polymers: fundamental research and practical applications. *Journal of Materials Chemistry* **2009,** *19* (47), 8907-8919.

48. Higashihara, T.; Ueda, M., Recent Progress in High Refractive Index Polymers. *Macromolecules* **2015,** *48* (7), 1915-1929.

49. Chung, W. J.; Griebel, J. J.; Kim, E. T.; Yoon, H.; Simmonds, A. G.; Ji, H. J.; Dirlam, P. T.; Glass, R. S.; Wie, J. J.; Nguyen, N. A.; Guralnick, B. W.; Park, J.; Somogyi, Á.; Theato, P.; Mackay, M. E.; Sung, Y.-E.; Char, K.; Pyun, J., The use of elemental sulfur as an alternative feedstock for polymeric materials. *Nature Chemistry* **2013,** *5*, 518.

50. Griebel, J. J.; Namnabat, S.; Kim, E. T.; Himmelhuber, R.; Moronta, D. H.; Chung, W. J.; Simmonds, A. G.; Kim, K.-J.; van der Laan, J.; Nguyen, N. A.; Dereniak, E. L.; Mackay, M. E.; Char, K.; Glass, R. S.; Norwood, R. A.; Pyun, J., New Infrared Transmitting Material via Inverse Vulcanization of Elemental Sulfur to Prepare High Refractive Index Polymers. *Adv. Mater.* **2014,** *26* (19), 3014-3018.

51. Lim, J.; Pyun, J.; Char, K., Recent Approaches for the Direct Use of Elemental Sulfur in the Synthesis and Processing of Advanced Materials. *Angew. Chem.-Int. Edit.* **2015,** *54* (11), 3249-3258.

52. Kloxin, C. J.; Scott, T. F.; Adzima, B. J.; Bowman, C. N., Covalent Adaptable Networks (CANs): A Unique Paradigm in Cross-Linked Polymers. *Macromolecules* **2010,** *43* (6), 2643-2653.

53. Bowman, C. N.; Kloxin, C. J., Covalent Adaptable Networks: Reversible Bond Structures Incorporated in Polymer Networks. *Angew. Chem.-Int. Edit.* **2012,** *51* (18), 4272-4274.

54. Kloxin, C. J.; Bowman, C. N., Covalent adaptable networks: smart, reconfigurable and responsive network systems. *Chem. Soc. Rev.* **2013,** *42* (17), 7161-7173.

55. Chen, X.; Dam, M. A.; Ono, K.; Mal, A.; Shen, H.; Nutt, S. R.; Sheran, K.; Wudl, F., A Thermally Re-mendable Cross-Linked Polymeric Material. **2002,** *295* (5560), 1698-1702.

56. Cromwell, O. R.; Chung, J.; Guan, Z., Malleable and Self-Healing Covalent Polymer Networks through Tunable Dynamic Boronic Ester Bonds. *J. Am. Chem. Soc.* **2015,** *137* (20), 6492-6495.

57. Rowan, S. J.; Cantrill, S. J.; Cousins, G. R. L.; Sanders, J. K. M.; Stoddart, J. F., Dynamic Covalent Chemistry. **2002,** *41* (6), 898-952.

58. Sheridan, R. J.; Bowman, C. N., A Simple Relationship Relating Linear Viscoelastic Properties and Chemical Structure in a Model Diels-Alder Polymer Network. *Macromolecules* **2012,** *45* (18), 7634-7641.

59. Sheridan, R. J.; Bowman, C. N., Understanding the process of healing of thermoreversible covalent adaptable networks. *Polymer Chemistry* **2013,** *4* (18), 4974-4979.

60. Berg, G. J.; Gong, T.; Fenoli, C. R.; Bowman, C. N., A Dual-Cure, Solid-State Photoresist Combining a Thermoreversible Diels-Alder Network and a Chain Growth Acrylate Network. *Macromolecules* **2014,** *47* (10), 3473-3482.

61. Lyon, G. B.; Baranek, A.; Bowman, C. N., Scaffolded Thermally Remendable Hybrid Polymer Networks. *Adv. Funct. Mater.* **2016,** *26* (9), 1477-1485.

62. Tasdelen, M. A., Diels–Alder “click” reactions: recent applications in polymer and material science. *Polymer Chemistry* **2011,** *2* (10), 2133-2145.

63. Montarnal, D.; Capelot, M.; Tournilhac, F.; Leibler, L., Silica-Like Malleable Materials from Permanent Organic Networks. *Science* **2011,** *334* (6058), 965-968.

64. Denissen, W.; Winne, J. M.; Du Prez, F. E., Vitrimers: permanent organic networks with glass-like fluidity. *Chem. Sci.* **2016,** *7* (1), 30-38.

65. Demongeot, A.; Groote, R.; Goossens, H.; Hoeks, T.; Tournilhac, F.; Leibler, L., Cross-Linking of Poly(butylene terephthalate) by Reactive Extrusion Using Zn(II) Epoxy-Vitrimer Chemistry. *Macromolecules* **2017,** *50* (16), 6117-6127.

66. Rottger, M.; Domenech, T.; van der Weegen, R.; Nicolay, A. B. R.; Leibler, L., High-performance vitrimers from commodity thermoplastics through dioxaborolane metathesis. *Science* **2017,** *356* (6333), 62-65.

67. Zou, W. K.; Dong, J. T.; Luo, Y. W.; Zhao, Q.; Xie, T., Dynamic Covalent Polymer Networks: from Old Chemistry to Modern Day Innovations. *Adv. Mater.* **2017,** *29* (14), 18.

68. Bowman, C. N.; Kloxin, C. J. J. A. C. I. E., Covalent adaptable networks: reversible bond structures incorporated in polymer networks. **2012,** *51* (18), 4272-4274.

69. Scott, T. F.; Schneider, A. D.; Cook, W. D.; Bowman, C. N., Photoinduced plasticity in cross-linked polymers. *Science* **2005,** *308* (5728), 1615-1617.

70. Worrell, B. T.; McBride, M. K.; Lyon, G. B.; Cox, L. M.; Wang, C.; Mavila, S.; Lim, C. H.; Coley, H. M.; Musgrave, C. B.; Ding, Y. F.; Bowman, C. N., Bistable and photoswitchable states of matter. *Nat. Commun.* **2018,** *9*, 7.

71. Scott, T. F.; Draughon, R. B.; Bowman, C. N., Actuation in Crosslinked Polymers via Photoinduced Stress Relaxation. **2006,** *18* (16), 2128-2132.

72. Park, H. Y.; Kloxin, C. J.; Abuelyaman, A. S.; Oxman, J. D.; Bowman, C. N., Stress Relaxation via Addition-Fragmentation Chain Transfer in High T-g, High Conversion Methacrylate-Based Systems. *Macromolecules* **2012,** *45* (14), 5640-5646.

73. Park, H. Y.; Kloxin, C. J.; Fordney, M. F.; Bowman, C. N., Stress Reduction and T-g Enhancement in Ternary Thiol-Yne-Methacrylate Systems via Addition-Fragmentation Chain Transfer. *Macromolecules* **2012,** *45* (14), 5647-5652.

74. Kloxin, C. J.; Scott, T. F.; Park, H. Y.; Bowman, C. N., Mechanophotopatterning on a Photoresponsive Elastomer. *Adv. Mater.* **2011,** *23* (17), 1977-1981.

75. Cox, L. M.; Li, Z.; Sowan, N.; Nair, D.; Xiao, J.; Bowman, C. N.; Ding, Y., Reconfigurable surface patterns on covalent adaptive network polymers using nanoimprint lithography. *Polymer* **2014,** *55* (23), 5933-5937.

76. McBride, M. K.; Hendrikx, M.; Liu, D. Q.; Worrell, B. T.; Broer, D. J.; Bowman, C. N., Photoinduced Plasticity in Cross-Linked Liquid Crystalline Networks. *Adv. Mater.* **2017,** *29* (17), 6.

77. Wang, C.; Mavila, S.; Worrell, B. T.; Xi, W. X.; Goldman, T. M.; Bowman, C. N., Productive Exchange of Thiols and Thioesters to Form Dynamic Polythioester-Based Polymers. *ACS Macro Lett.* **2018,** *7* (11), 1312-1316.

78. Wang, C.; Goldman, T. M.; Worrell, B. T.; McBride, M. K.; Alim, M. D.; Bowman, C. N., Recyclable and repolymerizable thiol-X photopolymers. *Mater. Horizons* **2018,** *5* (6), 1042-1046.

79. Worrell, B. T.; Mavila, S.; Wang, C.; Kontour, T. M.; Lim, C. H.; McBride, M. K.; Musgrave, C. B.; Shoemaker, R.; Bowman, C. N., A user's guide to the thiol-thioester exchange in organic media: scope, limitations, and applications in material science. *Polymer Chemistry* **2018,** *9* (36), 4523-4534.

80. Nair, D. P.; Cramer, N. B.; Gaipa, J. C.; McBride, M. K.; Matherly, E. M.; McLeod, R. R.; Shandas, R.; Bowman, C. N., Two-Stage Reactive Polymer Network Forming Systems. *Adv. Funct. Mater.* **2012,** *22* (7), 1502-1510.

81. Peng, H. Y.; Wang, C.; Xi, W. X.; Kowalski, B. A.; Gong, T.; Xie, X. L.; Wang, W. T.; Nair, D. P.; McLeod, R. R.; Bowman, C. N., Facile Image Patterning via Sequential Thiol-Michael/Thiol-Yne Click Reactions. *Chem. Mat.* **2014,** *26* (23), 6819-6826.

82. Peng, H. Y.; Nair, D. P.; Kowalski, B. A.; Xi, W. X.; Gong, T.; Wang, C.; Cole, M.; Cramer, N. B.; Xie, X. L.; McLeod, R. R.; Bowman, C. N., High Performance Graded Rainbow Holograms via Two-Stage Sequential Orthogonal Thiol-Click Chemistry. *Macromolecules* **2014,** *47* (7), 2306-2315.

83. Iha, R. K.; Wooley, K. L.; Nyström, A. M.; Burke, D. J.; Kade, M. J.; Hawker, C. J., Applications of Orthogonal “Click” Chemistries in the Synthesis of Functional Soft Materials. *Chem. Rev.* **2009,** *109* (11), 5620-5686.

84. Bruder, F.-K.; Hagen, R.; Rölle, T.; Weiser, M.-S.; Fäcke, T., From the Surface to Volume: Concepts for the Next Generation of Optical–Holographic Data-Storage Materials. *Angew. Chem.-Int. Edit.* **2011,** *50* (20), 4552-4573.

85. Gabor, D., A New Microscopic Principle. *Nature* **1948,** *161*, 777.

86. Toal, V., Introduction to holography. **2012**.

87. Gaylord, T. K.; Moharam, M. G., Thin and thick gratings: terminology clarification. *Appl. Opt.* **1981,** *20* (19), 3271-3273.

88. Klein, W. R.; Cook, B. D., Unified Approach to Ultrasonic Light Diffraction. *IEEE Transactions on Sonics and Ultrasonics* **1967,** *14* (3), 123-134.

89. Moharam, M. G.; Young, L., Criterion for Bragg and Raman-Nath diffraction regimes. *Appl. Opt.* **1978,** *17* (11), 1757-1759.

90. Kogelnik, H., Coupled wave theory for thick hologram gratings. *The Bell System Technical Journal* **1969,** *48* (9), 2909-2947.

91. Moharam, M. G.; Gaylord, T. K., Rigorous coupled-wave analysis of planar-grating diffraction. *J. Opt. Soc. Am.* **1981,** *71* (7), 811-818.

92. Hariharan, P., *Basics of holography*. Cambridge University Press: Cambridge, 2002.

93. Kowalski, B. A.; McLeod, R. R., Design concepts for diffusive holographic photopolymers. *J. Polym. Sci. Part B: Polym. Phys.* **2016,** *54* (11), 1021-1035.

94. Guo, J.; Gleeson, M. R.; Sheridan, J. T., A Review of the Optimisation of Photopolymer Materials for Holographic Data Storage. *Physics Research International* **2012,** *2012*, 16.

95. Close, D. H.; Jacobson, A. D.; Margerum, J. D.; Brault, R. G.; McClung, F. J., HOLOGRAM RECORDING ON PHOTOPOLYMER MATERIALS. **1969,** *14* (5), 159-160.

96. Colburn, W. S.; Haines, K. A., Volume Hologram Formation in Photopolymer Materials. *Appl. Opt.* **1971,** *10* (7), 1636-1641.

97. Dhar, L.; Hale, A.; Katz, H. E.; Schilling, M. L.; Schnoes, M. G.; Schilling, F. C., Recording Media That Exhibit High Dynamic Range for Digital Holographic Data Storage. *Opt. Lett.* **1999,** *24*, 487.

98. Guo, J.; Fujii, R.; Ono, T.; Klepp, J.; Pruner, C.; Fally, M.; Tomita, Y., Effects of chain-transferring thiol functionalities on the performance of nanoparticle-polymer composite volume gratings. *Opt. Lett.* **2014,** *39* (23), 6743-6746.

99. Tomita, Y.; Urano, H.; Fukamizu, T.-a.; Kametani, Y.; Nishimura, N.; Odoi, K., Nanoparticle-polymer composite volume holographic gratings dispersed with ultrahigh-refractive-index hyperbranched polymer as organic nanoparticles. *Opt. Lett.* **2016,** *41* (6), 1281-1284.

100. Hata, E.; Tomita, Y., Order-of-magnitude polymerization-shrinkage suppression of volume gratings recorded in nanoparticle-polymer composites. *Opt. Lett.* **2010,** *35* (3), 396-398.

101. Mitsube, K.; Nishimura, Y.; Nagaya, K.; Takayama, S.; Tomita, Y., Holographic nanoparticle-polymer composites based on radical-mediated thiol-yne photopolymerizations: characterization and shift-multiplexed holographic digital data page storage. *Opt. Mater. Express* **2014,** *4* (5), 982-996.

102. Suzuki, N.; Tomita, Y.; Kojima, T., Holographic recording in TiO2 nanoparticle-dispersed methacrylate photopolymer films. **2002,** *81* (22), 4121-4123.

103. Choi, K.; Chon, J. W. M.; Gu, M.; Malic, N.; Evans, R. A., Low-Distortion Holographic Data Storage Media Using Free-Radical Ring-Opening Polymerization. *Adv. Funct. Mater.* **2009,** *19* (22), 3560-3566.

104. Hata, E.; Mitsube, K.; Momose, K.; Tomita, Y., Holographic nanoparticle-polymer composites based on step-growth thiol-ene photopolymerization. *Opt. Mater. Express* **2011,** *1* (2), 207-222.

105. Gibson, I.; Rosen, D. W.; Stucker, B., *Additive Manufacturing Technologies: Rapid Prototyping to Direct Digital Manufacturing*. Springer-Verlag Berlin: Berlin, 2010; p 1-459.

106. Huang, S. H.; Liu, P.; Mokasdar, A.; Hou, L., Additive manufacturing and its societal impact: a literature review. *Int. J. Adv. Manuf. Technol.* **2013,** *67* (5-8), 1191-1203.

107. Poelma, J.; Rolland, J., Rethinking digital manufacturing with polymers. *Science* **2017,** *358* (6369), 1384-1385.

108. Melchels, F. P. W.; Feijen, J.; Grijpma, D. W., A review on stereolithography and its applications in biomedical engineering. *Biomaterials* **2010,** *31* (24), 6121-6130.

109. Lee, M. P.; Cooper, G. J. T.; Hinkley, T.; Gibson, G. M.; Padgett, M. J.; Cronin, L., Development of a 3D printer using scanning projection stereolithography. *Scientific Reports* **2015,** *5*, 9875.

110. de Beer, M. P.; van der Laan, H. L.; Cole, M. A.; Whelan, R. J.; Burns, M. A.; Scott, T. F., Rapid, continuous additive manufacturing by volumetric polymerization inhibition patterning. *Sci. Adv.* **2019,** *5* (1), eaau8723.

111. Kelly, B. E.; Bhattacharya, I.; Heidari, H.; Shusteff, M.; Spadaccini, C. M.; Taylor, H. K., Volumetric additive manufacturing via tomographic reconstruction. *Science* **2019**, eaau7114.

112. White, S. R.; Moore, J. S.; Sottos, N. R.; Krull, B. P.; Santa Cruz, W. A.; Gergely, R. C. R., Restoration of Large Damage Volumes in Polymers. *Science* **2014,** *344*, 620.

113. Podgorski, M.; Nair, D. P.; Chatani, S.; Berg, G.; Bowman, C. N., Programmable Mechanically Assisted Geometric Deformations of Glassy Two-Stage Reactive Polymeric Materials. *ACS Appl. Mater. Interfaces* **2014,** *6* (9), 6111-6119.

114. Toal, V., *Introduction to Holography*. 2012.

115. Peng, H.; Wang, C.; Xi, W.; Kowalski, B. A.; Gong, T.; Xie, X.; Wang, W.; Nair, D. P.; McLeod, R. R.; Bowman, C. N., Facile Image Patterning via Sequential Thiol–Michael/Thiol–Yne Click Reactions. *Chem. Mater.* **2014,** *26*, 6819.

116. Cody, D.; Gribbin, S.; Mihaylova, E.; Naydenova, I., Low-Toxicity Photopolymer for Reflection Holography. *ACS Appl. Mater. Interfaces* **2016,** *8*, 18481.

117. Ni, M.; Peng, H.; Liao, Y.; Yang, Z.; Xue, Z.; Xie, X., 3D Image Storage in Photopolymer/ZnS Nanocomposites Tailored by “Photoinitibitor.”. *Macromolecules* **2015,** *48*, 2958.

118. Tomita, Y.; Urano, H.; Fukamizu, T. a.; Kametani, Y.; Nishimura, N.; Odoi, K., Nanoparticle-Polymer Composite Volume Holographic Gratings Dispersed with Ultrahigh-Refractive-Index Hyperbranched Polymer as Organic Nanoparticles. *Opt. Lett.* **2016,** *41*, 1281.

119. Peng, H.; Bi, S.; Ni, M.; Xie, X.; Liao, Y.; Zhou, X.; Xue, Z.; Zhu, J.; Wei, Y.; Bowman, C. N.; Mai, Y. W., Monochromatic Visible Light “Photoinitibitor”: Janus-Faced Initiation and Inhibition for Storage of Colored 3D Images. *J. Am. Chem. Soc.* **2014,** *136*, 8855.

120. Urness, A. C.; Anderson, K.; Ye, C.; Wilson, W. L.; McLeod, R. R., Arbitrary GRIN Component Fabrication in Optically Driven Diffusive Photopolymers. *Opt. Express* **2015,** *23*, 264.

121. Sullivan, A. C.; Grabowski, M. W.; McLeod, R. R., Three-Dimensional Direct-Write Lithography into Photopolymer. *Appl. Opt.* **2007,** *46*, 295.

122. Yee, D. W.; Schulz, M. D.; Grubbs, R. H.; Greer, J. R., Functionalized 3D Architected Materials via Thiol-Michael Addition and Two-Photon Lithography. *Adv. Mater.* **2017,** *29*, 1605293.

123. Kress, B. C.; Gregory, G. G.; Davis, A. J.; Hahlweg, C. F., *Restocking the Optical Designers’ Toolbox for Next-Generation Wearable Displays (Presentation Recording)*. 2015; p 957903.

124. Kowalski, B. A.; Urness, A. C.; Baylor, M. E.; Cole, M. C.; Wilson, W. L.; McLeod, R. R., Quantitative Modeling of the Reaction/diffusion Kinetics of Two-Chemistry Diffusive Photopolymers. *Opt. Mater. Express* **2014,** *4*, 1668.

125. Liu, J. g.; Ueda, M., High Refractive Index Polymers: Fundamental Research and Practical Applications. *J. Mater. Chem.* **2009,** *19*, 8907.

126. Macdonald, E. K.; Shaver, M. P., Intrinsic High Refractive Index Polymers. *Polym. Int.* **2015,** *64*, 6.

127. Meka, C.; Jallapuram, R.; Naydenova, I.; Martin, S.; Toal, V., Development of a Panchromatic Acrylamide-Based Photopolymer for Multicolor Reflection Holography. *Appl. Opt.* **2010,** *49*, 1400.

128. Liu, S.; Gleeson, M. R.; Guo, J.; Sheridan, J. T., High Intensity Response of Photopolymer Materials for Holographic Grating Formation. *Macromolecules* **2010,** *43*, 9462.

129. Bunning, T., The Morphology and Performance of Holographic Transmission Gratings Recorded in Polymer Dispersed Liquid Crystals. *Polymer* **1995,** *36*, 2699.

130. Bunning, T. J.; Natarajan, L. V.; and, V. P. T.; Sutherland, R. L., Holographic Polymer-Dispersed Liquid Crystals (H-PDLCs). *Annual Review of Materials Science* **2000,** *30* (1), 83-115.

131. Natarajan, L. V.; Shepherd, C. K.; Brandelik, D. M.; Sutherland, R. L.; Chandra, S.; Tondiglia, V. P.; Tomlin, D.; Bunning, T. J., Switchable Holographic Polymer-Dispersed Liquid Crystal Reflection Gratings Based on Thiol–Ene Photopolymerization. *Chem. Mater.* **2003,** *15*, 2477.

132. White, T. J.; Natarajan, L. V.; Tondiglia, V. P.; Lloyd, P. F.; Bunning, T. J.; Guymon, C. A., Monomer Functionality Effects in the Formation of Thiol–Ene Holographic Polymer Dispersed Liquid Crystals. *Macromolecules* **2007,** *40*, 1121.

133. Chen, G.; Ni, M.; Peng, H.; Huang, F.; Liao, Y.; Wang, M.; Zhu, J.; Roy, V. A. L.; Xie, X., Photoinitiation and Inhibition under Monochromatic Green Light for Storage of Colored 3D Images in Holographic Polymer-Dispersed Liquid Crystals. *ACS Appl. Mater. Interfaces* **2017,** *9*, 1810.

134. Bruder, F. K.; Fäcke, T.; Rölle, T., The Chemistry and Physics of Bayfol HX Film Holographic Photopolymer. *Polymers* **2017,** *9*, 472.

135. Ayres, M. R.; Anderson, K.; Askham, F.; Sissom, B.; Urness, A. C.; Bjelkhagen, H. I.; Bove, V. M., Holographic Data Storage at 2+ Tbit/in 2. *Proceedings of SPIE* **2015,** *9386*, 93860G.

136. Heller, W., Remarks on Refractive Index Mixture Rules. *J. Phys. Chem.* **1965,** *69*, 1123.

137. Groh, W.; Zimmermann, A., What is the Lowest Refractive Index of an Organic Polymer? *Macromolecules* **1991,** *24*, 6660.

138. Bruder, F. K.; Hagen, R.; Rölle, T.; Weiser, M. S.; Fäcke, T., From the Surface to Volume: Concepts for the Next Generation of Optical-Holographic Data-Storage Materials. *Angew. Chem., Int. Ed.* **2011,** *50*, 4552.

139. Peng, H.; Nair, D. P.; Kowalski, B. A.; Xi, W.; Gong, T.; Wang, C.; Cole, M.; Cramer, N. B.; Xie, X.; McLeod, R. R.; Bowman, C. N., High Performance Graded Rainbow Holograms via Two-Stage Sequential Orthogonal Thiol–Click Chemistry. *Macromolecules* **2014,** *47*, 2306.

140. Alim, M. D.; Glugla, D. J.; Mavila, S.; Wang, C.; Nystrom, P. D.; Sullivan, A. C.; McLeod, R. R.; Bowman, C. N., High Dynamic Range (Δn) Two-Stage Photopolymers via Enhanced Solubility of a High Refractive Index Acrylate Writing Monomer. *ACS Applied Materials & Interfaces* **2018,** *10* (1), 1217-1224.

141. Coufal, H. J.; Psaltis, D.; Sincerbox, G. T., *Holographic data storage*. Springer: Berlin [etc.], 2000.

142. Castagna, R.; Vita, F.; Lucchetta, D. E.; Criante, L.; Simoni, F., Superior-Performance Polymeric Composite Materials for High-Density Optical Data Storage. *Adv. Mater.* **2009,** *21* (5), 589-592.

143. Ye, C.; McLeod, R. R., GRIN lens and lens array fabrication with diffusion-driven photopolymer. *Opt. Lett.* **2008,** *33* (22), 2575-2577.

144. Moore, D. T., Gradient-index optics: a review. *Appl. Opt.* **1980,** *19* (7), 1035-1038.

145. Žukauskas, A.; Matulaitienė, I.; Paipulas, D.; Niaura, G.; Malinauskas, M.; Gadonas, R., Tuning the refractive index in 3D direct laser writing lithography: towards GRIN microoptics. *Laser & Photonics Reviews* **2015,** *9* (6), 706-712.

146. Kaehr, B.; Scrymgeour, D. A., Direct-write graded index materials realized in protein hydrogels. *Applied Physics Letters* **2016,** *109* (12), 123701.

147. Ohmi, S.; Sakai, H.; Asahara, Y.; Nakayama, S.; Yoneda, Y.; Izumitani, T., Gradient-index rod lens made by a double ion-exchange process. *Appl. Opt.* **1988,** *27* (3), 496-499.

148. Liu, J.-H.; Chiu, Y.-H., Process equipped with a sloped UV lamp for the fabrication of gradient-refractive-index lenses. *Opt. Lett.* **2009,** *34* (9), 1393-1395.

149. Observatory, L. I. G. W. Silicate Bonding Procedure (Hydroxide-Catalysis Bonding) https://dcc.ligo.org/public/0013/E050228/001/E050228-00_Silicate%20bonding%20procedure.pdf (accessed 3/21/19).

150. Cramer, N. B.; O'Brien, C. P.; Bowman, C. N., Mechanisms, polymerization rate scaling, and oxygen inhibition with an ultra-rapid monovinyl urethane acrylate. *Polymer* **2008,** *49* (22), 4756-4761.

151. Beckel, E. R.; Stansbury, J. W.; Bowman, C. N., Effect of Aliphatic Spacer Substitution on the Reactivity of Phenyl Carbamate Acrylate Monomers. *Macromolecules* **2005,** *38* (8), 3093-3098.

152. Barner-Kowollik, C.; Bennet, F.; Schneider-Baumann, M.; Voll, D.; Rölle, T.; Fäcke, T.; Weiser, M.-S.; Bruder, F.-K.; Junkers, T., Detailed investigation of the propagation rate of urethane acrylates. *Polymer Chemistry* **2010,** *1* (4), 470-479.

153. Glugla, D. J.; Chosy, M. B.; Alim, M. D.; Childress, K. K.; Sullivan, A. C.; McLeod, R. R., Multiple patterning of holographic photopolymers for increased refractive index contrast. *Opt. Lett.* **2018,** *43* (8), 1866-1869.

154. Cho, Y. H.; Shin, C. W.; Kim, N.; Kim, B. K.; Kawakami, Y., High-Performance Transmission Holographic Gratings via Different Polymerization Rates of Dipentaerythritol Acrylates and Siloxane-Containing Epoxides. *Chem. Mat.* **2005,** *17* (25), 6263-6271.

155. Alim, M. D.; Glugla, D. J.; Mavila, S.; Wang, C.; Nystrom, P. D.; Sullivan, A. C.; McLeod, R. R.; Bowman, C. N., High Dynamic Range (Deltan) Two-Stage Photopolymers via Enhanced Solubility of a High Refractive Index Acrylate Writing Monomer. *ACS Appl Mater Interfaces* **2018,** *10* (1), 1217-1224.

156. Otsuka, H.; Nagano, S.; Kobashi, Y.; Maeda, T.; Takahara, A., A dynamic covalent polymer driven by disulfide metathesis under photoirradiation. *Chem. Commun.* **2010,** *46* (7), 1150-1152.

157. Rekondo, A.; Martin, R.; Ruiz de Luzuriaga, A.; Cabañero, G.; Grande, H. J.; Odriozola, I., Catalyst-free room-temperature self-healing elastomers based on aromatic disulfide metathesis. *Mater. Horizons* **2014,** *1* (2), 237-240.

158. Amamoto, Y.; Otsuka, H.; Takahara, A.; Matyjaszewski, K., Self-healing of covalently cross-linked polymers by reshuffling thiuram disulfide moieties in air under visible light. *Adv Mater* **2012,** *24* (29), 3975-80.

159. Fenoli, C. R.; Bowman, C. N., Synthesis of novel trithiocarbonate and allyl sulfide containing monomers. *Polymer Chemistry* **2014,** *5* (1), 62-68.

160. Kloxin, C. J.; Scott, T. F.; Bowman, C. N., Stress Relaxation via Addition−Fragmentation Chain Transfer in a Thiol-ene Photopolymerization. *Macromolecules* **2009,** *42* (7), 2551-2556.

161. Meng, Y.; Fenoli, C. R.; Aguirre-Soto, A.; Bowman, C. N.; Anthamatten, M., Photoinduced Diffusion Through Polymer Networks. *Adv. Mater.* **2014,** *26* (37), 6497-6502.

162. Xia, Y.; Kim, E.; Zhao, X.-M.; Rogers, J. A.; Prentiss, M.; Whitesides, G. M., Complex Optical Surfaces Formed by Replica Molding Against Elastomeric Masters. *Science* **1996,** *273* (5273), 347-349.

163. Calafiore, G.; Fillot, Q.; Dhuey, S.; Sassolini, S.; Salvadori, F.; Mejia, C. A.; Munechika, K.; Peroz, C.; Cabrini, S.; Piña-Hernandez, C., Printable photonic crystals with high refractive index for applications in visible light. *Nanotechnology* **2016,** *27* (11), 115303.

164. Pina-Hernandez, C.; Koshelev, A.; Digianantonio, L.; Dhuey, S.; Polyakov, A.; Calafiore, G.; Goltsov, A.; Yankov, V.; Babin, S.; Cabrini, S.; Peroz, C., Printable

planar lightwave circuits with a high refractive index. *Nanotechnology* **2014,** *25* (32), 325302.

165. Beadie, G.; Shirk, J. S.; Rosenberg, A.; Lane, P. A.; Fleet, E.; Kamdar, A.; Jin, Y.; Ponting, M.; Kazmierczak, T.; Yang, Y., Optical properties of a bio-inspired gradient refractive index polymer lens. *Opt. Express* **2008,** *16* (15), 11540-11547.

166. Fernández, R.; Bleda, S.; Gallego, S.; Neipp, C.; Márquez, A.; Tomita, Y.; Pascual, I.; Beléndez, A., Holographic waveguides in photopolymers. *Opt. Express* **2019,** *27* (2), 827-840.

167. Chen, X.; Liu, W.; Dong, B.; Lee, J.; Ware, H. O. T.; Zhang, H. F.; Sun, C., High-Speed 3D Printing of Millimeter-Size Customized Aspheric Imaging Lenses with Sub 7 nm Surface Roughness. *Adv. Mater.* **2018,** *30* (18), 1705683.

168. Gissibl, T.; Thiele, S.; Herkommer, A.; Giessen, H., Two-photon direct laser writing of ultracompact multi-lens objectives. *Nature Photonics* **2016,** *10*, 554.

169. Liu, J.-g.; Nakamura, Y.; Shibasaki, Y.; Ando, S.; Ueda, M., High Refractive Index Polyimides Derived from 2,7-Bis(4-aminophenylenesulfanyl)thianthrene and Aromatic Dianhydrides. *Macromolecules* **2007,** *40* (13), 4614-4620.

170. Fukuzaki, N.; Higashihara, T.; Ando, S.; Ueda, M., Synthesis and Characterization of Highly Refractive Polyimides Derived from Thiophene-Containing Aromatic Diamines and Aromatic Dianhydrides. *Macromolecules* **2010,** *43* (4), 1836-1843.

171. Tapaswi, P. K.; Choi, M.-C.; Jeong, K.-M.; Ando, S.; Ha, C.-S., Transparent Aromatic Polyimides Derived from Thiophenyl-Substituted Benzidines with High Refractive Index and Small Birefringence. *Macromolecules* **2015,** *48* (11), 3462-3474.

172. Matsuda, T.; Funae, Y.; Yoshida, M.; Yamamoto, T.; Takaya, T., Optical material of high refractive index resin composed of sulfur-containing aromatic methacrylates. **2000,** *76* (1), 50-54.

173. Okutsu, R.; Ando, S.; Ueda, M., Sulfur-Containing Poly(meth)acrylates with High Refractive Indices and High Abbe's Numbers. *Chem. Mat.* **2008,** *20* (12), 4017-4023.

174. Matsuda, T.; Funae, Y.; Yoshida, M.; Yamamoto, T.; Takaya, T., Optical material of high refractive index resin composed of sulfur-containing aliphatic and alicyclic methacrylates. *Journal of Applied Polymer Science* **2000,** *76* (1), 45-49.

175. Okutsu, R.; Suzuki, Y.; Ando, S.; Ueda, M., Poly(thioether sulfone) with High Refractive Index and High Abbe's Number. *Macromolecules* **2008,** *41* (16), 6165-6168.

176. Bhagat, S. D.; Chatterjee, J.; Chen, B.; Stiegman, A. E., High Refractive Index Polymers Based on Thiol–Ene Cross-Linking Using Polarizable Inorganic/Organic Monomers. *Macromolecules* **2012,** *45* (3), 1174-1181.

177. Suzuki, Y.; Higashihara, T.; Ando, S.; Ueda, M., Synthesis and Characterization of High Refractive Index and High Abbe's Number Poly(thioether sulfone)s based on Tricyclo[5.2.1.02,6]decane Moiety. *Macromolecules* **2012,** *45* (8), 3402-3408.

178. Chen, X.; Fang, L.; Wang, J.; He, F.; Chen, X.; Wang, Y.; Zhou, J.; Tao, Y.; Sun, J.; Fang, Q., Intrinsic High Refractive Index Siloxane–Sulfide Polymer Networks Having High Thermostability and Transmittance via Thiol–Ene Cross-Linking Reaction. *Macromolecules* **2018,** *51* (19), 7567-7573.

179. Chan, J. W.; Zhou, H.; Hoyle, C. E.; Lowe, A. B., Photopolymerization of Thiol-Alkynes: Polysulfide Networks. *Chem. Mat.* **2009,** *21* (8), 1579-1585.

180. Gao, P.; Xu, P.-F.; Zhai, H., Borax-catalyzed thiolysis of 1,2-epoxides in aqueous medium. *Tetrahedron Letters* **2008,** *49* (46), 6536-6538.

181. Suzuki, Y. K. S. I. Mercapto compound, a high refractive index resin and lens and a process for preparing them
. 1992.

182. Nebioglu, A.; Leon, J. A.; Khudyakov, I. V., New UV-Curable High Refractive Index Oligomers. *Industrial & Engineering Chemistry Research* **2008,** *47* (7), 2155-2159.

183. Okubo, T.; Kohmoto, S.; Yamamoto, M., Synthesis, characterization, and optical properties of polymers comprising 1,4-dithiane-2,5-bis(thiomethyl) group. **1998,** *68* (11), 1791-1799.

184. Okubo, T.; Kohmoto, S.; Yamamoto, M., Synthesis, characterization, and optical properties of polymers comprising 1,4-dithiane-2,5-bis(thiomethyl) group. *Journal of Applied Polymer Science* **1998,** *68* (11), 1791-1799.

185. Matsumoto, K.; Costner, E. A.; Nishimura, I.; Ueda, M.; Willson, C. G., High Index Resist for 193 nm Immersion Lithography. *Macromolecules* **2008,** *41* (15), 5674-5680.

186. Maheswara, M.; Oh, S.-H.; Ju, J.-J.; Park, S. K.; Park, S.; Do, J. Y., High refractive index of transparent acrylate polymers functionalized with alkyl sulfur groups. *Polymer Journal* **2009,** *42*, 249.

187. Nakagawa, Y.; Suzuki, Y.; Higashihara, T.; Ando, S.; Ueda, M., Synthesis of Highly Refractive Poly(phenylene thioether) Derived from 2,4-Dichloro-6-alkylthio-1,3,5-triazines and Aromatic Dithiols. *Macromolecules* **2011,** *44* (23), 9180-9186.

188. Nakabayashi, K.; Imai, T.; Fu, M.-C.; Ando, S.; Higashihara, T.; Ueda, M., Poly(phenylene thioether)s with Fluorene-Based Cardo Structure toward High Transparency, High Refractive Index, and Low Birefringence. *Macromolecules* **2016,** *49* (16), 5849-5856.

189. McNair, O. D.; Janisse, A. P.; Krzeminski, D. E.; Brent, D. E.; Gould, T. E.; Rawlins, J. W.; Savin, D. A., Impact Properties of Thiol–Ene Networks. *ACS Appl. Mater. Interfaces* **2013,** *5* (21), 11004-11013.

190. Zwiers, R. J. M.; Dortant, G. C. M., Aspherical lenses produced by a fast high-precision replication process using UV-curable coatings. *Appl. Opt.* **1985,** *24* (24), 4483-4488.

191. Norland Optical Adhesive 170. https://www.norlandprod.com/adhesives/NOA170.html (accessed 3/26/19).

192. Rahimi, A.; García, J. M., Chemical recycling of waste plastics for new materials production. *Nature Reviews Chemistry* **2017,** *1*, 0046.

193. Garcia, J. M.; Robertson, M. L., The future of plastics recycling. **2017,** *358* (6365), 870-872.

194. Shtukenberg, A. G.; Punin, Y. O.; Gunn, E.; Kahr, B., Spherulites. *Chem. Rev.* **2012,** *112* (3), 1805-1838.

195. Crist, B.; Schultz, J. M., Polymer spherulites: A critical review. *Prog. Polym. Sci.* **2016,** *56*, 1-63.

196. Carothers, W. H., Polymerization. *Chem. Rev.* **1931,** *8* (3), 353-426.

197. Mark, H., Intermolecular Forces and Mechanical Behavior of High Polymers. *Industrial & Engineering Chemistry* **1942,** *34* (11), 1343-1348.

198. Ozawa, T., Kinetics of non-isothermal crystallization. *Polymer* **1971,** *12* (3), 150-158.

199. Jeziorny, A., Parameters characterizing the kinetics of the non-isothermal crystallization of poly (ethylene terephthalate) determined by DSC. *Polymer* **1978,** *19* (10), 1142-1144.

200. Strobl, G., From the melt via mesomorphic and granular crystalline layers to lamellar crystallites: A major route followed in polymer crystallization? *The European Physical Journal* **2000,** *3* (2), 165-183.

201. Carothers, W. H., Polymers and polyfunctionality. *Transactions of the Faraday Society* **1936,** *32* (0), 39-49.

202. Mautner, A.; Qin, X.; Wutzel, H.; Ligon, S. C.; Kapeller, B.; Moser, D.; Russmueller, G.; Stampfl, J.; Liska, R., Thiol-ene photopolymerization for efficient curing of vinyl esters. *J. Polym. Sci. Part A: Polym. Chem.* **2013,** *51* (1), 203-212.

203. Alfrey, T.; Price, C. C., Relative reactivities in vinyl copolymerization. *J. Polym. Sci.* **1947,** *2* (1), 101-106.

204. Northrop, B. H.; Coffey, R. N., Thiol–Ene Click Chemistry: Computational and Kinetic Analysis of the Influence of Alkene Functionality. *J. Am. Chem. Soc.* **2012,** *134* (33), 13804-13817.

205. Gibson, I., *Additive Manufacturing Technologies*. Springer: New York, 2014.

206. Ngo, T. D.; Kashani, A.; Imbalzano, G.; Nguyen, K. T. Q.; Hui, D., Additive manufacturing (3D printing): A review of materials, methods, applications and challenges. *Composites Part B: Engineering* **2018,** *143*, 172-196.

207. Schwartz, J. J.; Boydston, A. J., Multimaterial actinic spatial control 3D and 4D printing. *Nat. Commun.* **2019,** *10* (1), 791.

208. Patel, D. K.; Sakhaei, A. H.; Layani, M.; Zhang, B.; Ge, Q.; Magdassi, S., Highly Stretchable and UV Curable Elastomers for Digital Light Processing Based 3D Printing. *Adv. Mater.* **2017,** *29* (15), 1606000.

209. Hegde, M.; Meenakshisundaram, V.; Chartrain, N.; Sekhar, S.; Tafti, D.; Williams, C. B.; Long, T. E., 3D Printing All-Aromatic Polyimides using Mask-Projection Stereolithography: Processing the Nonprocessable. *Adv. Mater.* **2017,** *29* (31), 1701240.

210. Herzberger, J.; Meenakshisundaram, V.; Williams, C. B.; Long, T. E., 3D Printing All-Aromatic Polyimides Using Stereolithographic 3D Printing of Polyamic Acid Salts. *ACS Macro Lett.* **2018,** *7* (4), 493-497.

211. Zhang, B.; Kowsari, K.; Serjouei, A.; Dunn, M. L.; Ge, Q., Reprocessable thermosets for sustainable three-dimensional printing. *Nat. Commun.* **2018,** *9* (1), 1831.

212. Seidler, K.; Griesser, M.; Kury, M.; Harikrishna, R.; Dorfinger, P.; Koch, T.; Svirkova, A.; Marchetti-Deschmann, M.; Stampfl, J.; Moszner, N.; Gorsche, C.; Liska, R., Vinyl Sulfonate Esters: Efficient Chain Transfer Agents for the 3D Printing of Tough Photopolymers without Retardation. *Angew Chem Int Ed Engl* **2018,** *57* (29), 9165-9169.

213. Sycks, D. G.; Wu, T.; Park, H. S.; Gall, K., Tough, stable spiroacetal thiol-ene resin for 3D printing. *Journal of Applied Polymer Science* **2018,** *135* (22), 46259.

214. Bhattacharjee, N.; Parra-Cabrera, C.; Kim, Y. T.; Kuo, A. P.; Folch, A., Desktop-Stereolithography 3D-Printing of a Poly(dimethylsiloxane)-Based Material with Sylgard-184 Properties. *Adv. Mater.* **2018,** *30* (22), 1800001.

215. Thrasher, C. J.; Schwartz, J. J.; Boydston, A. J., Modular Elastomer Photoresins for Digital Light Processing Additive Manufacturing. *ACS Appl. Mater. Interfaces* **2017,** *9* (45), 39708-39716.

216. Dolinski, N. D.; Page, Z. A.; Callaway, E. B.; Eisenreich, F.; Garcia, R. V.; Chavez, R.; Bothman, D. P.; Hecht, S.; Zok, F. W.; Hawker, C. J., Solution Mask Liquid Lithography (SMaLL) for One-Step, Multimaterial 3D Printing. *Adv. Mater.* **2018,** *30* (31), 1800364.

217. Leonards, H.; Engelhardt, S.; Hoffmann, A.; Pongratz, L.; Schriever, S.; Bläsius, J.; Wehner, M. M.; Gillner, A., Advantages and drawbacks of Thiol-ene based resins for 3D-printing. *Proceedings of SPIE* **2015,** *9353*, 7.

218. Chen, L.; Wu, Q.; Wei, G.; Liu, R.; Li, Z., Highly stable thiol–ene systems: from their structure–property relationship to DLP 3D printing. *Journal of Materials Chemistry C* **2018,** *6* (43), 11561-11568.

219. Wallin, T. J.; Pikul, J. H.; Bodkhe, S.; Peele, B. N.; Mac Murray, B. C.; Therriault, D.; McEnerney, B. W.; Dillon, R. P.; Giannelis, E. P.; Shepherd, R. F., Click chemistry stereolithography for soft robots that self-heal. *Journal of Materials Chemistry B* **2017,** *5* (31), 6249-6255.

220. Sycks, D. G.; Safranski, D. L.; Reddy, N. B.; Sun, E.; Gall, K., Tough Semicrystalline Thiol–Ene Photopolymers Incorporating Spiroacetal Alkenes. *Macromolecules* **2017,** *50* (11), 4281-4291.

221. Halloran, J. W., Ceramic Stereolithography: Additive Manufacturing for Ceramics by Photopolymerization. *Annual Review of Materials Research* **2016,** *46* (1), 19-40.

222. Fortman, D. J.; Brutman, J. P.; De Hoe, G. X.; Snyder, R. L.; Dichtel, W. R.; Hillmyer, M. A., Approaches to Sustainable and Continually Recyclable Cross-Linked Polymers. *ACS Sustain. Chem. Eng.* **2018,** *6* (9), 11145-11159.